Correlation between Morphology and Mechanical Properties of Polystyrene-b-Polybutadiene-b-Poly(methyl methacrylate) in Dependency of the Polybutadiene's Block Microstructure

DISSERTATION

zur Erlangung des akademischen Grades

Doktor der Naturwissenschaften

(Dr. rer. nat.)

der Technischen Fakultät

der Christian-Albrechts-Universität zu Kiel

vorgelegt von

Mohammad Rakibul Kabir

aus Chittagong/Bangladesch

Kiel, 2011

Correlation between Morphology and Mechanical Properties of Polystyrene-b-Polybutadiene-b-Poly(methyl methacrylate) in Dependency of the Polybutadiene's Block Microstructure

DISSERTATION

zur Erlangung des akademischen Grades

Doktor der Naturwissenschaften

(Dr. rer. nat.)

der Technischen Fakultät

der Christian-Albrechts-Universität zu Kiel

vorgelegt von

Mohammad Rakibul Kabir

aus Chittagong/Bangladesch

Kiel, 2011

1. Gutachter ..... Prof. Dr. Volker Abetz

(Institute of Polymer Research, Helmholtz-Zentrum Geesthacht)

2. Gutachter..... Prof. Dr. Klaus Rätzke

(Faculty of Engineering, Christian-Albrechts-University of Kiel)

Datum der mündlichen Prüfung 05.10.2011

Erklärung

Die vorliegende Arbeit wurde von mir selbstständig verfasst und ich habe dabei keine anderen als die angegebenen Hilfsmittel und Quellen benutzt.
Ferner habe ich nicht versucht, anderweitig mit oder ohne Erfolg eine Dissertation einzureichen oder mich der Doktorprüfung zu unterziehen.

Declaration on application for doctoral admission

I declare hereby that this doctoral theses was prepared by myself and all the publications are correctly cited here as references.
This work is neither published before by any other body nor is copied from other sources. This doctoral thesis has never been submitted in the present form or similar to any other university or board of examiners.

Geesthacht, 23/05/2011

Rakibul Kabir

TABLE OF CONTENTS

LIST OF ABBREVIATIONS

1,2-B	1,2-microstructure of polybutadiene
1,4-B	1,4-microstructure of polybutadiene
$\overrightarrow{\lvert a\rvert}, \overrightarrow{\lvert b\rvert}, \overrightarrow{\lvert c\rvert}$	Lattice vector in a direction of crystalline axis
(dn/dc)	Refractive index increment
A	cross section area of a specimen
$[A^-]$	concentration of the free ions
$[A^-C^+]$	concentration of the ion pairs
ABA	ternary triblock terpolymer from the block of A and B
ABC	ternary triblock terpolymer from the block of A, B and C
B	polybutadiene
B_0	external magnetic filed
BCC	Body-centered-cubic microphase
BHT	2,6-di-tert-butyl-4-methylphenol
$CDCl_3$	deuterated chloroform
CMA	cooperative motion algorithm
c_ac	cylinder at cylinder
c_ic	cylinder in cylinder
D	length of repeating unit in the composition profile
d_{hkl}	distance between two planes (hkl) [nm]
DIS	disordered phase
DME	1,2-dimethoxyethane
DMA	dynamic mechanical analysis
DPE	1,1-diphenylethene
DSC	differential scanning calorimetry
E	E- modulus or Young modulus (MPa)
E’	storage modulus (MPa)
E’’	loss modulus (MPa)
E*	complex modulus (MPa)
EPR	ethylene propylene plastics
EPDM	ethylene-propylene-dyne monomer
F	applied force producing extension of the specimens
ΔG_m	free energy of mixing
GPC	gel permeation chromatography
h	plank’s constant
(h,k,l)	miller indices
hS	polystyrene homopolymer
HEX or *hex*	hexagonally microphase
ΔH_m	enthalpy of mixing
I	intensity of primary beam that passes at an angle 0^0
$[I]_0$	concentration of the initiator
I_0	intensity of incident light
$iBAl(BHT)_2$	di[2,6-di(tert-butyl)-4-methyl phenoxy]isopropyl aluminium
ISP	polyisoprene-*b*-polystyrene-*b*-poly(2-vinylpyridine)
K	Kuhn length
k_1	propagation rate constant in contact ion pair system
k_2	propagation rate constant for dimeric aggregated species
k_4	propagation rate constant for tetrametric aggregates species
k_6	propagation rate constant for hexameric aggregates species

$k_{\pm}$	propagation rate constant for dissociated ion pairs
k_a	propagation rate constant for associated ion pairs
K_A	equilibrium constant for associated ion pairs
K_B	boltzman constant ($1.38*10^{-23}$ J/K)
K_D	equilibrium constant for dissociated ion pairs
K_d	dissociation constant
k_f	propagation rate constant in free ion pair system
k_i	rate constant of the initiation step
k_p	rate constant of the propagation step
k_p^{cis}	propagation rate constant for cis formation
k_p^{trans}	propagation rate constant for cis-trans formation
k_{obs}	observed rate constant for the propagation step
k_s	propagation rate constant in solvent seperated ion pair system
k_t	rate constant of the termination step
l	length of specimens
LAM or *ll*	lamellar microphase
ls	spheres on lamellae
lc	cylinder in lamellae
$I_q(\varphi)$	scattering intensity as a function of azimuthal angle
M	Methylmethacrylate
$[M]$	concentration of the monomer
$[M^*]$	concentration of all the living chain ends in the reaction system
M_e	molecular weight between the entanglements.
$[M_0]$	initial concentration of the monomer
M_i	molar mass of the i^{th} polymer chain
M_n	number average molar mass
M_n^{app}	apparent number average molar mass
M_n^{theo}	theoretical number average molar mass (monomer-initiator ratio)
M_z	Z average molecular weight
M_w	weight average molar mass
MPA	megapascal
N	overall degree of polymerization
N_i	number of polymer chains with molar mass M_i
NMR	nuclear magnetic resonance spectroscopy
ODT	order-disorder temperature
$[P]$	number of polymer chains
P2	orientation factor
P_n	degree of polymerization
PCL	poly (ε-caprolactone)
PDI	polydispersity index
PE	polyethylene
pK_a	dissociation constant
PP	polypropylene
PVC	polyvinyl chloride
q^*	wave vector
$\vec{q}$	scattering vector [nm^{-1}]
$Q_{Im\bar{3}m}$	body-centered cubic microphase
$Q_{Ia\bar{3}d}$	gyroid morphology
R	Universal gas constant (*8.315* J/Kmol)
RI	refractive index
R_i	rate of initiation
R_P	rate of polymerization
RV	retention volume
S	polystyrene
ΔS_m	entropy of mixing

T	temperature
TEM	Transmission Electron Microscopy
TPE	thermoplastic elastomer
T_g	glass transition temperature of the polymer
T_m	cystalline melting temperature
THP	tetrahydropyranyl ethers
THF	tetrahydrofuran
TMS	tetramethyl silane
SAXS	small angle X-ray scattering
SBM	polystyrene-b-polybutadiene-b-poly (methylmethacrylate)
SBS	polystyrene-b-polybutadiene-b- polystyrene
SEBS	styrene-Ethylene-Butadiene-Styrene
SCFT	self consistent field theory
SIS	polystyrene-b-polyisoprene-b-polystyrene
SIP	polystyrene-b-polyisoprene-b-poly(2-vinylpyridiene)
SIM	polystyrene-b-polyisoprene-b-poly(methyl methacrylate)
s_os	sphere on sphere
s_oc	sphere on cylinder
SSL	strong segregation limit
UV	ultraviolet
V_0	volume between the gel particles
V_e	elution volume
v_e	entanglement density
V_i	overall sum of all pore volumes
w_i	weight fraction of component i in copolymer
w	interfacial width
WSL	weak segregation limit
Y	electron withdrawing group
Z	number of nearest segments in other chains

LIST OF SYMBOLS

χ	Florry - Huggins interaction parameter
ε_{AB}	Interaction energy between segments A and B
φ_i	Volume fraction of the component i
φ_{2VP}	volume fraction of 2-vinyl pyridine
$\rho(A)$, $\rho(B)$	density profile of the components of A dn B in different phases
Å	angstrom
λ	wavelength [nm]
ΔE	Energy difference of the magnetic moment
μ	Magnetic moment of the nucleus
δ	chemical shift (ppm)
ν_0	operating frequency of a spectrometer
$\tan\delta$	damping factor
σ	stress (MPa)
σ_Y	stress at yield (MPa)
σ_M	stress at maximum (MPa)
σ_B	stress at break (MPa)
ε	strain (%)
ε_Y	strain at yield (%)
ε_M	strain at maximum (%)
ε_B	strain at break (%)
Θ	Bragg scattering angle [°]
φ	azimuth angle [°]

Chapter 01

Introduction

Self-assembled block copolymers offer diverse applications in the field of biology and medicine for drug delivery or drug carrier systems as well as in the field of material science for enhancing the mechanical, optical, and electrical properties in both bulk and thin film systems.[1] The covalently linked two or more polymeric chains, which are thermodynamically incompatible, allow the block polymer system to reform and reconfigure the morphology to a variety of microstructures. Hence the association properties can be customed for the potential applications of block copolymers in different application field. Since Szwarc's remarkable discovery of living anionic polymerization in the 1950s, the field of block copolymer based thermoplastic elastomers (TPE) have been successfully synthesized in a control manner with a fairly narrow polydispersity both in compositions and molar masses.[2, 3] In thermoplastic elastomers, two phases, a dispersed glassy (or semicrystalline) domain (hard phase) and an elastomeric matrix (soft phase) co-exist. The hard phase is brittle at service temperature and provides the physical crosslinks, while the elastomeric phase is soft as rubbery material and provides global flexibility. When the hard phase is melted or dissolved in a solvent, the material can be processed by conventional methods. Upon cooling of the material, the hard phase solidifies and the material regains its strength and elasticity. A high incompatibility and/or a high molar mass are disadvantageous in view of processing, as they result in a comparatively high melt viscosity.

In the early 1970s, Keller and co-workers investigated the mechanical properties of TPE's.[4, 5] Most of the studies have focused on glassy/ rubbery diblock and triblock TPEs consisting of polystyrene as a glassy blocks and polybutadiene and polyisoprene as rubbery blocks. In recent years, another new type of styrenic TPEs named, polystyrene-*b*-polybutadiene-*b*-poly(methyl methacrylate), (SBM), triblock terpolymer has received much attention to the researcher due to their possibility of forming various complex morphologies as well as improved mechanical properties compared to the commercially available SBS triblock TPEs. [6-10] As shown in Figure 1.1 a), in SBS type styrenic thermoplastic elastomer the two unlike block is such that the S-block assembles in a spherical fashion and the polybutadiene forms a bridge in between two S spheres. In some cases the B-type chains may loop back. However, in the same type of compositions but in SBM triblock terpolymer system, the B-type chain forms a bridge between the end blocks rather than loop back (Figure 1.1 b). [10] Therefore, the percentage of the B-type chain elastomeric bridges is higher compared to the SBS system. While the first case (SBS type), the loop forming

B chains leads to an elastic inactive middle block, the latter (SBM type) results in a higher elastic behavior. At larger elongations, some of the SBM triblock terpolymers show a higher resistance to deform than the corresponding SBS triblock copolymers.

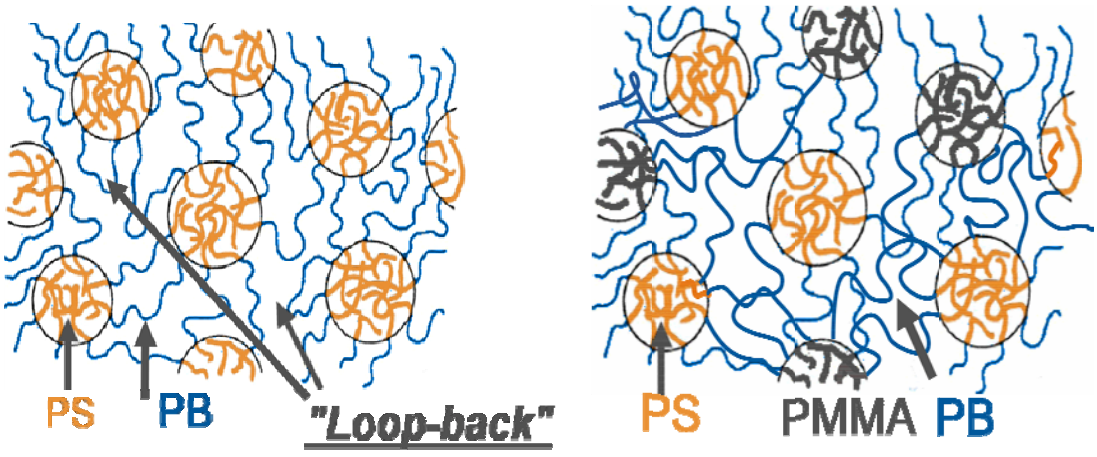

Figure 1.1: *Sketch of the loop-bridge formation of the polybutadiene middle block in SBS (left) and SBM (right) systems.*

Several works were reported on the formation of loop and the loop to bridge population ratio in well-segregated ABA triblock copolymers.[12-17] Based on Monte Carlo computer simulations using the Cooperative Motion Algorithm (CMA), an equilibrium bridge fraction of $\phi_{bridge} \cong 0.5$ to 0.37 was determined. This ratio depends on the total molar mass and has the tendency to decrease with an increasing molar mass of the ABA triblock copolymer. The effect of loop/bridge conformation ratio on the elastic properties of the sphere forming polystyrene-*b*-polyisoprene-*b*-polystyrene, (SIS) , triblock copolymers were investigated by Matsushita et al.[18, 19] They prepared a series of SIS samples having almost the same size of spherical S microdomains but different loop/bridge fractions by mixing a cyclic-SI diblock copolymer. The resulted stress-strain curves showed small shoulder-like enhancement of the stresses at low strains which mainly occurred due to the restoring force of lattice. This force depends linearly on the bridge fraction of the middle block chains in bulk states. The mechanical properties of TPE's can also be altered at similar morphologies by controlling the ratio of bridge to loop conformation. Again in ABABA pentablock copolymers where the bridge/loop ratio is higher than the ABA triblock copolymers show pronouncedly higher ductility in the pentablock system.[20]Again by controlling loop/bridge ratio of ABA copolymer, a desirable mechanical properties of the material can be obtained.[21]

The differences of the mechanical properties of different block copolymer are related to the interaction between the different phases and the resulting morphology. The mechanical testing

conditions as well as the molecular parameters such as total molar mass and microstructure of the rubber block segment differ significantly for the di- , tri- or multi- block systems. Comparing the tensile behavior of di- and tri-block systems of polystyrene and polybutadiene (cast from toluene), it has been found that the tri-block (SBS) systems exhibit rather rapid increase in the tensile stress compare to the di-block system after the macroscopic necking occurred at around a few hundred percent elongation.[22] Compared to linear di- or tri-block copolymers the multigraft or random copolymer TPE's show very high strain at break due to the enhanced degree of physical cross-linking sites of the block copolymer.[23-25] Weidisch et al. [25] reportaed strain at break around 2300% for styrene/isoprene graft copolymers having 10 branch points which are very high compared to the commercial TPE's Kraton. Investigations showed that the S block in the multigraft copolymer has a wormlike microphase-separated structure that lowers the long range order of multigraft copolymer than Kraton and allows the elastic backbone to couple into a large number of reinforcing S domains, resulting in huge elasticity. Again, in case of star block copolymers at equivalent chemical compositions of linear block copolymers, the star type copolymers show much larger plastic deformation. [26]

The micromechanical processes of the different domain's deformation also influence the mechanical properties of the block copolymer.[27] The mechanisms how the different domains are deformed can be investigated using mechanical, optical as well as microscopic techniques. Till now most of the deformation analysis were performed for styrenic TPEs copolymers.[4, 27-31] Investigations showed two types of plastic deformation mechanisms of the glassy component. In the first type, the deformation occurs through plastic flow or fragmentation of the blocks. In the other type, the deformation evolves as microcrazes at the phase boundary of the rubber like material. This crazes prolong through the glassy matrix. Both mechanisms are associated with a macro-necking of the bulk specimens rather than a micro-necking and are mostly observed for systems having a relatively high volume fraction of rubbery components (near 50%).[32] In case of SB diblock copolymer, plastic deformation was followed by cavitation mechanism.[23] However, the cavitation mechanism proposed for SB diblock copolymers is not valid for SBS triblock copolymers.[19]

The orientation of the domains as well as the mechanical properties of the block copolymers are also influenced by the deformation of microdomains. The orientation behavior of different domains of SBS and the blending homopolymer (hS) in the triblock copolymer (SBS), were investigated by Adhikari et al.[33] They obtained a rapid decrease in the degree of orientation of the polystyrene and the polybutadiene phases in the blend which is mainly due to the occurrence

of the ductile failure at the interface between the added hS and S blocks of the block copolymer. The orientation behavior is also influenced by the individual phases which is found as highly orientation in B phase than the S one because of the lower Young's modulus of B phase.

Although a broad range of scientific investigation correlating the polymeric structure and mechanical behavior have been found in literature, very few research activities have been focused on explaining the role of the B microstructure (with presence of lamellar morphology) i.e., 1,2-B and 1,4-B in styrenic TPEs on the mechanical behavior. So far the deformation and orientation behavior of the B microstructures of these polymers are still not fully understood. Significant scope still remains in understanding the orientation behavior of B polybutadiene microstructure in the deformation process of the morphology during tensile test.

Aim of this work

The primary goal in present research is to correlate the morphology and mechanical properties of different lamellar type of styrenic TPE, i.e., polystyrene-*b*-polybutadiene-*b*-poly (methyl methacrylate), SBMs. The SBM system is of particular interest, because increasing the molar mass the domains will segregate more strongly. As a consequence the mechanical properties will improve, which means the behavior of deformation and orientation will exhibit a molar mass dependency. Therefore, the mechanical properties will be different for different lamellar type SBMs.In case of SBM, due to different type of end blocks and B microstructures, the expected deformation mechanism will not be same as SBS. In this work a few hypotheses shall be proposed which might help to understand the correlation between morphology and mechanical properties as well as the deformation and orientation behavior of the B microstructure.

To accomplish the present goal following tasks will be performed:

i) SBM triblock terpolymers will be synthesized via anionic polymerization to obtain a unique control of the polymerization reactions along with narrow polydispersities. Molar masses are targeted from 30 - 300 kg/mol which exhibit good segregation, hence improved mechanical properties. Polar and non-polar solvents will be used to synthesize SBMs with various contents of 1,2- and 1,4-polybutadiene microstructure.

ii) Mechanical properties will be analyzed for different lamellar types of SBMs with varying polybutadiene microstructures. The analysis will be performed

for different morphologies, weight percentage of polybutadiene and total molar mass of the polymers.

iii) Morphological deformations will be analyzed via in-situ tensile tests and small angle X-ray scattering (SAXS). Transmission electron microscopy (TEM) will be applied to investigate the morphology change due to deformation. For this purpose, two sets of polymers containing same weight fraction and molar mass but different polybutadiene microstructures will be synthesized. Investigation will be performed to analyze the effects of the B microstructure on deformation morphology during the elongation.

iv) The effect of the blended residual blocks on the morphologies and the mechanical properties will be discussed. After synthesis, some residual blocks (polystyrene homopolymer or polystyrene-*b*-polybutadiene diblock copolymer) remained blended with the SBM triblocks.

In this thesis the above mentioned tasks and ideas are presented as follows: the segregation behavior and the deformation of block copolymers' morphology are emphasized in **Chapter 2** where different segregation models and the deformation patterns of diblock and triblock copolymers are described. **Chapter 3** describes the theoretical background of anionic polymerization and synthesis techniques of different blocks. Here, the reactions principles for different polar and non-polar monomers in different solvents as well as the presence of additives and catalysts in the polymerization reactions have been explained. The morphological, mechanical and thermal characterization techniques are described in **Chapter 4.** Different synthesis techniques for SBM triblocks in both THF and toluene are given in **Chapter 5** where the optimum conditions of the reactions are discussed in greater detail. The morphological characterizations (Transmission Electron Microscopy (TEM), Small Angle X-ray Scattering, (SAXS)) of different lamellar SBMs are studied in **Chapter 6** where the discussion is focused on the morphological and mechanical properties of SBMs having various contents of 1,2- and 1,4- B as well as molar masses. Besides the segregation behavior of the triblocks is discussed based on the thermal analysis (differential scanning calorimetry (DSC) and dynamic mechanical (DMA) results. In **Chapter 7,** the results of sequential deformations experiments on the different domains analyzed by *in-situ* SAXS and tensile tests. The results are correlated with the TEM micrographs. A special emphasis is given to the deformation and orientation behavior of the different domains and the B microstructures which play an important role during the deformation process. The effects of the residual blocks on the morphology and mechanical properties are discussed in **Chapter 8**. **Chapter 9** summarizes the results and concludes of the present work.

Reference

[1] V. Abetz, N. Hadjichristidis, H. Iatrou, M. Pitsikalis, P. F. W. Simon, "*Block Copolymers I, Advances in Polymer Science"*, Springer-Verlag Berlin Heidelberg, 2005.

[2] M. Levy, *Bulletin of the Israel Chemical Society* **2005**, *18*.

[3] Editorial, *Prog. Polym. Sci* **2006**, *31*, 1039.

[4] J. A. Odell, A. Keller, *Polym. Eng. Sci.* **1977**, *17*, 544.

[5] R. G. C. Arridge, M. J. Folkes, *J. Phys. D: Appl. Phys.* **1972**, *5*, 344.

[6] H. Königsmann, "Kinetische Untersuchungen zur Synthese von Blockcopolymeren mit Methacrylatsegmenten durch neue anionische Polymerisationssysteme", in *am Fachbereich Chemie und Pharmazie*, der Johannes Gutenberg-Universität Mainz, 2001.

[7] T. Goldacker, "Überstrukturen in Mischungen aus Blockcopolymeren", in *im Fach Chemie der Fakultät für Biologie, Chemie und Geowissenschaften*, Univerrsität Bayreuth, 1999.

[8] S. Brinkmann-Rengel, "Thermoplastic Elastomere auf Basis von ABA und ABC Dreiblockcopolymer", in *am Fachbereich Chemie und Pharmazie*, der Johannes Gutenberg-Universität Mainz, 1998.

[9] U. Breiner, "Morphologische Studien zum Phasenverhalten mikrophasenseparierter ABC Dreiblockcopolymer", in *am Fachbereich Chemie und Pharmazie*, der Johannes Gutenberg-Universität Mainz, 1996.

[10] S. Brinkmann-Rengel, V. Abetz, R. Stadler, E. L. Thomas, *Kautschuk Gummi Kunstoffe* **1999**, *12*, 806.

[11] H. Schmalz, A. Böker, R. Lange, G. Krausch, V. Abetz, *Macromolecules* **2001**, *34*, 8720.

[12] E. Zhulina, A. Halperin, *Macromolecules* **1992**, *25*, 5730.

[13] M. W. Matsen, *J. Chem. Phys* **1995**, *102*, 3884.

[14] M. W. Matsen, M. Schick, *Macromolecules* **1994**, *27*, 187.

[15] R.L. Jones, L. Kane, R. Spontak, *J. Chem. Eng. Sci.* **1996**, *51*, 1365.

[16] H. Watanabe, *Macromolecules* **1995**, *28*, 5006.

[17] K. Karatasos, S.H. Anastasiadis, T. Pakula, H. Watanabe, *Macromolecules* **2000**, *33*, 523.

[18] Y. Takahashi, Y. Song, N. Nemoto, A. Takano, Y. Akazawa, Y. Matsushita, *Macromolecules* **2005**, *38*, 9724.

[19] A. Takano, I. Kamaya, Y. Takahashi, Y. Matsushita, *Macromolecules* **2005**, *38*, 9718.

[20] Y. Mori, L. S. Lim, F. S. Bates, *Macromolecules* **2003**, *36*, 9879.

[21] Y. Sliozberg, J. Andzelm, M. VanLandingham, J. K. Brennan, V. Pryamitsyn, V. Ganesan, in *Nanoscale Science and Engineering Forum*, Philadelphia, PA The 2008 Annual Meeting.

[22] H. Kawai, T. Hashimoto, K. Miyoshi, H. Uno, M. Fujimura, *J. Macromol. Sci. Phys.* **1980**, *B17(3)*, 427.

[23] R. Weidisch, M. Ensslen, G.H. Michler, H. Fischer, *Macromolecules* **1999**, *32*, 5375.

[24] R. Weidisch, M. Ensslen, G. H. Michler, M. Arnold, H. Budde, S. Höring, H. Fischer, *Macromolecules* **2001**, *34*, 2528.

[25] R. Weidisch, S. P. Gido, D. Uhrig, H. Iatrou, J. Mays, N. Hadjichristidis, *Macromolecules* **2001**, *34*, 6333.

[26] R. Adhikari, G. H. Michler, W. Lebek, S. Goerlitz, R. Weidisch, K. Knoll, *J. App. Polym. Sci.* **2002**, *85*, 701.

[27] R. Adhikari, "Correlations Between Molecular Architecture, Morphology and Deformation Behavior of Styrene/Butadiene Block Copolymers and Blends", in *Mathematisch-Naturwissenschaftlich-Technischen Fakultät*, der Martin-Luther-Universität Halle-Wittenberg, 2001.

[28] T. A. Huy, R. Adhikari, G. H. Michler, *Polymer* **2003**, *44*, 1247.

[29] C. C. Honeker, E. L. Thomas, *Chem. Mater.* **1996**, *8*, 1702.

[30] C. C. Honeker, E. L. Thomas, *Macromolecules* **2000**, *39*, 9407.

[31] A. S. Argon, R. E. Cohen, B. Z. Jang, J. B. V. Sande, *J. Polym. Sci.: Polym. Phys. Ed.* **1981**, *19*, 253.

[32] H. Kawai, T. Hashimoto, K. Miyoshi, H. Uno, M. Fujimura., *J. Macromol. Sci. Phys.* **1980**, *B17(3)*, 427.

[33] R. Adhikari, T. A. Huy, S. Henning, G. H. Michler, K. Knoll, *Colloid Polym. Sci.* **2004**, *282*, 1381.

Chapter 02

Segregation and Deformation of Block Copolymers

The unique properties of block copolymers in solution and in the solid state increase the importance and interest in block copolymers research field. The topology of block copolymers also enhances the possibility of varying molecular shape like linear, star or branch. The simplest block copolymers where two different blocks are joined end to end display usually four different morphologies, namely, spherical, cylindrical, gyroidal, and lamellae. Contrary, the triblock copolymers and three or four arm miktoarm star copolymers provide a vast multitude of structures.[1] In most cases it is not favorable to mix the unlike blocks of the macromolecules. They often phase separate, although their monomers mix homogeneously. This is due to very low entropy of mixing, as because, a system of two polymer chains of N monomers each, roughly exhibits a $1/N$ times smaller entropy of mixing than that of mixing the monomers they are made of. [2] Thermodynamically speaking, the microphase separation occurs because of the competition of repulsive interaction and conformational entropy. In order to provide the fundamentals of the behavior of segregation that will help to understand the different morphological patterns in later chapters, different segregation models of di- and tri-block copolymers need to be discussed first.

2.1 Microphase separation in block copolymers

The phase behavior of $(AB)_n$ (where n is the number of junction point) block copolymers are governed by three factors: i) the overall degree of polymerization, N, ii) the volume fraction of individual blocks (φ_A, $\varphi_B = 1 - \varphi_A$) which is determined by the ratio of two monomers and their molar volume, and iii) the Flory-Huggins parameter, χ. The first two parameters are governed by the polymerization stoichiometry, the influence of translational and configurational entropy, whereas the third parameter, χ, is affected by the selection of corresponding monomers.[3] For compatibility or the miscibility of two polymers, the free enthalpy of mixing ΔG_m should be decreased ($\Delta G_m < 0$) which is defined as follows:

$$\Delta G_m = \Delta H_m - T\Delta S_m \qquad \text{Equation 2.1}$$

Here, ΔH_m is the mixing enthalpy which describes the energetic interactions between the block sequences.

This is explained by the theory of Flory-Huggins-Staverman[4-6] segmental interaction parameter (χ), which can be applied for polymer solutions as well as for polymer blends.

$$\Delta H_m = RT\,\chi_{AB}\varphi_A\varphi_B \qquad \text{Equation 2.2}$$

R = universal gas constant
T = temperature
φ_i = volume fraction of component i.

The Flory-Huggins-Staverman parameter χ_{AB} (for a diblock) is expressed by the following equation

$$\chi AB = \frac{Z}{K_B T}\,[\varepsilon_{AB} - \frac{1}{2}(\varepsilon_{AA} + \varepsilon_{BB})] \qquad \text{Equation 2.3}$$

Z = number of nearest segments in other chains
K_B = Boltzman constant
ε_{AB} = interaction energy between segments A and B

The entropy of mixing ΔS_M is given by the following equation

$$\Delta S_M = -R\,(\frac{\varphi_A}{N_A} ln\varphi_A + \frac{\varphi_B}{N_B} ln\varphi_B) \qquad \text{Equation 2.4}$$

N_i = degree of polymerization of component i
φ_i = the volume fraction of the i^{th} component.

The positive mixing entropy ΔS_M leads to a negative contribution to the free enthalpy. As the volume fraction logarithm ($\log\varphi_i$) is always negative, according to Equation 2.4, ΔS_M will be positive, giving an overall negative contribution to ΔG_m (Equation 2.1). Especially for high degrees of polymerization, N_i, the entropic contribution decreases and even slight repulsive interactions between the segments ($\Delta H_m > 0$) result in a positive value to ΔG_m . Therefore, macrophase separation occurs in homogeneous polymer blends. [7] In case of block copolymers, due to the chemical link between the different blocks macrophase separation is no longer possible. The block copolymers undergo microphase separation at a length scale of the size of the macromolecules, typically in the range of 10 - 100 nm.[8]

Hence, the microphase separation as well as the morphology of the block copolymers is influenced by both enthalpic and entropic contributions. The unfavorable interfacial energy between the different segments tends to be minimized in order to achieve the smallest possible ratio between the interface

and volume. However, the entropy lost associated with chain stretching drives the chain into a random coil conformation and a weakly segregated (or large or diffuse) interface between the blocks are resulted.[9]

Again the interaction parameters of the different blocks in the block copolymers have the temperature dependency as expressed by the Equation 2.5[3]

$$\chi = \alpha T^{-1} + \beta \qquad \text{Equation 2.5}$$

Here, α and β are constants for given volume fraction, φ and the number of repeating units, *N*. For a decreasing temperature, the interaction parameter increases ($\alpha > 0$) favoring the reduction of repeating unit contact A-B. The blocks are separated at a microscopic scale and A / B rich domains are formed with an extensive amount of internal interfaces. At higher temperatures the interaction parameter decreases and an order-disorder transition occurs leading to a homogeneous mixture of A and B, as sketched in Figure 2.1.

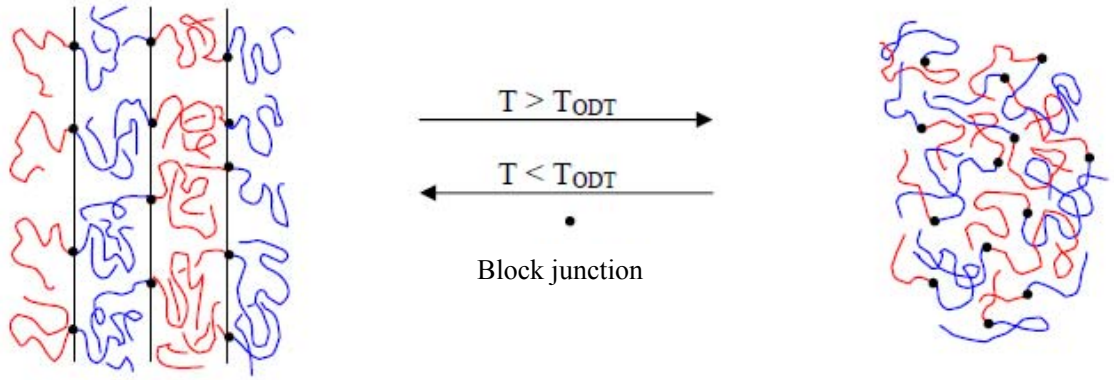

Figure 2.1: *Sketch of temperature induced ordered (lamellar) - disordered transition of AB diblock copolymers.*

For AB diblock copolymers the different microphases which are thermodynamically stable are presented in Figure 2.2. When A is the minority component ($\varphi_A << \varphi_B$), A forms spheres and are arranged in a body centered cubic structure. If the volume fraction φ_A is increased, a hexagonal array of cylindrical A phases, embedded in a B-type matrix, is formed. Increasing φ_A further a gyroid A block pattern in the B-type matrix is formed. For $\varphi_A = 0.5$, the AB diblock copolymer assembles into a

lamellar pattern of *A*-rich and *B* -rich domains. If the majority components are A, i.e., $\varphi_A > \varphi_B$, the inverse sequence of the morphologies is observed. In this case the sequence starts from the lamellar microphase to the body-centered-cubic (bcc) spheres of the B phase in the A matrix.

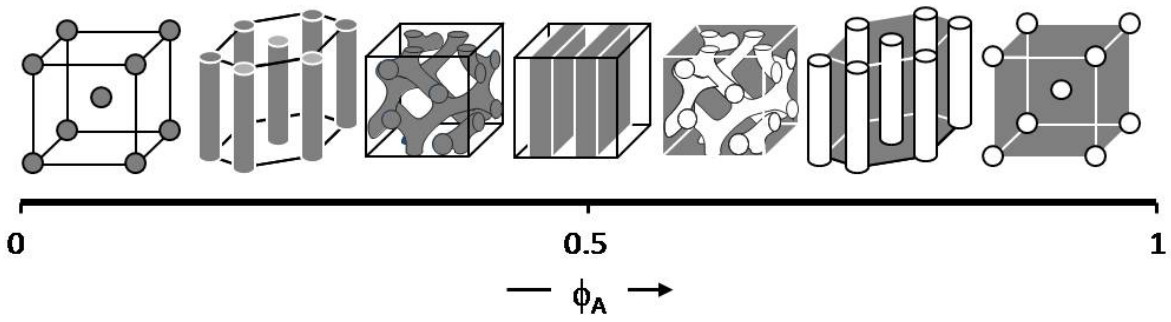

Figure 2.2: *Equilibrium morphologies of AB diblock copolymer with increasing volume fraction of φA. From left to right: spheres on a body-centered cubic (bcc) lattice, hexagonally packed cylinders, double gyoid, lamellae and the inverse sequence of the morphologies.*

2.2 Theoretical model of phase separation of diblock copolymers

As described above, the entropic and enthalpic contributions to the free energy density in a diblock copolymer are related to $1/N$ and χ, respectively. The product χN expresses the state of block copolymer phase and enthalpic-entropic balance. This product can also be interpreted as a measure of incompatibility between different blocks. The degree of incompatibility, χN, controls the degree of segregation between A and B blocks. Depending on χN, the segregation behavior is categorized into weak, intermediate and strong segregation. For $\chi N << 10$, the system is in an isotropic so-called disordered state as the entropic contributions are dominating the enthalpic term.

In the following three theoretical approaches are discussed to explain the microphase separation of block copolymers: i) Weak Segregation Limit (WSL), ii) Strong Segregation Limit (SSL) and iii) Self Consistent Field Theory (SCFT).

2.2.1 Weak Segregation Limit (WSL)

The Weak Segregation Limit theory was developed by Leibler [10] and Erukhimovich[11]. It describes the order-disorder transition of a microphase-separated block copolymer to a disordered melt. Here, the entropic effects dominate over the tendency of the block configuration to minimize the unfavorable interfacial energy of the two different segments (Figure 2.3). As a result, a mixed, isotropic phase is observed. The chain segments of both components penetrate each other. Here the segregation regimes vary not only with N but also with lamellar spacing, D, and interfacial width, w. In the disordered phase at $\phi = 0.5$, the characteristic length scale D is $2\pi/q^* = 1.318\ k\ N^{0.5}$, where '$k$' is the Kuhn length, q^* is the wave vector by which the structure function attains its maximum, and $N^{0.5}$ scaling associates the absence of segregation. When χN approaches 10, a disorder to order phase transition is produced by a delicate balance of energetic and entropic factors. In the vicinity of this transition, the A-B interactions are sufficiently weak; therefore, the individual copolymers remain largely unperturbed. The ordered composition profile is approximately sinusoidal. This results in a broad interface (cf. 'a' in Figure 2.3) lead to a weak segregation of the two domains. [12, 13]

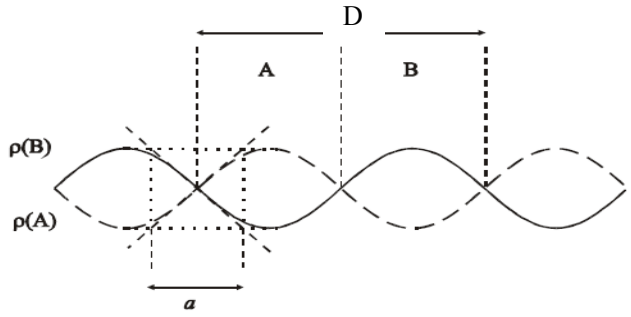

Figure 2.3: *Sinusoidal composition profile for phase-separated AB diblock copolymers in the weak segregation limit (WSL).*[13, 14]
D: length of repeating unit in the composition profile
a: thickness of the shared interface of the two components
ρ(A), ρ(B): density profile of the components A and B in the different phases.

A phase diagram for weakly segregated diblock copolymers was first calculated by Leibler using Landau's mean field approximation (Figure 2.4, a).[10] In symmetrical diblock copolymers ($\phi_A = 0.5$ and $\chi N = 10.495$), a second order phase transition to a lamellar microphase occurs. On the other hand for an asymmetric diblock copolymer ($\phi_A \neq 0.5$), a first order phase transition to a body-centered-cubic (bcc) microphase is predicted at $\chi N > 10.495$. Further transitions from the bcc structure to a hexagonal microphase and subsequently to the lamellar microphase are observed when χN increases either by

lowering the temperature or by increasing *N*. Experimentally a direct transition to the lamellar microphase has been observed without passing the intermediate bcc and hexagonal phases. Leibler himself already mentioned the need for fluctuation corrections, which are necessary for the description of finite chain lengths (in his theory he considered infite chain lengths). To overcome this problem, Fredrickson and Helfand[15] have extended the Leibler's theory by introducing such fluctuation corrections. For a finite $N = 10^6$, a direct transition from a disordered melt to a lamellar ($0.475 < \phi_A < 0.5$) or hexagonal phase ($0.42 < \phi_A < 0.475$) is predicted; for $\phi_A < 0.42$, a disorder-order transition to a bcc phase (Figure 2.4, b) is calculated.

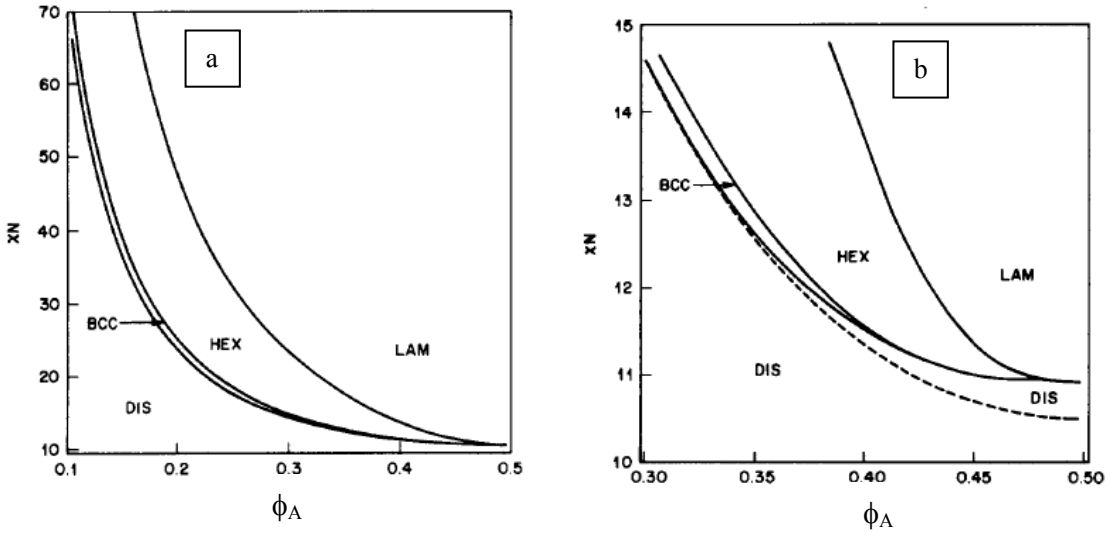

Figure 2.4: *Phase diagrams for diblock copolymers in WSL calculated by Leibler[10] (a) and by Fredrickson et al.[15] (b). The dashed curve is the classical spinodal computed by Leibler.*
LAM: lamellar microphase
HEX: hexagonal microphase
BCC: body-centered cubic microphase
DIS: disordered phase

2.2.2 Strong Segregation Limit (SSL)

The theory of the Strong Segregation Limit (SSL) was developed by Meier[16], Helfand[17, 18], and Semenov[19]. This theory describes the free energy contributions of a block copolymer chain, where the free energy is governed by the interfacial tension due to incompatibility and elastic contribution of the different blocks. Diblock copolymers belonging to the SSL regime show a high incompatibility especially if the product χN exceeds a value of 100. Phase separation occurs even for a low degree of polymerization, *N*, and the copolymers exhibit microphase separation of pure A and B with a sharp or narrow interface, see 'a' in Figure 2.5.

In this case the total contact area of the interfacial regions of segment A and B is minimized by extending their chain configuration and maintaining the density homogeneous near the interface. The entropic effects oppose the enthalpic energy associated with the contacts between the A and B segments, hence the chain configurations and microdomain periods are perturbed. Therefore, the tendency to extend the chain configuration creates a dependency of the domain size *D* on $N^{2/3}$. [17, 19]

$$D \propto N^{2/3} \chi^{1/6} \qquad \text{Equation 2.6}$$

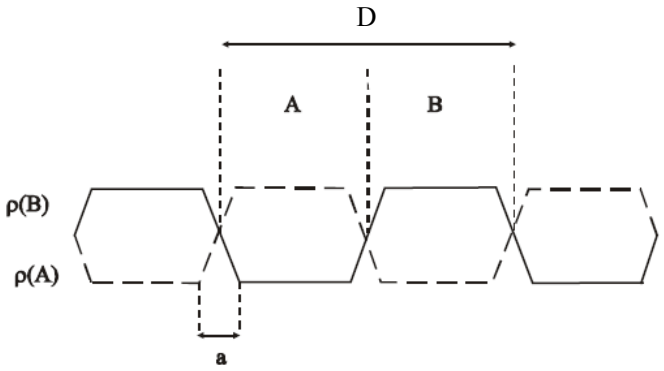

Figure 2.5: *Characteristic composition profile in the case of strong segregation limit (SSL)*[14]
D: length of repeating unit in the composition profile
a: thickness of the shared interface of the two components
ρ(A), ρ(B): density profile of the components A and B in the different phases.

2.2.3 Self Consistent Field Theory (SCFT)

Matsen and Bates[20] combined both approaches using self consistent field theory (SCFT). Further modification of the approach is done by Fredrickson and Helfand.[15] The theory predicts a region of finite composition where a direct transition between disordered and lamellar phases is possible and where the fluctuation effects disappear for an infinite large *N*. In Figure 2.6 the A segment density $\varphi_A(r)$ of the lamellar phase ($\varphi_A = 0.5$) at several degrees of segregation has been shown as a representative example. The weak segregation can be observed for $\chi N \sim 12$. This profile exhibits a sinusoidal shape as indicated by the dotted line (see also Figure 2.3) and can be well approximated by its first harmonic. This value ($\chi N \sim 12$) is close to the critical point of the mean-field $\chi N = 10.495$. For $12 \leq \chi N \leq 50$ the weak to intermediate crossover occurs. In this region the block copolymer adopt a sharp interface that indicates a strong segregation with strongly stretched blocks in different microdomains. However, to reach $\varphi_A(r) > 0.9999$ in the middle of an A-rich domain, i.e., a crossover

from intermediate to strong segregation, χN should exceed 50. For very high values of χN ~ 100, the middle of each domain consists of pure blocks. In this case the internal interfaces become very narrow (as described in Figure 2.5). However, the theory of strong segregation does not allow an accurate prediction of domain spacing (D) and interfacial widths (a) until the product χN exceeds 100.[10, 20]

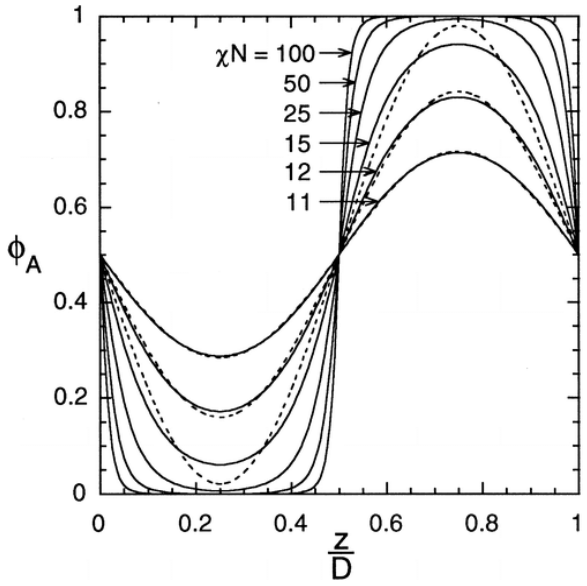

Figure 2.6: *A-segment density ($\phi_A(r)$) profile for a symmetric (f = 0.5) lamellar AB diblock melt for χN = 11, 12, 15, 25, 50, and 100. Dashed lines denote first-harmonic approximations for the profiles at χN = 11, 12, and 15. [20]*

The formation of a particular morphology as a function of components volume fraction has been explained in the paper of Matsen et al[20] using this mean-field theory. A mean-field phase diagram for conformationally symmetric diblocks and asymmetric triblock copolymer melts using the standard Gaussian polymer model is presented in Figure 2.7. It describes the corresponding order-order transitions with the recently discovered gyroid structure.

In Figure 2.7a the phase diagram for χN ~ 150 is shown. In accordance with the Semenov prediction, a narrow stable region along with the order-disorder transition for centered packed spheres (CPS) is found. This region extends towards the strong-segregation limit and is located between disordered phase (DIS) and body-centered cubic microphase ($Q_{Im\bar{3}m}$) with the triple points at χN = 17.67 and φ_A = 0.235 (Figure 2.7b, circle 1). While the regions of stability for the lamellae, helix and body-centered cubic ($Q_{Im\bar{3}m}$) phases grow with an increasing χN, the region of stability for the bicontinous gyroid ($Q_{Ia\bar{3}d}$) phase decreases monotonically beyond χN ~ 18. Initially it decreases gradually but later it becomes faster with increasing χN. The phase boundary of bincontinous phase originated at the triple point with χN = 11.14 and φ_A = 0.452 can be seen in Figure 2.7b circle 2. Increasing the product χN

from 40 to 60, the gyroid ($Q_{Ia\bar{3}d}$) phase becomes unstable and the phase boundaries of gyroid ($Q_{Ia\bar{3}d}$) disappear, see Figure 2.7a (circle 3).[20]

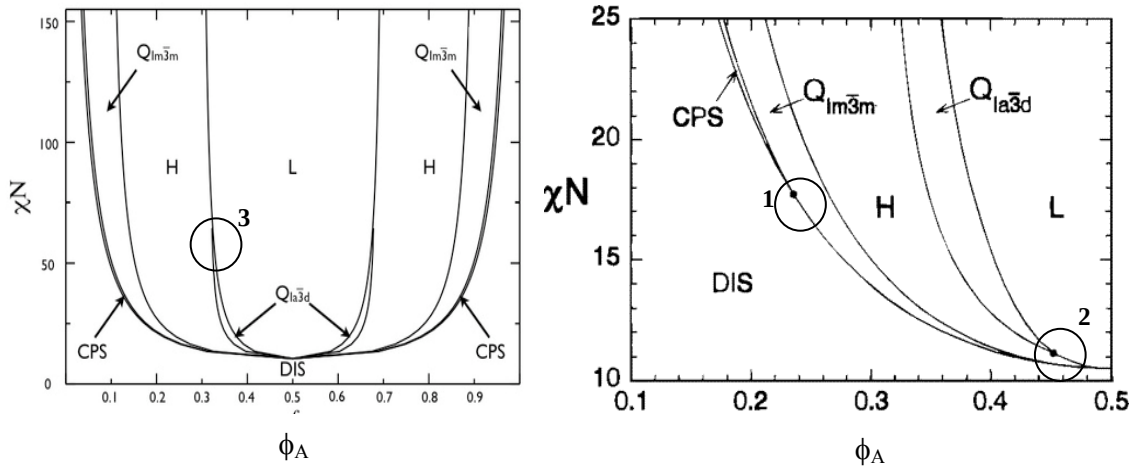

Figure 2.7: *Phase diagram for diblock copolymers in the strong segregation limit (SSL) calculated by matsen et al.*[20]
L = lamellar microphase
H = helix
CS = centered packed spheres
DIS = disordered phase
$Q_{Im\bar{3}m}$ *= body-centered cubic microphase*
$Q_{Ia\bar{3}d}$ *= gyroid*
ϕ_A *= volume fraction of the component A.*

2.3 Theoretical model of phase separation of ABC triblock terpolymers

For last three decades the concept of phase separation has been extended to ABC triblock terpolymers. In most cases the morphologies expected in ABC systems are composed of basic structural features which are already known from the diblock copolymers, such as spheres, cylinders or lamellae. Compared to AB diblock copolymers, a limited number of theoretical models have been developed to explain morphological structures in linear ABC triblock terpolymers. The free energy of various triblock's morphologies has been described in literature.[21-23] Compared to the diblocks, the triblocks display even larger variety of morphologies. Also topological variations, i.e., changing the blocks sequence can be realized. So ABC triblock terpolymers show a richer morphological behavior due to their two independent composition variables (ϕ_A, ϕ_B) and their three binary segmental interaction parameters, χ_{AB}, χ_{BC} and χ_{CA}.[21, 24] In the case of ABC triblocks where the condition $\chi_{AB} \sim \chi_{BC} > \chi_{AC}$ is fulfilled, an interface can be generated between the non-chemically linked end blocks. In such system

spheres on spheres, spheres on cylinders, rings on cylinders, and cylinders in lamellae morphology are formed.[21, 25, 26] However, when the interaction parameter of the two endblocks is significantly larger than those of the middle and end blocks, i.e., $\chi_{AC} > \chi_{AB} = \chi_{BC}$ (for fixed interaction parameters of $\chi_{AB}N = \chi_{BC}N = 13$ and $\chi_{AC}N = 35$), an ordered structure with no AC interface is observed.[26] In this system, core-shell spheres, cylinders, gyroid, lamellae, and alternating versions of the sphere, cylinder, and gyroid phases, in which the A and C domains form alternating equivalent sublattices within a B matrix are observed. Again in the systems where χ_{AC} is intermediate between the other interaction parameters, i.e., $\chi_{AB} < \chi_{AC} < \chi_{BC}$, the observed phases show alternating spheres on a BCC lattice as observed in a CsCl crystal, coreshell gyroid, core-shell cylinders, perforated-lamellar, and pillared-lamellar. [26]

Different segregation theories are published in literature for the investigation of phase behavior of triblock copolymers. Spontak et al.[27] Semenov et al.[28], Mogi et al.[29], and Stadler et al.[30, 31] followed the SSL approach. Using the SSL model only the morphology of a symmetric ABC triblock in which the center B block forms the matrix and the outer A and C blocks are embedded as cylinders or spheres can be explained.[32] This model only considers the interaction of directly linked blocks and is not able to explain all the complex microstructures formed by ABC triblock terpolymers. [22] Wang et al.[33] modified the model by introducing a relative strength of the interaction within the triblock terpolymers and derived six different classes of phase diagrams, which can predict more complex morphologies. Matsen et al. [34] used SCFT theory to compare different compositions ($\phi_A = \phi_B$) whereas Tyler et al.[26] calculated the phase behavior of ABC triblock terpolymer melts. However, SSL theory gives a good explanation for co-continuous morphologies which are mostly considered to be stable or metastable in weak or intermediate segregation regime.

Matsushita and coworkers investigated the morphology of polyisoprene-*b*-polystyene-*b*-poly (2-vinylpyridine), (ISP) where the volume fractions of end blocks are the same ($\phi_I = (\phi_{2VP})$ but the fraction of the middle block, $\phi_{S;}$ is varied from 0.3 to 0.8. From the analysis a three-phase four-layer lamellar structure for the same volume fractions of all the three blocks has been obtained. For this polymer a phase diagram in terms of volume fraction of the middle block polymer has been described, and the results are explained in terms of the theory of diblock copolymers.[35-37] The same triblock components but with a different block sequence of polystyrene-*b*-polyisoprene-*b*-poly(2-vinlypyridine), (SIP) were investigated by Gido et al.[38]. Here, a core shell cylinder morphology instead of lamellar one were found although the volume fractions of the three blocks were same ($(\phi_S \approx \phi_I \approx \phi_{2VP}$). This is due to the role of interfacial tension coefficients in the superstructure formation as described in Birshtein et al.[39]

When investigating the morphology of symmetric[21] and asymmetric[40] linear triblock terpolymers, Stadler and his co-workers[30, 41-45] obtained previously unknown morphologies for polystyrene-*b*-polybutadiene-*b*-poly (methyl methacrylate), SBM triblock terpolymers. They followed a procedure analogous to the Matsushita group where the volume fractions of the end blocks S and M are kept constant and the volume fraction of the center B block have been varied. The obtained morphologies are given in Figure 2.8. The minority component B is placed at the S/M lamellar interface by forming spherical domains. The B spheres are turned into cylinders with a certain increase of the B volume fraction. When all the three blocks have same volume ratio, a lamellae pattern is observed. For φ_B = 0.54 the S and M blocks assemble as cylinders which are embedded in the B matrix (Figure 2.8d). When the amount of middle block is greater (φ_B = 0.82), both the end blocks form a mixed phase and assemble themselves in a body centered cubic phase embedded in the B matrix.

In case of asymmetric SBM triblocks where the matrix is formed by M endblocks, spheres or cylinders of the second S end block are obtained[47] Increasing the volume fraction of the middle B block, φ_B, from 0.04 to 0.22 gradually, different fascinating morphologies were found (Figure 2.9). Stadler and coworkers also obtained the same morphological series with S as matrix and M as spheres or cylinders.[13, 31, 45]

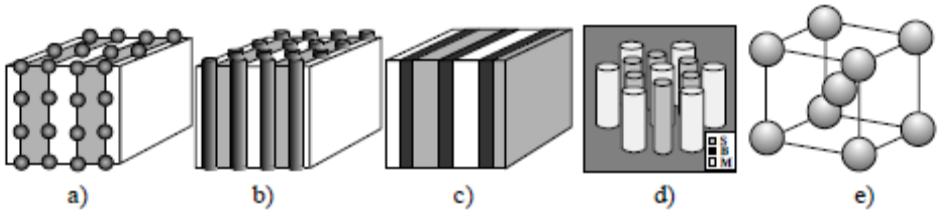

Figure 2.8: *SBM-morphologies with symmetric end blocks and from left to right with increasing the middle block. (The color code as stained with OsO4 is : S = gray, B = black, M = white)* [46]
a) ls = spheres on lamellae,
b) lc = cylinder in lamellae ,
c) ll = lamellae ,
d) cylinder in B-Matrix
e) (mixed M und S spheres) in B-Matrix. color code: B = transparent, S and M = gray)

To illustrate the theoretical model of the linear ABC triblock terpolymers, Riess et al.[48] proposed a model which describes polystyrene-*b*-polyisoprene-*b*-poly(methyl methacrylate), SIM, systems. However, most of the proposed morphologies showed a core-shell type structure. Subsequently, Semenov et al.[19] established a theory, which allowed the calculation of the free energy for spherical, cylindrical and lamellar morphologies for binary block copolymers. Stadler et al. extended Semenov's strong segregation theory to explain the morphologies of linear SBM, triblock terpolymers in terms of

the minimization of interfacial energy.[30, 31, 44, 45, 49-51] With this theory almost all complex SBM triblock morphologies can be explained (Figure 2.10).

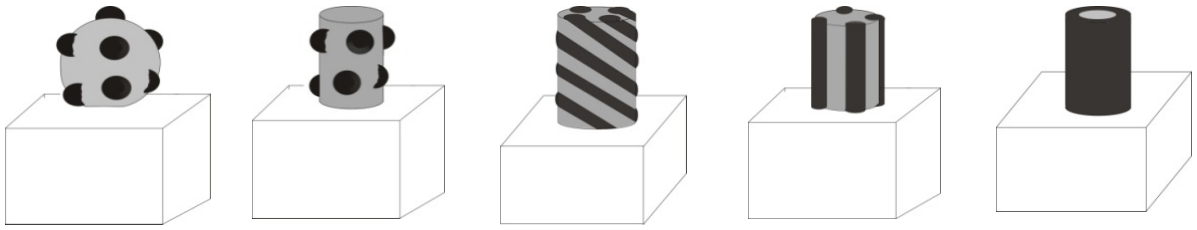

a) $S_{17}B_{07}M_{76}^{200}$ b) $S_{21}B_{05}M_{74}^{248}$ c) $S_{31}B_{16}M_{53}^{127}$ d) $S_{28}B_{14}M_{58}^{200}$ e) $S_{20}B_{25}M_{55}^{86}$

Figure 2.9: *Microphase separated morphologies of SBM triblock terpolymers. Here, the symbol* $S_xB_yM_z^n$ *indicates,* ***x****,* ***y****,* ***z*** *= weight fractions of the corresponding blocks, n = molar mass of the polymers. Color code: gray = S, black = B, white = M*

a) spheres on spheres (s_0s)
b) spheres on cylinder (s_0c)
c) helix
d) cylinder at cylinder (c_ac)
e) cylinder in cylinder (c_ic)

However from Figure 2.10, more complex ordered phases of triblock terpolymers cannot be derived. Based on Stadler's theory, Qui et al[53] employed a diagram considering generic Fourier space method. The essential idea is to expand all the spatially varying functions into a generic set of basic functions. They focused on the frustrated ABC triblock terpolymers where the interaction between the two end blocks is the smallest one, i. e., $\chi_{AC} << \chi_{AB} \approx \chi_{BC}$. From the new phase diagram a number of new phases (e.g., combination or interfaces of lamellar, gyroid, cylinder or sphere) for the triblock terpolymer systems of SBM[30], polystyrene-*b*-polyisoprene-b-poly (methyl methacrylate), SIM[54] and polystyrene-*b*-polybutadiene-*b*-ε-caprolactone[55] could be predicted. Furthermore, the capability of the method to predict the experimentally observed structures of the so-called knitting pattern of triblock terpolymers can also be demonstrated.

2.4 Thermoplastic Elastomers (TPE) of ABC type triblock terpolymers

Several commercial thermoplastic elastomers can be categorized mainly in three different classes: i) styrene block copolymers containing styrene as a hard block and isoprene or butadiene as soft block, ii) multiblock elastomers containing crystalline blocks like polyurethane, polyester, polyamide or

polyethylene, and iii) hard polymer-elastomer blends, i.e., polypropylene with ethylene propylene plastics (EPR) or ethylene-propylene-diene monomer (EPDM) blended with thermoplastic elastomers.[52, 56] In Table 2.1. the glass transition temperature (T_g) and the crystalline melt temperatures (T_m) of some of those TPEs are given.

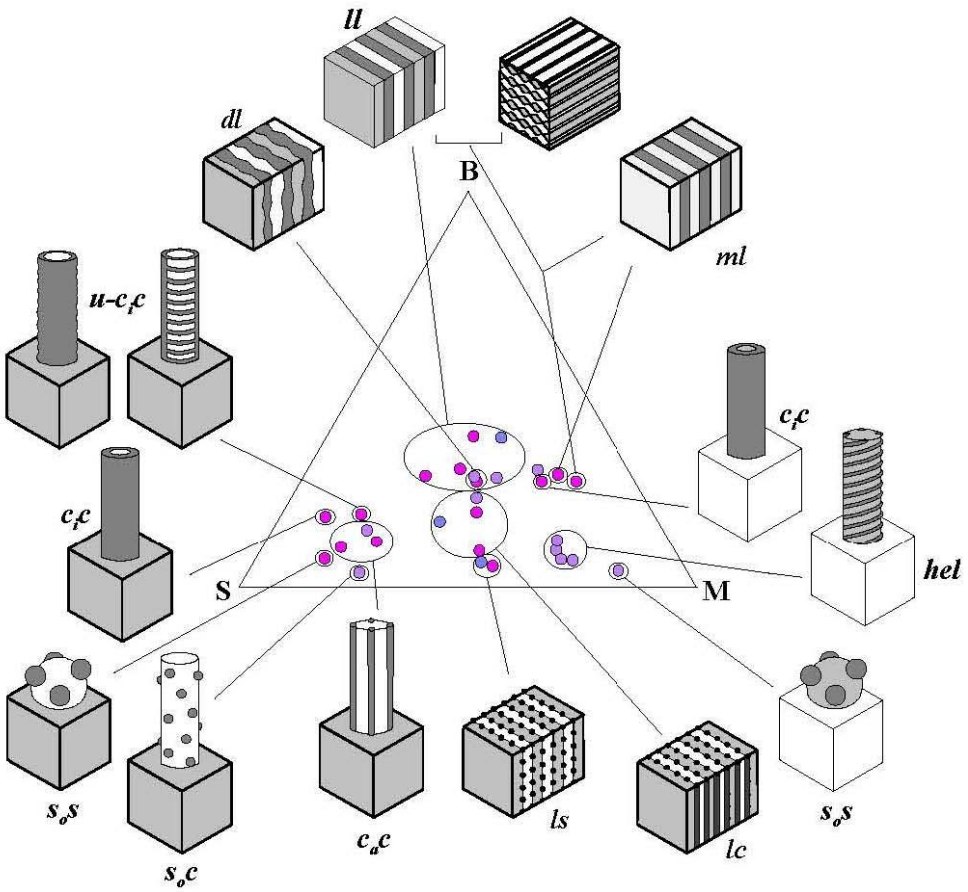

Figure 2.10: *Microphase separated morphologies for polystyrene-b-polybutadiene-b-poly(methyl methacrylate), (SBM), triblock terpolymers (the colors correspond to the OsO_4 staining in the TEM micrographs: S- gray, B-black, M-white).* [52]

The individual phases of the TPE retain their specific glass transition temperature (T_g) or crystalline melting temperature (T_m) as shown in Figure 2.11. Below the glass transition temperature of the rubbery phase, a very high modulus is obtained for both the hard and soft phases. However, when the temperature is raised to the service temperature, the elastomeric phase becomes softer and their modulus decreases. The reduction in modulus is less for the hard phases compared to the soft one. When decreasing the temperature beyond the glass transition temperature, the material turns viscous or starts to melt due to softening of the hard phase. The modulus of the hard elastomeric material starts to decrease more than the soft one and at a certain point; both the materials attain the same moduli.

Table 2.1: *Glass transitions and crystalline melt temperatures of major TPEs* [57]

Thermoplastic elastomer type	**Soft, Rubbery phase T_g (°C)**	**Hard Phase T_g or T_m (°C)**
Styrenic block copolymer		
S-B-S	-90	95 (T_g)
S-I-S	-60	95 (T_g)
S-EB-S	-55	95 (T_g) and 165 (T_m)[a]
S-B-M	-70 to -90	90- 135 (T_g)[c]
Multiblock copolymers		
Polyurethane elastomers	-40 to -62	190 (T_m)
Polyester elastomers	-40	185 to 220 (T_m)
Polyamide elasomers	-40 to -60	220 to 275 (T_m)
Hard polymer-elastomer combinations		
Polypropylene-hydrocarbon rubber[b]	-60	165 (T_m)
Polypropylene-nitrile rubber	-40	165 (T_m)
PVC-(nitrile rubber + DOP)	-30	80 (T_g) and 210 (T_m)

[a] In blends containing polypropylene, [b] EPDM, EPR, butyl rubber, and natural rubber. [c] current PhD work.

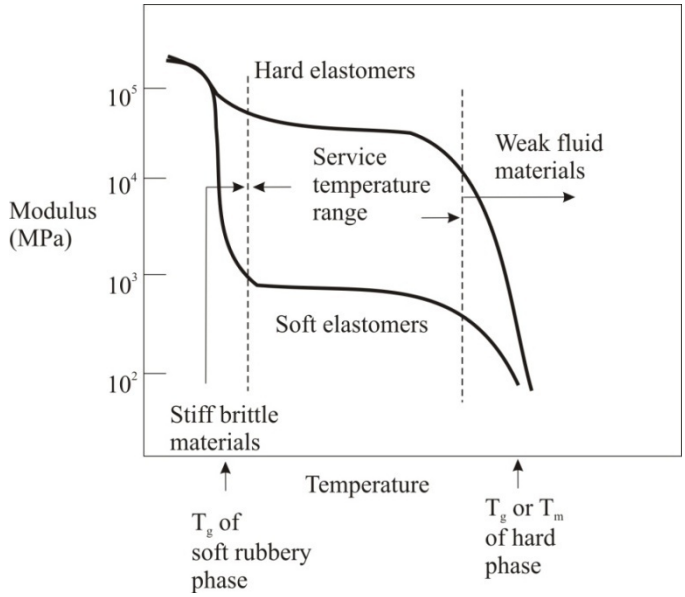

Figure 2.11: *Modulus of typical thermoplastic elastomers (TPE) in dependence on the temperature.* [57]

According to Figure 2.11 the range of the service temperature is in between the glass transition of the elastomeric phase (lower service temperature) and the glass transition or melting of the hard phase (upper service temperature). The exact values of a final product are dependent on the service conditions, for example, the amount of hardening that will be tolerated or the amount of stress applied. Thus, sometimes the actual lower service temperature will be higher than glass transition of the

elastomer and the actual upper service temperature will be lower than the glass transition or transition to melt of the hard phase.

Depending on the length of the polymer chains, the polymeric materials exhibit flexibility, mobility and deformability. In solid-like crystalline or glassy materials, the chains are linked to form a network structure that prevents flexible mobility under external pressure, as a result exhibit rigid behavior.

When ordinary solids, such as crystalline or glassy materials are subjected to external forces, the recovery of deformation between two atoms is altered only by a few angstrom (Å). Therefore, at higher deformation either flow or fracture of these materials occurs. In contrast, the response of rubber like materials is entirely intramolecular. On removal of the external forces, these rubber-like materials rapidly relax to their original dimensions, essentially with no residual or non-recoverable strain. When an external applied force is transmitted to the long chains through their network, the chains start to vibrate and each chain acts like an individual spring. In bulk or at high concentrations, polymer chains entangle themselves; (Figure 2.12). The spacing between two inter-twining points is expressed by the molecular weight between the entanglements (M_e).

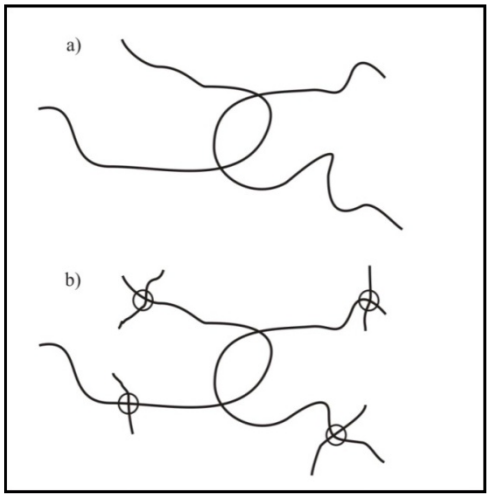

Figure 2.12: *Molecular entanglements in a high molar mass polymer. b) Entanglements are locked by cross-linking (indicated by small circles).* [57]

The representative values of the average molecular weight between the entanglements (M_e) are 7000 for polymer melts of cis-1,4-polybutadiene, 14,000 for cis-1,4-polyisoprene and as high as 35,000 for polystyrene. In a crosslinked elastomer, the entanglements are permanently locked as shown in Figure 2.12.b. In this case the elastic response of the material is obtained considering the presence of both chemical crosslinks and physically trapped entanglements.

The mechanical strength of the solid and the flow behavior of the molten state are largely controlled by the entanglements of TPE materials. For example, at room temperature the soft phase polybutadiene (B) is a viscous liquid, whereas the hard polystyrene phase of SBS is a rigid transparent solid that transforms into a viscous liquid above 100 °C. Below the T_g of the hard phase, the crosslink between S with long and flexible B chains are transformed into rubber-like soft solid, which is capable

of recovering deformations. In semicrystalline polymers, like polyethylene (PE), rigid crystalline regions exist in which the chains are periodically stacked and act as physical crosslinks between rubbery amorphous regions.

2.5 Mechanical properties and deformation behavior of thermoplastic elastomer

In the present section the theoretical principles of mechanical and deformation behavior of thermoplastic elastomers will briefly be highlighted. Figure 2.13 shows a typical stress-strain curves of polymer materials that gives a straightforward measure to characterize and compare the mechanical behavior.

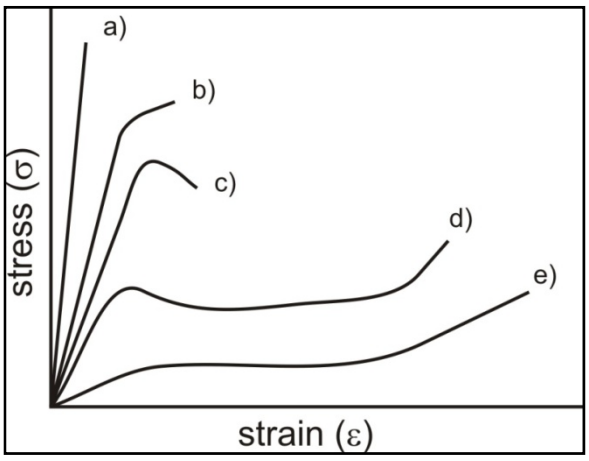

Figure 2.13: *Typical stress-strain curves for different polymers types. a) high modulus material(e. g.reinforced TPE), b) brittle material (e. g. polystyrene and poly(methyl methacrylate), c) ductile material (e. g. PVC), d) toughened thermoplastic elastomer (e.g. PE or PP), e) rubbery material.* [58]

Figure 2.13 a) represents the high modulus of a thermoplastic elastomer (e.g., reinforced thermoplastics) which shows a linear relationship of increasing stress and high tensile strength at very

low strain at break. The curve b) shows a brittle material in which the fracture occurs at low strains. This behavior can be observed in polystyrene and poly(methyl methacrylate) copolymer system.

Materials like rubber modified thermoplastics or PVC show a ductile behavior which is characterized by a yield stress followed by a yielding drop (see curve c). Again, a strain softening occurs after the yield stress in semicrystalline types of thermoplastic elastomers (e.g., PE or PP) as shown in curve d). In this case the stress remains constant up to certain elongations and afterwards for further elongations the strain hardening can be observed. Rubbery materials show stress-strain curves where the stress increases in a non-linear way without yielding during elongation.

The tensile stress at break and tensile strain at break of some commercial TPEs are highlighted in the Table 2.2.

Table 2.2: *Mechanical properties of commercially available TPEs*[59]

Material	**Tensile stress at break (MPa)**	**Tensile strain at break (%)**	**service temperature (°C)**
Styrene-butadiene rubber	15	500	high[59]
Natural rubber	30	500	high[59]
Polyethylene	10	high	-10-50[59]
SBS	25	800	-20-80[59]
Polyurethane	50	600	-20-80[59]
Kraton D 5152 (SBS or SIS)	3,9	550	room temperature[52]
Estane 58133 (polyurethane, Polyether/ester)	35	500	room temperature[52]

The deformation behavior and the resulting mechanical properties are mainly controlled by the molecular structure, the morphology, the nature of interface between the blocks, as well as the organization of the polymeric material's microscopic building blocks.[58] Figure 2.14 compares the idealized stress-strain behavior of a diblock TPE and triblock TPE. In case of an ABA type triblock copolymer (here A and B represent glassy and rubbery blocks) strain hardening is observed at higher elongation compared to an AB type thermoplastic elastomer. Again, a comparative study of the mechanical properties of ABA and ABC type triblock TPEs were reported by Brinkmann et al.[52] They correlated the mechanical properties of SBS and SBM triblock copolymers and found higher mechanical properties in SBM type triblock terpolymers. Based on their initial findings, the mechanical properties of different SBM triblock TPEs shall be compared as a function of the polybutadiene microstructure and the molar mass of the polymers' building blocks in the present work.

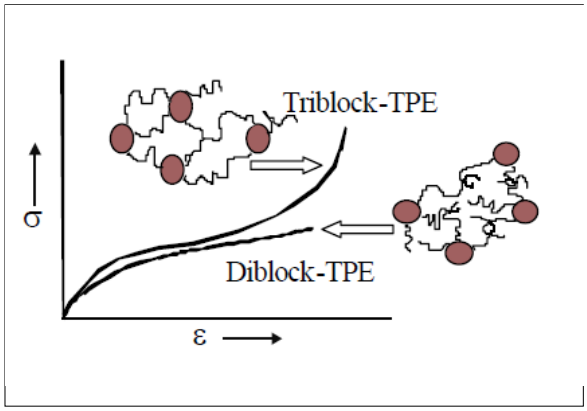

Figure 2.14: *Effect of the molecular architecture the on mechanical properties in case of TPEs composed of AB diblock and ABA triblock copolymers*[58].

2.6 Morphological deformation of block copolymers: Fundamentals of deformation mechanism

The deformation behavior of the polymers' morphology after applying mechanical stress can related to the different parameters like composition and molar mass of the polymers, phase morphology, interface, size and orientation of the different blocks etc.[60-62] If a cylindrical domains are embedded in a glassy matrix application of a tensile stress *parallel* to the oriented cylinders leads to a ductile behavior whereas a *perpendicular* application of the tensile loading results in brittleness.[63]According to Thomas et al.[64]who investigated the dependency of the deformation mechanism on the loading angle for thermoplastic elastomers composed of poly(styrene) and poly(butadiene) blocks the strain is accommodated primarily in the soft rubbery matrix with the rubbery chains orienting along the stretch axis if spherical or cylindrical S domains are present. If, however, the soft B domains are embedded as spheres or cylinders in the S matrix, fracture will mainly occur by crazing. In case of a lamellar pattern, the fracture mechanism occurs as a combination of both mechanisms crazing and shear yielding.[65]Huy et al.[60]investigated the deformation behavior of SBS triblock copolymers with respect to the orientation of the individual block domains by means of tensile tests and Fourier transform infrared (FT-IR) spectroscopy. They demonstrated that the B phase shows a stronger orientation than the S phase because of its lower E modulus.

The segregation behavior of the different domains plays an important role during the deformation process. In case of a system showing a weak segregation the orientation process is dominated by the migration of the grain boundaries, whereas for stronger segregated systems, the orientation is dominated by the rotation of the grains. For weakly segregated block copolymers, however, a

significant improvement of tensile strength and Young's modulus can be found due to the broadened interfacial width between the blocks.[66] An increasing interface width leads to a decreasing interfacial energy which causes a decreasing stress concentration at the interface. As a result a premature failure of the samples are decreased and a larger craze initiation stress is occurred at the region of the transversely oriented cylinder axes compared to the stronger segregated block copolymer systems.[67]

2.6.1 Influence of cylindrical morphology on triblock copolymer deformation

2.6.1.1 Copolymers having glassy domains in the rubbery matrix

Seguela and Prud'homme[68] have investigated the deformation behavior of SBS triblock copolymers having spherical and cylindrical S domains in the B matrix. By using SAXS, they observed the spherical S domains to orient in an ellipsoidal pattern along the stress axis. Pakula and co-workers[69] stated that the deformation of cylindrical domains of SBS TPE copolymers are controlled by the molecular orientation of the rubbery blocks at high strain. However, at low strain the deformation is governed by the initial morphology of the samples.

For example, when the stretching direction is parallel, perpendicular or 45° with respect to the cylindrical domain axis, a chevron structure of broken glassy cylinders is formed as the final morphology (Figure 2.15, 5). Its evolution begins with expanding the cylindrical domains along the stretching direction. At the yield point, the S domains are fragmented into smaller regions as indicated in Figure 2.15, 3. These fragmented domains can now orient more easily with the flexible B domains resulting in a zig-zag pattern (Figure 2.15, 5). A detailed study on the mechanical response up to moderate strains (< 120%) was performed by Odell and Keller[70] by using a combination of SAXS, TEM, and birefringence techniques. Their results show that the deformation of the morphology occurs in an affine manner at low strains. However, the behavior is highly affected whether the strain is applied perpendicular or parallel to the cylinder direction: In the first case an affine deformation can be observed for strains up to 20%. In the second case, however, the affine deformation ceases at 3% strain where the material reaches its yield point. Thus, the deformation process in a block copolymer composed of a rubbery matrix and minor glassy components completes via chain and domain orientation along the stretching direction.

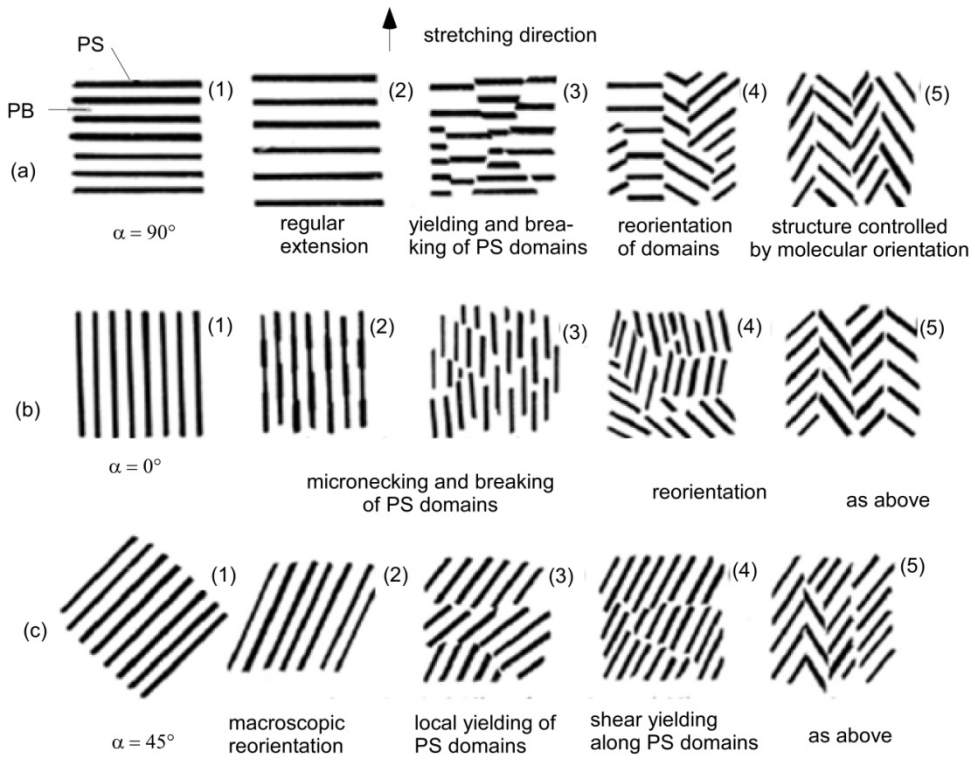

Figure 2.15: *Deformation mechanisms in cylindrical block copolymers having glassy cylinders in a rubbery matrix suggested by Pakula et al. [69]The directions of the stretching are(a) perpendicular, (b) parallel, and (c) 45° to the original orientation of the cylindrical domains.*

2.6.1.2 Copolymers having rubbery domains in the glassy matrix

Argon and co-workers[71] proposed a two-step craze growth mechanism for SB diblock copolymers having their B domains embedded in the S matrix as hexagonally packed cylinders (Figure 2.16).First the material is elastically deformed up to a critical strain then at elevated stresses cavitation can be observed within the domains, and finally a necking with a fibril formation of S matrix occurs.

2.6.2 Influence of lamellar morphology on triblock copolymer deformation

The deformation behavior of lamellar morphologies at large strains has not been studied as extensively as the deformation behavior of the cylindrical morphology. Yamaoka et al.[72]investigated the orientation behavior of the lamellar domains of SBS triblock copolymers where the oriented lamellae shows excellent Izod impact strength and large elongation. At large strains the material reaches its yield points followed by necking. A chevron-like morphology appears at 85% stretching and a random

arrangement of broken S domains is observed at 500% elongation. For deformations exceeding 500%, the destroyed and randomly dispersed S domains in the B matrix caused the observed '*diffuse scattering*' pattern. [73]

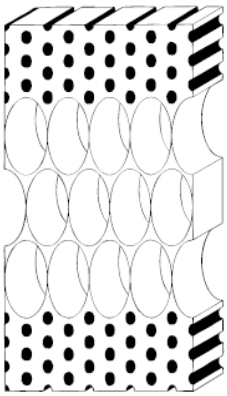

Figure 2.16: *Cavitation model proposed by Argon et al [71] where the black domains represent the B cylinders embedded in the white S matrix. The cavitation occurs in the B rods followed by the plastic deformation of the S matrix resulting in crazed structures. [67]*

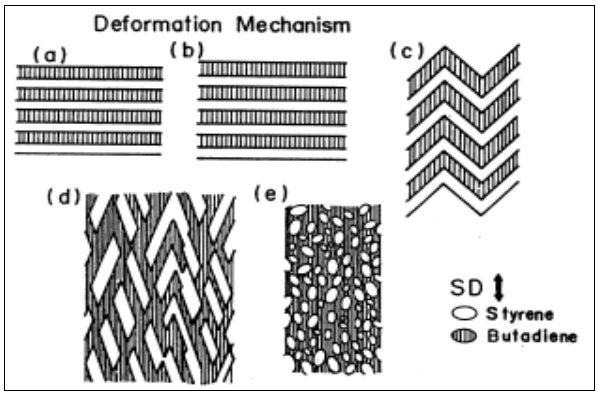

Figure 2.17: *Schematic representation of the deformation processes involved in the strain-induced plastic-to-rubber transition:a) initially, b) microdomain deformation prior to the yield point, c) necking and formation of the chevron pattern, d) breaking of the lamellar domains, and e) dispersion of the glassy domains in the rubbery matrix. [73]*

Figure 2.17 shows the morphology changes during deformation of a SBS system which involves kinking, shearing, destruction, and orientation of the lamellae domains. The change of the structure from (a) to (b) illustrates the initial stage of regular deformation of the microdomains before reaching the yield point. When the stress is applied perpendicular to the lamellae, the domains are expanded. At the yield point the necking starts and the lamellar domains collapse. With further stretching, the

remains of the lamellar domains are rearranged along the stretching direction (cf. (c) to (d)). Finally, the fragmented S domains are randomly dispersed in the rubbery matrix as shown in Figure 2.17 (e).

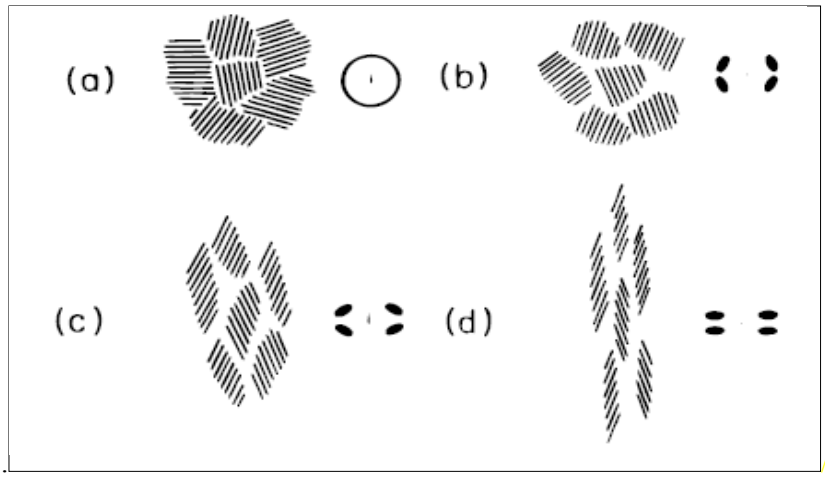

Figure 2.18: *Schematic description of the grain arrangement at different stages of neck deformation together with the corresponding first order SAXS diffraction maximum. Stretching direction is vertical. a) isotropic ring, b) formation of four points lobe, c)lateral breadths of the lobes increase, and d) further orientation leading to an approach of the lobes.* [68].

When this deformation is followed by SAXS, the scattering pattern initially exhibits isotropic rings as sketched in Figure 2.18a. At minor stretching, some of the domains are oriented in the stretching direction (Figure 2.18b). It is suggested that the necking proceeds through local extension and contraction of the rubbery phase with little ductile deformation of the glassy one[68]

At large deformations the lobes of the four-point pattern rotate at a fixed azimuthal angle. Hence, the stacking axis as well as the lamellar normal is oriented along the stretching direction (Figure 2.18c). At the end of the necking process, the elongated stacks of tilted parallel lamellae form a fiber-like chevron structure resulting in a SAXS-pattern where the four point lobes further approach (Figure 2.18d). [68]

2.6.3 Influence of lamellae/cylinder mixed domain on triblock copolymer deformation

The deformation process of triblock copolymer where lamellae and cylinders are co-exist follows the combination of the mechanisms of the pure cylinder and lamellae stress pattern. In a hexagonal

cylindrical pattern with S blocks content of 76%, the crazes propagate preferentially through the regions where the cylinder axes are transversely oriented to the direction of the external stress applied. For samples where lamellar and cylindrical structures coexist and the content of the S block is 72-74%, the crazes diverge through the grains of lamellae. However, if the lamellar domains are perpendicular to the craze direction, the crazes propagation ceases at the borderline of the lamellae stacks and the stacks are destroyed the higher strains.[67]

2.6.4 Role of entanglements on mechanical properties

Entanglements play an important role to describe the mechanical behavior of thermoplastic elastomers. Phenomena like shear deformation, crazing, macro ductility as well as brittleness of block copolymers are highly influenced by the presence of entanglements. In its glassy and rubbery state the amorphous polymer is often idealized as a network of entangled strands linked at entanglement points. The entanglement network is characterized either by the density of entanglements points, v_e, in space or by the molar mass of the entanglements, M_e. [74-76] The influence of physical entanglements on the mechanical response are more pronounced rather at lower strains than at large ones. In case of triblock copolymers the ultimate tensile strength increases if the M_e of the soft, rubbery midblock is decreased. When the entanglement density, v_e, is low, strain softening is more pronounced than strain hardening. For a successful enhancement of the mechanical properties, the molar mass of the matrix should exceed the entanglement molar mass by eight times. Only then the number of entanglements per chain is sufficient to withstand the evolution of stress under deformation.[63] In Table 2.3, the entangled molecular weights of different blocks are given.

The toughness and the brittleness of a polymer can also be described with respect to the "entanglement molar mass", M_e. Regarding the data in Table 2.3, the high values of M_e in case of S and M indicate brittleness and ductility. In case of 1,2- and 1,4-B at a molar mass ranging of 40 kg/mol the difference in M_e is negligible. However, the 1,4-B shows more flexibility due to its chemical structure, which allows the formation of an intramolecular network and shows an increasing tendency to withstand stress at high elongation.

Table 2.3: Molar mass of entanglements, M_e, of different blocks of polymers.

Polymer	**S**[77]	**B (1,2-)**[78] **(39 kg/mol)**	**B (1,4-)**[78] **(39 kg/mol)**	**M**[79] **(66 kg/mol)**	**S-M**[79] **(69 kg/mol)**
M_e (g/mol)	20000	1660*	1690*	6000	11500

**Note that the 1,4-B is 93 % and 1,2-B is 94 % for those particular polymers. Values were calculated from the literature data. (Here S = polystyrene, B = polybutadiene, M = poly (methyl methacrylate), S-M = diblock of polystyrene-poly (methyl methacrylate) at 50:50 weight percent ratio).*

The post-yield behavior plays a key role to determine whether a material in its glassy state is brittle or ductile. In principle two different responses of the material after reaching the yield point may occur: i) strain softening (i. e. a drop in true stress after yield) or ii) strain hardening (the subsequent rise in stress after softening) (cf. Figure 2.19a). The 'strain softening' that is observed in entangled systems, leads to a redistribution of stresses in larger volumes in the vicinity of propagating cracks, whereas strain hardening stabilizes this localization and transfers the strain over the whole sample.[63] However, in case of amorphous polymers the process of plastic deformation is mainly controlled by the molecular motion on a segmental scale. [77]

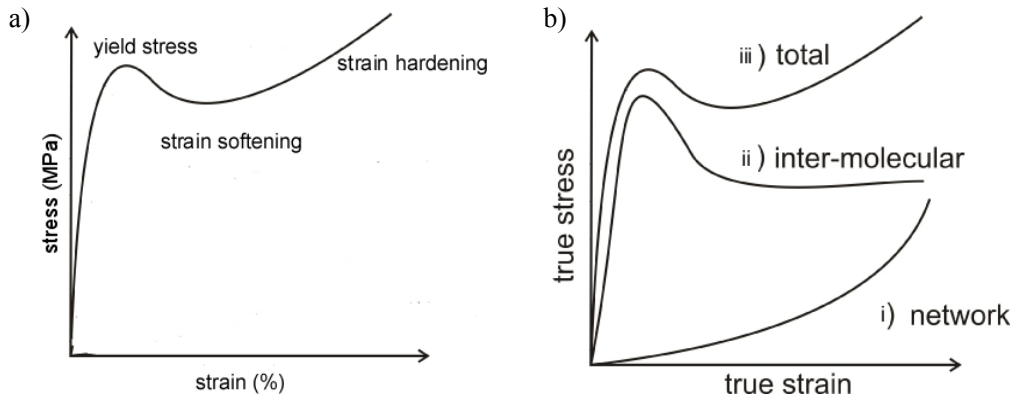

Figure 2.19: *a) strain softening and strain hardening after post-yield behavior*[63]*, b) the influence of intramolecular and intermolecular effects upon stretching during tensile tests.*[77]

In Figure 2.19b), the characteristic strain-stress curves of polymer materials made-up of intramolecular and intermolecular networks is shown. For intramolecular network the stress increases exponentially under increasing strain, as shown in curve (i). In case of intermolecular networks (ii) a linear elastic response upto the yield point is observed, which is followed by a stress drop due to the deformation of the continuous glassy domains. At higher strains, the stress remains constant mainly due to the presence of an intermolecular network of the soft domains. The combined stress-strain response under

the influence of both intramolecular and intermolecular interaction is similar to curve (iii), where the non-linear elastic regime is followed by yielding, then strain softening occurs and finally for a further increase strain hardening takes place.[77]

2.6.5 Morphological deformation of Poly (methyl methacrylate), M, containing block copolymers

Poly (methyl methacrylate), M, is ductile at temperatures well below the T_g. The ductility of M can be reduced by blending it with S, which leads to an increase of the blend's molar mass of entanglements, M_e. In case of triblock copolymers very high tensile strengths can be achieved by using a rubbery middle block with a low entanglement molar mass. Therefore, the tensile strength increases when B ($M_e \approx$ 1690 g/mol) is used as a middle block instead of poly(n-butyl acrylate, $M_e \approx$ 28000 g/mol). This variation also results in strain softening, i. e. to a redistribution of stresses at larger volume units in the vicinity of a damage zone.[75, 76]

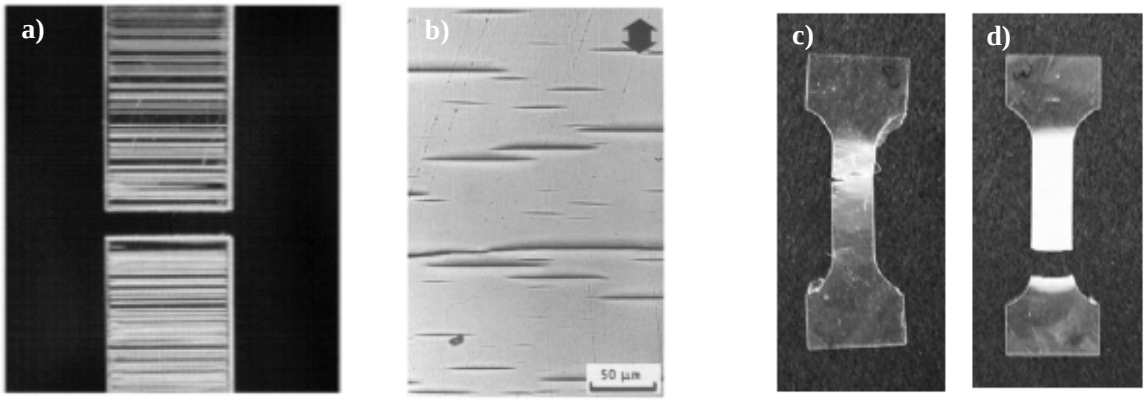

Figure 2.20: *a) S film (crazes occurs homogeneously)[77], b) Optical micrograph of M after applying 2.4% plastic strain,[80] c) Optical image of a tensile test sample of poly(methyl methacrylate) (PMMA)-b-poly(butyl acrylate) (PBA)-b-poly(ε-caprolactone) (PCL) (MBC) (MBC) triblock copolymers after deformation, pure triblock, d) 50 wt% of MBC blend with M.[63]*

Figure 2.20a) and 2.20b) illustrate the damage of S and M by crazing the damage mechanism. Stress whitening can be seen in Figure 2.20c) and 2.20d) where blends of M are fractured during stretching.

Kierkels et al[63] investigated the effect of the chain lengths of the M block on the mechanical deformation by X-ray scattering. Their results show strong craze-like scattering patterns for a copolymer consisting of random M and a few percent of methyl acrylate which is similar to the

scattering patterns of S. For very high M block lengths (500 kg/mol), no delocalization and deformation is noticed whereas for a very low M block lengths (23 kg/mol), no craze-like structures are observed. Hence, it is obvious that the craze behavior of the M domains is significantly influenced by its chain length.

2.6.6 Morphological deformation of polystyrene-*b*-polybutadiene-*b*-poly (methyl methacrylate),(SBM), triblock terpolymer

In case of polystyrene-*b*-polybutadiene-*b*-poly(methyl methacrylate), SBM, type thermoplastic elastomers a detailed discussion of the deformation mechanisms of the different blocks is hardly found in literature. Stadler and coworkers[81] have investigated the deformation mechanism of symmetric and asymmetric SBMs where mainly the failure of the M phase of lamellar triblock copoylmers during tensile test was reported. When the SBMs are symmetrical (lamellae (*ll),* lamellae cylinder *(lc)* and lamellar sphere (*ls*), the deformation mostly took place in M phase. Compared to symmetrical triblock terpolymers, the asymmetrical ones (cylinder at cylinder (c_ac), cylinder in cylinder (c_ic)) showed a plastic deformation in the S matrix. It is reported that the 1,2-B isomer mostly contributes to the craze formation and yielding while the 1,4-B one contributes to strain hardening (network forming).[82] Hence, the processes of deformation strongly depend on the morphological patterns, molar mass, type of the B microstructure as well as the stretching direction during the tensile tests.

Reference

[1] F. J. Balta´ Calleja, Z. Roslaniec, "*Block Copolymer"*, Marcel Dekker, Inc, New York, 2000.

[2] A. V. Ruzette, L. Leibler., *Nature materials.* **2005**, *4*, 19.

[3] F. S. Bates, *Science* **1991**, *251*, 898.

[4] P. J. Flory, *J. Am. Chem. Soc.* **1940**, *62*, 1561.

[5] M. L. Huggins., *J. Phys. Chem.* **1942**, *46*, 151.

[6] M. L. Huggins., *J. Am. Chem. Soc.* **1942**, *64*, 1712.

[7] H. Schmalz., "Development of Thermoplastic Elastomers with Improved Elastic Properties Based on Semicrystalline Block Copolymers", Universität Bayreuth., 2003.

[8] V. Abetz, N. Hadjichristidis, H. Iatrou, M. Pitsikalis, P. F. W. Simon, "*Block Copolymers I, Advances in Polymer Science"*, Springer-Verlag Berlin Heidelberg, 2005.

[9] A. H. E. Müller, K. Matyjaszewski, "*Controlled and Living Polymerizations"*, Wiley-VCH Verlag GmbH & Co. KGaA, 2009.

[10] L. Leibler, *Macromolecules* **1980**, *13*, 1602.

[11] I. Y. Erukhimovich., *Polym. Sci. U.S.S.R* **1982**, *24*.

[12] G. Cantea, "Shear-induced alignment in block copolymer solutions", in *im Fach Chemie der Fakultät für Biologie, Chemie und Geowissenschaften*, Universität Bayreuth, 2005.

[13] T. Breiner, "Block copolymers with functionalized poly(2-hydroxyethyl methacrylate) segments for optical data storage - Synthesis and structural characterization." in *am Fach Chemie der Fakultät für Biologie, Chemie und Geowissenschaften*, Universität Bayreuth, 2001, p. /.

[14] F. S. Bates, G. H. Fredrickson, *Annu. Rev. Phys. Chem.* **1990**, *41*, 525.

[15] G. H. Fredrickson, E. Helfand., *J. Chem. Phys* **1987**, *87*, 697.

[16] D. J. Meier., *J. Polym. Sci. Part C: Polym. Symp.* **1969**, *26PC*, 81.

[17] E. Helfand, Z. R. Wasserman, *Macromolecules* **1976**, *9*, 879.

[18] E. Helfand, *Acc. Chem. Res* **1975**, *8*, 295.

[19] A. N. Semenov, *Sov. Phys. JETP* **1985**, *61*, 733.

[20] M. W. Matsen, F. S. Bates, *Macromolecules* **1996**, *13*, 1091.

[21] R. Stadler, C. Auschra, J. Beckmann, U. Krappe, I. G. Voigt-Martin, L. Leibler., *Macromolecules* **1995**, *28*, 3080.

[22] Y. V. Lyatskaya, T. M. Birshtein., *Polymer* **1995**, *36*, 975.

[23] V. Abetz, R. Stadler, L. Leibler., *Polym. Bull.* **1996**, *37*, 135.

[24] V. Abetz, R. Stadler., *macromol. Symp.* **1997**, *113*, 19.

[25] C. Auschra, R. Stadler., *Macromolecules* **1993**, *26*, 2171.

[26] C. A. Tyler, J. Qin, F. S. Bates, D. C. Morse, *Macromolecules* **2007**, *40*, 4654.

[27] R. J. Spontak, J. M. Zielinski., *Macromolecules* **1992**, *25*, 663.

[28] A. N. Semenov., *Macromolecules* **1989**, *22*, 2849.

[29] Y. Mogi, K. Mori, H. Kotsuji, Y. Matsushita, I. Noda., *Macromolecules* **1993**, *26*, 5129.

[30] R. Stadler, C. Auschra, J. Beckmann, U. Krappe, I. G. Voigt-Martin, L. Leibler, *Macromolecules* **1995**, *28*, 3080.

[31] U. Breiner, U. Krappe, V. Abetz, R. Stadler, *Macromol. Chem. Phys.* **1997**, *198*, 1051.

[32] H. Nakazawa, T. Ohta, *Macromolecules* **1993**, *26*, 5503.

[33] W. Zheng, Z. G. Wang., *Macromolecules* **1995**, *28*, 7215.

[34] M. W. Matsen., *J. Chem. Phys.* **1998**, *108*, 785.

[35] Y. Mogi, H. Kotsuji, Y. Kaneko, K. Mori, Y. Matsushita, I. Noda, *Macromolecules* **1992**, *25*, 5412.

[36] Y. Mogi, K. Mori, Y. Matsushita, I. Noda, *Macromolecules* **1994**, *25*, 5412.

[37] Y. Matsushita, M. Tamura, I. Noda, *Macromolecules* **1994**, *27*, 3680.

[38] S. P. Gido, D. W. Schwark, E. L. Thomas, *Macromolecules* **1993**, *26*, 2636.

[39] Y. V. Lyatskaya, T. M. Birshtein, *Polymer* **1995**, *36*, 975.

[40] U. Breiner, U. Krappe, V. Abetz, R. Stadler., *Macromol. Chem. Phys.* **1997**, *198*, 1051.

[41] C. Auschra, R. Stadler, *Macromolecules* **1993**, *26*, 2171.

[42] J. Beckmann, C. Auschra, R. Stadler, *Macromol. Rapid Commun.* **1994**, *15*, 67.

[43] U. Krappe, R. Stadler, I. G. Voigt-Martin, *Macromolecules* **1995**, *28*, 4458.

[44] S. Brinkmann, R. Stadler, E. L. Thomas, *Macromolecules* **1998**, *31*, 6566.

[45] U. Breiner, U. Krappe, T. Jakob, V. Abetz, R. Stadler, *Polym. Bull.* **1998**, *40*, 219.

[46] T. Goldacker, "Überstrukturen in Mischungen aus Blockcopolymeren", in *im Fach Chemie der Fakultät für Biologie, Chemie und Geowissenschaften*, Univerrsität Bayreuth, 1999.

[47] R. Kabir, *Unpublished results* **2010**.

[48] G. Riess, M. Schlienger, S. Marti., *J. Macromol. Sci. Phys.* **1980**, *B17(2)*, 355.

[49] K. Jung, V. Abetz, R. Stadler, *Macromolecules* **1996**, *29*, 1076.

[50] V. Abetz, R. Stadler, *macromol. Symp.* **1997**, *113*, 19.

[51] U. Krappe, R. Stadler, I. Voight-Martin, *Macromolecules* **1995**, *28*, 7583.

[52] S. Brinkmann-Rengel, "Thermoplastic Elastomere auf Basis von ABA und ABC Dreiblockcopolymer", in *am Fachbereich Chemie und Pharmazie*, der Johannes Gutenberg-Universität Mainz, 1998.

[53] Z. Guo, G. Zhang, F. Qiu, H. Zhang, Y. Yang, *Physical Review Letters* **2008**, *101*, 028301.

[54] C. Koulic, R. Jerome, *Macromolecules* **2004**, *37*, 888.

[55] V. Balsamo, F. V. Glydenfeldt, R. Stadler, *Macromolecules* **1999**, *32*, 1226.

[56] H. Schmalz, "Development of Thermoplastic Elastomers with Improved Elastic Properties Based on Semicrystalline Block Copolymers", in *im Fach Chemie der Fakultät für Biologie, Chemie und Geowissenschaften*, Universität Bayreuth., 2003.

[57] J. G. Drobny, *Handbook of Thermoplastic Elastomers* **2007**, William Andrew Publishing.

[58] R. Adhikari, "Correlations Between Molecular Architecture, Morphology and Deformation Behavior of Styrene/Butadiene Block Copolymers and Blends", in *Mathematisch-Naturwissenschaftlich-Technischen Fakultät*, der Martin-Luther-Universität Halle-Wittenberg, 2001.

[59] J. E. Mark, B. Erman, R. R. Eirich, "*The Science and Technology of Rubber"*, First Edition edition, 2005.

[60] T. A. Huy, R. Adhikari, G. H. Michler, *Polymer* **2003**, *44*, 1247.

[61] R. Adhikari, T. A. Huy, S. Henning, G. H. Michler, K. Knoll, *Colloid Polym. Sci.* **2004**, *282*, 1381.

[62] Y. Cohen, R. J. Albalak, B. J. Dair, M. S. Capel, E. L. Thomas, *Macromolecules* **2000**, *33*, 6502.

[63] J. T. A. Kierkels, "Tailoring the Mechanical Properties of Amorphous Polymers", Technische Universiteit Eindhoven, 2006.

[64] C. C. Honeker, E. L. Thomas, *Chem. Mater.* **1996**, *8*, 1702.

[65] F. Ramsteiner, W. Heckmann, *Polym. Commun.* **1984**, *25*, 178.

[66] R. Weidisch, M. Ensslen, G. H. Michler, M. Arnold, H. Budde, S. Höring, H. Fischer, *Macromolecules* **2001**, *34*, 2528.

[67] R. Weidisch, M. Ensslen, G.H. Michler, H. Fischer, *Macromolecules* **1999**, *32*, 5375.

[68] R. Seguela, J. Prud'homme, *Macromolecules* **1981**, *14*, 197.

[69] T. Pakula, K. Saijo, H. Kawai, T. Hashimoto, *Macromolecules* **1985**, *18*, 1294.

[70] J. A. Odell, A. Keller, *Polym. Eng. Sci.* **1977**, *17*, 544.

[71] C. E. Schwier, RA. S. Argon, R. E. Cohen, *Polymer* **1985**, *26*, 1985.

[72] I. Yamaoka, M. Kimura, *Polymer* **1993**, *34*, 4399.

[73] M. Fujimura, T.Hashimoto, H. Kawai, *Rubber Chem Technol* **1978**, *51*, 215.

[74] C. J. G. Plummer, N. C. Mauroux, H. H. Kausch, *Polym. Eng. Sci.* **1994**, *34*, 318.

[75] C. Creton, G.Hu, F. Deplace, L. Morgret, K. R. Shull, *Macromolecules* **2009**, *42*, 7605.

[76] J. D. Tong, R. Jerome, *Polymer* **2000**, *41*, 2499.

[77] H. E. H. Meijer, L. E. Govaert, *Prog. Polym.Sci.* **2005**, *30*, 915.

[78] C. G. Robertson, C. M. Rademacher, *Macromolecules* **2004**, *37*, 10009.

[79] P. Tordjeman, J. L. Halary, L. Monnerie, A. M. Donald, *Polymer* **1995**, *36*, 1627.

[80] H. Kawabe, Y. Natsume, Y. Higo, S. Nunomura, *Journal of Material Science* **1992**, *27*, 5547.

[81] R. Weidisch, S. Goerlitz, G. H. Michler, R. Stadler, in *10th Int. Conf. Deformation, Yield and Fracture of Polymers*, Cambridge, UK, 1997.

[82] S. S. Bhagawan, D. K. Tripathy, *Materials Chemistry and Physics* **1987**, *17*, 415.

Chapter 03

Anionic Polymerization Method

3.1 Introduction

The discovery of anionic polymerization has a tremendous impact on polymer and material science. An interest in the synthesis of a polymer by anionic polymerization concept first arised when Karl Ziegler[1] attempted to synthesize dienes by sodium or lithium containing aromatic hydrocarbons as initiators. Later on in 1956, Szwarc and his coworkers[2-4] reported the successful anionic living polymerization of styrene and diene monomers by sequential monomer addition. They termed the polymerization as "living" due to the absence of spontaneous termination and chain transfer reactions. The synthesis of polymer compounds involving lithium initiator and non-polar monomers allow narrow molar mass distributions and predictable molar masss. The living nature of the propagating chain and termination in a controlled manner lead to block copolymers with different morphologies and functional groups at one or both chain ends. Stadler and coworkers.[5-7] employed this polymerization technique to synthesize ABA and ABC type triblock copolymers to investigate their complex morphologies.

3.2 Mechanism of anionic polymerization

As in all other chain polymerizations, the mechanism of anionic polymerization can also be divided into three principal steps: Initiation, propagation, and termination. An important aspect of anionic polymerization is the relationship of monomer reactivity and stability of the propagating species.[8] The mechanism of the polymerization depends strongly on the solvent polarity.

3.2.1 Initiation

For a successful initiation the reactivity of the monomer has to be matched with the appropriate initiating species to form a stabilized negative charge. When such a nucleophilic initiator attacks a monomer, a propagating species is formed. For a highly reactive propagating anion (e.g. styrene

anion), a powerful nucleophile is required as an initiator whereas for stable propagating anions (e.g. ethylene oxide anion), a weak nucleophile can be used. The polymerization of monomers with strong electron withdrawing groups like acrylonitrile, vinyl chloride, styrene and methyl methacrylate can be initiated by metal amides, alkoxides, or organometallic compounds.

Organolithium compounds are unique initiators among the organic derivatives since they generally exhibit the characteristics of covalent and ionic compounds. Thus, they are soluble not only in common polar solvents such as ethers, but also in non-polar hydrocarbon ones.[9] A general initiation of styrene is given in Equation 3.1.

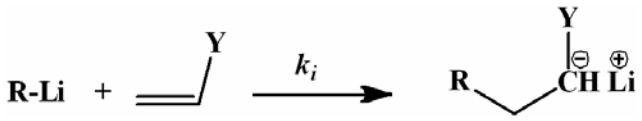

Equation 3.1

Here,

R-Li = *initiator*
k_i = *rate constant of initiation step*
Y = *electron withdrawing group*

The nucleophilic attack of the initiator on the vinyl group or any other polymerizable functional group of the monomer proceeds with a rate constant k_i. The living propagating species then attacks other monomer units present in the system.

3.2.1.1 Initiation in polar solvents

The properties of carbanions in polar solvent are mostly dependent on the intermolecular ionic interactions of the solvent, monomer, initiator and the size of metallic counterion. Depending on the carbanion stability, in polar solvents different associated states called aggregates are formed. The tight associates of carbanion with the counter cation are termed as contact ion pairs whereas loosely associated carbanions and cations lead to so-called solvent-separated ion-pairs. The solvent separated ion pairs can further dissociate into free ions especially at low concentrations. These different types of associated ions exist in equilibrium in solution (Scheme 3.1), and the equilibrium is influenced by the polarity of the solvent.

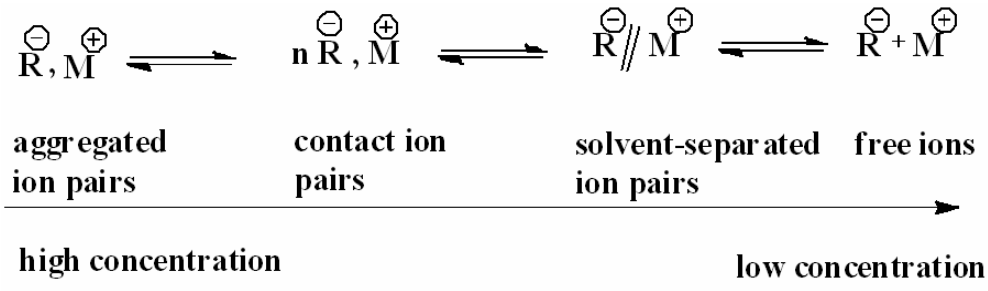

Scheme 3.1: *Ion pairs in a polar solvent for different concentration*[10]

The degree of dissociation of contact or solvent separated ion pairs into free ions (which are the propagating species) influences the overall polymerization rate tremendously. Hence the equilibrium of free anions, ion pairs, contact ions, and aggregated ion pairs plays an important role when polymerization is carried out in polar media.[10] At -108°C in THF, *t*-BuLi is present as a dimer (cf. trimers in benzene, hexane), *sec*-BuLi exists in a monomer-dimer equilibrium (trimers in cyclohexane, benzene) and *n*-BuLi is a mixture of dimers and trimers (hexamer in benzene).[11, 12] Degrees of association of ion pairs also vary on temperature. A lower degree of association is favored when temperature is decreased.

3.2.1.2 Initiation in non-polar solvents

Alkyllithium copounds generally exist in aggregated form as dimers, tetramers, and hexamers in hydrocarbon solvents. Some initiators show a concentration dependent association behavior in hydrocarbon solvents, some others show sterical hindrance depending on the side groups. An unhindered initiator like *n*-butyllithium and ethyllithium exists as hexamers in hydrocarbon solvent whereas alkyllithium compounds with substitued α- or β- carbon tend to associate into tetramers. Other factors, i.e., delocalization of the charge, decreasing the concentration, increasing the temperature, and substitution of an aromatic solvent by an aliphatic one also decreases the degree of association. Hence, the anionic polymerization of styrene and dienes using *n*-butyllithium as initiator in hydrocarbon medium is sluggish and often incomplete due to the high aggregation.

3.2.1.3 Kinetics of initiation process

The overall kinetics of the initiation process in hydrocarbon and aromatic solvents are highly dependent on the reaction conditions. As a rule of the thumb the reactivity of initiators is inversely proportional to the degree of association of the alkyllithium compound.[13]

The kinetics of *n*-butyllithium with styrene in benzene exhibits a first-order dependence on styrene concentration and assumes an aggregation of a hexameric form. This hexameric aggregates must be in an unassociated form to react with styrene monomer and this unassociated species is formed by dissociation of the BuLi hexamers (Equation 3.2). Both states are in a dynamic equilibrium[14]

$$(n\text{-}BuLi)_6 \underset{}{\overset{K_d}{\rightleftharpoons}} 6\,(n\text{-}BuLi) \qquad \text{Equation 3.2}$$

and

$$R_i = k_i K_d [BuLi]^{1/6}[M] \qquad \text{Equation 3.3}$$

K_d = *dissociation constant*
R_i = *rate of initiation where*

$$R_i = -d[I]/dt \qquad \text{Equation 3.4}$$

3.2.2 Propagation

Propagation is the continuous regeneration of reactive intermediates through a repetitive cycle of elementary steps as shown in Equation 3.5

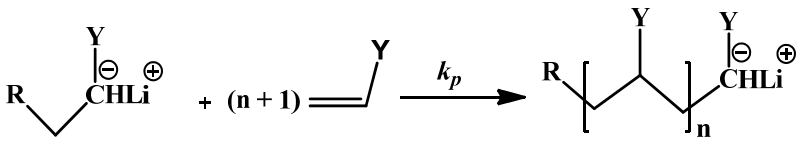

Equation 3.5

k_p = *rate constant of the propagation step*

To obtain a narrow molar mass distribution, all chains should grow to the same length. That is only possible if the rate of initiation is fast enough to propagate all chains at the same moment ($k_i >> k_p$) and in the absence of any termination (and negligible back reaction even at high conversions).

3.2.2.1 Propagation in polar solvents

The solvating ability of polar solvents like THF weakens the carbon-metal bond (C-M) and consequently the activation energy of the propagation reaction becomes lower. Szwarc[15] has noted that the loose or solvent-separated ion pairs will exist only when at least one of the ions possesses a tight solvation shell. On the contrary, if the interaction of both ions with the solvent is weak, only tight or contact ion pairs will exist. Hence, the average degree of chain association of ion pairs decreases

and the dissociation processes of aggregates increases in polar solvent. Thus, most n-alkyllithium (*n*-BuLi) compounds that are hexameric in hydrocarbon solution are associated into tetramers in polar solutions at room temperature. The reaction rate is reported 10^2-10^3 faster in polar solvents than in non-polar ones.[8]

The complexity of the propagation reaction arises from the contribution of various propagating species in the system, i.e. contact ion pairs, solvent-separated ion pairs, and free ions. These carbanionic intermediates are active as propagating centers and each carbanionic species reacts with the monomer with its own unique rate constant (k_1, k_s, k_f) as shown in Scheme 3.2 As a result, propagating chains will not grow at the same time and different propagating rates broaden the molar mass distribution.

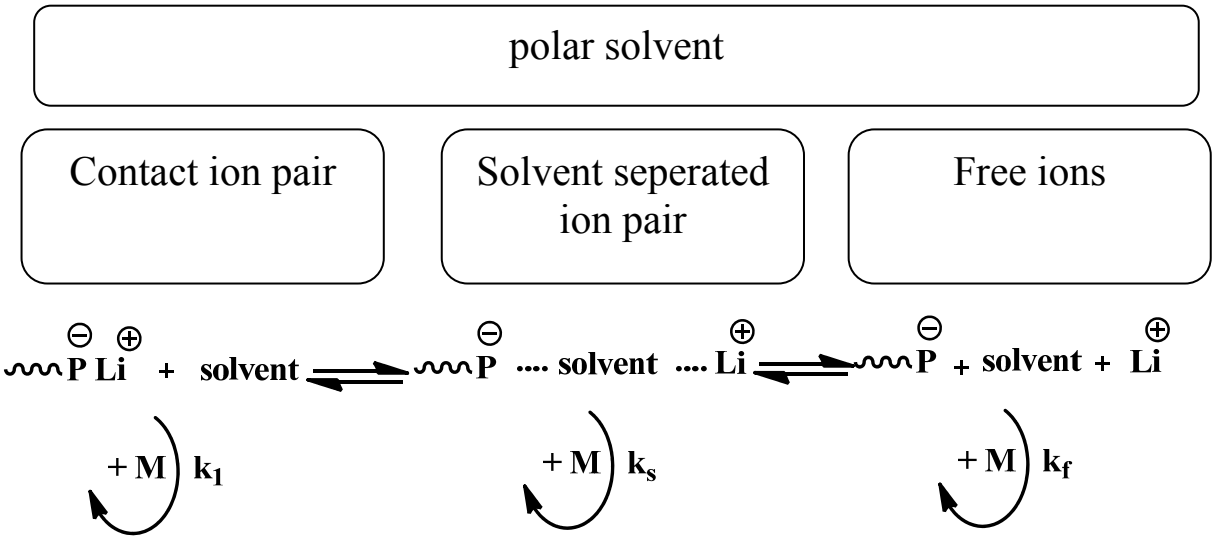

Scheme 3.2: *Different propagating species present in polar solvent.*

The propagation rate increases in presence of Lewis bases that decreases the average degree of association of polymeric organolithium aggregates decreases. When additives or impurities i.e, lithium alkoxides (e.g. *t*-BuOLi) are present, the rate of propagation may decrease. It is assumed that the alkoxides coordinate with the organolithium to form mixed aggregates which are less reactive towards monomers than the organolithium itself.[16]

3.2.2.2 Propagation in non-polar solvents

The alkyllithium compounds in hydrocarbon solvent are associated into dimers, tetramers, and hexamers. The degree of association is depending on the organic moiety, the solvent concentration, and the temperature as well. When an unhindered initiator like *n*-BuLi is used, the aggregation is

mostly into hexamers however, by increasing steric hindrance of the alkyl group like in *sec*-BuLi and *t*-BuLi, tetrameric aggregates are formed.

The apparent propagation rates are heavily influenced by the nature of the solvent employed which can be seen in Scheme 3.3. For example under equivalent conditions, the polymerization proceeds faster in benzene than in an aliphatic solvents due to the higher degree of aggregation in the latter case. For a given solvent system, the apparent propagation rates also depend on the type of the monomer reactivity ratio in the following order.

styrene > isoprene > butadiene.

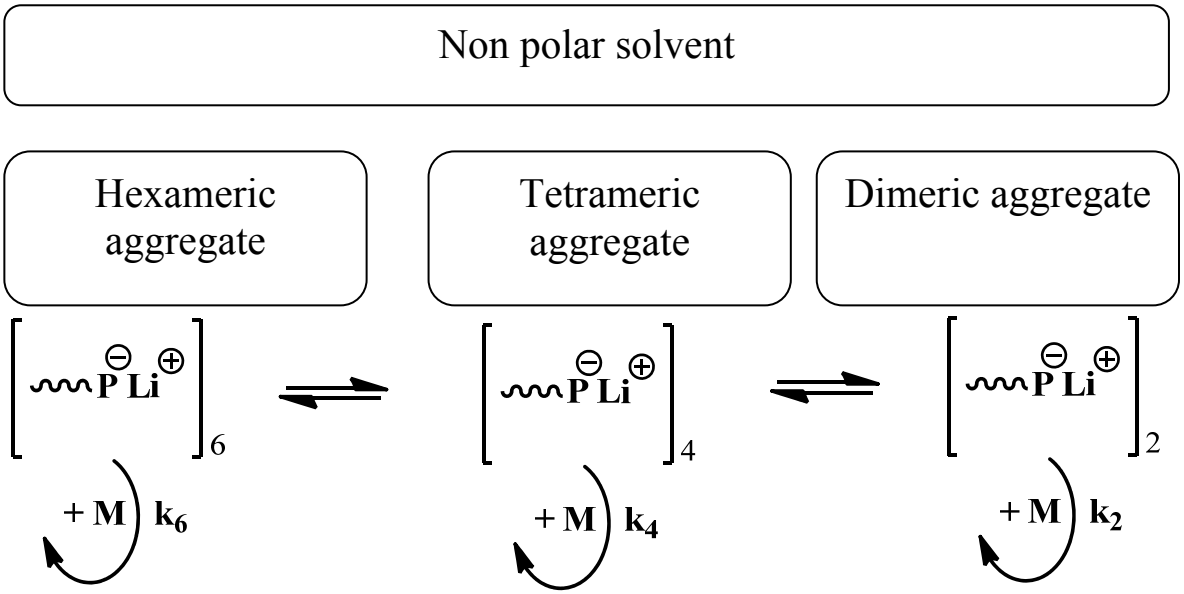

Scheme 3.3: *Different propagating species present in non-polar solvent*

3.2.3 Termination and chain transfer reaction

Termination occurs when the active species are destroyed or become inactive. Under ideal conditions anionic polymerization should be free of termination reactions. In reality, termination mainly occurs by a proton transfer agent which is either present or introduce into the system. After complete consumption of the monomer the reaction is usually terminated by adding a protic agent which reacts with the carbanionic centers of the polymer chain yielding a neutral species. However, as the concentration of the carbanion centers decay over time, a spontaneous termination also occurs.

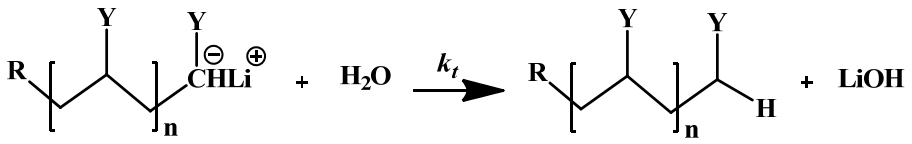

Equation 3.6

Here,

k_t = *rate constant of termination*

During termination different groups can be functionalized at the living chain end by chain transfer reaction. As an example, carboxylation of the end group occurs when CO_2 is used and an alcohol group is introduced when ethylene oxide is used during termination.

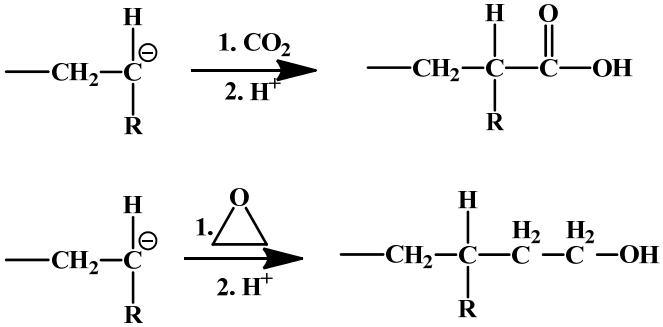

Scheme 3.4: *Chain transfer carboxylation reaction during termination*

3.3 Molar mass distribution in living polymerizations

The molar mass of a polymer is not a unique value like small molecules. Rather, a given polymer sample has a distribution of molar masses. These distributions will depend on the different polymerization techniques. To define molar mass distribution, different molar mass averages need to be considered. There are two very commonly used averages, the number average molar mass, $\bar{M}_n$ and the weight average molar mass, $\bar{M}_w$. $\bar{M}_n$ is defined as the total mass of the polymer divided by the number of molecules and is expressed by Equation 3.7. Here, N_i is the number of molecules and M_i is the molar mass of a polymer consisting of *i* repeat units

$$\bar{M}_n = \frac{\sum N_i M_i}{\sum N_i} \qquad \text{Equation 3.7}$$

The weight average molar mass corresponds to the sum over the products of total mass of each polymer species N_iM_i and its mass M_i divided by the total mass of the polymer as expressed by Equation 3.8.

$$\bar{M}_w = \frac{\sum N_i M_i^2}{\sum N_i M_i} \qquad \text{Equation 3.8}$$

The polydispersity index which also describes the distribution of a polymer is defined by the ratio of weight average molar mass and the number average molar mass.

$$\text{PDI} = \frac{\bar{M}_w}{\bar{M}_n} \qquad \text{Equation 3.9}$$

A very narrow distributed polymer can be obtained when an instant initiation takes place. Hence, all the active centers will generate at once and each of those has an identical propagation rate. According to Flory[17] and Schulz[18] a polymerization with fast initiation and absence of chain transfer and termination reactions leads to a well-defined polymer forming narrow distributed chain lengths.[8] If the conversion is high enough to polymerize each active centre at the same time and the rate of initiation is much larger than the propagation ($k_i >> k_p$), the chain lengths follow a Poisson distribution as expressed by Equation 3. 10.

$$P_w = P_n + 1 - \frac{1}{P_n}$$

i.e., $$\text{PDI} = \frac{P_w}{P_n} = 1 + \frac{1}{P_n} - \frac{1}{P_n^2} \approx 1 + \frac{1}{P_n} \qquad \text{Equation 3.10}$$

with $M_w = P_w . M$

$M_n = P_n . M$

and M = *molar mass of the repeating units.*

The ratio of $\frac{\bar{M}_w}{\bar{M}_n}$ must exceed unity, but when all the polymer chains approach a uniform chain length, the polydispersity index approaches unity. However, the polydispersity index may reach above 100 if the polymers are branched or prepared with coordination catalysts.[19]

If no termination and chain transfer occur, the concentration of the propagating chains remains constant during the course of the reaction and the number average molar mass depends linearly on the conversion. Thus, for a full conversion the number average degree of polymerization can be written as

$$M_n = \frac{[M]_0}{[I]_0} \qquad \text{Equation 3.11}$$

Here,

$[M]_0$= initial concentration of the monomer
$[I]_0$ = concentration of the initiator

More generally, at a finite conversion at any time t $M_n(t)$ is given by

$$M_n(t) = \frac{[M]_0 - [M]_t}{[I]_0}$$ Equation 3.12

3.4 Synthesis of block copolymers by anionic polymerization

The rate of anionic polymerization of styrene using alkyllithium as initiators strongly depends on the solvent. It is very fast in polar solvents like THF, comparatively slower in aromatic hydrocarbons such as benzene, and even slower in aliphatic hydrocarbons such as cyclohexane. This is due to the different states of solvation and aggregation of carbanions in these solvents.[10] Therefore, the mechanism of anionic polymerization is complex due to the contribution of the different forms of ion pairs. An important aspect in anionic polymerization is the relationship among monomer reactivity, the stability of the corresponding propagating carbanion, and the appropriate initiating species. There is a general relationship between the monomer reactivity and the stability of the anions formed by nucleophilic addition. The term 'dissociation constant', (pK_a), which measures the dissociation of a molecule into an anion and a proton, can also be used to describe the monomer reactivity. The monomers which form the least stable anions have the largest pK_a values of the corresponding conjugate acids and they are the least reactive monomers in anionic polymerization. These least reactive monomers require the use of the most reactive organometallic initiators (Table 3.1). In general, an appropriate initiator that has a similar reactivity to the propagating carbanionic species is used to form an anionic species.

Table 3.1: *Comparison of initiators and pKa values at solvent dimethylsulfoxide (DMSO) for different monomer types.*

Monomer type	***pKa* (DMSO)**	**initiators**
Styrene [20]	43	*NR_2-, RLi, RMt, Napthalene radical anions*
Butadiene [20]	44	*Same as styrene*
Methyl methacrylate [21]	30-31	*$Fluorenyl^-$, Ar_2C^-, Ketyl radical anions*

Another aspect of the block copolymer synthesis is the reactivity of the polymeric anionic initiator with a second block forming monomer. The more reactive propagating anions corresponding to a less reactive monomer (i.e., higher carbanion conjugate acid, *pKa*). These monomers can initiate the polymerization of more reactive monomers that form more stable anions (i.e., lower carbanion conjugate acid *pKa*), but not vice versa[22] During a sequential monomer addition one monomer should crossover to the chain end of a different monomer. This crossover is generally occurring to monomers that have the same or smaller conjugate acid pK_a values than the initiating carbanionic chain ends (Table 3.1).[8]

In the present work, linear triblock terpolymers consisting of polystyrene-*b*-polybutadiene-*b*-poly (methyl methacrylate) were synthesized. The synthetic strategies of the three different blocks will be discussed in the following sections to better understand the mechanism of the triblock terpolymer synthesis.

3.4.1 Styrene

3.4.1.1 Polymerization in polar solvents

Anionic polymerization of styrene is influenced by the solvent polarity, initiator type, and temperature. First polymerization of styrene was reported where the synthesis was performed at low temperature in THF using sodium napthalenide. The results show no side reactions.[3, 23] However, during the kinetic investigations in polar solvents, a high reactivity of all types of ion and ion pairs was found at ambient temperatures (cf. section 3.2.2.1). All those ions, especially the solvated ion pairs and free ions, revealed the highest reactivity with the styrene monomer. Under these conditions, the apparent rate constant of propagation is too high even for the less reactive contact ion pairs. Therefore, the difficulties arise to control the reaction. In order to avoid this phenomenon, polymerization of styrene in THF is usually performed at lower temperatures like -70 ^{0}C. Although various species of the ion pairs are present in the solution, the rate of chain propagation remains lower than the rate of dissociation. As a result, a dynamic equilibrium between solvation and association can be reached during the propagation reaction and the molar mass distribution remains narrow.

In Scheme 3.5, $K_{c,s}$ (here, $K_{c,s} << 1$) is the equilibrium constant for the interconversion of contact to solvent-separated ion pairs. Since the polarity of the solvent increases with decreasing temperature, this interconversion is exothermic. Thus, at low temperature, the more reactive solvent-separated ion pairs are favored and the overall rate constant increases until the majority of monomer additions occur via the solvent-separated ion pairs.

3.4.1.2 Polymerization in non-polar solvents

The initiation and the propagation of styrene in hydrocarbon solvent are significantly influenced by the aggregates of the alkyllithium compounds (cf. section 3.2.2.2). The reaction order with respect to the propagating anions is 0.5 in benzene, toluene, and cyclohexane which indicates a less reactive dimer of polystyryllithium anions in equilibrium with the reactive unimers.[24] Since the dissociation of lithium ion pairs into free ions is not possible in a non-polar solvent, it is assumed that the less active dimeric anions are aggregated with the coexisting tiny amounts of reactive unimer. [10].

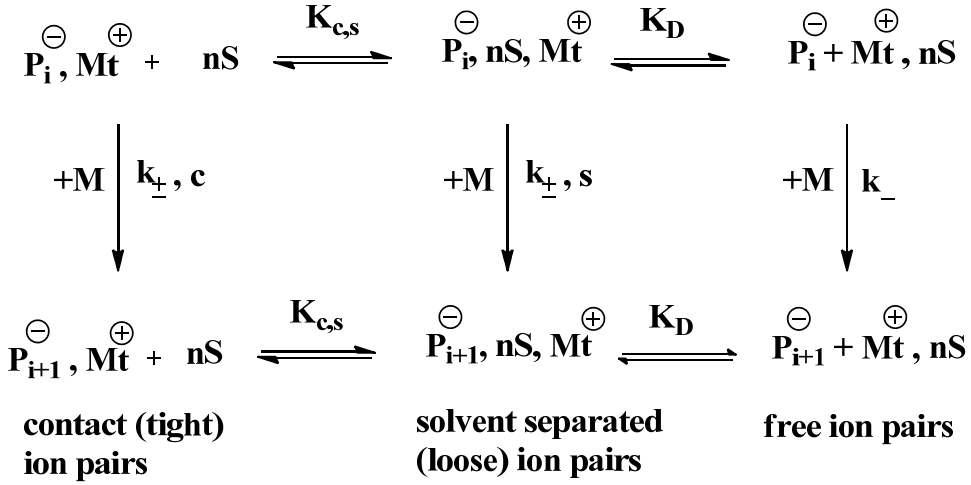

Scheme 3.5: *Three state mechanism of styrene polymerization involving contact and solvent-separated ion pairs and free anions with* $k_{\pm,c} << k_{\pm,s} < k_{-}$*.*[10]

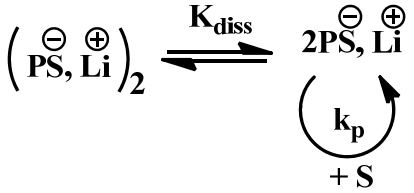

Scheme 3.6: *Dimers and unimers in the anionic polymerization of styrene in a nonpolar solvent.*

The relative reactivity of various alkyllithium compounds as initiators for the anionic polymerization of styrene in hydrocarbon solvents decreases in the following order (the degree of association is indicated in brackets):

menthyllithium (2) > sec-BuLi (4) > i-PrLi (4-6) > i-BuLi > n-BuLi (6) > t-BuLi (4)

Among the organolithium initiators, *n*-BuLi is preferred because of its high degree of association (hexameric) and its stability even at elevated temperature (> 50 ^{0}C). However, *sec*-BuLi is the second

most important organolithium initiator because of its rapid initiation reaction in styrene polymerization, its solubility in almost all solvents, and also for its commercial availability.[8]

The reaction order of styrene monomer concentration is first order in heptane, cyclohexane, benzene and toluene. The dependency of the reaction order on total chain end concentration is one-half as shown in the following equation. The poly(styryl)lithium anion is predominantly associated into dimers in hydrocarbon solvents. [14]

$$R_p = -\frac{d[S]}{dt[M]} = k_{obs}[\text{PSLi}]_0^{1/2}[S] \qquad \text{Equation 3.13}$$

Here,

R_p = *rate of polymerization*

k_{obs} = *observed rate constant of propagation*

3.4.1.3 Tacticity of polystyrene

The lithium alkyl initiated polymerization in THF results in polystyrene with an atactic microstructure due to the similar energy of the two possible carbanionic isomer chain ends during the propagation step.[25]

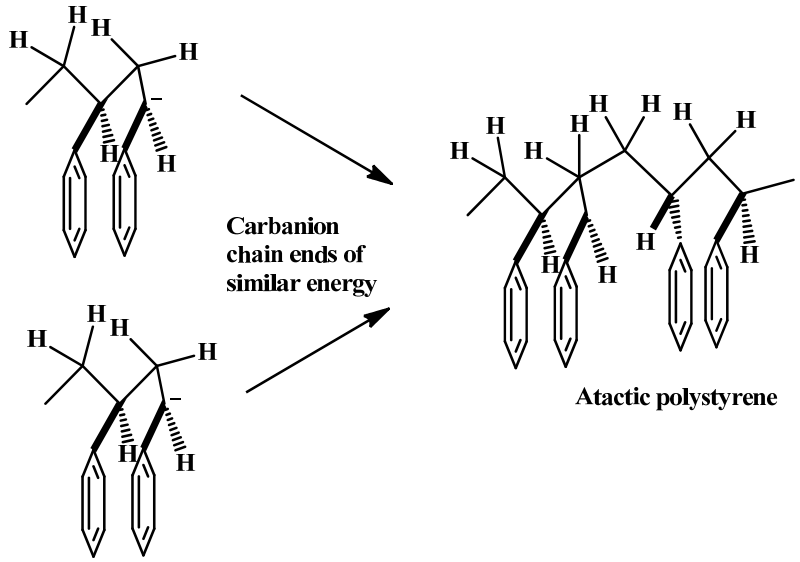

Scheme ***3.7:*** *Formation of atactic polystyrene by anionic polymerization with lithium alkyl intiator in THF.*[26]

The dependency of the polymer tacticity on the nature of the alkali metal and the associated metal alkyl is strong especially in the hydrocarbon media, i.e., methylcyclohexane as reported by Marechal et al. Around 85% of isotactic polystyrene can be obtained in a binary systems like potassium derivatives/dialkylmagnesium system.[27]

3.4.2 Butadiene

Anionic polymerization of 1,3-butadiene is significantly different from styrene due to the presence of two double bonds. Moreover, butadiene shows strong dependency on the type of solvent resulting in different regiochemistry of the polymer. The kinetic studies of the propagating species show a one-half-order dependency on the initiator concentration. However, the recent studies by Morton et al.[28] indicate a one-fourth or one-sixth-order dependency on initiator concentration when greater precautions were taken to eliminate impurities. The relative reactivities of alkyllithiums as polymerization initiators are intimately linked to their degree of association (indicated in brackets) as shown below.

menthyllithium (2) > sec-BuLi (4) > i-PrLi (4-6) > t-BuLi (4) > i-BuLi> n-BuLi (6)

3.4.2.1 Polybutadiene of 1,2- microstructure

Generally, when a polar solvent like THF is used, the microstructure of butadiene is high of a 1,2-configuration. It is reported that at low temperature and in presence of polar solvent a higher 1,2-polybutadiene content is obtained.[9, 28-31] In fact, there is a tendency towards higher 1,4-content with increasing size of the counterion in polar media. As an example, if lithium is used as counterion it undergoes specific solvation due to a short interionic distance compared to the other bulkier metal cations and highest 1,2-content is observed. On the contrary, cesium counterion leads the polybutadiene unit to highest 1,4-content. In polar media the propagating allyl organoalkali compounds show less charge on the (α)-carbon and more charge on the (γ)-carbon (cf. Scheme 3.8). When more negative charge is present on the (γ)-carbon, the highly solvated lithium cation shields the alpha position and consequently the γ-position is favored for the formation of 1,2-units.[10]

The chain end concentration also influences to obtain high content of 1,2-microstructure. For an alkyllithium-initiated anionic synthesis of polydienes, under normal polymerization conditions, only 5-10% of vinyl side chain is formed (1,2 -PB). However, 38-47% of the 1,2-microstructure can be obtained for polybutadiene at a chain end concentration of 0.5 M in cyclohexane or benzene.

3.4.2.2 Polybutadiene of 1,4- microstructure

1,4-polybutadiene microstructure is mostly obtained in non-polar solvents. When organolithium compound are used as initiator the negative charge of the lithium counterion is more localized on the (α)- carbon. Therefore, the next monomer is more likely to the (α)-carbon and a 1,4- microstructure unit is dominant in the final product. However, cis and trans isomers are coexisting in 1,4-polybutadiene.

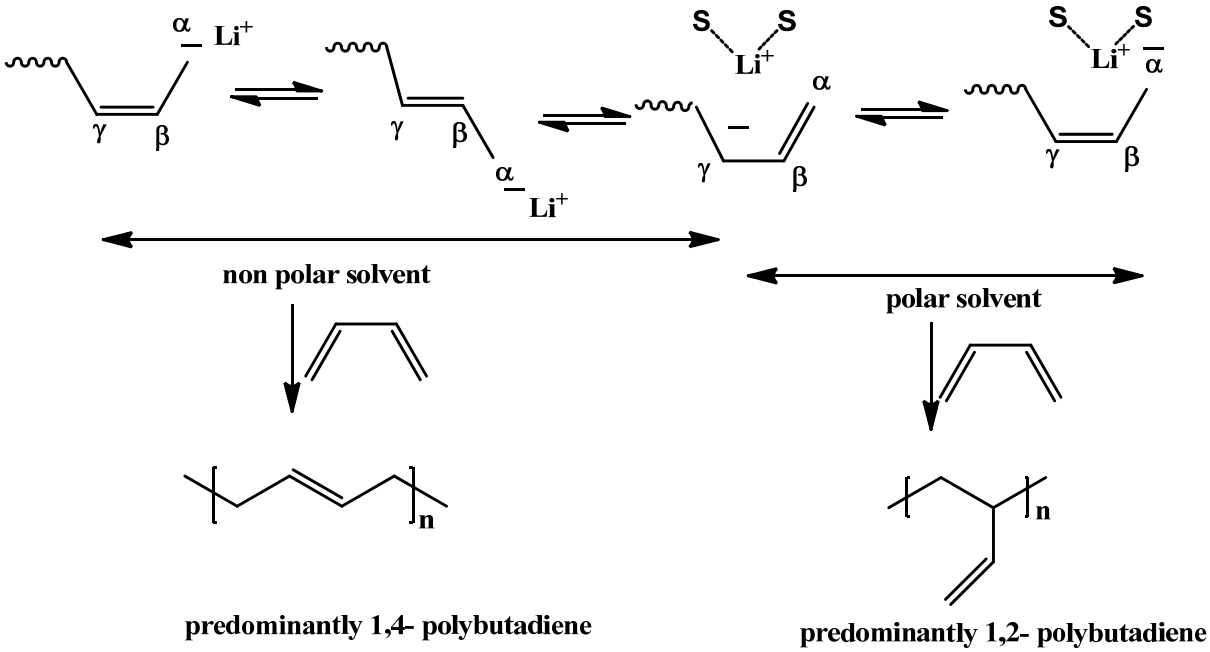

Scheme 3.8: *Polybutadiene active centers in different type of solvents and the formation of 1,2- and 1,4-polybutadiene*

3.4.2.3 Polybutadiene of cis- trans isomers

In absence of any solvent and at low concentrations of organolithium initiator (10^{-6}M), 86 % of 1,4-cis, 9 % of 1,4-trans, and 5 % of 1,2- polybutadiene are obtained.[8] Van der Arend et al.[32] has performed a controlled polymerization of polybutadiene with a high 1,4-cis content by using aliphatic solvents like cyclohexane. As the polymerization proceeds too fast at the polymerization temperature, a small amounts (0.1 to 2 wt %) of alkyl substituted benzenes (i. e. *o*-, *m*-, *p*-xylene, 1,3,5-trimethylbenzene etc.) were used to slow down the reaction. Pires et al.[33] employed a catalyst composed of neodynium versatate, trans-butyl chloride and diisobutylaluminum hydride in the synthesis. Almost 99 % cis 1,4-repeating units were obtained by this method. Gerbert et al.[34] reported that the initially formed cis isomer of the poly(dienyl)lithium chain end can isomerize to the trans isomer in competition with monomer addition. Worsfold and Bywater[35] hypothesized the mechanism

of the associated form of the poly(dienyl)lithium isomerize chain ends as shown in Scheme 3.9. After formation of *cis*-isomer the first-order conversion of the *cis*-isomer cannot compete effectively with further monomer addition ($k_{-1} << k_p^{cis}$; i.e., $k_p^{cis} >> k_p^{trans}$). But at low concentration of monomer relative to chain ends significant amounts of the *trans*-isomer will be in equilibrium with the *cis*-form. The temperature has also an influence on the regiochemistry of the butadiene polymerization. At higher temperatures the 1,4- trans form is converted to the more stable *cis*- one because of the higher rate of isomerization.

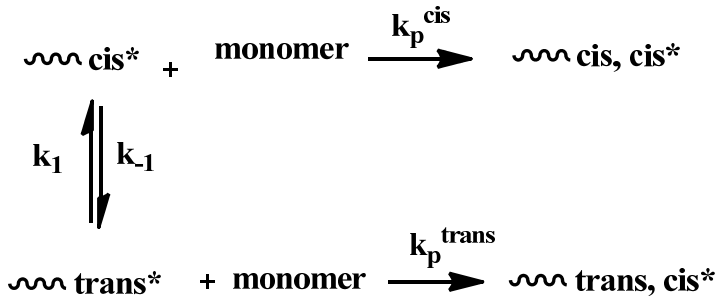

Scheme 3.9: *cis-trans isomerisation in dependency of monomer and chain end concentrations*[8]

The effects of the different types of solvents as well as the counterions on polybutadiene microstructure are outlined in Table 3.2 and Table 3.3.[8, 36-39]

Table 3.2: *Dependence of the solvent used in polymerization of butadiene on the polybutadiene microstructure.*

solvent		**temperature (°C)**	**polybutadiene microstructure (%)**		
			cis-1,4	**trans-1,4**	**1,2**
polar solvent	THF	0	6	6	88
	THF	-78	~0	8	92
	Et_2O	0	8	17	75
	Dioxan	15	-	13	87
non-polar solvent	Benzene	20	62		38
	cyclohexane	20	53		47
	hexane	20	30	60	8

Table 3.3: *Dependence of the counterion type on the polybutadiene microstructure.*

counterion	temperature (°C)	Polybutadiene microstructure (%)		
		cis-1,4	trans-1,4	1,2
Li	70	35	52	13
Na	20	10	25	65
K	50	15	40	45
Rb	60	7	31	62
Cs	60	6	35	59

3.4.2.4 Practical consequences of polybutadiene synthesis in polar and non-polar solvent

3.4.2.4.1 Polymerization of butadiene in polar solvent

The slow propagation rate and low stability of living polybutadiene chain end of polybutadiene propagation in THF causes longer reaction times that favour termination. To avoid that side reaction, polymerization of butadiene was investigated between -40 °C and -75 °C, however, at those temperatures it was found to be free of termination. Sigwalt et al.[40] proved that temperatures below -40 °C are necessary to obtain block copolymers of PS-*b*-PB without termination. Halasa et al.[41] has reported almost 100% of 1,2-polybutadiene at -5 °C to +20 °C can be achieved when the polymerization is performed in the presence of butyllithium initiators modified by *bis*-piperidino ethane. Furthermore, the presence of inorganic salts like lithium tetraphenylborate or LiCl also enhances the stability of the polybutadienyl carbanion.[42-44] A very efficient method to synthesis stabilizing alkoxide compounds was introduced by Auschra et al.[45]. They proposed adding *n*- or *sec*-BuLi in THF at room temperature to pretreat the solvent (Scheme 3.10). After 12 h the reaction of the alkyllithium compounds is completed as the resulting mixture shows no capability of initiating any polymerization of vinyl monomers. Furthermore, the impurities present in the reaction mixture are also eliminated by this procedure. Due to the stabilizing effects of the additive formed on the polyisobutadienyl anion, it is possible to polymerize at higher temperatures (between -5 °C to -15 °C) without any termination.

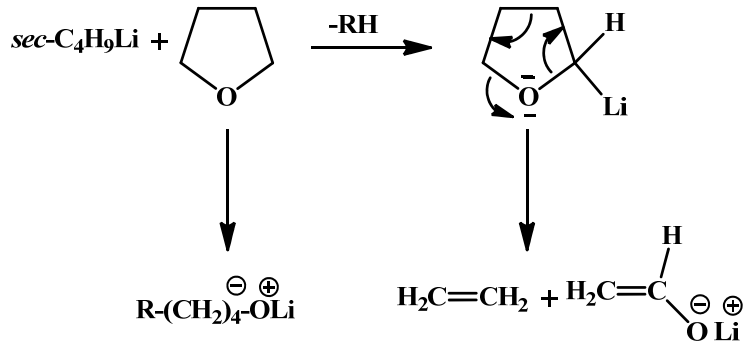

***Scheme 3.10**: Alkoxide formation in situ according to Auschra et al.[45]*

3.4.2.4.2 Polymerization of butadiene in non-polar solvent

The anionic polymerization of dienes proceeds via active dienyl lithium species which associated into dimers, tetramers and sometimes more higher aggregates in hydrocarbon solvents. Kinetic measurements indicated that the propagation for butadiene is of fractional order in the range of 0.16–0.25 with respect to the active chain-end concentration indicating hexameric or tetrameric aggregates. The association into aggregation has been reported different by different researchers though same characterization methods were used.[8, 10]

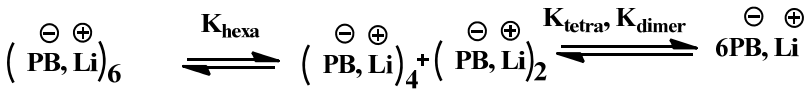

Equation 3.14

To circumvent the aggregation of the chain ends, the polymerization of butadiene is performed at or above room temperature depending on the type of the non-polar solvent. In most cases, 30 °C to 40 °C were used in case of toluene or benzene when alkyllithium species are used as initiators.

3.4.2.4.3 Results of ^{1}H- NMR

Typical ^{1}H - NMR spectra of polybutadiene exhibiting different microstructures are shown in Figure 3.1 where the 1,2-B is predominant in polar solvent and the 1,4-B microstructures are obtained in non-polar solvent. The details of the ^{1}H-NMR analysis will be discussed in section 4.1 of Chapter 4.

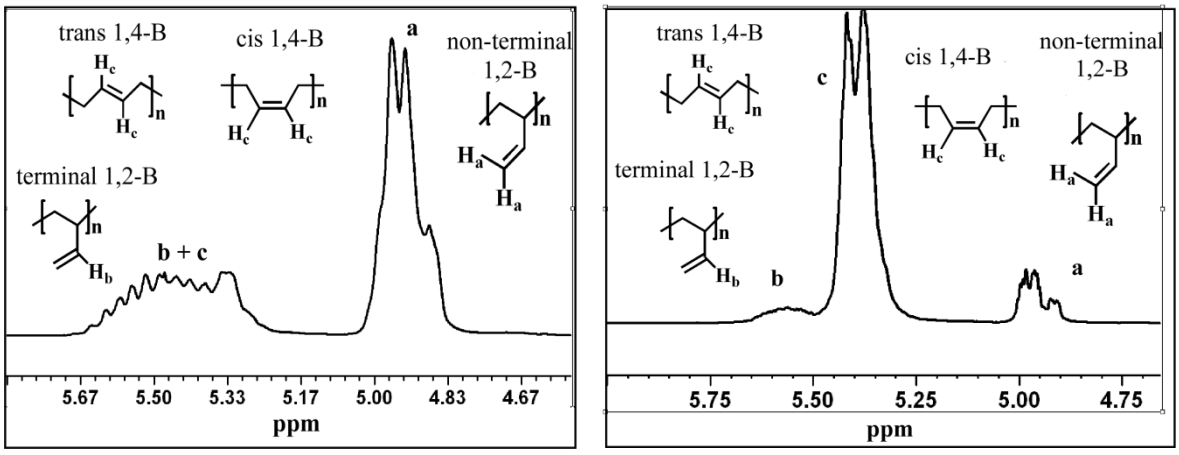

Figure 3.1: *^{1}H- NMR of polybutadiene; Left: in polar solvent (THF), (high 1,2-PB content). Right: in non-polar solvent (toluene) (high in 1,4-PB content).*

The ratio of 1,2- and 1,4- polybutadiene is calculated from ^{1}H-NMR spectra.

$$\frac{1,2}{1,4} = \frac{I(H_a)}{I(H_b,H_c) - 0.5I(H_a)} \qquad \text{Equation 3.15}$$

Here,

H_a = hydrogen atom of the β - carbon of 1,2- polybutadiene (5.10 to 487 ppm)
H_b = hydrogen atom of the α - carbon of 1,2- polybutadiene (5.70-5.50 ppm)
H_c = hydrogen atoms of the cis-trans polybutadiene of 1,4- polybutadiene (5.51-5.2 ppm)
I = integral of specified hydrogen atoms in ^{1}H-NMR

3.4.2.5 Tacticity of polybutadiene

It is possible to control the tacticity (e.g., rr, mr and mm triads) of polybutadiene by using various catalyst system including cobalt catalysts.[46] There are three types of polybutadiene isomers e.g., syndiotactic, isotactic, and atactic can exist in 1,2-polybutadiene.[47] The properties of the polymers are highly influenced by these configurations of polybutadines. In case of 1,2-isotactic and 1,2-syndiotactic isomers the polybutadiene shows rigid and crystalline behavior with poor solubility whereas for atactic isomer the polybutadiene shows softness and poor recovery character.[48]

3.4.3 Methyl methacrylate

3.4.3.1 Polymerization of MMA in polar solvents

Methyl methacrylate (MMA) can be polymerized in a controlled manner in polar solvents such as THF and DME if intramolecular solvation of the counterion is absent and the backbiting reaction (cleavage of the ester bond in the side group) is suppressed as discussed in previous research works.[49-51] It can be polymerized anionically in different solvents with a variety of initiators.[52] The optimum conditions can be summarized as : polar solvents (DME >THF >> THP), low temperatures, $T = -75^0$C for THF and large counterions, ($Cs^+ > K^+ > Na^+ > Li^+$).[53]

In Scheme 3.11, the equilibrium of associated and non-associated ion pairs is sketched (constants: K_D and K_A) with their corresponding propagation rate constants (k_a, $k_\pm$). It is found that the equilibrium is shifted in the direction of the associated ion pairs (i.e. $K_A >> K_D$) and the aggregation of the chain ends is preferred. As the propagation rate constant of associated ion pairs, k_a, is much smaller than that of the non-associated ion pairs, $k_\pm$, the coexistence of the two propagating species will result in a broad molar mass distribution.

To circumvent the aggregation of the carbanion chain ends the polymerization is usually performed at lower temperatures.[53] Compared to a polystyrene or polybutadiene polymerization which propagates by a purely carbanion active chain end in polar solvents, the living methyl methcrylate anion uses its carboxyl group to delocalize its negative charge. Consequently, the initiation of MMA by organolithium initiators is troublesome because they may attack MMA in different ways (Scheme 3.12). Firstly, the initiator could attack the vinyl carbon of methyl methacrylate and form a carbanion that can propagate the reaction. Secondly, the alkyl group can be attacked resulting in the evolution of butane. Finally, the carbonyl group could be approached by the initiator; this is especially damaging as a lithium alkoxide is produced that interferes with the propagation reaction.

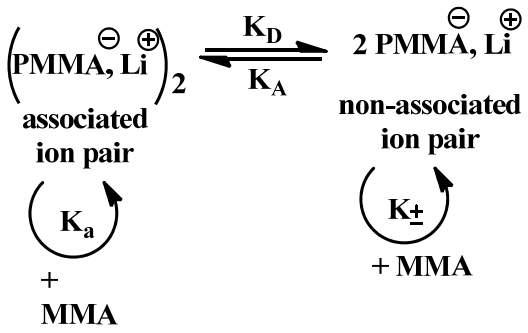

Scheme 3.11: *Equilibrium between associated and non-associated ion pairs.*[10]

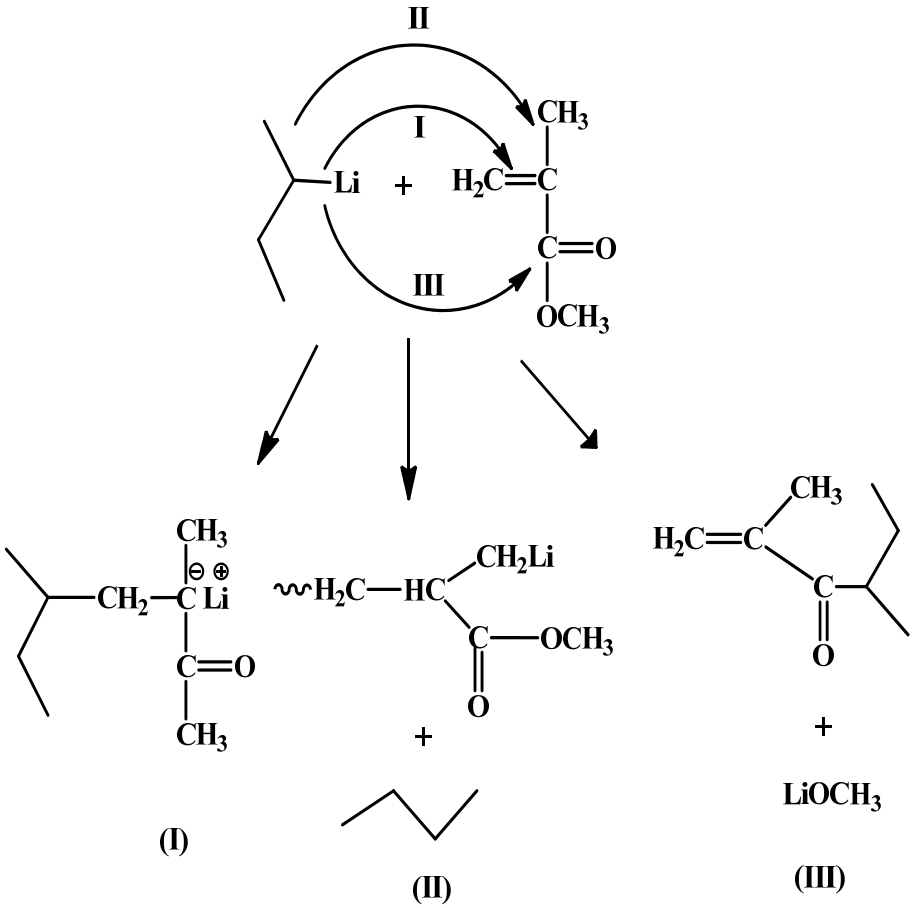

Scheme 3.12: *Different possibilities of reactions during initiation*[54]

To avoid the reactions II and III, initiators with lower reactivity need for the polymerization of MMA. Their reactivity can be lowered for example, by a higher delocalization of the negative charge or by increasing the sterical hindrance. An initiator, which fulfils both the requirements is 1,1-diphenyl-3-methyl pentyl lithium. This can be produced in situ by direct reaction of *sec*-BuLi on 1,1-diphenylethylene in THF (Scheme 3.13).

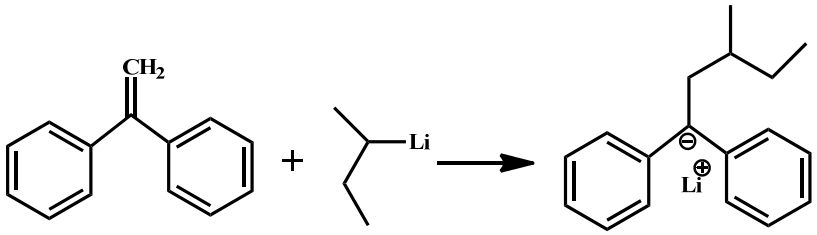

Scheme 3.13: *Synthesis of the initiator 1,1- diphenyl-3-methylpentyl lithium*

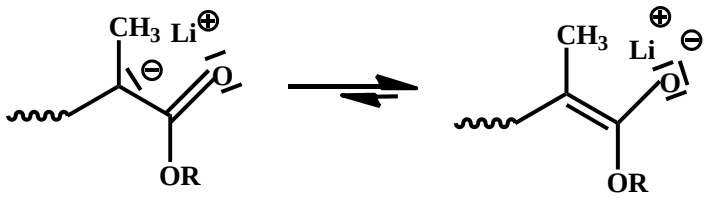

Scheme 3.14: *Formation of esternolate structure during MMA polymerization*

The stabilized esterenolate species formed in case of butyllithium initiator is an in equilibrium with the carbanion species (Scheme 3.14). It is most abundant (almost 80%) because the negative charge prefers to reside on the most electronegative oxygen atom.[55] The solvation energy of the enolate structure does not allow a cleavage of the lithium-oxygen bond and must therefore be considered as an dormant species. Hence, no further reactions can take place and the propagation fails. [56]

Furthermore, the esterenolate has the tendency to form aggregated species resulting in problems to control the polymerization. It has been observed that the slow exchange of aggregated and non-aggregated ion pairs leads to an increase in polydispersity.[57] Consequently, to achieve polymers of a narrow polydispersity, side reactions have to be avoided and aggregation has to be suppressed. It is evident from recent publications that the termination reaction mainly occurs during the propagation step by the attack of propagating enolate anion into the antepenultimate ester carbonyl group. Hence, a cyclic β-ketoester which can be identified by IR spectroscopy at a distinct band at 1712 cm^{-1} as well as in the UV at λ = 300 nm.[10, 49, 50]

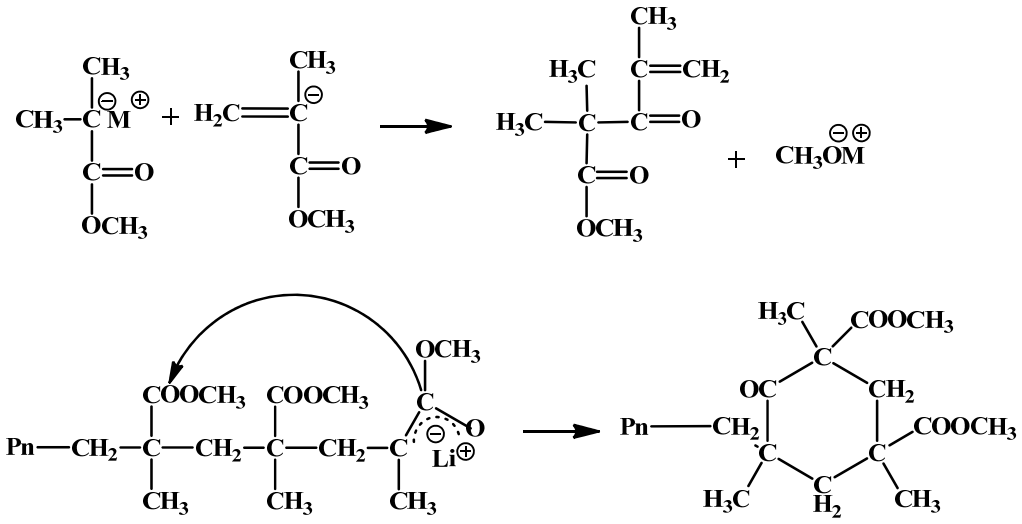

Scheme 3.15 : *Cyclization with penultimate ester groups (backbiting reaction)* [52]

3.4.3.2 Polymerization of MMA in non-polar solvents

The anionic polymerization of MMA in toluene is complicated because of slow equilibrium between the multiple aggregates of ion pairs which leads to a very broad molar mass distribution. As lithium ions at living chain ends coordinate to the in-chain ester carbonyl group, a coordinative polymer network is formed. This network forms a physical gel at higher conversion (Scheme 3.16). Hence, the approach of monomer units to the methacrylate anions is hindered and an additional broadening of the molar mass distribution is resulted.

Müller and his coworkers[58] have investigated the kinetics of the gel formation of a coordinative polymer network of ester enolate groups during the polymerization in the presence of the $AlEt_3$ at -65 °C. They observed that the concentration of enolate chain ends is much higher in the gel-phase compared to the sol-phase and the association equilibrium is shifted towards the aggregated chain ends as shown in Scheme 3.17. In species (**1**), the aluminium alkyl coordinates to the oxygen atom of the ester alcohol. Hence, a dimeric associated lithium esterenolate is formed which is the dormant species. But the propagating species are mostly occurred through the unimeric lithiated esterenolate-aluminum alkylate complex (**2**).[58] Hence, in the following case, the sol-gel equilibrium will shift to the gel side with increasing conversion.

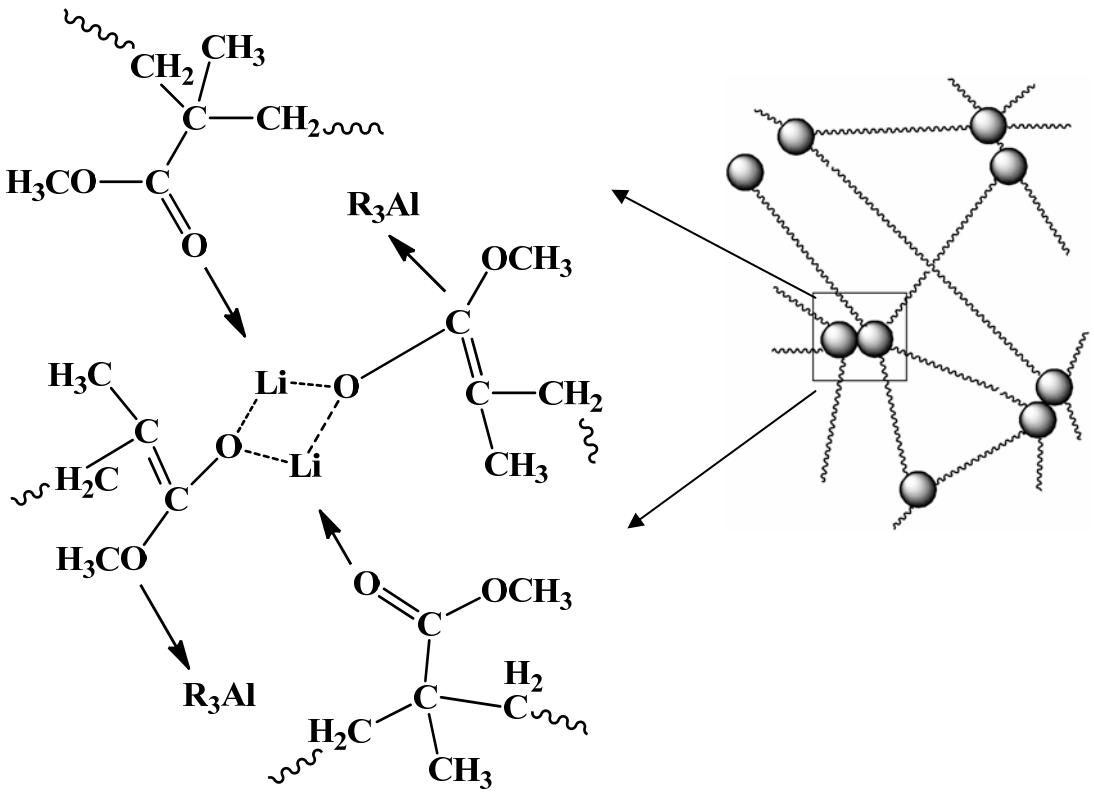

Scheme 3.16: *Structure of the coordinative network of living PMMA chains in non-polar solvents.*

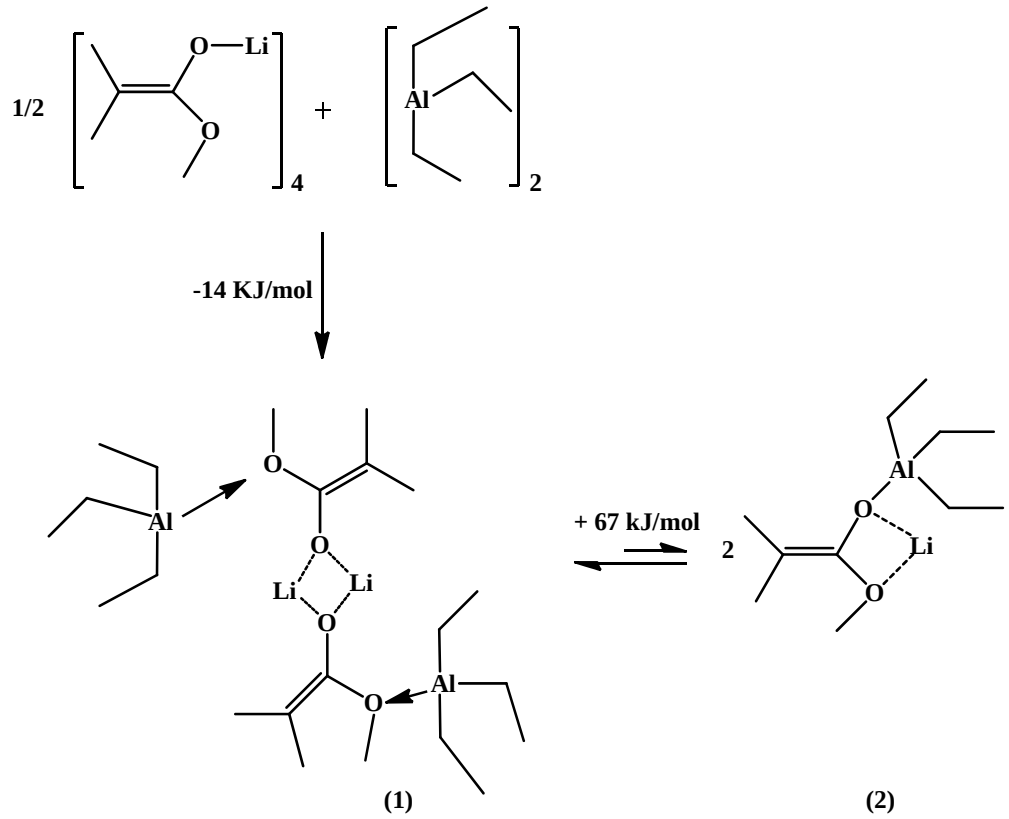

Scheme 3.17: *Interaction of ester enolates with aluminum alkyls*[58]

To overcome the aggregation of the polymer network, Hamada and coworkers[59] employed various aluminium alkyls, $AlEt_3$, additives and *tert*-butyllithium as initiator in the polymerization of MMA in toluene at -78 °C. Ballard and his coworkers[55] shielded the ester oxygen in the dimer of the lithium enolate by coordination with the aluminium central atom. Among various method to circumvent the network formation two strategies were followed in present work.

3.4.3.2.1 Using Additives

Schlaad and Müller[58] used several additives e.g. esters, ethers as well as Lewis bases to suppress the network formation by blocking the free coordination sites of the lithium ion during the polymerization. It was found that a high concentration of Lewis base is required to suppress the formation of the network. Schulz et al. [52] employed an external solvation of the metal ion by a polar medium at low temperatures to control the aggregation of the ion pair and to minimize the side reactions. They observed the existence of equilibrium between different types of contact ion pairs as shown in Scheme 3.18. By using the polar co-solvent 1,2-dimethoxyethane, (DME), and benzyl-oligo-α-methylstyrylsodium as initiator, MMA polymerization was performed without any termination even at 0 °C. In solvents like DME, the equilibrium between the intramolecularly solvated species (A) and (B)

shifts towards the solvated ion pair (C). The use of DME as a co-solvent increases the external solvation of the ion pairs presumably due to its higher polarity. For the Li^+ counterion in DME, the rate is lower compared to THF and the coordinating efficiency with both the anion and DME is higher. As a result, the incoming monomer could not displace DME from the complex (C) and the intramolecular solvation (A and B) which could lead to a termination of the propagating species by backbiting reaction is no longer possible.[50]

However, narrow polydispersity polymer can only be obtained in non-polar solvents at temperatures in the range of -40 °C to -100 °C. But at this temperature the polymerization is extremely slow and only low molar mass polymer can obtain. Hence, these conditions are not appropriate in an industrial scale. Also termination occurs at higher temperatures where the carbanion reacts with the penultimate ester groups (Scheme 3.14).[55]

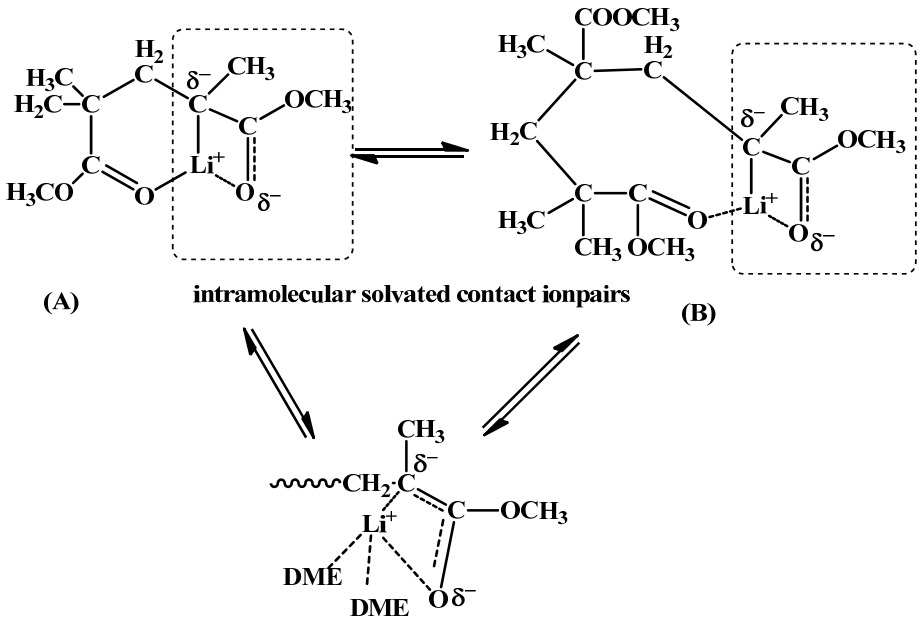

Scheme 3.18: *Propagation via contact ion pairs in MMA polymerization.*

3.4.3.2.2 Using Al catalysts

Various research groups have attempted to overcome side reactions and to influence the equilibrium dynamics of aggregated ion pairs by using sterically hindered alkyl metal initiators in combination with ligands. Kitayama's group[60-62] modified the triethlyaluminum system introducing the bulky diphenoxyalkylalumium ligand and obtained very good control of the stereoregularity. Hamada et

al.[59] and Schlaad et.al.[58, 63] have introduced organoaluminium complexes as catalysts which are used with lithium counterion and with a base to perform anionic polymerization of MMA. The base increases the rate and improves the uniformity of the polymerization. On the other hand, the organoalumium catalyst coordinates to the growing chain end. Thus, the chain end can be stabilized and its nucleophilicity can be lowered. As a result, the control over the polymerization is retained. Consequently, suitable lewis bases (e.g. methyl pivalate) prevent the network formation up to high monomer conversions and at its high concentration a linear time conversion plots as well as narrow molar mass distributions could be obtained.[58]

Ballard et. al.[55] have introduced another Al catalyst, di[2,6-di(*tert*-butyl)-4-methyl phenoxy]isopropyl aluminium, *i*BAl(BHT)$_2$, (Figure 3.2) with more bulky side groups that cause sterical hindrance and suppress the formation of an enolate structure. Furthermore, polymerization can be carried out in a temperature range of 0 to 40 °C leading to highly syndiotactic PMMA. A detailed synthesis procedure of *i*BAl(BHT)$_2$ will be discussed in Chapter 05.

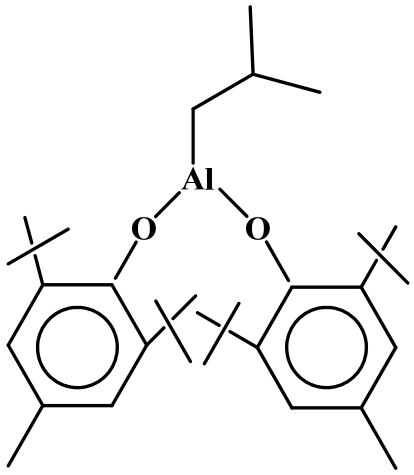

Figure 3.2: *Chemical formula of* ***i****BAl(BHT)$_2$*

This catalyst can only be used in non-polar solvents. When the organoaluminium/lithium system is used in polar solvents such as tetrahydrofurane or dioxane, a strong coordination with the catalyst was observed. As a result the compound total disrupts into lithium and aluminum alkyls and coordinates separately to the cyclic ether. When the Al catalyst is used in hydrocarbon solvents such as benzene, toluene or cyclohexane, a complex is formed that removes the Li counterion from the enolate structure. This enolate structure enables other monomers to attack the chain end. Molecular dimensions measured by wide angle X-ray scattering show that no direct bond between Li and Al is present in this system.[55, 64]

Generally certain additives need to be present when an Al catalyst system is employed. Hence, the rate of the polymerization increases and the resulting molar mass distribution remains narrow. This additive could be an ester compound such as methyl pivalate, diisooctyl phthalate, or a crown ether such as 12-crown-4. Among the ether group, tetrahydrofurane, 1,2- dimethoxyethane (DME), *N*-methylpyrrolidine are used.[58] A propagating center of a living chain end in presence of Al catalyst and DME can be proposed as shown in Scheme 3.19.

Thus, a number of novel ways to tailor poly(methyl methacrylate) have been found during the recent past. Among them only the use of an appropriate additive/ligand combination in conjunction with an initiator leads to a perfect control of the polymerization both in polar and non-polar solvents.

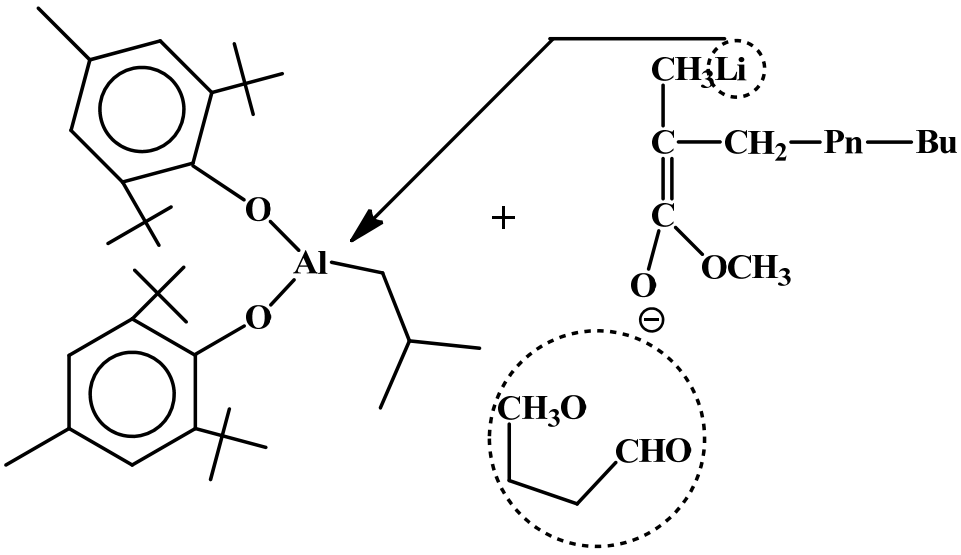

Scheme 3.19*: Proposed scheme of the propagating centers of living chain end in presence of Al catalyst and DME.*

3.4.3.3 Tacticity of poly (methyl methacrylate)

Pure isotactic poly (methyl methacrylate),M, can be prepared in toluene by reacting with phenlymagnesium bromide and MMA at 0 °C under argon atmosphere. When hexane is used as solvent in the presence of *n*-BuLi, a mixture of isotactic, heterotactic and syndiotactic M are formed. Highly syndiotactic M is produced by using a free-radical catalyst, tert-butyl peroxypivalate in mineral oil. The reaction needs to be performed in chloroform at 45 °C.[65]

3.5 Summary

Anionic polymerization technique is the unique technique among the others to obtain polymers of controlled polydispersity. The mechanisms of polar and non-polar monomers are well understood in all types of solvent. Among the monomers, the polymerization of styrene is easily controlled and irrespective of the solvent. Polybutadiene microstructures can be tailored by using different solvents. However, the controlled polymerization of poly (methyl methacrylate) is demanding in non-polar solvents. Aggregation and network formation of living carbanion chain ends can be avoided by using certain additives and catalysts.

.

Reference

[1] K. Ziegler, H. Colonius, O. Schäfer, *Justus Liebigs Ann Chem* **1929**, *473*, 36.

[2] M. Szwarc, "*Living polymers and Electron Transfer Processes"*, New York : Interscience Publishers, 1968.

[3] M. Szwarc, *Nature* **1956**, *178*, 1168.

[4] M. Szwarc, M. Levy, R. Milkovich, *J. Am. Chem. Soc.* **1958**, *78*, 2656.

[5] R. Stadler, U. Krappe, U. Breiner, *Polymer Preprints (ACS)* **1996**, *37*, 434.

[6] R. Stadler, C. Auschra, J. Beckmann, U. Krappe, I. G. Voigt-Martin, L. Leibler, *Macromolecules* **1995**, *28*, 3080.

[7] U. Breiner, U. Krappe, V. Abetz, R. Stadler, *Macromol. Chem. Phys.* **1997**, *198*, 1051.

[8] H. L. Hsieh, R. P. Quirk, "*Anionic Polymerization- Principles and Practical Application"*, Mercel Dekker, New York, 1996.

[9] R. N. Young, R. P. Quirk, L. J. Fetters, *Advance in polymer science* **1984**, *56*, 1.

[10] A. H. E. Müller, K. Matyjaszewski, "*Controlled and Living Polymerizations"*, Wiley-VCH Verlag GmbH & Co. KGaA, 2009.

[11] W. Bauer, W. R. Winchester, P. v. R. Schleyer, *Organometallics* **1987**, *6*, 2371.

[12] W. Bauer, D. Seebach, *Helv. Chim. Acta* **1984**, *67*, 1972.

[13] H. L. Hsieh, *J.Polym. sci. Part A: General Papers* **1965**, *A3*.

[14] D. J. Worsfold, S. Bywater, *Can. J. Chem.* **1960**, *38*, 1891.

[15] M. Szwarc, "*Ions and ion pairs in organic reactions."* Wiley interscience, New York, 1972.

[16] H. L. Hsieh, W. H. Glaze, *Rubber Chem. Technol* **1970**, *43*.

[17] P. J. Flory., *J. Am. Chem. Soc.* **1940**, *62*, 1561.

[18] G. V. Z. Schulz, *Physik. Chem* **1939**, *B-43*, 25.

[19] G. C. Eastmond, A. Ledwith, S. Russo, P. Sigwalt, "*Comprehensive Polymer Sci."* Pergamon Press, London, 1989.

[20] F. G. Bordwell, *Acc. Chem. Res.* **1988**, *21*, 456.

[21] F.G.Bordwell, D. J. Algrim, *J. Am. Chem. Soc.* **1988**, *110*, 2964.

[22] R. P. Quirk, D. J. Kinning, L. J. Fetters, "*Comprehensive Polymer Sci."* Pergamon Press, 1989.

[23] M. Szwarc, M. Levy, R. Milkovich, *J. Am. Chem. Soc.* **1956**, *78*, 2656.

[24] M. Morton, L. J. Fetters, E. E. Bostick, *J. Polym. Sci.* **1963**, *Part C,1*, 311.

[25] T. Kawamura, T. Uryu, T. Seki, K. Matsuzaki, *Makromol. Chem.* **1982**, *183*, 1647.

[26] T. Breiner, "Block copolymers with functionalized poly(2-hydroxyethyl methacrylate) segments for optical data storage - Synthesis and structural characterization." in *am Fach Chemie der Fakultät für Biologie, Chemie und Geowissenschaften*, Universität Bayreuth, 2001.

[27] J. M. Marechal, S. Carlotti, L. Shcheglova, A. Deffieux, *Polymer* **2004**, *45*, 4641.

[28] M. Morton., "*Anionic Polymerization, Principles and Practice."* Academic Press, New York, 1983.

[29] S. Bywater, "*Encyclopedia or Polymer Science and Engineering"*, Wiley-Interscience, New York, 1985.

[30] M. J. M. Abadie, L. Satibi, *Eur. Polym.J* **1987**, *23*, 423.

[31] M. Morton, L. J. Fetters, *Rubber Chem Tech* **1975**, *48*, 359.

[32] Amsterdam, Neterlands. 5,691,429 (1997), invs.: J. C. M. Van Der Arend, M. D. B. Wildschut, A. A. Van Der Huizen, M. J. E. Kersten;

[33] N. M. T. Pires, F. M. B. Coutinbo, M. A. S. Costa, *European Polymer Journal* **2004**, *40*, 2599.

[34] W. Gerbert, J. Hinz, H. Sinn, *Mackromol. Chem.* **1971**, *144*, 97.

[35] D. J. Worsfold, S. Bywater, *Macromolecules* **1978**, *11*, 582.

[36] R. Milner, R. N. Young, *Polymer* **1982**, *23*, 1636.

[37] S. Bywater, Y. Firat, P. R. Black, *J. Polym. Sci. Polym.Chem.Ed.* **1984**, *22*, 669.

[38] F. C. Foster, J. L. Binder, *Adv.Chem.Series.Am. Chem.Soc.* **1957**, *19*, 26.

[39] S. Bywater, D. J. Worsfold, G. Hollingsworth, *Macromolecules* **1972**, *5*, 389.

[40] A. Gourdenne, P. Sigwalt, *Eur. Polym.J* **1967**, *3*, 481.

[41] A. F. Halasa, D. F. Lohr, J. E. Hall, *J. Polym. Sci: Polym. Chem. Ed.* **1981**, *19*, 1357.

[42] A. Garton, S. Bywater, *Macromolecules* **1975**, *8*, 694.

[43] P. Teyssie, R. Fayt, J. P. Hautekeer, C. Jacobs, R. Jerome, L. Leemans, S. K. Varshney, *Macromol. Symp.* **1990**, *32*, 61.

[44] S. K.Varshney, P. Bayard, C. Jacobs, R. Jerome, R. Fayt, P. Teyssie, *Macromolecules* **1992**, *25*, 5578.

[45] C. Auschra, R. Stadler., *Polymer Bull* **1993**, *30*, 257.

[46] G. Leone, A. Boglia, F. Bertini, M. Canetti, G. Ricci, *Macromol. Chem. Phys.* **2009**, *210*, 279.

[47] J. R. White, S. K. De, "*Ruber Technologist's Handbook"*, Rapra Technology Limited, 2001.

[48] M. Morton, "*Rubber Technology"*, Third Edition edition, Springer, 1987.

[49] P. Vlcek, L. Lochmann, *Prog. Polym.Sci.* **1999**, *24*, 793.

[50] D. Baskaran, *Prog. Polym.Sci.* **2003**, *28*, 521.

[51] C. Johann, A. H. E. Müller, *Macromool.Chem.Rapid Comm.* **1981**, *2*, 687.

[52] R. Kraft, A. H. E. Müller, H. Höcker, G. V. Schulz, *Macromool.Chem.Rapid Comm.* **1980**, *1*, 363.

[53] A. H. E. Müller, "*Comp. Polym. Sci. Chain Polymerization."* 1989.

[54] M. Szwarc, "*Living Polymers and Mechanisms of Anionic Polymerization"*, Springer-Verlag Berlin Heidelberg, New York 1983.

[55] D. G. H. Ballard, R. J. Bowles, D. M. Haddleton, S. N. Richards, R. Sellens, D. L. Twose, *Macromolecules* **1992**, *25*, 5907.

[56] D. J. Worsfold, *J. Polym. Sci. Polym.Chem.* **1967**, *5*, 11.

[57] D. Kunkel, A. H. E. Müller, L. Lochmann, M. Janata, *Makromol Chem, Macromol Symp* **1992**, *60*, 315.

[58] H. Schlaad, B. Schmitt, A. H. E. Müller, S. Jüngling, H. Weiss, *Macromolecules* **1998**, *31*, 573.

[59] K. Hamada, K. Ishiura, M. Kato, S. Yaginuma, "*Anionic Polymerization process, and process for producing a polymer by the anionic polymerization process"*, European patent application, 2001.

[60] M. Tabuchi, T. Kawauchi, T. Kitayama, K. Hatada, *Polymer* **2002**, *43*, 7185.

[61] T. Hirano, T. Kitayama, K. Hatada, *Polymer Journal.* **1998**, *30*, 736.

[62] T. Kitayama, Y. Zhang, K. Hatada, *Polymer Journal.* **1994**, *26*, 868.

[63] H. Schlaad, B. Schmitt, A. H. E.Müller, *Angew. Chem. Int. Ed* **1998**, *37*, 1389.

[64] H. Ruckdäschel, J. K. W. Sandler, V. Altstädt, C. Rettig, H. Schmalz, V. Abetz, A. H. E. Müller, *Polymer* **2006**, *47*, 2772.

[65] E. V. Thompson, *J. of Polym. Sci.* **1966**, *4*, 199.

Chapter 04

Characterization Techniques

4.1 ^{1}H-Nuclear Magnetic Resonance (NMR) Spectroscopy

^{1}H- Nuclear Magnetic Resonance (^{1}H -NMR) is a technique which provides information about the electronic environment of hydrogen in polymeric materials. By using this method structural fragment information of polymer materials through the chemical shifts can be determined. The nuclei of certain isotopes have an intrinsic spinning motion that generates a magnetic moment along the spin axis. The simultaneous application of a strong external magnetic field B_0 and an energy from a second and weaker radio-frequency source (ΔE) (applied perpendicular to B_0) to the nuclei results in the rotation of the macroscopic nuclear magnetization away from its equilibrium position parallel to the applied magnetic field.[1] The transitions between the energy states of the nuclear spin are shown in the following equation.

$$\Delta E = \frac{\boldsymbol{\mu h B_0}}{\boldsymbol{2\pi}} \qquad \text{Equation 4.1}$$

here

μ = magnetic moment of the nucleus
h = Planck's constant

For different molecules the electron density around each nucleus are different. Hence, the opposing field and the effective field for each nucleus will also be different. Thus, the chemical shift of a nucleus can be measured by the difference between the resonance frequency of the nucleaus of interst molecule and a standard (reference) medium. The tetramethyl silane, TMS, is mainly used as a standard due to the presence of 12 equivalent protons. These protons give a very intense peak at a chemical shift of 0 ppm (parts-per-million). Generally, the hydrogen nuclei of a polymer with electron withdrawing groups tend to resonate at higher frequencies, $\nu_{hydrogen}$, than the frequency of TMS, ν_{TMS}. The chemical shift of a hydrogen atom in the molecule is defined as.

$$\delta = \frac{\boldsymbol{\nu_{hydrogen} - \nu_{TMS}}}{\boldsymbol{\nu_0}} \qquad \text{Equation 4.2}$$

where,

ν_0 = operating frequency of the spectrometer

The magnitude or the intensity of NMR signals is displayed along the vertical axis of the spectrum. This intensity is proportional to the concentration of each type of hydrogen nucleus, so to say molar concentration. Thus, a small or a dilute sample will give a weak signal. The signal strength increases proportionally with the sample's concentration. An arbitrary number, which is the relative intensity of signal, is reflected together with the chemical shift for assigning the set of hydrogen. The intensities are integrated electronically and they are displayed at the bottom of each peak. A typical ^{1}H-NMR spectrum of a polystyrene-*b*-polybutadiene-*b*-poly(methyl methacrylate) (SBM) triblock terpolymer is shown in Figure 4.1.

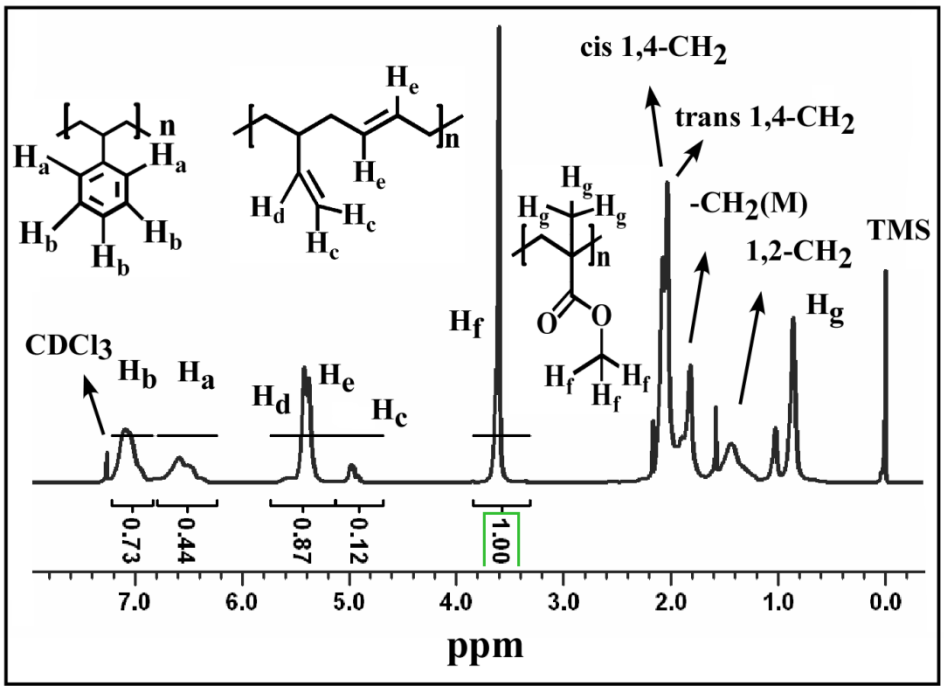

***Figure 4.1**: ^{1}H-NMR of polystyrene-b-polybutadiene-b-poly(methyl methacrylate), SBM, triblock terpolymer measured in $CDCl_3$.*

When $CDCl_3$ is used as a solvent due to its non-purity one signal for the residual protons is observed at 7.26 ppm. The protons of polystyrene are shifted downfield (shifted to the left, 6.3 to 7.2 ppm) because of the de-shielded protons of the aromatic ring. Among five protons of polystyrene, three (symbolized as H_b) show higher shift respective of low shielding effect, whereas the other two (named as H_a) show lower chemical shift with high shielded effect. In case of polybutadiene the double bond is oriented perpendicular to the external field with 'π' electrons circulating at a right angle. The induced magnetic fields are parallel to the external fields at a location of the alkene protons. These fields are shifted with their peaks to the downfield from 4.5 ppm to 5.7 ppm. At 3.6 ppm three protons of the methyl group of poly(methyl methacrylate) (M) are found. The 1,4-*cis* and *trans* olefinic

protons appear at 2.0 ppm, while the protons from the methylene groups of polystyrene (S) and M resonate between 1.3 to 1.8 ppm. The 12 protons of the internal standard, TMS, are observed at 0 ppm.

4.2 Gel Permeation Chromatography (GPC)

Gel Permeation Chromatography (GPC) is used to determine the molar mass and the polydispersity of polymeric materials. The GPC is also known as 'Size Exclusion Chromatography' (SEC) because of its ability of separating the polymer molecules according to the molecular size. The molecules are separated by introducing a column filled with cross-linked polymer gel, composed of e.g., polystyrene and divinylbenzene, porous glasses or silica gels. The gel has small pores of specific size (ca. $10^3 – 10^7$ Å diameters). When a polymer passes through this column the larger particles elute first, then the smaller molecules diffuse through the pores of the column resulting in a longer retention time.[2]

In GPC, the molecules are separated based on the hydrodynamic volume, not the molecular weight. If no mass-sensitive detectors (e. g. light-scattering photometer or viscosimeter) are available, a calibration curve must be generated to obtain the molar mass distribution and the corresponding averages. Depending on the detector, a conventional or a universal calibration curve is defined. A conventional calibration curve is employed when a single concentration detector, typically Refractive Index (RI) or UV detector is used. In general a standard substance, which covers the entire molar mass of the sample, is used for calibration. The detector detects the concentration at a given elution volume or elution time. Then a plot of log [M] vs retention volume (RV) is drawn. A relationship between the retention volume and the molar mass can be obtained from the plotted curve (Figure 4.2).

However, the sample, which is analyzed by conventional calibration curves, is chemically different from the standard one. To determine the molar mass of a polymer, the sample should have the same density as the standards. In fact, it is often not the case when a conventional calibration curve is used. Usually, a narrow distributed polystyrene reference with known molar masses is used to calibrate. Thus, only polystyrenes but not the other types of polymers show their true molar masses. For all other polymers, the calculated molar masses will be an apparent value. To overcome this problem a universal calibration curve is constructed considering the hydrodynamic volume instead of molar masses. In this curve the hydrodynamic volume is plotted against the retention volume, RV. At a given retention volume and a given concentration of an unknown polymer, the molar mass or their distribution can be calculated from this curve. However, by using MALLS (Multi-angle Laser Light Scattering) detector, the molar mass of the macromolecular species can be determined directly without any previous calibration or comparison.

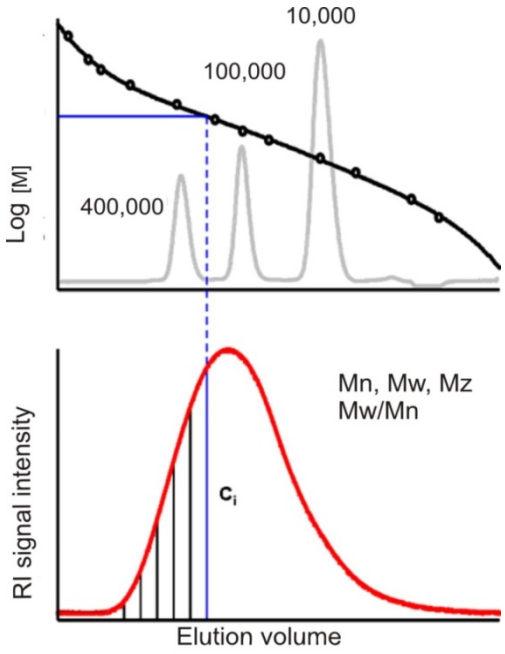

Figure 4.2: *Schematic sketch depicting the calibration of a GPC instrument.*

The molar mass distribution as well as other parameters, e.g., weight average molar mass (M_w), number average molar mass (M_n), and z average molar mass (M_z), are defined by the following equations:

$$\overline{M_n} = \frac{\sum N_i M_i}{\sum N_i} = \frac{\sum c_i}{\sum \frac{c_i}{M_i}} \qquad \text{Equation 4.3}$$

$$\overline{M_w} = \frac{\sum N_i M_i^2}{\sum N_i M_i} = \frac{\sum c_i M_i}{\sum c_i} \qquad \text{Equation 4.4}$$

$$\overline{M_z} = \frac{\sum N_i M_i^3}{N_i M_i^2} = \frac{\sum c_i \ M_i^2}{\sum c_i M_i} \qquad \text{Equation 4.5}$$

Here, the number of i repeating unit is N_i, their molar mass is M_i and c_i is the concentration of the molecules i.

The polydispersity index (PDI) which indicates the uniformity of the chain lengths is obtained from Equation 4.3 and Equation 4.4.

$$\text{PDI} = {M_w}/{M_n} \qquad \text{Equation 4.6}$$

4.2.1 Detectors

The detectors monitor the concentration of investigated polymer in the eluting solvent. There are many detectors used in GPC. Typically they are categorized as concentration sensitive and molar mass sensitive. Among them the following two concentration sensitive detectors were used in the present work.

4.2.1.1 UV Detector

This detector can detect only the functional groups in the analyte, which are absorbing at the particular wavelength, for example, the phenyl ring at a wavelength of 254 nm. The sensitivity depends on the molar absorption coefficient at the particular wavelength. If molecules do not absorb this wavelength they are invisible. The solvent being used should not absorb at the operating wavelength. The advantage of UV detectors is their insensitivity towards temperature and pressure variation.

4.2.1.2 Differential Refractometer (RI)

The overall refractive index of the eluate (solvent + sample) is determined using a differential refractometer. It detects the concentration of all present units in a polymer unless the refractive index of the polymer is similar to the refractive index of the solvent (i.e., $RI_{pol} \neq RI_{solvent}$). Disadvantages of this type of detectors are the dependency on temperature and pressure fluctuations.

The RI signal is not only proportional to sample concentration but also to a sample-dependent parameter called refractive index increment, *dn/dc*. By using the calibration constant, *RI.Cal*, and *dn/dc* of a sample, the RI signal is obtained (Equation 4.7).

$$\text{RI. Signal} = RI.Cal.\frac{n-n_0}{n_0}.c.\frac{dn}{dc} \qquad \text{Equation 4.7}$$

n = refractive index of the sample solution
n_0= refractive index of the reference solvent
c = concentration of the sample.

The changes in the polymer composition are determined by the ratio UV/RI. In a pure polystyrene system the ratio UV/RI remains constant at 0.35, as shown in Figure 4.3. If the polystyrene units are 'diluted' by other components, e.g., SB diblock or SBM triblock, the intensity of the UV signal will be lower, and the UV/RI ratio will be decreased.

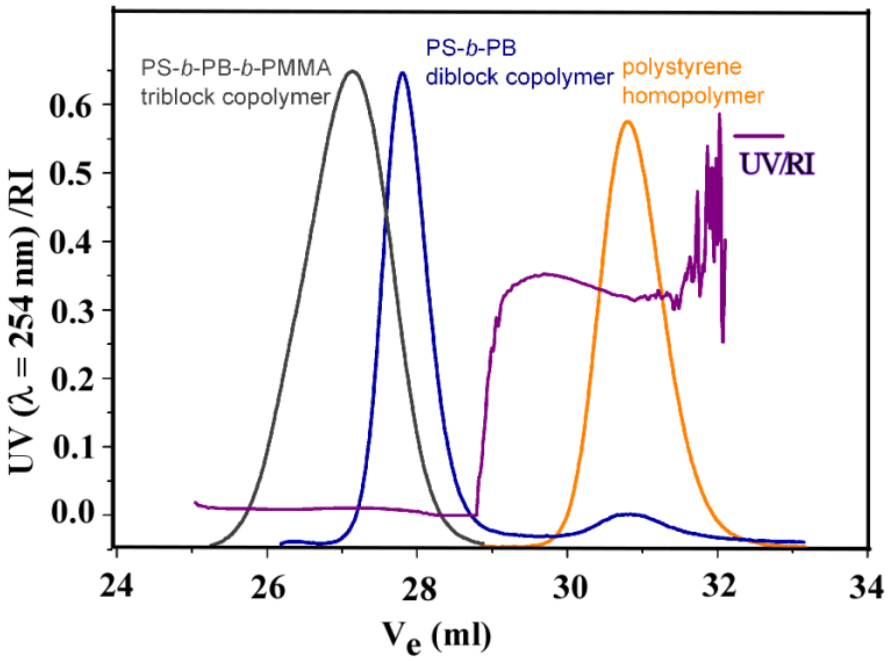

Figure 4.3: *GPC elution curve vs UV/RI ratio of polystyrene-b-polybutadiene-b-poly(methyl methacrylate) triblock terpolymer.*

4.3 Transmission Electron Microscopy (TEM)

Transmission electron microscopy (TEM) is one of the most versatile analytical tools for the investigation of polymer morphologies, especially when multiphase polymer morphologies and polymer blends are needed to be investigated.[3] In TEM analysis the electron beam is transmitted through an ultra thin polymer specimen. During transmission the electrons can be absorbed, scattered, or inelastically scattered. The transmitted electrons which interact with the specimen are captured by a sensor or a detector.

The objective lens and the objective apertures are the most important parts of a TEM that generates a bright-field (bf) or a dark-field (df) images of a specimen. Bright-field is the most widely used mode of TEM imaging. Here, an aperture is placed in the back focal plane of the objective lens. Only the weakly scattered and transmitted electrons from the specimens are captured at a location of objective aperture on the optical axis. For dark-field images, the beam is scattered strongly while the direct beam is blocked by the aperture. One or more diffracted beams are allowed to pass the objective aperture and a dark region on the image is emerged.

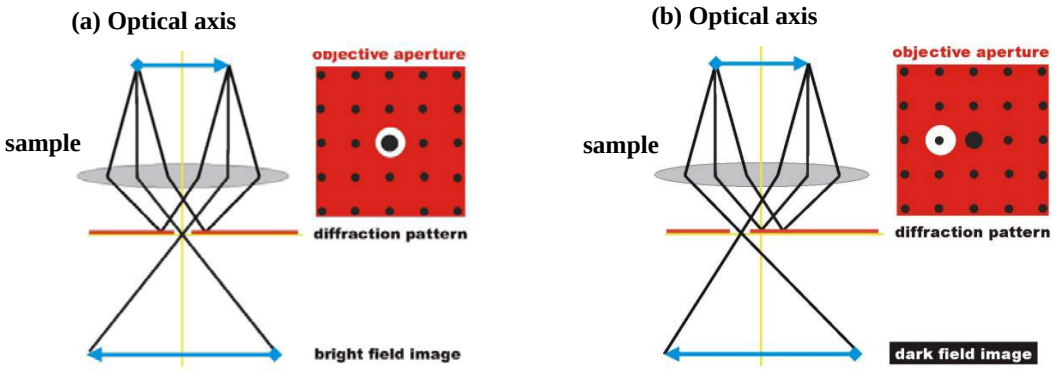

Figure 4.4: *Schematic sketch of bright-field (a) and dark-field (b) imaging.*

4.3.1 Staining of polymer samples

As in most organic polymers the electron densities are rather similar, the bright-field or dark-filed imaging gives very limited information.[4] Hence, it is difficult to distinguish different phases of polymer by a direct microphase investigation using TEM. Therefore, atoms with high number of electrons, i.e. heavy elements are used to stain the polymer by which the phase contrast can be increased. Heavy elements such as ruthenium or osmium oxides are used as staining agent. The contrast of the stained region increases with the atomic number of the staining atom as well as the number of stained sites per volume unit.

Among the staining agents that are used for polymers only OsO_4 and RuO_4 are discussed here. The OsO_4 agent stains the amino, alcohol and aldehyde functional groups as well as the olefinic double bonds, but not the aromatic rings, esters or nitrile groups (Kato's method).[5]

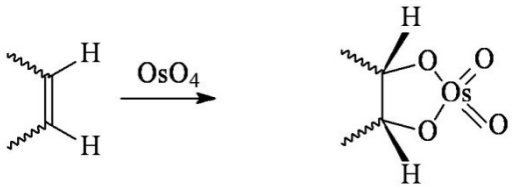

Equation 4.8

As an alternative, ruthenium tetroxide (RuO_4), which is a stronger oxidizing agent than OsO_4, reacts with both aromatic and olefinic double bonds.[6] The RuO_4 readily cleaves double bonds to yield carbonyl products. It stains polystyrene rings but does not react with the ester groups present in the polymers like poly (methyl methacrylate). [7] The reaction of RuO_4 with the polystyrene is given in Equation 4.9.

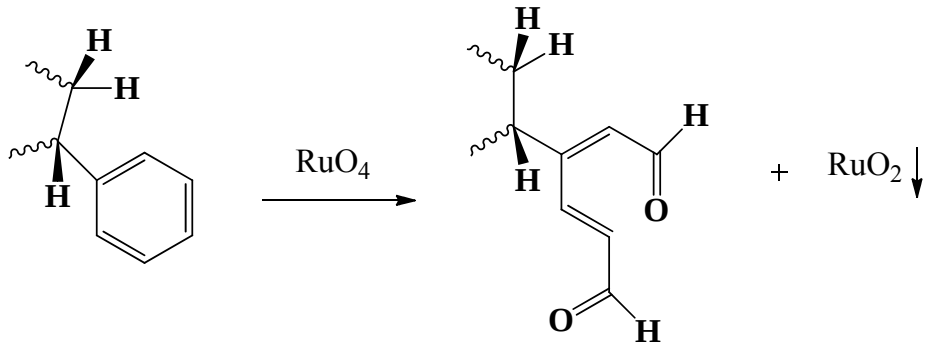

Equation 4.9

In contrast to OsO_4, the selectivity of RuO_4 strongly depends on the staining time and concentration of its vapour. Polystyrene-*b*-polybutadiene-*b*-poly (methyl methacrylate), SBM, triblock terpolymer can be stained by OsO_4 as well as RuO_4. When OsO_4 is used, only the polybutadiene part is affected and appears dark in the micrograph. On the contrary, the RuO_4 leads to black domains of S. Both agents do not react with M; hence the corresponding domains will always appear white in the micrographs. In Table 4.1 the "colors" of the different blocks of SBM are given.

Table 4.1: *"Color" of polystyrene-b-polybutadiene-b-poly(methyl methacrylate), SBM, triblock terpolymer in TEM images.*

Staining agent	**S**	**B**	**M**
OsO_4	gray	black	white
RuO_4	black	gray	white

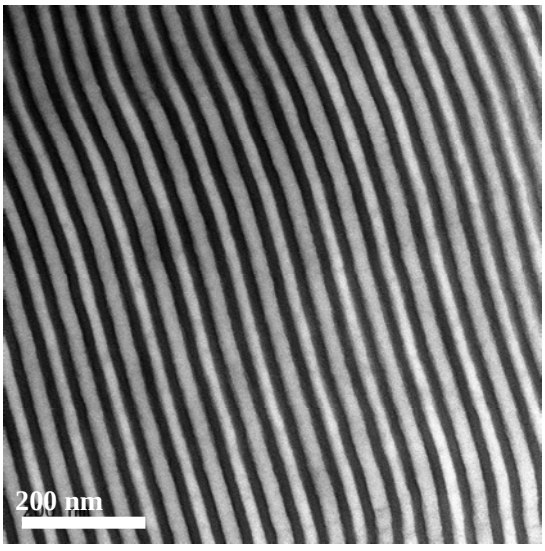

Figure 4.5: *TEM images of polystyrene-**b**-polybutadiene-**b**-poly(methyl methacrylate), SBM, triblock terpolymer stained with OsO_4, color code: gray = S, black = B, white = M.*

4.3.2 Radiation Damage

During TEM measurements the electron beam interacts with the material resulting in some crosslink reactions. In addition, the bonds may break leading to disorder and continuous loss of masses.[8] Thus, the micrographs of the polymer films are altered. This phenomenon is called radiation damage. Radiation damages in aromatic compounds are less a problem for TEM analysis than in aliphatic ones, as in the aromatic compounds the electron liberation by damaging can be delocalized or distributed.[9] Due to this radiation damage the M domain often becomes narrower than the S domain in TEM micrographs. Moreover, the phenyl group stabilizes the environment of S rather than such stabilization can occur in M. Hence, the sensitivity of the radiation damage of the other chemical groups attached to the M is increased resulting in narrower domains.[10-12]

4.4 Dynamic Mechanical Analysis (DMA)

The dynamic mechanical analysis (DMA) is used to measure the viscoelastic behavior of polymeric materials. As the polymers have both elastic and viscous properties, they store and dissipate energy upon applied sinusoidal forces. This behavior is expressed by dynamic storage modulus, *E*', dynamic loss modulus, *E*", and mechanical damping, δ. Depending on the polymer type, temperature and frequency, the dynamic moduli may vary between 10 MPa and 10^5 MPa.[13]

The viscoelastic response of a material under applied stress is shown in Figure 4.6. For an applied sinusoidal stress, σ, with time, t, a viscoelastic material responds with a sinusoidal strain, ε. The sinusoidal variation in time, i.e., the rate, is usually described in terms of, ω. ([ω] = rad/sec). Upon applied stresses, the material phases shift along the wave. This phase shifting mainly occurs due to additional time which is pretty high compared to the time necessary for molecular motion and relaxation. This phase shift is denoted by delta, δ.

The stress of a viscoelastic material is not in phase with the strain, but proceeds with a phase shift, δ, as expressed by Equation 4.10.

$$\sigma = \sigma_0 \sin(\omega t + \delta)$$
$$= \sigma_0 \sin(\omega t) \cos\delta + \sigma_0 \cos(\omega t) \sin\delta \qquad \text{Equation 4.10}$$

And

For a sinusoidal strain the motion is described by Equation 4.11

$$\varepsilon = \varepsilon_0 \sin(\omega t) \qquad \text{Equation 4.11}$$

ω is the angular frequency.

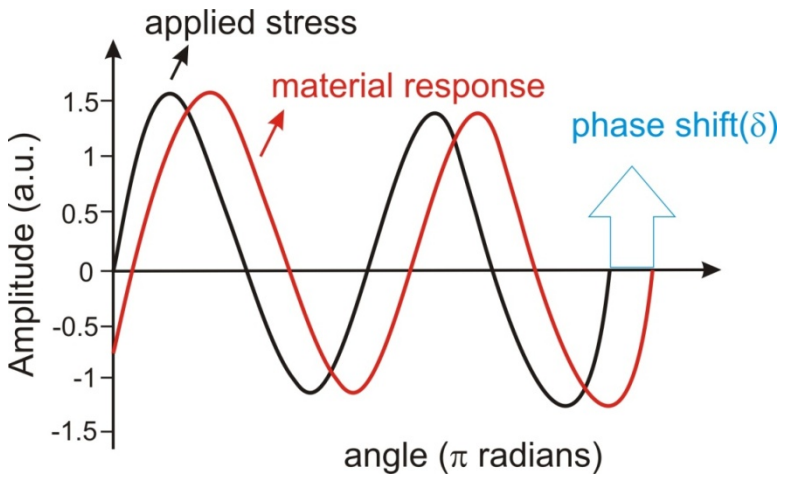

Figure 4.6: *The response of a viscoelastic material upon applied stress at certain amplitude. The DMA supplies an oscillatory force, causing a sinusoidal stress to be applied to the sample, which generates a sinusoidal strain. By measuring both the amplitude of the deformation at the peak of the sine wave and the lag between the stress and strain sine waves, quantities like the modulus, the viscosity, and the damping can be calculated.*[13, 14]

To account for both the plastic and elastic nature of the response a complex modulus *E** is introduced, as expressed by Equations 4.12.

$$E^* = \sigma / \varepsilon \qquad \text{.Equation 4.12}$$

To describe the complex modulus, the exponential forms of Equation 4.10 and Equation 4.11 were used.

$$\sigma = \sigma_0 \sin(\omega t + \delta) = \sigma_0 e^{i(\omega t + \delta)} \qquad \text{Equation 4.13}$$

$$\varepsilon = \varepsilon_0 \sin(\omega t) = \varepsilon_0 e^{i(\omega t)} \qquad \text{Equation 4.14}$$

Combining Equation 4.12, 4.13, and 4.14, the complex modulus can be derived.

$$E^* = \sigma/\varepsilon = \frac{\sigma_0 e^{i(\omega t+\delta)}}{\varepsilon_0 e^{i(\omega t)}} = \frac{\sigma_0}{\varepsilon_0} e^{i(\omega t+\delta-\omega t)} = \frac{\sigma_0}{\varepsilon_0} e^{i\delta} \quad \text{Equation 4.15}$$

$$E^* = \frac{\sigma_0}{\varepsilon_0}(\cos\delta + i\sin\delta) = \underbrace{\frac{\sigma_0}{\varepsilon_0}\cos\delta}_{E'} + \underbrace{i\,\frac{\sigma_0}{\varepsilon_0}\sin\delta}_{E''} \quad \text{Equation 4.16}$$

In other words

$$E^* = E' + iE'' \quad \text{Equation 4.17}$$

From Equation 4.16 and 4.17, the storage modulus as well as the loss modulus can be redefined in a straightforward manner. The storage module, E′, which represent the stiffness of a viscoelastic material, is proportional to the energy stored during a loading cycle.

$$E' = \frac{\sigma_0}{\varepsilon_0}\cos\delta \quad \text{Equation 4.18}$$

The loss modulus, E′′, is the energy dissipation by heat during one loading cycle due to viscous flow.

$$E'' = \frac{\sigma_0}{\varepsilon_0}\sin\delta \quad \text{Equation 4.19}$$

The phase angle,δ, in a viscoelastic material is defined by the phase difference (ratio) between the dynamic stress and the dynamic strain during a sinusoidal oscillation. The phase angle can be defined in terms of "tan δ" by combining the Equations 4.18 and 4.19

$$\tan\delta = \frac{E''}{E'} \quad \text{Equation 4.20}$$

The phase angle is expressed in radians (rad). A tan δ value larger than unity indicates that the non-elastic strain component is higher in a material, while a lower value indicates that the material is predominantly elastic.

In a purely elastic material (Figure 4.7) the stress and the deformation are always in phase, i.e. at '0' phase angle. The complex modulus, *E**, can be expressed by the ratio of the stress amplitude to the deformation amplitude and is equivalent to the storage modulus, *E,′* (δ = 0, therefore, cos(0) = 1; sin(0) = 0, and *E** = *E′*). Steel is an example of an almost purely elastic material. In an ideally viscous material the phase angle is 90°. In this case, *E** is equal to the loss modulus, E′′, i.e., the viscous part of the complex modulus.

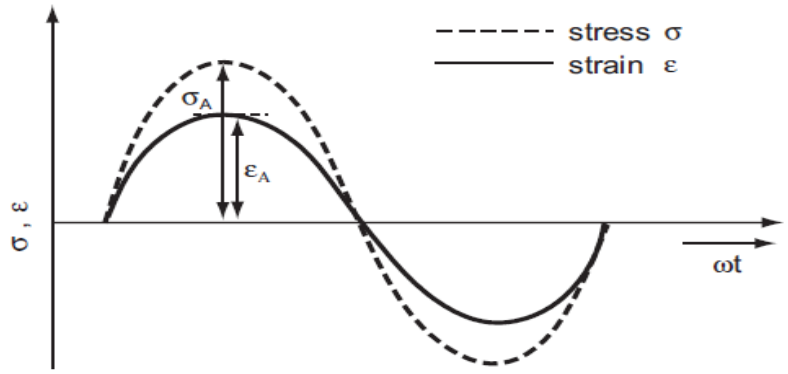

Figure 4.7: *Stress-strain behavior of a purely elastic material.*

In Figure 4.8, the storage modulus, E′, loss modulus, E′′ and the damping factor, δ**,** are plotted against temperature. The molecules at low temperature are highly immobile so that they are unable to resonate with the oscillatory loads. The storage modulus, *E′,* has been found considerably higher than the loss modulus, *E′′*. When the temperature reaches the glass transition of the polybutadiene segments (1,2-unit) at approximately -12 °C, the mobility of the B domain increases and are easily resonated. This is reflected by the local maxima of both *E′′*and tan δ. On the other hand *E′* decreases in a stepwise manner. With further increase of temperature, the storage modulus, *E′,* decreases, and at 110 °C a sharp change of the loss modulus, *E′′* can be detected. This temperature indicates the glass transition of S. The polymer becomes very soft with further increase of the temperature at above 130 °C. Very low storage modulus and a sharp change of loss modulus are detected around 136 °C, which indicates the glass transition temperature of M.

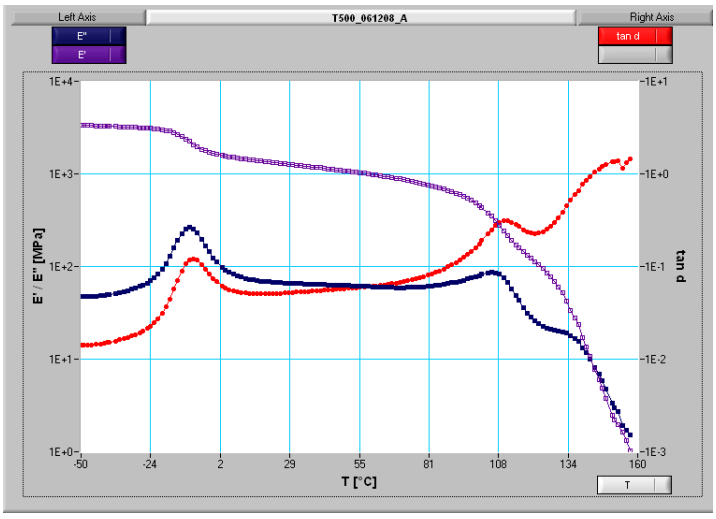

Figure 4.8: *Representative DMA analysis of a polystyrene-b-polybutadiene-b-poly(methyl methacrylate), SBM triblock terpolymer. Storage modulus, E′, loss modulus, E′′, and the damping factor, δ, were monitored against temperature.*

4.5 Differential Scanning Calorimetry (DSC)

Differential scanning calorimetry or DSC is a thermo analytical technique where thermal transition of a polymer is measured as a function of temperature. In this technique a reference material with a precise thermal transition has to be taken along with the polymer sample. This reference sample provides a direct comparison of temperature measurement from the polymer sample. The basic principle is that, when a polymer sample undergoes a physical transformation such as phase transitions, more (or less) heat needs to flow to (or from) the polymer than the reference material in order to maintain a equilibrium temperature at the both samples. An aluminium disc is used generally as a sample holder to obtain a fairly constant heat capacity.[15] For both the sample and the reference nearly same temperature should be maintained throughout the experiment. In this work, the heat flow difference is monitored continuously during the heating and cooling down of the samples.[16] The temperature at which the related enthalpy of the sample changes is recorded. From the DSC measurement the most important physical property, e.g., glass transition temperature of a polymer is detected. Depending on the different methods (e.g., DMA and DSC) and heating/cooling rate, the glass transition temperature is varied by several degrees.

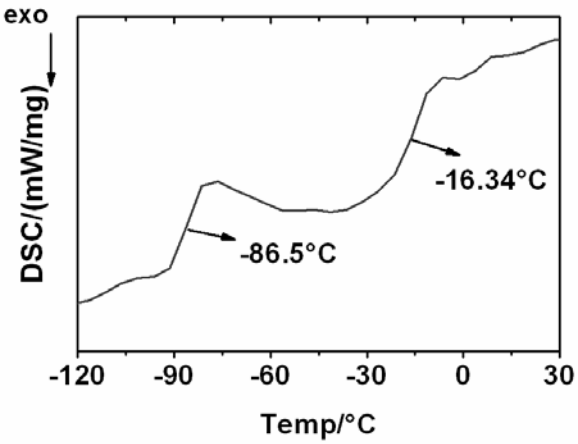

Figure 4.9: *Glass transition temperature of 1,2- and 1,4- polybutadiene measured at DSC at a heating rate of 20 k/min (2nd heating curve was shown).*

Figure 4.9 shows a DSC curve of a blend of 1,2- and 1,4-polybutadiene. Two thermal changes at -86.5 °C and -16.3 °C were found. Those temperatures are very close to the glass transition temperatures of the homopolymers of 1,4- and 1,2- B which indicates the microphase separation of 1,2- and 1,4-B in the blend mixture.

4.6 Stress-strain experiments

When a certain force, *F*, is applied to a material, a deformation,δ, occurs which is proportional to the force. This can be expressed by the following equation:

$$\delta = \frac{Fl}{AE}$$

or, $E = \frac{Fl}{A\delta}$ Equation 4.21

Where:

F = applied force producing extension of the specimens
l = length of specimens
A = cross section area of specimens
E = Modulus of elasticity, Young modulus
δ = deformation of the specimens

Tensile stress, or simply stress, is expressed as the load per unit area or force applied per cross-sectional area perpendicular to the force.

$$\sigma = \frac{F}{A}$$ Equation 4.22

Tensile strain, or the elongation of a bar per unit length, is determined by Equation 4.23.

$$\varepsilon = \frac{\boldsymbol{\delta}}{\boldsymbol{l}}$$ Equation 4.23

Combination of Equation 4.21-23 renders

$$E = \frac{F.\,l}{A.\,\delta} = \frac{\sigma}{\varepsilon}$$ Equation 4.24

Where

E = Young's Modulus (MPa)
σ = stress (MPa)
ε = strain (%)

The quantity *E*, the ratio of the unit stress to the unit strain, is the modulus of elasticity of the material in tension or compression and is often called *Young's Modulus*.

Figure 4.10 highlights a typical stress-strain curve of a polymer material. For low strain (ε), a linear elongation is observed up to a certain stress. The slope indicates the *Young's modulus*, i.e., the sample's resistance to deformation. When a high elongation is applied, a plastic deformation of the sample occurs. The point where the plastic deformation starts is called the yield point. If the elongation is further increased, the sample breaks at a maximum of stress and strain value. The area under the curve is the energy that is needed to deform, and eventually break the material.

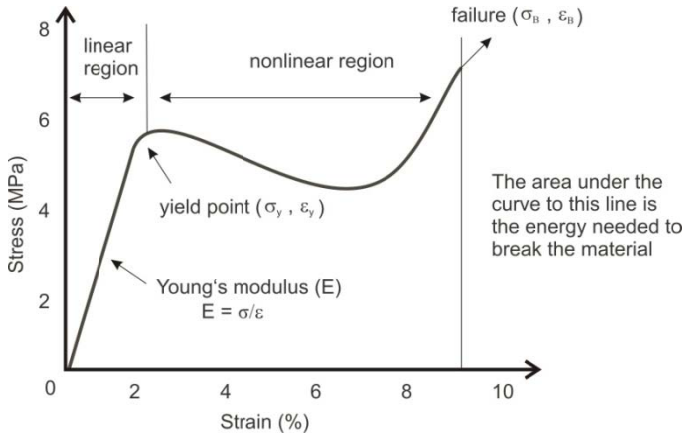

Figure 4.10*: Typical stress- strain curve for a polymer material.*

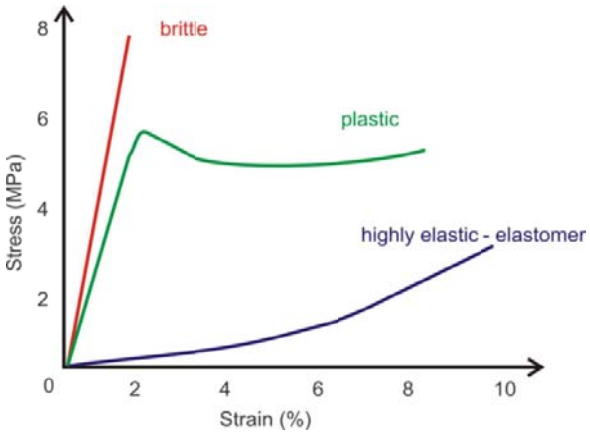

Figure 4.11: *Stress-strain curve for different types of polymer materials.*

Typical stress-strain curves of elastic and plastic materials are depicted in Figure 4.11. A brittle polymer exhibits very large Young's modulus. A plastic material shows a linear stress-strain dependency for lower strains, whereas once the yield point is reached the plastic deformation

commences. An elastomer deforms mostly elastically, showing extremely low Young's modulus and low stiffness.

4.7 Small Angle X-ray Scattering (SAXS)

The Small Angle X-ray Scattering (SAXS) is the most widely used technique to study polymer materials related to periodic structures on large scales (2 to 200 nm). This technique provides more reliable information of polymer's bulk properties than the TEM. The principle of SAXS is based upon the scattering pattern of a crystalline material, but that can be successfully employed also for amorphous materials like the polymers.

4.7.1 Lattice Parameters

The unit cell is the smallest unit of a crystalline material where the atoms are arranged within a given type of crystal structure. A three dimensional crystal structure is described by the lattice parameters: the length of the cell edges, the angles between them, and the atomic positions inside a unit cell. To describe lattice parameters via a reciprocal lattice or the inverse intercepts along the lattice vectors, three values are chosen, i.e., $|\vec{a}|$, $|\vec{b}|$ and $|\vec{c}|$. They are arranged to obtain the lowest possible integer named Miller Indices (h, k, l). Miller index (100) represents a plane orthogonal to direction h; index (010) represents a plane orthogonal to direction k, and index (001) represents a plane orthogonal to l. Figure 4.12 shows Miller indices for a cubic crystal system.

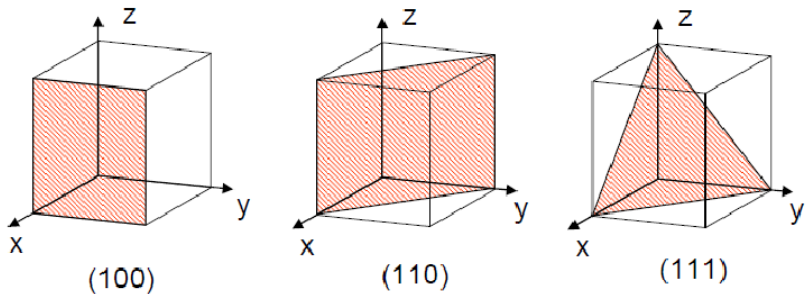

Figure 4.12: *Miller indices for a cubic crystal system.*

4.7.2 Scattering Theory

Depending on the spatial structure (morphology) of the polymer system different scattering methods, i.e., light, X-ray or neutron scattering can be used. Small angle X-ray scattering (SAXS) is a technique where a nm-range sample structure can be detected. A detector at very low angles (0.1 – 10°) records the elastic scattering of X-rays (wavelength of 0.1 to 0.2 nm). A well-collimated incident X-ray beam is very important to measure the scattered intensities close to the primary beam. The analyses are performed under vacuum to avoid gas scattering.[15]

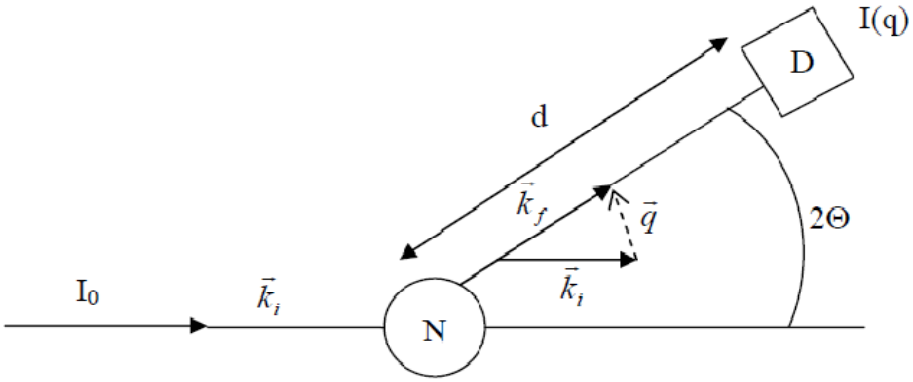

Figure 4.13: *Scattering pattern where a beam with intensity I_0 with identical wavelength approach a crystalline solid and is scattered off with one atom (N). The reflected beam I (q) traverses with angle 2Θ.*[17]

Here;

I_0 = intensity of the incident beam
I(q) = intensity of the scattered beam as a function of q
$\overrightarrow{k_i}$, $\overrightarrow{k_j}$ = wave vector [nm^{-1}]
d = distance between scattering object and detector [nm]
$\vec{q}$ = scattering vector [nm^{-1}],
D = detector
N = particle
Θ = angle of incidence [°].

A simple scattering pattern is given in Figure 4.13. When a monochromatic radiation with an intensity, I_0, and a wavelength, λ, passes through a polymer, most of the beam is transmitted and the remaining is absorbed or scattered. The intensity, $I(\vec{q})$, of the scattered waves at different angles, Θ, is recorded by a detector D at a distance, d. The scattering vector, $\vec{q}$, is equal to the difference between the wave

vectors of the incident, $\overrightarrow{k_i}$ and the scattered, $\overrightarrow{k_f}$, plane waves. The scattering vector,$\vec{q}$, is related to the angle of incident Θ, represent by Equation 4.25.

$$\vec{q} = |q| = \frac{4\pi sin\ \Theta}{\lambda} \qquad \text{Equation 4.25}$$

Θ = angle of incidence [°]
$\vec{q}$ = scattering vector [nm^{-1}]

The scattering pattern arising from a microphase separated block copolymer is similar to the diffraction pattern obtained from a crystalline solid which can be explained from Bragg's diffraction pattern as given in Figure 4.14. Bragg diffraction occurs when an electromagnetic radiation or subatomic particle waves with a wavelength comparative to atomic spacings of the crystalline sample hits the crystal at an arbitrary angle. The interference of the reflected waves can be either destructive or constructive. To obtain constructive interference, the path difference between the two incident and the scattered waves, which is 2dsinΘ, has to be a multiple of the wavelength λ. Hence, the Bragg's law gives the relation between interplanar distance d and diffraction angle Θ:

$$n\lambda = 2d_{hkl} \sin \Theta \qquad \text{Equation 4.26}$$

Θ = Bragg angle [°]
d_{hkl} = distance between two planes (hkl) [nm]
n = an integer representing the number of wavelengths required for constructive interference to occur. At the smallest angle of incidence (θ) for a maxima n = 1, at the next smallest angle n = 2, etc.

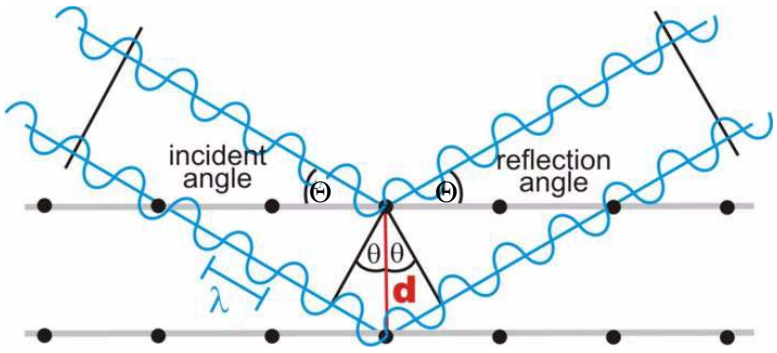

Figure 4.14: *Bragg diffraction. Two beams with identical wavelength, (λ) and phase (Θ) approach a crystalline solid. The scattered wave is considered as 2dsinΘ due to travel an extra length by photon which enters the second layer. d is the distance between two planes.*

To monitor the morphology of the material by SAXS, the segment of the block copolymers need to be different in their electron density. Hence, during passing the X-ray beam through crystalline or amorphous material, the scattering X-rays from different electrons are interfered with each other and a diffraction pattern is produced at different scattering angle. The different intensity maxima for different regularity of the morphology can be detected.

Using Equation 4.25 and 4.26 the spacing of the two lattice plane, d_{hkl}, can be defined

$$d_{hkl} = \frac{2\pi n}{q} \qquad \text{Equation 4.27}$$

The observed values for the spacing can be compared with the characteristic sequences of model lattices. The ratio of the characteristic peaks, d_{hkl}, with the first peak, d_{100}, the different special arrangements, such as lamellae, hexagonally or tetragonally packed cylinders and body centered cubic (bcc) spheres can be defined, see Table 4.2. The 2D SAXS images as well as the corresponding 1D-SAXS pattern of a SBM triblock are shown in Figure 4.15. The relative positions of the peaks obtained at 1q*, 2q*, 2.9q*, 3.9q*, 4.9q* indicate lamellar patterns. By using Equation 4.27, the long periodicity of lamellar domains for the first intense peak (n = 1) was calculated 73 nm.

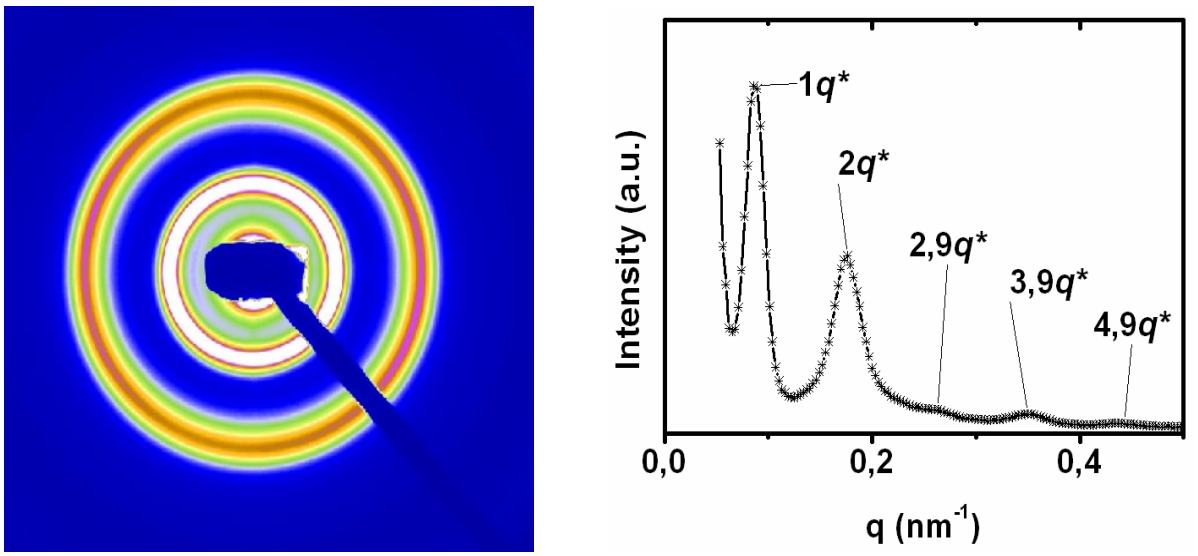

Figure 4.15: *2D-SAXS images (left) and 1D-SAXS pattern (intensity vs. q nm^{-1}) obtained of a lamellar type $S_{32}B_{31}M_{32}^{106}$ triblock terpolymer.*

Table 4.1: *Ratios of consecutive Bragg spacings for different model morphologies by bcc spheres, hexagonally and tetragonally packed cylinders, lamellae and gyroid*[17-20].

Morphology		**reflections**					
		1	2	3	4	5	6
Spheres bcc	d_{hkl}/d_{100}	1	0.707	0.577	0.5	0.447	0.408
	(hkl)	110	200	211	220	310	222
	rel.pos.	1	√2	√3	√4	√5	√6
Cylinders Hexagonal	d_{hkl}/d_{100}	1	0.577	0.5	0.378	0.333	0.289
	(hkl)	100	110	200	210	300	320
	rel.pos.	1	√3	√4	√7	√9	√12
Cylinders Tetragonal	d_{hkl}/d_{100}	1	0.707	0.5	0.447	0.333	0.316
	(hkl)	100	110	200	210	300	320
	rel.pos.	1	√2	√4	√5	√9	√10
Lamellae	d_{hkl}/d_{100}	1	0.5	0.333	0.25	0.20	0.167
	(hkl)	100	200	300	400	500	600
	rel.pos.	1	2	3	4	5	6
Gyroid	d_{hkl}/d_{100}	1	0.866	0.655	0.612	0.548	
	(hkl)	211	220	321	400	420	
	rel.pos.	√3	√4	√7	√8	√10	

4.8 In-situ tensile test and SAXS

In-situ tensile test and SAXS experiment hold particular interest because of the ability to study large deformation at several angles with respect to the deformation direction. The distribution of scattering intensity at different planar sections gives sequential data to analyze the morphology change due to the deformation. These patterns give additional evidence to interpret the deformation of the domains grain consisted of a zigzag or chevron pattern (corresponding to a 4-point pattern in reciprocal space) of broken cylinders or lamellae.[21] The 2D X-ray scattering patterns are presented in Figure 4.16. This scattering pattern is subdivided in 360 cake sections of 1 degree each (Figure 4.16a), which are subsequently integrated over the accessible *q*-range to determine the amount of scattering in each direction. The distribution of the scattered intensity in the different directions relative to the tensile

direction can be constructed by azimuthal angles vs intensity (Figure 4.16b). Intensities at 90 ° and 270 ° correspond to the tensile direction which is referred to as *meridional scattering*. The appearance of these streaks is related to the formation of crazes. Whereas at 0 and 180 ° are related to the perpendicular direction as referred *equatorial scattering* which is the indication of the shear yielding.[22]

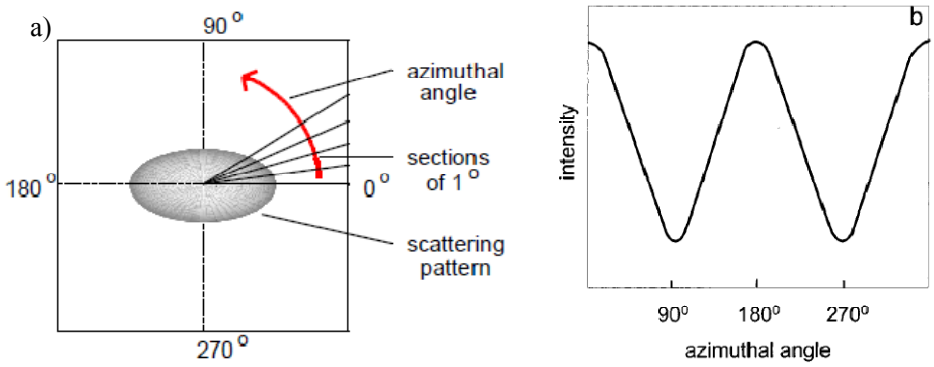

Figure 4.16: *Schematic representation of data analyses as performed in SAXS measurements. (a) Division of the 2D scattering patterns and (b) the resulting azimuthal plot which describes the relation between the intensity and the azimuthal angle.*[22, 23]

The orientation distribution function of chain segments of the block copolymer is expressed by a second coefficient of the Legendre polynomial, P_2,which is termed as '*orientation factor*', can be obtained by integrating the scattering intensity $I_q(\varphi)$ as a function of azimuthal angle φ from $\varphi = 0°$ to 360°.[24]

$$P_2 = \frac{3<cos^2\varphi> -1}{2} \qquad \text{Equation 4.28}$$

where

$$< cos^2\varphi > = \frac{\int_0^{2\pi} d\varphi (I_q(\varphi) cos^2(\varphi) |sin(\varphi)|)}{\int_0^{2\pi} d\varphi (I_q(\varphi) |sin\,(\varphi)|)} \qquad \text{Equation 4.29}$$

Depending on the type of chain alignment, two different ranges of the orientation factor (P_2) can be obtained. When the chains are perfectly aligned to the reference axis (maximum scattering intensity at φ= 0°), P_2 are ranged from 0 to 1. For P_2 = 0 indicates a perfect random orientation of the lamellar spacing whereas for P_2 = 1 corresponds to a perfect lamellar alignment to the reference axis. For an

alignment of the lamellae along the field direction (maximum scattering intensity at φ= 90°), P_2 ranges from 0 to -0.5. When P_2 = -0.5, the chains are more perpendicular to the reference axis. The normals of the lamellae are lying with random orientation in the plane perpendicular to the reference direction.

Reference

[1] J. A. Dean, *The Analytical Chemistry Handbook* **2004**, *2nd Edition*, 15.1.

[2] J. M. G. Cowie., *Polymers: Chemistry and Physics of Modern Materials.* **2001**, Nelson Thornes.

[3] M. Tsuji., *Com. Polym. Sci.* **1989**, *Vol I* 785.

[4] L. C. Sawyer, D. T. grubb, *Fundamentals of microscopy, Polymer Microscopy.* **1996**, *Chapman & Hall, London*.

[5] K. Kato., *J. Polym. Sci. Polym. Lett.* **1966**, *4*, 35.

[6] J. S. Trent., *Macromolecules* **1984**, *17*, 2930.

[7] G. Mao, J. Wang, S. R. Clingmann, C. K. Ober, J. T. Chen, E. L. Thomas, *Macromolecules* **1997**, *30*, 2556.

[8] D. T. Grubb, *J. Mat. Sci.* **1974**, *9*, 1715.

[9] B. Pullman, A. Pullman., *Quantum Biochemistry, Interscience, New York* **1963**.

[10] U. Breiner, U. Krappe, E. L. Thomas, R. Stadler, *Macromolecules* **1998**, *31*, 135.

[11] V. Abetz, T. Goldacker, *Macromol. Rapid Commun.* **2000**, *21*, 16.

[12] P. Alexander, A. Charlesby, *Nature* **1954**, *173*, 578.

[13] K. S. Kwan, "The Role of Penetrant Structure in the Transport and Mechanical Properties of a Thermoset Adhesive", in *Materials Engineering and Science*, Virginia Polytechnic Institute and State University, 1998.

[14] K. P. Menard, "*Dynamic Mechanical Analysis-A Practical Introduction"*, CRC Press LLC, New York, 1999.

[15] D. Campbell, R. A. Pethrick, J. R. White, *Polymer Characterization- Physical Techniques* **2000**, *Second Edition*, Stanley Thornes (Publishers) Ltd.

[16] J. A. Dean, *The Analytical Chemistry Handbook* **1995**, *2nd Edition*, 15.1.

[17] G. Cantea, "Shear-induced alignment in block copolymer solutions", in *im Fach Chemie der Fakultät für Biologie, Chemie und Geowissenschaften*, Universität Bayreuth, 2005.

[18] S. Brinkmann-Rengel, "Thermoplastic Elastomere auf Basis von ABA und ABC Dreiblockcopolymer", in *am Fachbereich Chemie und Pharmazie*, der Johannes Gutenberg-Universität Mainz, 1998.

[19] U. Breiner, "Morphologische Studien zum Phasenverhalten mikrophasenseparierter ABC Dreiblockcopolymer", in *am Fachbereich Chemie und Pharmazie*, der Johannes Gutenberg-Universität Mainz, 1996.

[20] T. Goldacker, "Überstrukturen in Mischungen aus Blockcopolymeren", in *im Fach Chemie der Fakultät für Biologie, Chemie und Geowissenschaften*, Univerrsität Bayreuth, 1999.

[21] C. C. Honeker, E. L. Thomas, *Chem. Mater.* **1996**, *8*, 1702.

[22] J. T. A. Kierkels, "Tailoring the Mechanical Properties of Amorphous Polymers", Technische Universiteit Eindhoven, 2006.

[23] B. J. P. Jansen, S. Rastogi, H. E. H. Meijer, P. J. Lemstra, *Macromolecules* **2001**, *34*, 4007.

[24] A. Böker, H. Elbs, H. Hänsel, A. Knoll, S. Ludwings, H. Zettl, A. V. Zvelindovsky, G. J. A. Sevink, V. Urban, V. Abetz, A. H. E. Müller, G. Krausch, *Macromolecules* **2003**, *36*, 8078.

Chapter 05

Anionic Polymerization of SBM Triblock Terpolymers

5.1 Synthesis of SBM in THF

The SBM triblock terpolymers were synthesized in THF by sequential addition of the monomers to obtain higher microstructure of 1,2- polybutadiene. It was already mentioned in chapter 03 that the ability of forming block copolymer depends strongly on the stability of the carbanionic chain ends and the completeness of the monomer conversion of each block. Hence, the triblock terpolymers were synthesized according to the following procedure. 500 ml of THF (2 days refluxed over potassium) were collected in a reactor and then pre-treated with ~8 ml *sec*-BuLi at -30 °C. When the color of the solution turns yellowish and does not change at least for 30 minutes, then the solution is supposed to be free of impurities. The solution was slowly stirred overnight at 20 °C to obtain the alkoxide additives as discussed in chapter 03. On the next day the solution is supposed to be colorless.

The synthesis was started with styrene homopolymerization as a first block because of the high nucleophilicity of the styrene carbanion.[1] As a typical example, freshly distilled styrene (12.62 ml, 110 mmol) was added to the pretreated THF at -65 °C and the polymerization was initiated by 0.5 ml (0.7 mmol) *sec*-BuLi. The solution turned to yellowish indicating the livingness of the S chains. As a next step, 19 ml (232 mmol) butadiene were added to the living S-anion at -65 ^{0}C and the solution was slowly warmed up to -10 °C. The color of the solution became light yellowish. The reaction was allowed to continue at this temperature for 4-5 hours to ensure the conversion of all butadiene that was present in the system. Before adding MMA, the living chain ends of the polybutadiene were capped with 0.8ml (4.5 mmol) of 1,1 diphenylethylene (DPE) at -30 °C in order to reduce the reactivity. The instantaneous red color in the solution clearly indicated the presence of living diphenylmethane anion. The reaction was kept for additional 30 minutes at this temperature and then the solution was cooled down to -70 °C for MMA polymerization. The color of the solution instantly disappeared when 12 ml (112 mmol) MMA was added. After one hour, a mixture of MeOH and HCl (20 ml) were used to terminate the reaction. The precursors of S, SB diblock and SBM triblock were collected throughout the reaction for further investigations using ^{1}H-NMR and GPC. The overall reaction scheme is given as follows:

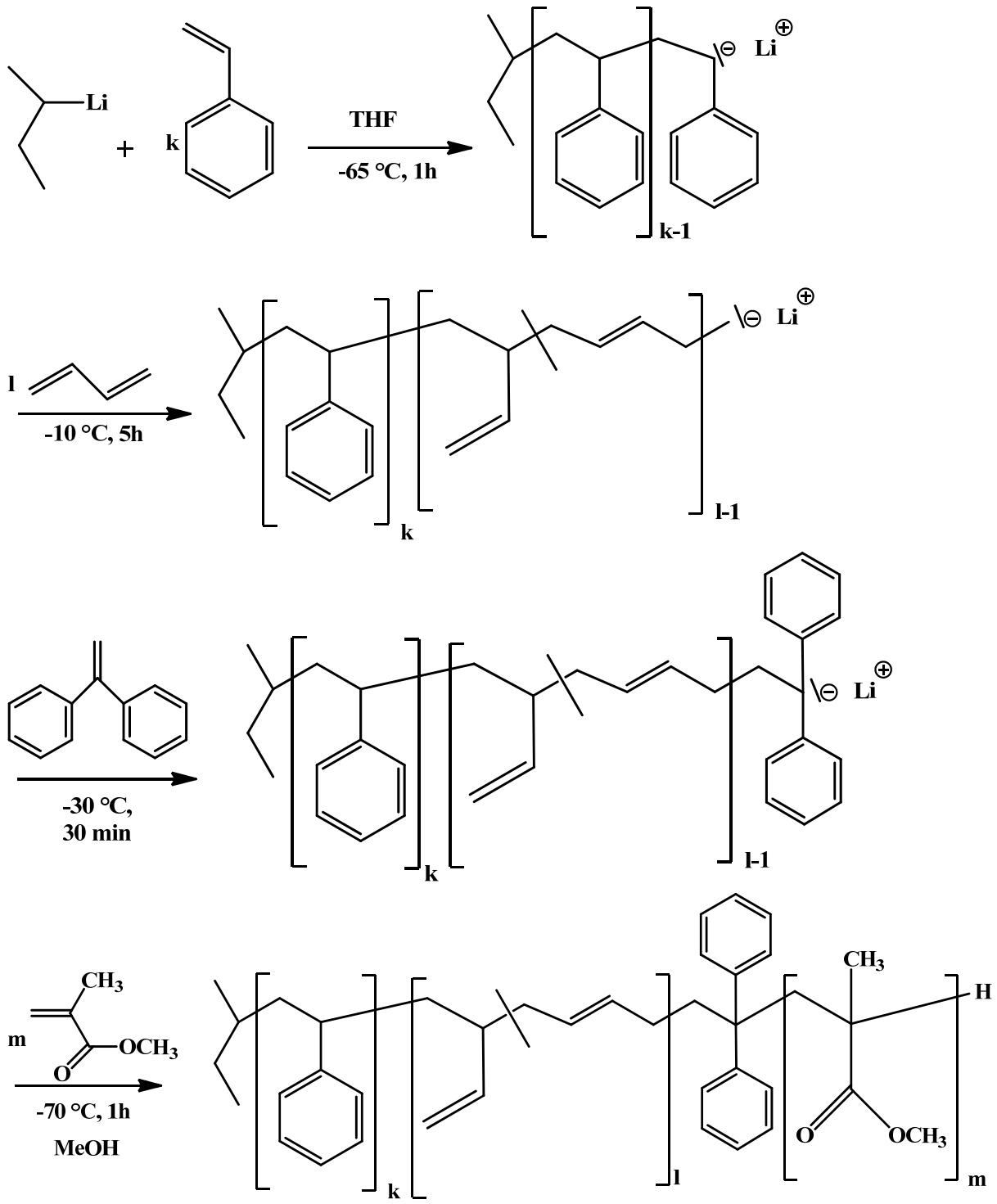

Scheme 5.1*: Reaction scheme of SBM triblock synthesis in THF.*

5.1.1 ^{1}H-NMR

The compositions of the different polymer blocks were calculated from ^{1}H-NMR spectra. $CDCl_3$ was used as NMR solvent. As the microstructure of polybutadiene (B) was the main focus of the investigation, only the characteristic signals of B are shown in Figure 5.1.

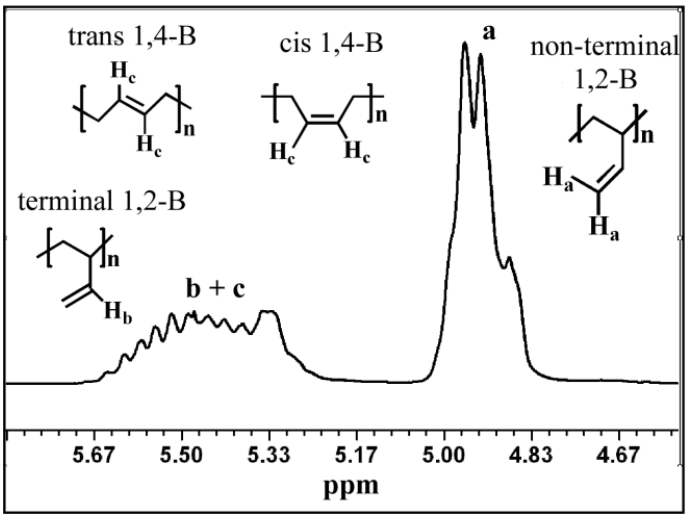

***Figure 5.1**: ^{1}H-NMR spectra in $CDCl_3$. The range of the spectra was highlighted from 4.7 to 5.7 ppm only to show the polybutadiene units. The synthesis was performed in THF.*

Here, the broad peaks between 5.2 and 5.67 ppm correspond to the two protons of the double bond of 1,4- unit (marked as c) and one proton of the vinyl group of 1,2- unit (marked as b). The other two vinyl protons of 1,2- unit appeared between 4.7 and 5.1 ppm (marked as a). From the two butadiene signals the ratio of 1,2- and 1,4- isomers as well as the weight fraction of polybutadiene blocks were determined. The different polybutadiene microstructures were calculated from ^{1}H-NMR spectrum by using Equation 3.15 in chapter 03. The final product contains almost 90% of 1,2-B and 10% of 1,4-B. The proton signals of the remaining blocks were already described in section 4.1, chapter 04.

5.1.2 GPC

The molar mass and the polydispersity of the polymers were obtained from GPC. At an elution volume ranging from 25.5 to 32.5 mL, three peaks were detected, see Figure 5.2. The first peak emerged from 29 to 32.5 mL elution volume due to the contribution of S homopolymer. The presence of S homopolymer was confirmed by the ratio of UV (λ= 254 nm)/RI. The typical value of the UV/RI ratio was found to be 0.35 for S. The diblock copolymer of SB was detected by the peak between 26.5

and 31 mL in the figure. The final product, SBM, was found at the elution volume ranging from 25.5 to 29 mL. From GPC, only the M_n and M_w of the PS precursor can be obtained in the "correct" way as only a polystyrene calibration curve was available. Hence, the absolute molar mass of S is M_n = 15 kg/mol. On the other hand it was taken as an apparent value for diblock and triblock, e.g., M_n^{app} = 39 kg/mol for SB diblock, and M_n^{app} =54 kg/mol for SBM triblock.

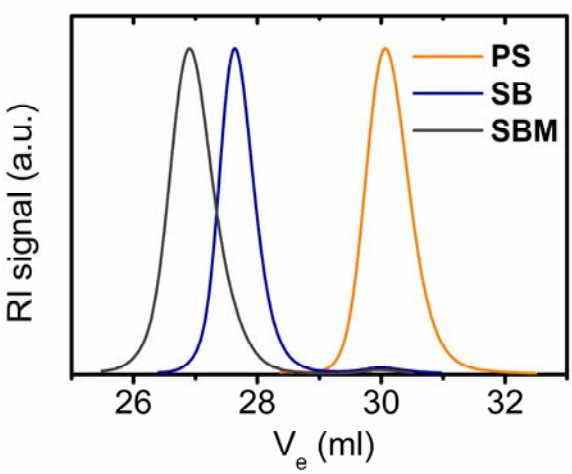

Figure 5.2: *Idealized GPC elugram (RI-signal) showing the, S homopolymer (—), SB diblock (—) and the SBM triblock (—). Note, that part of the peaks overlap. To improve the visibility, all elugrams are normalized to their maxima.*

The number average molar masses of S, SB and SBM are shown in Table 5.1. The results were obtained by a combination of ^{1}H-NMR and GPC analysis (see section 10.4 in appendix C). Significant differences of the molar masses can be noticed in the results. This is due to the differences in the methodic approach of ^{1}H-NMR and GPC analysis. Due to S calibration apparent molar masses were obtained from GPC measurement, whereas absolute molar masses were obtained from ^{1}H-NMR calculations.

Table 5.1: *Molecular weights as calculated from GPC and ^{1}H-NMR data.*

Method	**S (kg/mol)**	**SB (kg/mol)**	**SBM (kg/mol)**
GPC (1)	15	40	55
NMR(2)	-	30	49

(1) GPC data (apparent values, S calibration)
(2) GPC and 1H-NMR

5.2 Synthesis of SBM in Toluene

The polymerization of MMA in a non-polar solvent is not straight forward as described in chapter 03. An Al catalyst is needed to be introduced during MMA polymerization. The synthesis of Al catalyst is described in the following sections.

5.2.1 Synthesis of Al Catalyst

The following process has been performed to synthesize di[2,6-di(*tert*-butyl)-4-methyl phenoxy]isopropyl aluminium *i*BAl(BHT)$_2$. Commercial triisobutyl aluminium 25 wt% (1.0 M) solution in toluene and 2,6-di-tert butyl-4-methylphenoxy (BHT) were used.

Reaction procedure

A 100 ml schlenk flask with a magnetic stirrer was set up on the vacuum line. 20 g of BHT were transferred into the flask and dried under vacuum conditions for at least 14 hours. 40 ml of triisobutylaluminium were added subsequently to the BHT. The valve of the schlenk flask was kept open for 1 hour in N_2 environment to discharge the isobutane gas produced during the reaction. When no more gas was released, the solution was heated up to 70 °C and stirred overnight. The reaction was allowed to continue until the desired product, *i*BAl(BHT)$_2$, was reached to 98 % of its purity. The reaction pathway is described in the reaction scheme 5.2.

Table 5.2: *The chemical shifts of the different protons of the product,* ***i****BAl(BHT)$_2$, side product, Al(BHT)$_3$, and non-reacted BHT. The results obtained from ^{1}H-NMR spectra.*

symbol	chemical shift/ (ppm)	Interpretation
a	2.3	protons from the *para* methyl group of BHT and the product, *i*BAl(BHT)$_2$
b	2.5	6 protons of the methyl group. These protons are present in the *para* position of phenoxy group of BHT
c	2.15	3 proton of the alkyl group of toluene
d	1.42	18 protons of tert butyl group of BHT
e, f	0.93-1.08	6 protons of alkyl group from isobutyl chain, it's a doublet due to the coupling effect of the adjacent proton of h and k.
g, i	0.66 and 0.26	2 protons from methylene group of isobutyl chain adjacent to Al
h, k	1.9-2.05	Proton multiplett adjacent to 6 alkyl protons (e,f) and 2 methylene protons

		(g,i) of isobutyl group
j	1.8	36 protons of tert butyl group from the product, *i*BAl(BHT)$_2$
l	1.56	protons from the product Al(BHT)$_3$

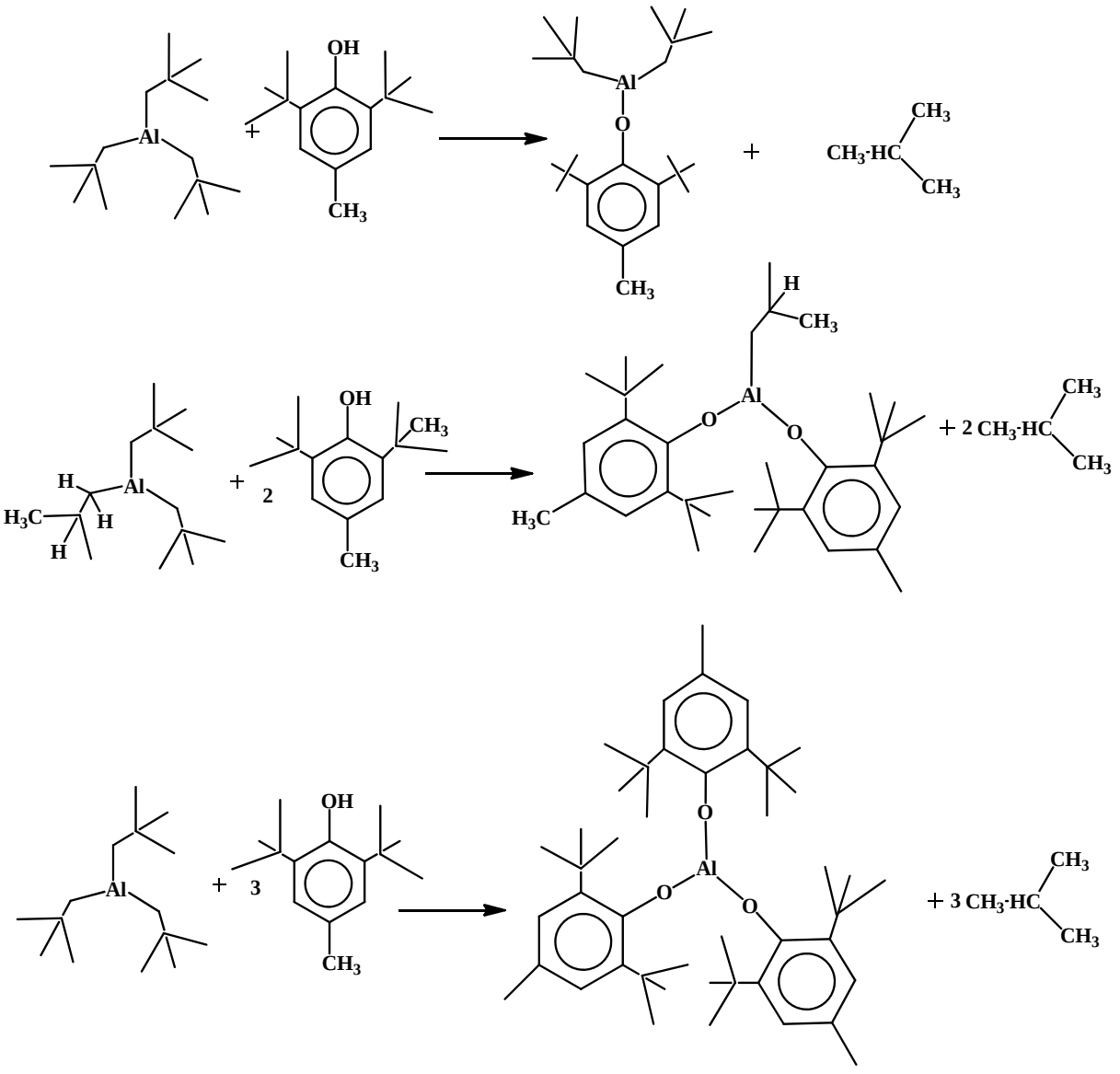

Scheme 5.2: *Reaction scheme of the* ***i****BAl(BHT)$_2$ synthesis from* ***i****B$_3$Al and BHT. First, second and third iso-butylgroup are replaced by the BHT and isobutane gas are released.*

To monitor the conversion of BHT several samples were taken in a dried NMR tube during the reaction. ^{1}H-NMR was done as quickly as possible to avoid any decomposition of catalyst. For this

analysis 0.6 ml d_8-toluene with 0.4 ml typical sample volume was taken in the NMR tube. The NMR of the targeted product *i*BAl(BHT)$_2$, pure BHT and triisobutyl aluminium (*i*B$_3$Al) were integrated and overlaid as shown in Figure 5.3. The chemical shifts of the different protons are given in Table 5.2

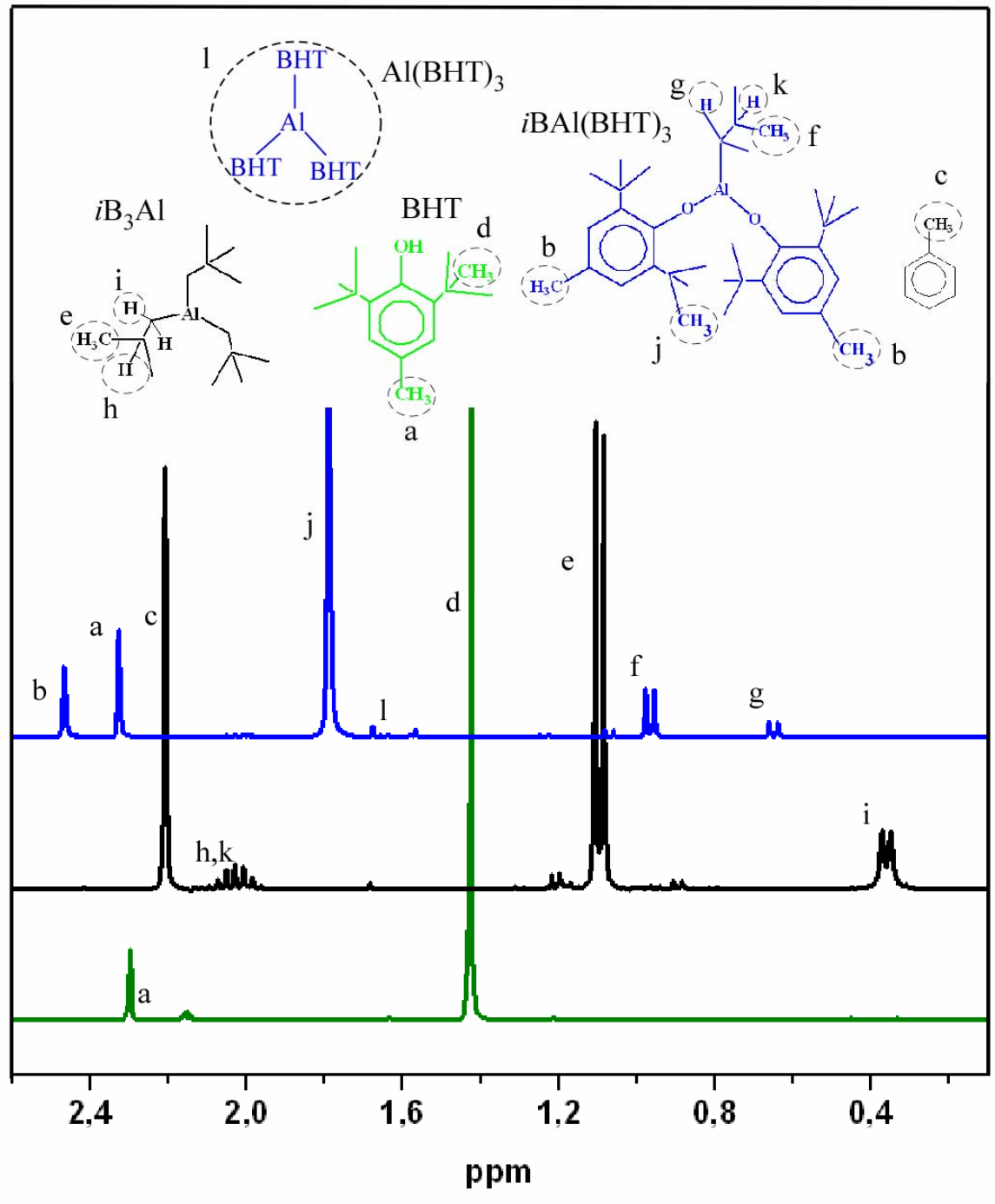

Figure 5.3: *Overlay of the ^{1}H- NMR spectra of BHT, iB$_3$Al and iBAl(BHT)$_2$.*

The sequential product formation during the reaction of BHT and iB$_3$Al are highlighted in Figure 5.4. The conversion of the iB$_3$Al to iBAl(BHT)$_2$ was dominant for the first 3 days and can be observed clearly from the peak between 1.75 and 1.88 ppm. But a new peak, with high intensity (intensity ratio of product and side product is ***1.5 : 1***) was detected at 1.56 ppm after 6 days. This new peak corresponds to the side product, Al (BHT)$_3$. The other side product, iB$_2$Al (BHT) was noticed at 1.67 - 1.7 ppm. When excessive BHT was present, all the three isobutyl groups of iB$_3$Al were substituted by BHT, however, took a long reaction time. The reaction continued even after 28 days at room temperature.

When the catalyst was completely synthesized, toluene, the major part of the solvent, was distilled off. The remaining slurry was stored for several days at 4 °C until the crystals of iBAl(BHT)$_2$ were formed. The catalyst was washed with small quantities of toluene, then re-dissolved in toluene in order to obtain a solution of typical concentration, c = 1 mol /L. The purity of the Al catalyst needs to be around 98% for the synthesis of SBM triblock in toluene. However, in the present case, 93% purity was obtained.

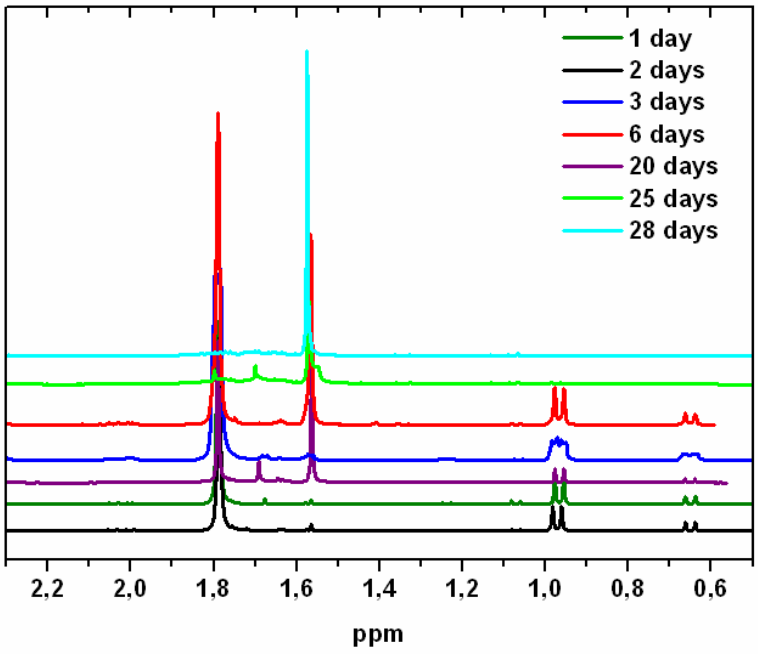

Figure 5.4: *Evolution of ^{1}H-NMR spectra during the formation of iBAl(BHT)$_2$. Note that the signals which can be assigned to the sideproducts increase for extended reaction times.*

5.2.2 Synthesis of SBM in toluene by using Al catalysts

In this approach the toluene was first refluxed over sodium (Na) for at least two days. One day before starting synthesis it was pretreated with a few drops of styrene together with enough *sec*-BuLi. The pale yellowish color was obtained after this treatment, basically due to the presence of styryl anion. The polymerization was started with 14.90 ml (117.60 mmol) freshly distilled styrene. As an initiator 0.3 ml (4.2 mmol) *sec*-BuLi was used. The solution became orange-yellowish due to the presence of living chain end of S. The reaction was continued at 25 °C for 120 minutes for a complete conversion of S. As a second block, butadiene (21.7 ml, 263.57 mmol) was added to the solution at 0 °C. The temperature was increased to 40 °C and the reaction was continued for 4 hours. After certain time the color of the solution turned to light yellowish. A mixture of 9 ml (5.28 mmol) *i*BAl(BHT)$_2$ and 3 ml (28.90 mmol) DME were added to the reaction mixture at -10 °C.[2] Then 15.71 ml (146.85 mmol) of MMA were added to the solution. After this process the color of the solution turned to light green-yellowish. After one hour the solution was heated up to 25 °C and then for another 2 hours the polymerization has been carried on. The reaction was terminated by adding a mixture of MeOH and HCl. Then the polymer was precipitated into isopropanol and dried in *vacuo* at 30 °C for one day. The sample was then supplied for GPC and ^{1}H-NMR measurements. Scheme 5.3 shows the total reaction scheme.

5.2.2.1 ^{1}H-NMR

In Figure 5.5 ^{1}H-NMR spectra in $CDCl_3$ are shown. The protons of the 1,2-B (a) unit appear within 5.1 to 4.8 ppm. The broad peak between 5.4 and 5.2 ppm is detected for the two protons of the double bond of 1,4- unit (c). The remaining proton of the vinyl group of 1,2- unit (b) can be seen at 5.7 to 5.5 ppm. The different polybutadiene microstructures were calculated from ^{1}H-NMR spectrum by using Equation 3.15 in chapter 03. The final product contains almost 88 % of 1,4-B microstructure.

The resulted M was calculated to be 4 wt % by ^{1}H-NMR spectra. However, the target was to obtain 33 wt%, as this amount is required to obtain a lamellar type morphology. That means the Al catalyst/DME mixture was most likely not able to eradicate the aggregated species of the carbonyl group of MMA.

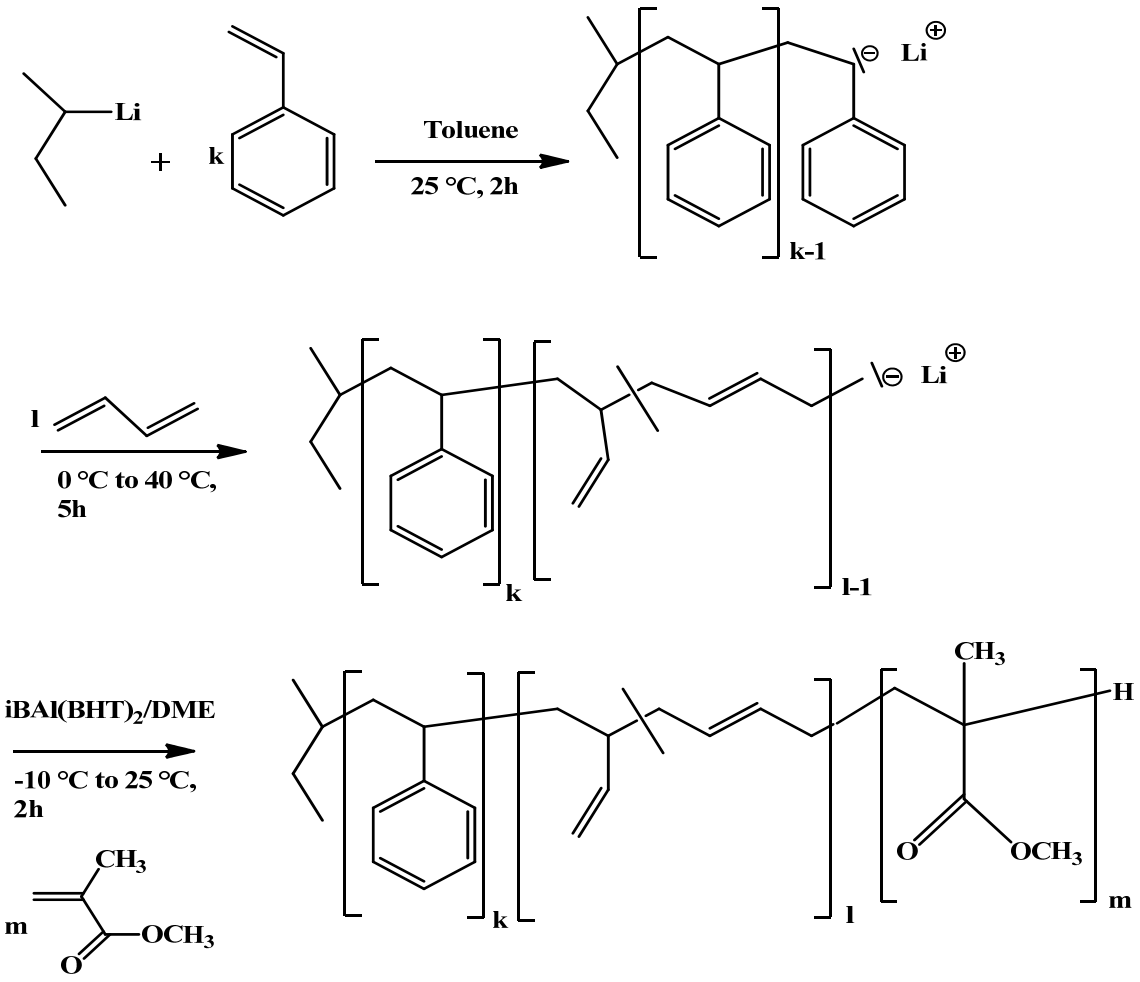

Scheme 5.3: *Reaction scheme for the synthesis of SBM in toluene in the presence of Al catalyst.*

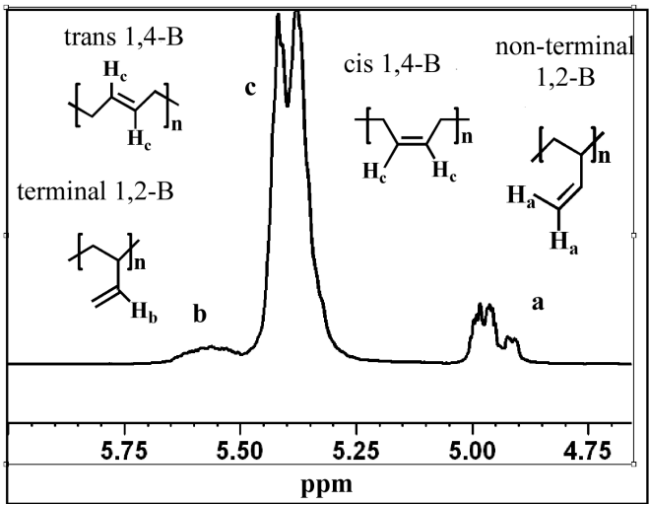

Figure 5.5: *^{1}H-NMR spectra in $CDCl_3$. The range of the spectra was highlighted from 4.7 to 5.7 ppm only to show the polybutadiene units. The synthesis was performed in toluene and in presence of Al catalyst.*

5.2.2.2 GPC

The GPC elugram in Figure 5.6 shows the traces of S precursor at the elution volumes from 27 to 30 mL with a molecular weight (M_n) of 33 kg/mol and polydispersity of 1.03. The overlapping elugrams of the SB diblock and SBM triblock exhibit only slight volume differences due to the formation of very little amount of M block. The apparent molar mass of SBM observed from the GPC is, M_n^{app} (SBM) = 150 kg/mol

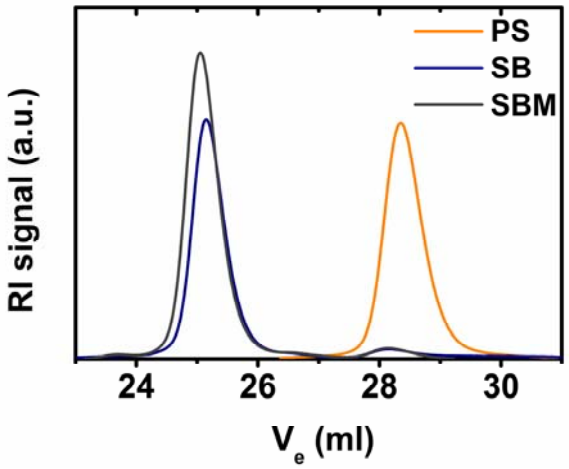

Figure5.6: *GPC elugram (RI signal) of S homopolymer (—), SB diblock copolymer (—) and SBM triblock terpolymer (—). The polymerization was performed in toluene by using the Al catalyst.*

The molar masses of the different blocks were calculated from the combination of GPC and ^{1}H-NMR data. The calculated values are shown in Table 5.3. The values are different mostly due to the differences of the measuring techniques of GPC and NMR.

Table 5.3: *Molecular weight of the different blocks calculated from GPC and ^{1}H-NMR*

	S	**SB**	**SBM**
GPC	33 kg/mol	143 kg/mol[(1)]	150 kg/mol[(1)]
NMR	-	76 kg/mol [(2)]	79 kg/mol[(2)]

(1) GPC data (apparent values, S calibration)
(2) GPC and ^{1}H-NMR

5.3 Synthesis of SBM by combination of polar and non-polar solvents

5.3.1 By using diethyl ether (Et_2O) as co-solvent

The challenges of the SBM polymerization in toluene in the presence of an Al catalyst have been mentioned in the previous section. When no Al catalyst is used, DPE has to be added before the polymerization of MMA. However, in this case the control over the reaction in toluene solution is very poor. The possibility of deactivation of the living chain ends is then very high, especially when the reaction continues for a longer time (overnight). Zune et.al.[3] found by ^{7}Li-NMR investigation that the reaction rate decreases gradually when a small amount of polar solvent is present in the system.[4] They have found that the rate of reaction decreases due to the presence of lithium hydroxide and other salts (LiOH, sBuOLi,….) which are produced during the pretreatment of THF with *sec*-BuLi.

The deactivation of the chain ends occurs during the addition of DPE by the following three possible reactions: i) all living chain ends react with the DPE resulting in a controlled MMA polymerization and a narrow polydispersity, ii) the presence of some non-reactive SB chains and iii) the termination of the SB diblock.

i) $PS\text{-}b\text{-}PB^- Li^+ + DPE \longrightarrow PS\text{-}b\text{-}PB\text{-}DPE^- Li^+$

ii) $PS\text{-}b\text{-}PB^- Li^+ + DPE \longrightarrow PS\text{-}b\text{-}PB\text{-}DPE^- Li^+ + PS\text{-}b\text{-}PB^- Li^+$

iii) $PS\text{-}b\text{-}PB^- Li^+ + DPE \longrightarrow PS\text{-}b\text{-}PB$

To avoid the deactivation of chains and formation of aggregates, the polarity of the reaction medium needs to be increased during DPE addition. Hence, the following procedures are followed.

i) The different propagation rate of the living species has been tackled by adding 10 vol% of diethyl ether (Et_2O) instead of THF. As no other additives were required in case of Et_2O addition, the living carbanions were not deactivated. 5 equiv DPEs have been added for end-capping the living SB chain.

ii) The reaction was continued at ambient temperature until all the living chain ends were completely end-capped by DPE. The duration of the reaction was reported to be 70 to 120 min for a living chain end with a concentration of 0.01M in toluene and with the presence of Et_2O as co-solvent.[3]

iii) The polymer solution was cooled down to -30 °C when the conversion of the living chain ends with DPE were completed. Afterwards, THF was added to the toluene mixture at

-30 °C until the ratio (toluene: THF) = (***1 : 1.5)***. The polarity of the solvent mixture should then be suitable for MMA polymerization.

The reaction scheme is given in below Scheme 5.4.

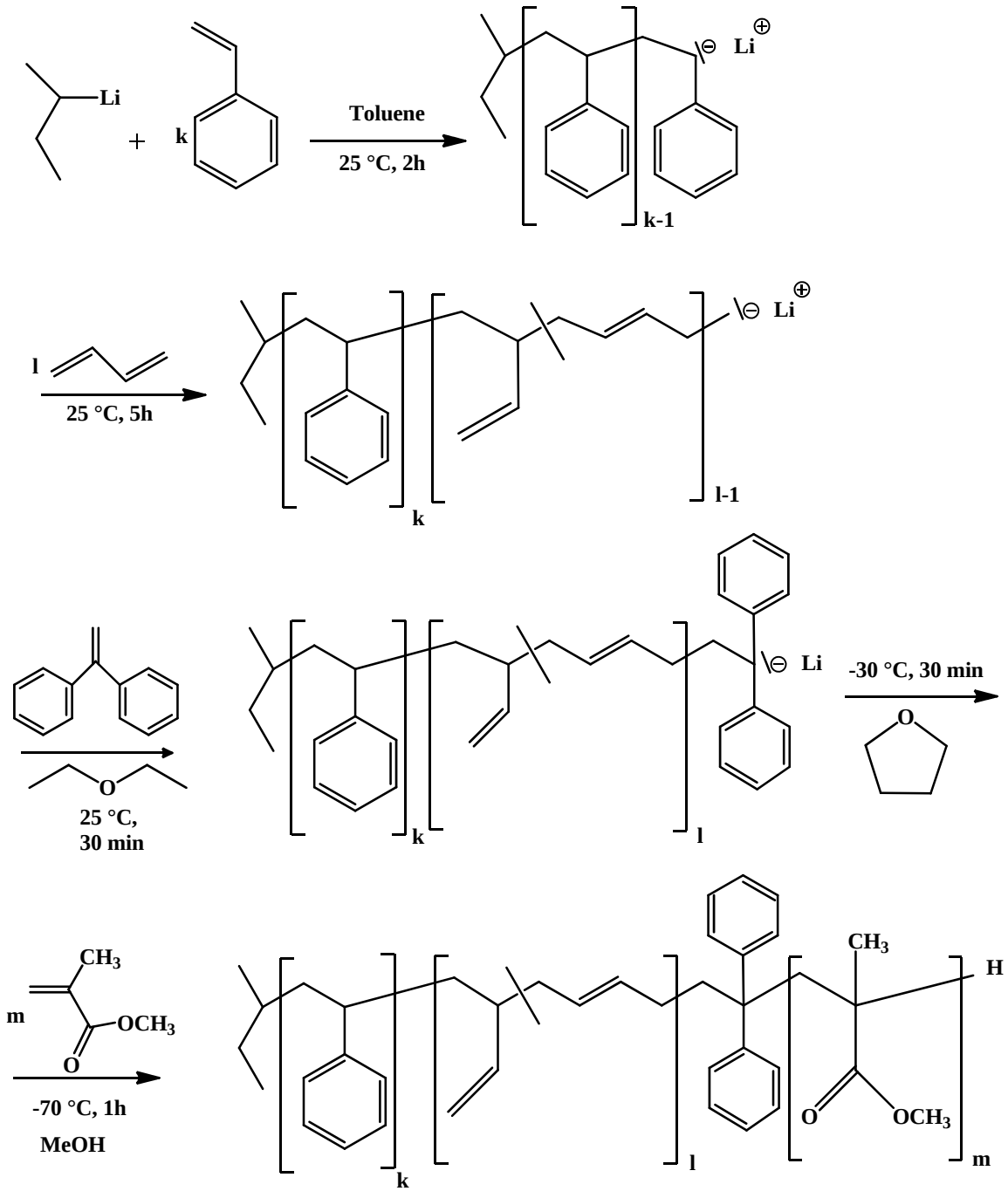

Scheme 5.4: *Synthesis of SBM triblock in a toulene-THF mixture in absence of Al catalyst.*

GPC results

Figure 5.7 shows the elution curve of the S homopolymer at an elution volume ranging from 27.5 to 31 mL. Besides the SB diblock's main peak ranging from 25.5 to 27.5 mL, a small peak at 27.5 to 30 mL is seen resulting from the residual S homopolymer. This termination has occurred during the crossover from styrene to butadiene polymerization. The peak corresponding to the SBM triblock arises at an elution volume ranging from 24 to 30 ml. In the SBM elugram, a large quantity of termination is noticed within 25.5 to 28 mL, the same area of the SB diblock. This termination might occur due to the impurities which were introduced during the addition of DPE, Et_2O, or THF. A long tubing (connector) during the transfer of THF might also introduce the impurities in the solution resulting in unexpected termination. It has to be considered that the conversion of butadiene must be completed before adding DPE and sufficient time has to be allowed for the reaction of SB chain with DPE.

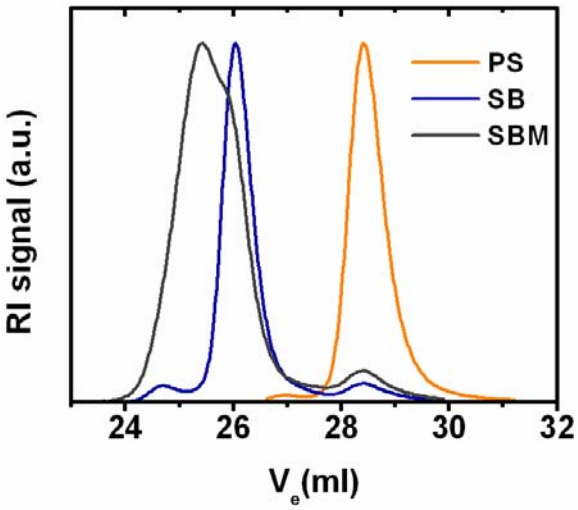

Figure 5.7: *GPC elugram (RI signal) of S homopolymer (—), SB diblock copolymer (—) and SBM triblock terpolymer (—). The polymerization was performed in a mixture of THF and toluene at 1:1.5 volume ratio.*

This technique can only be applied for molar masses up to 150 kg/mol. As described above, the kinetics of the reaction mostly depends on the concentration of active species. When the concentration of active species decreases below 10^{-4} mol/l, particularly for the polymer of high molar mass, some chains are deactivated by unavoidable impurities (i.e. in the nitrogen atmosphere).

5.3.2 Without diethyl ether (Et_2O) as co-solvent

5.3.2.1 Experiment 1 (THF and DPE added at -60 °C)

In every addition steps of the additives and solvents some termination reactions occur. Therefore, to reduce terminations, THF was used as co-solvent at -60 °C. At -60 °C the probability of the side reactions is lower for the control reaction rate. DPE was also added to the solution at the same temperature. In order to study the chain end termination, two SB precursors were collected. The first precursor (SB1) was collected at -60 °C before adding THF. The second precursor (SB2) was collected after adding DPE. The interval between the THF and DPE additions was kept at 5 minutes. Afterwards, DPE was allowed to react at -30 °C for 1 hour and at -60 °C for another 30 minutes. Finally, MMA was polymerized at -60 °C for 1 hour.

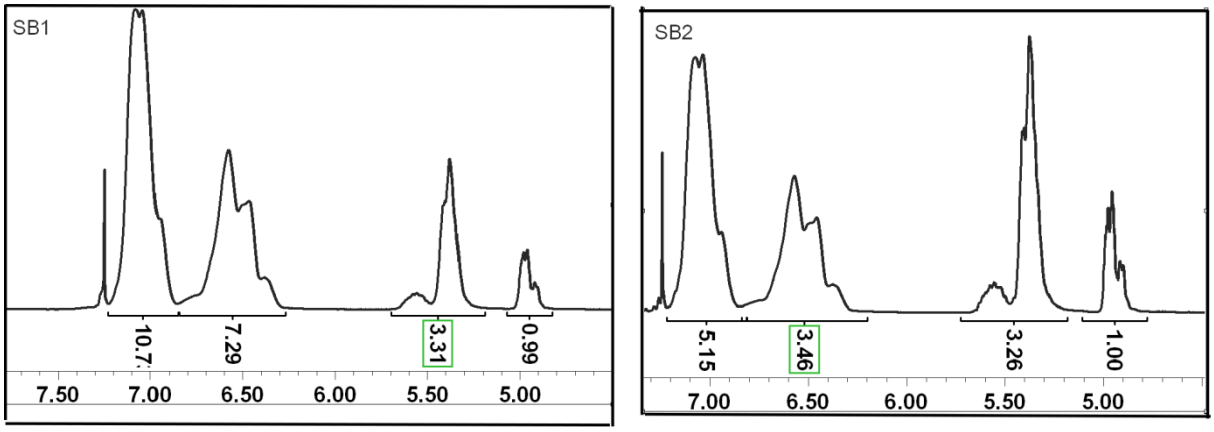

Figure 5.8: *^{1}H-NMR of SB1 (left), collected before addition of DPE and THF. SB2 (right), collected after addition of DPE and THF.*

5.3.2.2 ^{1}H-NMR and GPC Results

The ^{1}H-NMR spectra of the SB1 and SB2 are shown in Figure 5.8. The weight percentages of the different blocks and the percentages of the polybutadiene units were calculated from the ^{1}H-NMR spectra, see Table 5.4. The amount of x_B was calculated to be 21% for SB1, and 36% for SB2. This significant increase of SB indicates the continuation of butadiene polymerization in the polar media, although the reaction has been continued 24 hours in the non-polar media to ensure the consumption of all B chains. Despite the different weight percentage (x_B) of B, both the SB1 and SB2 show 74% of 1,4-polybutadiene microstructure. It needs to be mentioned that in both cases the solvents were identical only the mode of DPE addition was varied. Hence, the same ratio of 1,2 / 1,4 but different

chain length of the SB1 and SB2 are obtained indicating that in the latter case the conversion of polybutadiene was not complete (see Table 5.5).

Table 5.4: *Weight percent of S and B block and polybutadiene microstructures calculated by GPC and ^{1}H-NMR.*

Sample	**x_S (%)**	**x_B (%)**	**1,2- (%)**	**1,4- (%)**
SB1	77	21	26	74
SB2	64	36	26	74

Table 5.5: *Molar masses and polydispersity of different blocks calculated by GPC and ^{1}H-NMR.*

Sample	**M_n (kg/mol)**	**M_w (kg/mol)**	**PDI**
S	130	137	1,06
SB1	161	326	1,43
SB2	221	326	1,47
SBM	234	364	1,56

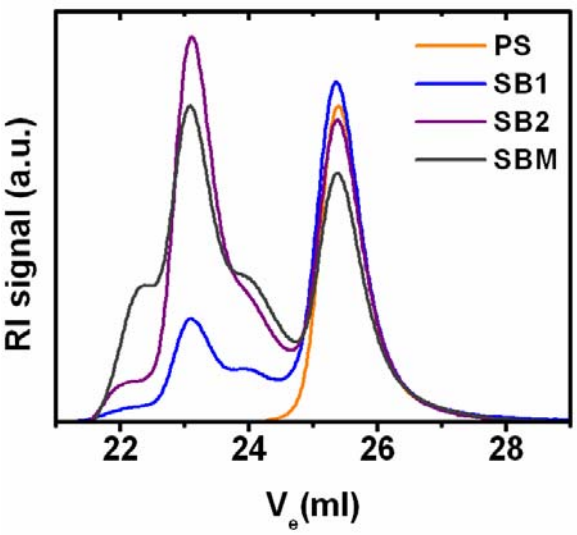

Figure 5.9: *GPC elugram (RI signal) of SBM triblock terpolymer with S homopolymer and SB diblock copolymer. Polymerization was performed in THF-toluene mixtures where THF and DPE were added at -60 °C.*

Figure 5.9 shows the GPC elugram of multimodal peak of the triblock, indicating the terminations during the cross-over reaction from butadiene chain end to MMA. The S is located at the elution

volume range from 24 to 28 mL. But three multimodal peaks are observed in the SB1 elugram. Almost 67% S and 24% SB diblock were calculated (deconvolution using *Gaussian curve*) (see section 10.5 in appendix D). The amount of diblock fraction increases up to 45% in SB2, which also supports the continuation of the butadiene polymerization in THF.

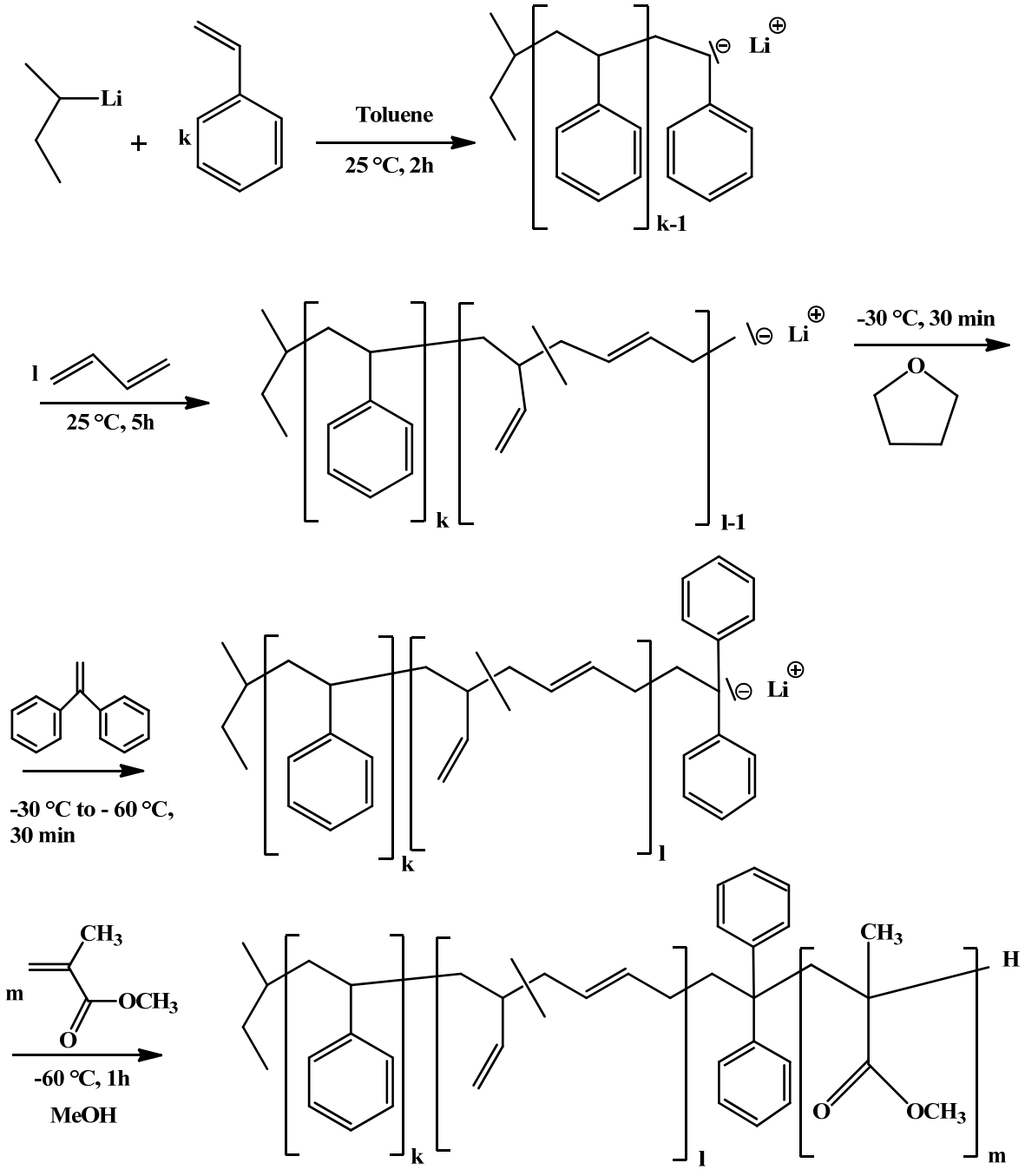

Scheme 5.5: *Reaction scheme of SBM in presence of THF and toluene mixture. THF and DPE were added at -30°C.*

5.3.2.3 Experiment 2 (THF and DPE added at -30 °C)

In experiment 1 it has been shown that the THF and DPE addition at a very low temperature (-60 °C) during synthesis cannot be suppressed the termination. In the present experiment, THF and DPE were added at -30 °C to obtain better results. A SB precursor was collected before adding MMA (see scheme 5.5).

5.3.2.4 ^{1}H-NMR and GPC Results

Figure 5.10 shows the GPC elugram and ^{1}H-NMR of the resulted polymer. The GPC traces show no S or SB diblock impurities in the final product. The molar mass and the polydispersity obtained from the GPC agreed very well with the calculated data (50 kg/mol). From ^{1}H- NMR, the resulting weight fractions of different blocks are almost same with the aimed value (see Table 5.6). The 1,4- PB microstructure is calculated 84%.

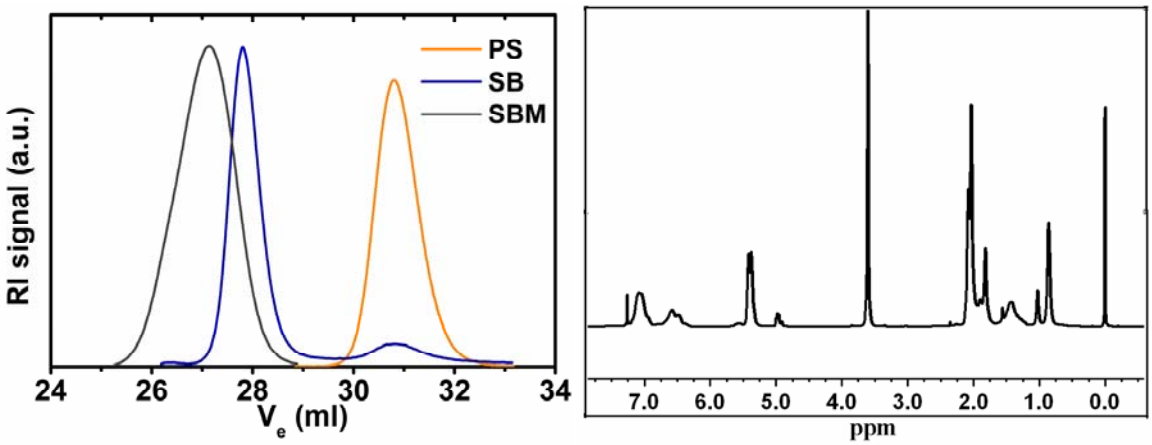

Figure 5.10: *GPC elugram (RI signal) of S homopolymer (—), SB diblock copolymer (—), SBM triblock terpolymer (—) and ^{1}H-NMR spectra of SBM. Polymerization was performed in a THF / toluene mixture.*

Table 5.6: *Molar masses, weight fractions of different blocks and the contents of B microstructures are obtained from GPC and ^{1}H-NMR.*

Sample	**M_n (kg/mol)**	**M_w (kg/mol)**	**PDI**
PS	11	12	1,03
SB	29	35	1,24
SBM	54	57	1,06

Sample	x_S (%)	x_B (%)	x_M (%)	1,2- B (%)	1,4-B (%)
SBM	30	30	40	16	84

5.4 Purification techniques of SBM triblock

In most cases the anionic polymerization of the SBM triblock terpolymer leads to a few terminations. The blend of homopolymer or diblock copolymer is present with the desired triblock terpolymer. The purity can be achieved by separating the residual blocks from the final product. Several works have been published where various techniques have been introduced for triblock purification. [5-11] In this work the following methods were applied for SBM purification.

5.4.1 Thin Layer Chromatography (TLC)

In this method several drops of high concentrated SBM polymer solution were placed one centimeter above the base of TLC plate as shown in Figure 5.11 (a). The solvents were chosen according to the composition of the SBM triblocks. Gankina et al.[12] reported that benzene was good solvent in a diblock copolymer of polystyrene-*b*-poly(methyl methacrylate) (SM). The S shows highest migration, whereas the M remains at the beginning. Again, in a mixture of chloroform and methyl ethyl ketone (MEK), the block copolymer can be separated from the M homopolymer. The difficulties arise when the polarity of the polymers are similar, for example, in the case of S and B. Both the homopolymers are easily soluble in cyclohexane-toluene mixture. Nevertheless, the B phases move faster than the S at a lower toluene concentration in eluent and separates first from the SB mixture.

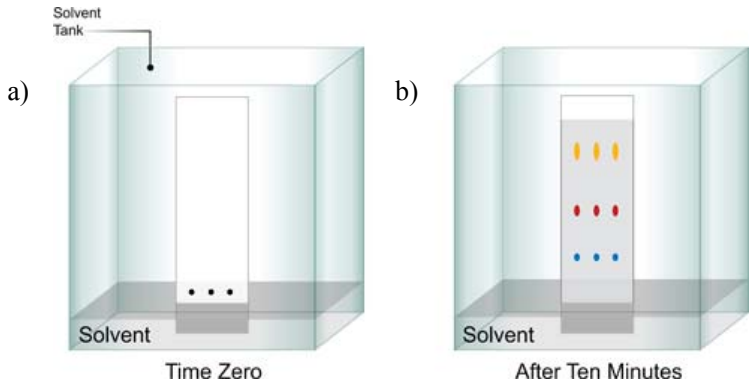

Figure 5.11: *Schematic sketch of the TLC method. a) the black drops are the polymer solution, b) the solvents are mixed with the polymer solution and depending on the solubility parameter, different blocks are migrated along the stationary phase.*

When the TLC plate was placed in the solvent, the SB was moved faster as well as the S along the stationary phase. Therefore, the SBM triblock was remained at the bottom of the plate (Figure 5.11 b). The plate was then taken out from the jar and dried slightly with the heatgun until the black spots appeared on the plate. Then the retention factor (R_f) was calculated by Equation 5.1 to determine the solvent polymer interaction behavior for a particular polymer system.

$$R_f = \frac{\boldsymbol{migration\ distance\ of\ polymer}}{\boldsymbol{migration\ distance\ of\ solvent\ front}} \qquad \text{Equation 5.1}$$

When this technique was used in SBM triblock system, very long time was needed for purifying the polymer. Hence, the following method was attempted.

5.4.2 Adsorption Chromatography Method

A chromatography tube was uniformly packed with cotton and then filled with aluminum oxide as an adsorbent. The adsorbent was 25 – 50 (vol.%) times more than the polymer sample. As a top layer very fine and clean sand were used. The column was rinsed five to ten times with cyclohexane before pouring the polymer solution (see Figure 5.12). The polymer solution was absorbed by the layers of sand and aluminum oxide. The column was then rinsed several times with 100 ml cyclohexane. As a result the easily dissolved polymer blocks in cyclohexane elute separate at first and then the partially dissolved parts. The solution coming out through the adsorption layer was collected. All the collected samples were then precipitated, filtrated, dried, and analyzed by GPC. The disadvantage of this method is, only a low amount (few mg) of polymer sample can be separated.

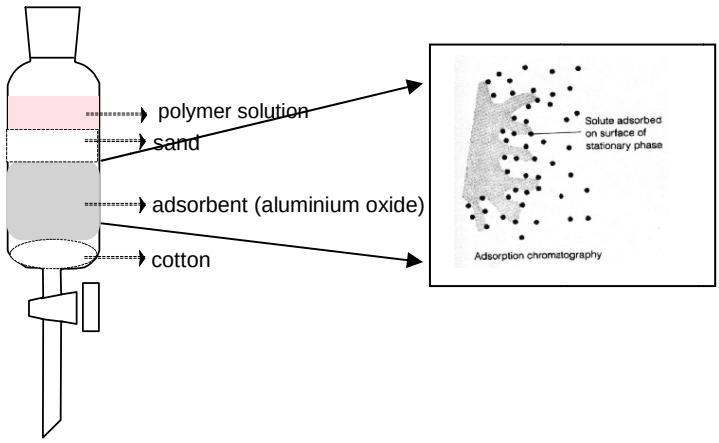

Figure 5.12: *Schematic sketch of adsorption chromatography.*

5.4.3 Mixtures of two different solvents

Jung et al.[13] have reported a method of separation residual S and SB blocks where a combination of different solvents was used. Following their work, in the present work five different mixtures of cyclohexane and isopropanol, 10:90 …. 50:50 were used to purify the polymer at a concentration of 0.4 g/L. Two experiments were performed, one at room temperature and the other at 80 °C. For the first experiment, the SBM triblock was dissolved in cyclohexane and the solution was stirred overnight at room temperature.

As the S and SB are dissolved in cyclohexane, the non-dissolved parts should be the purified triblock. However, from GPC elugram, no significant improvements of the purification are seen (see Figure 5.13 a). For the second experiment, the SBM solution was used in the solvent ratios 20:80, 50:50 and 80: 20 at 80 °C. However, only the solvent ratio 20:80 showed a very little amount of purified triblock (Figure 5.13 b). This technique was also not suitable for purifying the SBM triblock at a large scale.

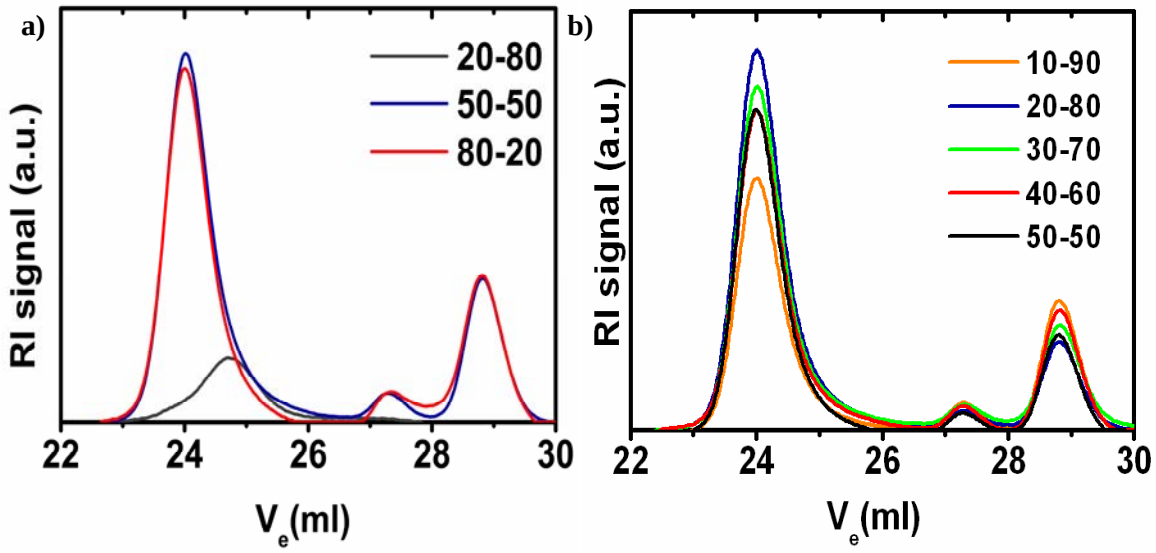

Figure 5.13: *GPC elugrams (RI signal) of the SBMs purified with cyclohexane and isopropanol at different volume ratios. (a: without any temperature, b: applying temperature at 80 °C).*

5.4.4 Using theta (Θ) solvent

In most cases, the theta solvent is used to purify the SBM triblocks. In general the cyclohexane is used as the theta solvent for polystyrene at 34 °C, the *n*-heptane is used at -1 °C for polybutadiene (1,4- cis 97%), and the acetone is used at -126 °C for poly(methyl methacrylate). In this work cyclohexane was

kept at 60 °C for 4-5 hours. After this treatment the residual S homopolymer and SB diblock were dissolved in the solvent and were separated off. The insoluble parts were rinsed 3-4 times with cyclohexane and dried at 30 °C in vacuum. For the *n*-heptane solvent it was kept 110 °C for 18-20 hours. After cooling down the solution, the insoluble parts were filtered and separated. This solvent is generally used depending on the weight fraction and the molar mass of the polymers. The acetone was used as a separated solvent when M content was higher in SBM. The SBM part was dissolved in acetone and came out with the solvent. The solvent was then partly removed by using rotavapor and the remaining parts were precipitated in methanol.

In Figure 5.14 the GPC elugram is shown where one can see almost all the SB impurities were removed from the crude triblock by using theta solvent method. This technique is less time consuming and high amount of SBM can be purified (10-15 g) at a time.

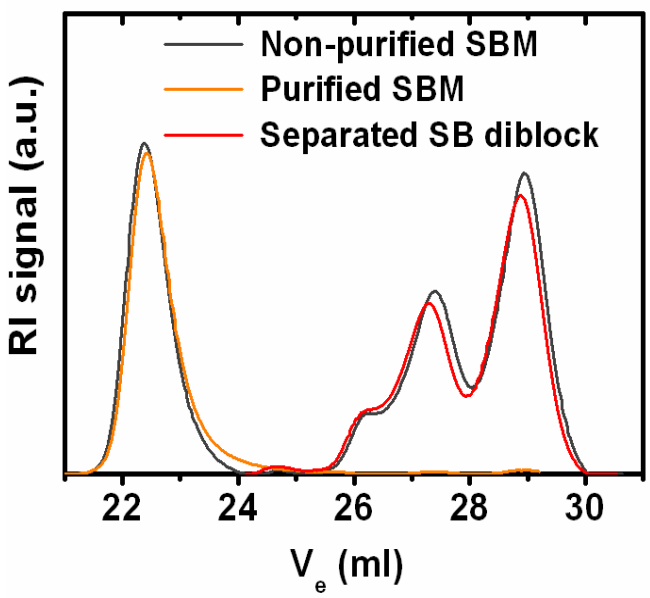

Figure 5.14: *GPC elugram (RI signal) of purifying SBM (—), non-purifying SBM triblock (—) and the separated SB diblock (—) by using theta solvent (cyclohexane).*

Reference

[1] H. L. Hsieh, R. P. Quirk, "*Anionic Polymerization- Principles and Practical Application"*, Mercel Dekker, New York, 1996.

[2] H. Ruckdäschel, J. K. W. Sandler, V. Altstädt, C. Rettig, H. Schmalz, V. Abetz, A. H. E. Müller, *Polymer* **2006**, *47*, 2772.

[3] C. Zune, P. Dubois, R. Jerome, T. Werkhoven, J. Lugtenburg, *Macromol. Chem. Phys.* **1999**, *200*.

[4] C. A. Ogle, S. L. Wang, *Polym. Prepr. (Am. Chem. Soc., Div. Polym. Chem.)* **1992**, *33*, 190.

[5] S. Ritzenthaler, F. Court, E. G. Reydet, L.Leibler, J. P. Pascault, *Macromolecules* **2003**, *36*, 118.

[6] H. Königsmann, "Kinetische Untersuchungen zur Synthese von Blockcopolymeren mit Methacrylatsegmenten durch neue anionische Polymerisationssysteme", in *am Fachbereich Chemie und Pharmazie*, der Johannes Gutenberg-Universität Mainz, 2001.

[7] L. Corte, K. Yamauchi, F. Court, M. Cloitre, T. Hashimoto, L. Leiber, *Macromolecules* **2003**, *36*, 7695.

[8] B. Jaffrennou, J. Portal, F. Méchin, J. P. Pascault, *European Polymer Journal* **2008**, *44*, 3439.

[9] T. Goldacker, "Überstrukturen in Mischungen aus Blockcopolymeren", in *im Fach Chemie der Fakultät für Biologie, Chemie und Geowissenschaften*, Univerrsität Bayreuth, 1999.

[10] S. Ritzenthaler, F. Court, L. David, E. G. Reydet, L.Leibler, J. P. Pascault., *Macromolecules* **2002**, *35*, 6245.

[11] D. Yamaguchi, M. Cloitre, P. Panine, L.Leibler, *Macromolecules* **2005**, *38*, 7798.

[12] E. S. Gankina, I. I. Efimova, J. J. Kever, B. G. belenkii, *Talanta* **1987**, *34*, 167.

[13] K. Jung, "Polybutadien-*block*-polystyrol-*block*-polymethylmethacrylat-Dreiblockcopolymere-Vom Spiel mit der Monomersequenz zu nicht-zentrosymmetrischen Schichtstrukturen." in *an Fachbereich Chemie und Pharmazie*, der Johannes Gutenberg-Universität Mainz, 1996.

Chapter 06

Influence of the Polybutadiene Microstructure on the Morphology and the Mechanical Properties of Lamellar Type SBM Triblock Terpolymers

6.1 Introduction

Block copolymers have been widely studied for their ability of tailoring the chemical and mechanical properties by adjusting their constituent blocks. Depending on the weight fractions and the interfacial tensions of the blocks, the morphologies can be varied between spherical[1], cylindrical[2], lamellar[3], or helix[4] as well as gyroid, knitting pattern[5] and some complex morphologies that are absent in the linear ABC triblock as described elsewhere.[6] Considering the volume fractions of the three blocks, Arai et al.[7] obtained a lamellar morphology consisting of polystyrene-*b*-polybutadiene-*b*-poly(4-vinylpyridine) (SBVP) with the volume fraction ratio of $\phi_S : \phi_{B} : \phi_{P4VP}$ =1.0: 1.28: 1.52. Further investigation on the dimensions of the lamellar domains were described by Mogi and his coworkers[8] where the triblock copolymer of polyisoprene-*b*-polystyrene-*b*-poly(2-vinylpyridine) with the volume fraction ratio of $\phi_I : \phi_S : \phi_{P2VP} = 1 : 1 : 1$ was in the focus. Auschra et al.[9] described a lamellar pattern of polystyrene-*b*-polybutadiene-*b*-poly(methyl methacrylate), $S_{24}B_{38}M_{38}^{245}$ triblock and its hydrogenated analogue polystyrene-*b*-poly(ethylene-*co*-1-butene)-*b*-poly(methyl methacrylate), $S_{24}EB_{38}M_{38}^{248}$. Both the polymers contain very high molar mass at a volume fractions ratio $\phi_S : \phi_{EB} : \phi_M = 1.0 : 1.58 : 1.58$. The first small angle X-ray scattering (SAXS) patterns of a lamellar morphology of a triblock terpolymer containing polystyrene-*b*-poly(4-vinylbenzyl dimethylamine)-*b*-polyisoprene were investigated by Shibayama et al.[10] Later on Breiner et al.[11] investigated the effects of polybutadiene hydrogenation on the symmetric, non-symmetric and the mixed lamellar patterns of SBM's morphology by transmission electron microscopy (TEM) and SAXS. The influence of blending the lamellar SBM triblocks with SB diblocks as well as the influence of changing the block sequence from SBM to BSM on the morphological pattern were reported elsewhere.[12, 13] The correlation of the mechanical properties and the morphologies of SBM and SBS were performed by Brinkmann et. al.[3] However, very few data are available where the mechanical properties of different lamellar SBM morphologies are discussed. As the rubbery polybutadiene domains consist of two different microstructures, according to Honeker et al.[14] the polymers properties will strongly be affected by the polybutadiene microstructures. .

As we can see from the above literature review that the influences of polybutadiene microstructure on the morphology and the mechanical properties were hardly discussed, hence, in present work the correlation of B microstructure and mechanical properties of SBM triblock terpolymers were investigated. For this, different subtypes of the lamellar SBMs containing 1,2- and 1,4-B microstructures were chosen.

In the first section of this chapter, the morphologies of lamellar type SBMs are classified and characterized with TEM and SAXS techniques. Moreover, differential scanning calorimetry (DSC) and dynamic mechanical analysis (DMA) are employed to analyze the thermal property and segregation behavior of the polymers. Five different morphologies are categorized as follows:

i) well segregated lamellae

ii) well segregated but short domain size lamellae

iii) mixed lamellae

iv) chain like oriented lamellae and

v) transitional lamellae.

In the second section, the mechanical properties are investigated for all subtype lamellar patterns. These properties are then correlated with the morphologies and polybutadiene microstructures. The results are divided into following two categories:

i) symmetric type having the same weight fraction of the blocks, and

ii) asymmetric type having the higher poly(methyl methacrylate), (M) than the polystyrene (S) and the polybutadiene (B).

The mechanical properties of a polymer are influenced by various factors, e.g., varying morphologies, total molar mass, chain topology as well as the solvents used for sample preparation.[3, 14] In SBM triblock terpolymers, the polybutadiene block is usually a combination of 1,2- and 1,4-isomers. Depending on the chain length, the B microstructure has an enormous influence on the polymers properties. In Figure 6.1 the microstructures of polybutadiene (1,4-B and 1,2-B) are shown. In a 1,4-B microstructure four carbon atoms exist in the back bone whereas in a 1,2-B microstructure two carbon atoms are present in the backbone and the remaining two stay as a pendant group. Depending on the presence of 1,2-B and 1,4-B, different thermal properties can be obtained. The glass transition temperatures (T_g) vary significantly for 1,2-B and 1,4-B, e.g., T_g,(1,2-B) = -12 °C and T_g (1,4- B) =

-90 °C. These structural and thermal differences in B microstructures influence the polymer properties significantly.

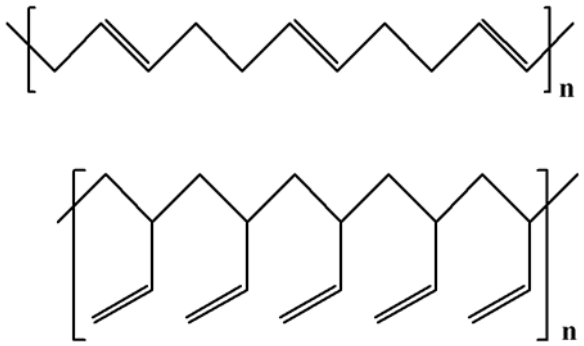

Figure 6.1: *Structural formula of 1,4- (top) and 1,2- (below) polybutadiene .*

The thermodynamic behavior (e.g., the interaction parameter, solubility parameter or the cohesive energy density) between the different blocks plays an important role in the formation of morphology. In Table 6.1, differences in the cohesive energy density of the three blocks of SBM are given. The relation between cohesive energy density (CED) and the solubility parameter, δ, is given in Equation 6.1.

$$\delta = \frac{\sqrt{\Delta E}}{V} \qquad \text{Equation 6.1}$$

The solubility parameters of two substances are directly related to their interaction parameter which is expressed by Equation 6.2.

$$\chi_{AB} \propto (\delta_a - \delta_b)^2 \qquad \text{Equation 6.2}$$

According to Flory-Huggins-Staverman enthalpic segmental interaction parameters, Equation 6.2 can be expressed as follows

$$\chi_{AB} = \frac{v}{RT} (\delta_a - \delta_b)^2 \qquad \text{Equation 6.3}$$

Here, *v* is the geometric average of the molar segmental volume calculated from the densities at room temperature. *RT* is the molar thermal energy at a given temperature. The solubility parameter δ is taken from Table 6.1. For the Flory- Huggins interaction parameter, the following values are obtained at 25 °C: χ_{SB} = 0.0623, χ_{BM} = 0.1029 and χ_{SM} = 0.0411.[3]

Above stated thermodynamic parameters indicate that for two nearly identical substances the enthalpy of mixing (cf. Equation 2.2, chapter 2) will approach zero and the mixing process is entirely entropy driven, as $\Delta G = - T\Delta S$ (cf Equation 2.1 chapter 2). The final substance will be then miscible.

Table 6.1*: Comparison of the differences of the cohesive energy density of the polymer pairs present in SBM for 1,2- and 1,4- B isomers.*[3]

Polymer pair	**1,4-B** $(\delta_A - \delta_B)^2$ **in [cal/cm^3]**	**1,2- B** $(\delta_A - \delta_B)^2$ **in [cal/cm^3]**
S/B	0.49	1.10
B/M	0.81	1.56
S/M	0.04	

Table 6.2 : *The solubility parameters of different blocks of SBM triblock*[15]

Polymer	**Polystyrene**	**1,4-polybutadiene**	**1,2-polybutadiene**	**Poly(methyl methacrylate)**
Solubility parameter δ $[MPa]^{1/2}$	9.10	8.40	8.05	9.30

Table 6.3: *Solubility parameters of different solvent*[15]

Solvent	**Chloroform**	**Toluol**	**THF**
Solubility parameter δ $[MPa]^{1/2}$	9.30	8.90	9.10

According to Table 6.2, poly (methyl methacrylate), M, has the highest solubility parameter, while polybutadiene, B, has the lowest value. Furthermore, from Table 6.1 one can see that the differences in the cohesive energy density of 1,4- B is considerably lower than the cohesive energy density of 1,2- B. As a result, the incompatibility of both the end blocks S and M with the 1,4- B is stronger. This leads to a stronger segregation in 1,4-B containing SBM's compared to the 1,2- B ones. However, the cohesive energy density between S and M is much lower compared to the cohesive energy between S and B or M and B. Therefore, segregation of S and M can be observed.

According to Table 6.1 and 6.2, the presence of 1,2- B or 1,4- B as a middle block does not have significant influences on the segregation of other two blocks. Following relation holds for this case.

$$\delta_{(1,2-B)} \approx \delta_{(1,4-B)} < \delta_S < \delta_M \qquad \text{Equation 6.4}$$

Not only the solubility parameters of B microstructure but also the types of solvent influence the segregation of different blocks. Table 6.3 shows the solubility parameters of different solvents. The effects of solvent on the morphology will be discussed in the forthcoming sections.

The investigated polymers along with the weight fractions, the number of repeating units (N) of the different blocks and the resulted morphologies are listed in the Table 6.4.

Table 6.4: *List of SBMs with their weight fractions, molar masses and the number of repeating units (N). The resulted morphologies are also shown. Here,* $^{m}S_xB_yM_z^{n}$ *represents: m = polybutadiene microstructure, (x,y,z) = weight fraction of the different blocks, n = total molar mass of the polymer.*

	polymers	N_S	N_B	N_M	**morphology**
SBM1	$^{1,4}S_{34}B_{31}M_{35}^{80}$	261	459	280	well segregated lamellae
SBM2	$^{1,2}S_{37}B_{31}M_{32}^{106}$	398	643	358	well segregated lamellae
SBM3	$^{1,4}S_{32}B_{32}M_{36}^{170}$	522	1007	611	well segregated lamellae
SBM4	$^{1,2}S_{31}B_{31}M_{38}^{55}$	122	235	156	well segregated short domain lamellae
SBM5	$^{1,2}S_{32}B_{27}M_{41}^{43}$	132	215	176	well segregated short domain lamellae
SBM6	$^{1,2+1,4}S_{31}B_{38}M_{31}^{38}$	113	267	118	chain type-oreinted lamellae
SBM7	$^{1,4}S_{30}B_{29}M_{41}^{53}$	153	284	217	mixed lamellae
SBM8	$^{1,4}S_{21}B_{27}M_{52}^{75}$	151	375	390	mixed lamellae
SBM9	$^{1,4}S_{24}B_{25}M_{51}^{54}$	124	250	275	transitional lamellae
SBM10	$^{1,2}S_{32}B_{31}M_{37}^{91}$	273	511	329	transitional lamellae
SBM11	$^{1,4}S_{26}B_{29}M_{45}^{148}$	369	794	665	transitional lamellae

Part I (Analysis of Morphology)

6.2 Morphology of lamellar type SBM triblock terpolymers

In all SBM triblock terpolymers, the volume fraction of B middle block was varied from 0.34 to 0.50. The total molar mass of the polymers were ranged from 38 to 170 kg/mol. The 1,2-B contents were ranged from 18 to 87%.

6.2.1 Well segregated lamellar morphology

The volume fractions of all the three blocks and the microstructures of polybutadiene are listed in Table 6.5. The total molar masses of the polymers are varied from 80 to 170 kg/mol. The weight fractions of the three blocks are found to be same. However, the polybutadiene microstructures differ from each other with respect to their lower and higher 1,2-B contents. In the following section well segregated polymers SBM1, SBM2 and SBM3 are discussed on the basis of morphological (by means of TEM, SAXS) and thermal (by using DMA, DSC) analyses.

Table 6.5: *Volume fraction ratios' and polybutadiene microstructures of well segregated lamellar SBMs.*

Polymer		ϕ_S	ϕ_B	ϕ_M	ϕ_S:	ϕ_B:	ϕ_M	***x*(1,2-B)**	***x*(1,4-B)**
SBM1	$^{1,4}S_{34}B_{31}M_{35}^{80}$	0.26	0.43	0.31	1 :	1.6 :	1.2	18	82
SBM2	$^{1,2}S_{37}B_{31}M_{32}^{106}$	0.29	0.43	0.28	1 :	1.5 :	1	87	13
SBM3	$^{1,4}S_{32}B_{32}M_{36}^{170}$	0.25	0.43	0.32	1 :	1.7 :	1.3	30	70

The TEM micrographs and the SAXS patterns of the three polymers are given in Figure 6.2. Figure 6.2a shows the TEM image of SBM1 ($S_{34}B_{31}M_{35}^{80}$) where the three domains are very well segregated. As the films were stained with OsO_4, the gray color indicates the S domain, the black one is the B domain and the white one represents the M domain. In this case a centrosymmetric type (SBMMBS) long periodicity lamellae is observed. The morphology is further analyzed by SAXS experiments (see Figure 6.2b). In the 1D-SAXS pattern, SBM1 showed nicely ordered reflection peaks of lamellar pattern at a relative positions of 1q*, 2q*, 3q*, 4q*,4,9q*, 5,8q* and 6.9q*. The TEM image of the second polymer SBM2 ($S_{37}B_{31}M_{32}^{106}$) is given in Figure 6.2c. Though the color contrasts of the different domains are not clear but the long periodicity of centrosymmetric lamellar pattern can be

identified. The scattering peaks from the 1D-SAXS pattern in Figure 6.2d also shows lamellar pattern with six ordered reflection peaks. Finally, the third polymer SBM3 ($S_{32}B_{32}M_{36}^{170}$) also shows very well segregated lamellar pattern which can be identified from the color code of the TEM image (see Figure 6.2e). The first four reflection peaks from the 1D-SAXS pattern also supports the TEM interpretation.

The long periodicity and the domain sizes of different blocks were calculated from TEM micrographs as well as 1D-SAXS patterns. The domain sizes of the different blocks were found to vary depending on the total molar masses of polymers, see Table 6.6. Among the three domains, S domain was broader compared to B and M domains. The M domains were narrower than S domains which could be due to the effect of radiation damage of M during TEM measurement. However, the radiation damage of S domains is negligible in TEM analysis as in the aromatic compounds the electron liberation by damaging can be delocalized or distributed. The values of SBMB long periodicity obtained by TEM measurement were smaller than that of SAXS which are as understood due to the effect of the radiation decay of the M domains. The B domains were the narrowest among others.

The domain sizes of the different blocks are smaller for SBM2 than the SBM1 though the molar mass of SBM2 is higher than the molar mass of SBM1. The lower domain size for SBM2 can be explained considering the presence of B microstructures. The SBM2 is composed of 87% of 1,2- B, whereas the other two SBMs have predominantly 1,4- B (see Table 6.5). As the cohesive energy density is higher for 1,2- B than for 1,4- B (cf. Table 6.1), the incompatibility of 1,2- B with the S and M is less. So the phase boundaries of S/B and M/B are more pronounced in the 1,2-B containing polymer. Therefore, a broad region of a mixed phase can be observed (see section 2.2.1, chapter 02) resulting in narrow 1,2-B domains. Again, the incompatibility of 1,4- B with the S and M is higher. Hence, the phase boundary is much more distinct and the mixed phases of the two domains are reduced. The resulting segregation shows broad 1,4-B domains (see section 2.2.2, chapter 02).

Table 6.6: *Domain sizes (**d**) of the different segregated blocks (S, B, M in nm scale) and the long periodicity are calculated by TEM and SAXS.*

	polymer	d_S **(nm)**	d_B **(nm)**	d_M **(nm)**	d_{SBMB} **(nm)**	
					TEM	**SAXS**
SBM1	$^{1,4}S_{34}B_{31}M_{35}^{80}$	17	12	16	53	80
SBM2	$^{1,2}S_{37}B_{31}M_{32}^{106}$	11	6	8	34	73
SBM3	$^{1,4}S_{32}B_{32}M_{36}^{170}$	20	17	19	76	96

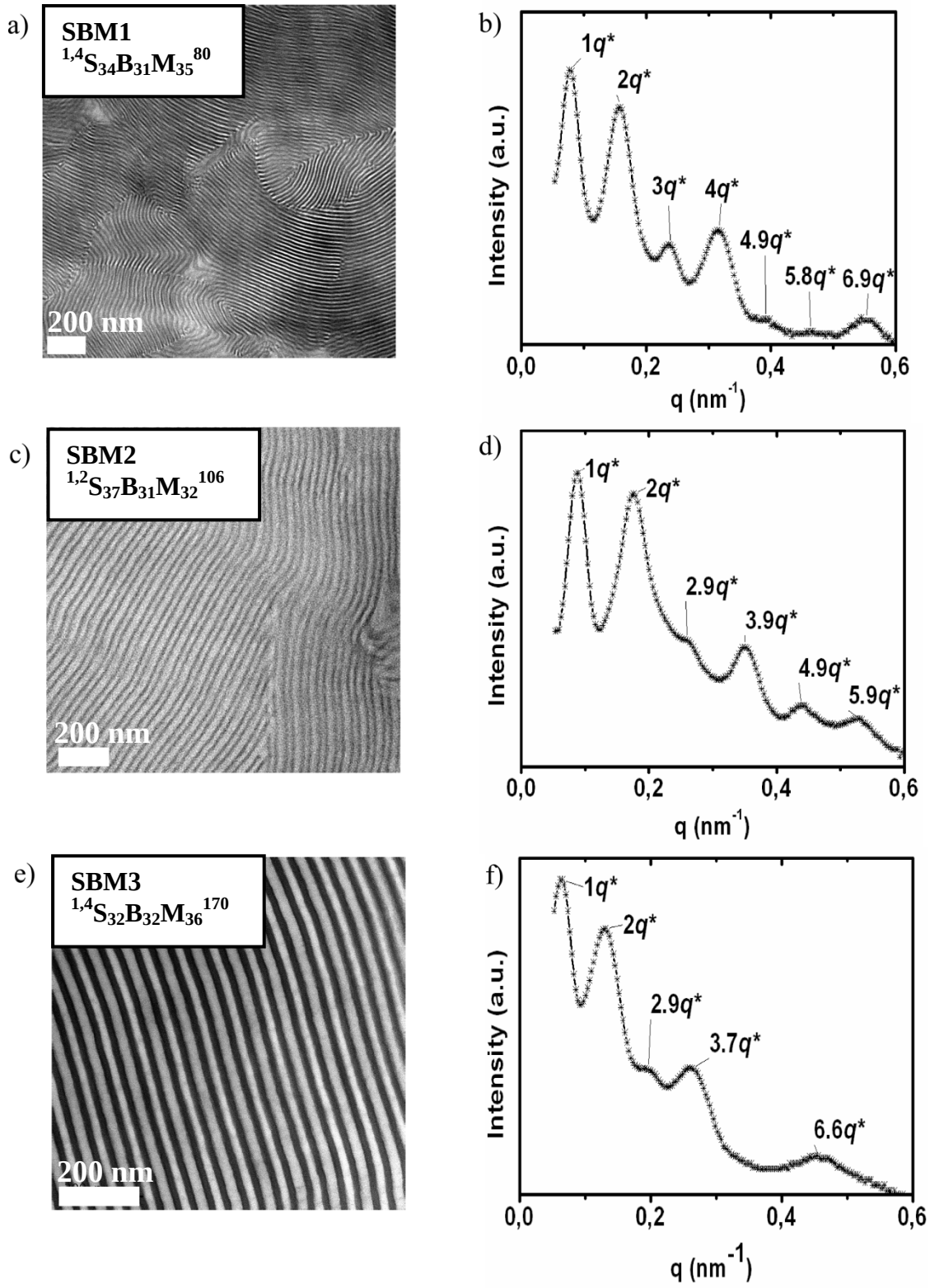

Figure 6.2: *TEM and 1D-SAXS patterns of $^{1,4}S_{34}B_{31}M_{35}^{80}$(a,b), $^{1,2}S_{37}B_{31}M_{32}^{106}$(c,d) and $^{1,4}S_{32}B_{32}M_{36}^{170}$(e,f). Polymer films were casting in $CHCl_3$ and stained in OsO_4. The color code of the TEM images, S = gray, B = black, M = white.*

A schematic drawing of a well segregated lamellae pattern is shown in Figure 6.3, where the B lamellae are surrounded by one S and one M lamellae. A single SBM chain can be formed by a bridge formation of B to the endblocks of S and M. In this consequence, no loop back formation with the residing end blocks (S or M) is possible.

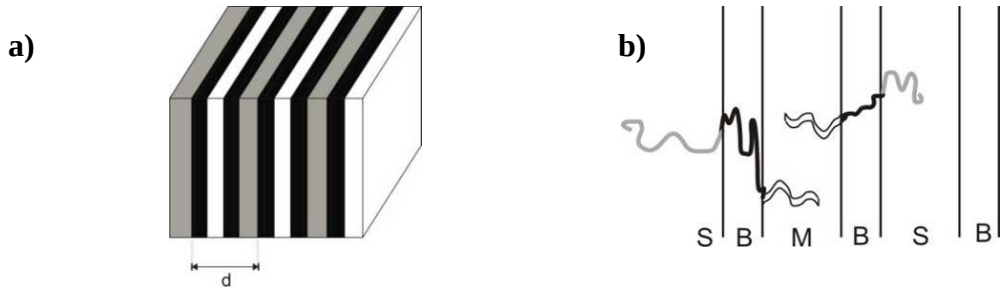

Figure 6.3: *Schematic sketch of centrosymmetric SBMB type lamellar morphology (a) and the bridge formation of B with the end blocks (S and M).*

6.2.2 Well segregated but short domain length lamellar morphology

The molar masses of the following two SBMs are 55 kg/mol and 43 kg/mol. In both cases the 1,2-B microstructure is predominant. The ratios of the volume fractions for both the polymers are given in Table 6.7.

In Figure 6.4a and 6.4c the TEM images of SBM4 ($S_{31}B_{31}M_{38}^{55}$) and SBM5 ($S_{32}B_{27}M_{41}^{43}$) are shown. As seen from the TEM images, both the polymers show same type of lamellar morphology. The different lamellar patterns are highlighted with circles. Circle 1 shows a clear segregation of the three domains whereas in circle 2, only the S and M domains can be recognized. The segregation of the mixed S/M lamellae along with the B domains is focused in circle 3. Some non-segregated areas are observed in circle 4. However, the non homogeneity of the different domains in circles 2, 3 or 4 are most probably due to the different projection views or the less contrast of the TEM micrographs. It should be mentioned that in the case of the low molar mass polymers when prepared by solvent casting method, fast evaporation causes moderate segregation of the domains. In fact, both SBM4 and SBM5 show good segregation which can be confirmed by the DSC curves in Figure 6.4e and 6.4f. Three distinct glass transitions (T_g) of the respective three blocks (T_g-B ≈ -14 °C, T_g-S ≈ 90 °C and T_g-M ≈ 125 °C) are detected from the curves.

Table 6.7: *Volume fraction ratio and polybutadiene microstructure of well segregated short domain lamellar SBMs*.

polymer		ϕ_S	ϕ_B	ϕ_M	ϕ_S:	ϕ_B:	ϕ_M	***x*(1,2-B)**	***x*(1,4-B)**
SBM4	$S_{31}B_{31}M_{38}^{55}$	0.24	0.42	0.33	1 :	1.8 :	1.4	90	10
SBM5	$S_{32}B_{27}M_{41}^{43}$	0.25	0.38	0.37	1 :	1.5 :	1.5	89	11

The morphologies of SBM4 and SBM5 are further investigated by the SAXS experiments, as shown in Figure 6.4b and 6.4d. In 1D-SAXS pattern of SBM4 the first peak appeared at the shoulder of the second peak. The relative positions of the peaks are 1q*, 1.2q* and 2q* which doesn't fit for any structural assignment as given in the Table 4.1, chapter 04. However, the two intense peak which is raised at 0.17 nm^{-1} and 0.28 nm^{-1} resembles a relative positions of 1q* and 1,65q*. The peaks positions are very close to the hexagonally cylindrical pattern which is 1q* and 1,73q*. But from TEM images in Figure 6.4a, no cylindrical patterns are identified. Hence, the TEM is performed again on samples stained at an extended time (3 minutes instead of 1) in OsO_4 to obtain better contrast of the different domains. The new TEM images are shown in Figure 6.5. The higher magnified image of the circle area 1 is shown in the inset where the B cylinders can be distinguished as pseudo-hexagonal assemblies in the S cylinder (see the sketched cartoon). The M domain exists as a continuous phase. The cylinders of B and S are embedded in the M phases. The resulted morphology also agrees with the 1D-SAXS diffraction pattern as shown in Figure 6.4b. However, this type of cylindrical morphology can be found in $S_{65}B_{14}M_{21}^{129}$ as well as in $S_{64}B_{12}M_{24}^{78}$ as reported by Breiner et al.[2] Hence, the pseudo-hexagonal pattern in case of $S_{31}B_{31}M_{38}^{55}$ is somehow unexpected as the weight fractions present in this polymer generally favor the formation of lamellar morphology. When the other polymer SBM5 was interpreted, whose compositions are quite similar to SBM4, a lamellar morphology is obtained. Analyzing the six scattering peaks at the relative positions of 1q*, 2q*, 3q*, 4q*, 5q* and 6q* as identified from the 1D-SAXS pattern as well as from the TEM images (Figure 6.4c and 6.4d), the lamellar pattern of SBM5 is confirmed. The unexpected pseudo-hexagonal pattern of SBM4 is, as understood, could be the effect of entropy lost of the low molar mass of 1,2-B domains (12 kg/mol) for fast solvent evaporation during the preparation of the film.

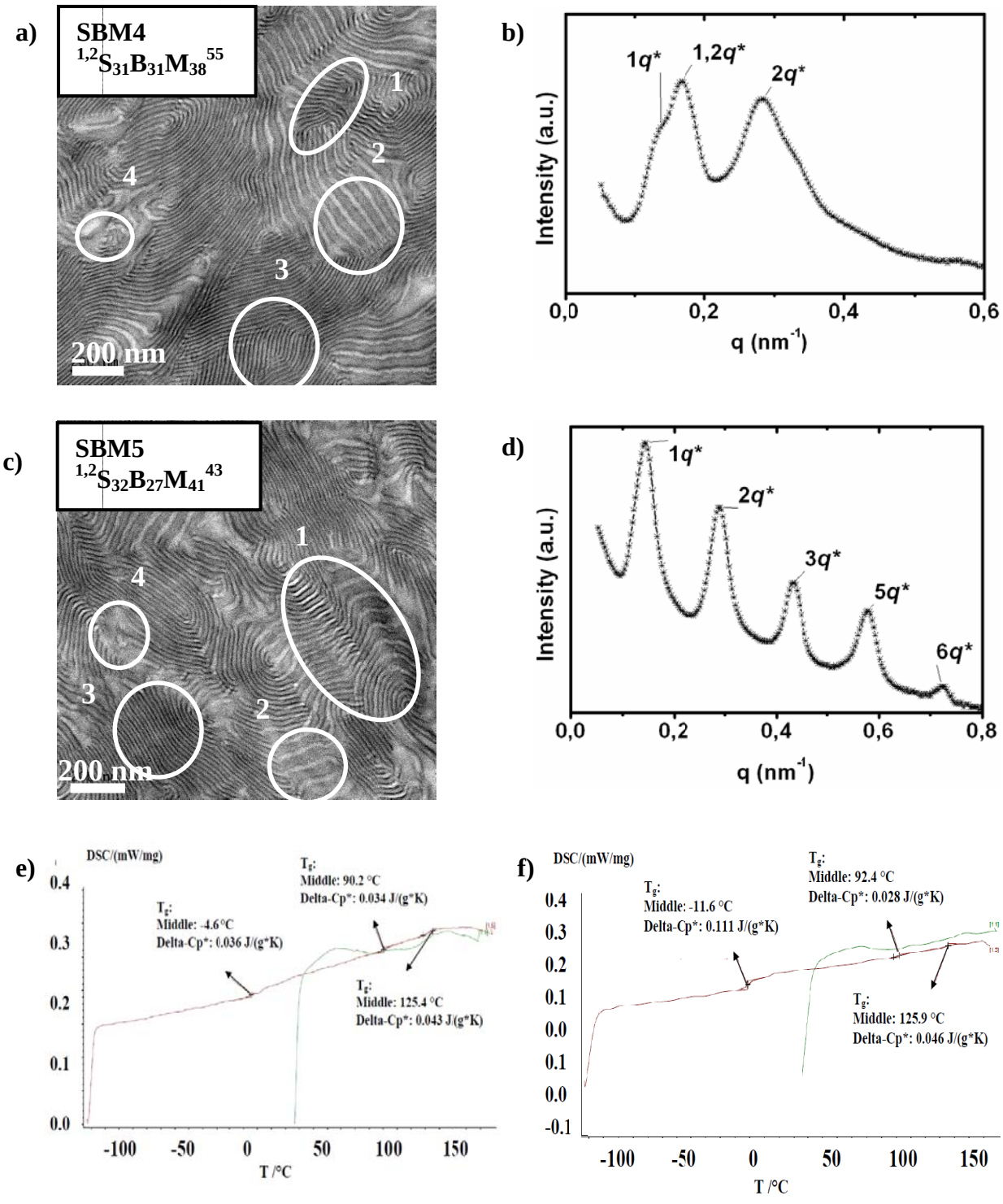

Figure 6.4: *a) and c) show the TEM images of SBM4 ($^{1,2}S_{31}B_{31}M_{38}^{55}$) and SBM5 ($^{1,2}S_{32}B_{27}M_{41}^{43}$). Here, 1 = clear segregation of the three domains, 2 = segregation of S and M domains, 3 = mixed S/M lamellae along the B domains, 4 = non-segregated area. b) and d) show the 1D-SAXS patterns. e) and f) show the DSC curves of SBM4 and SBM5. The heating rate for DSC is 20K/min and the temperature range is -120 °C to 160 °C.*

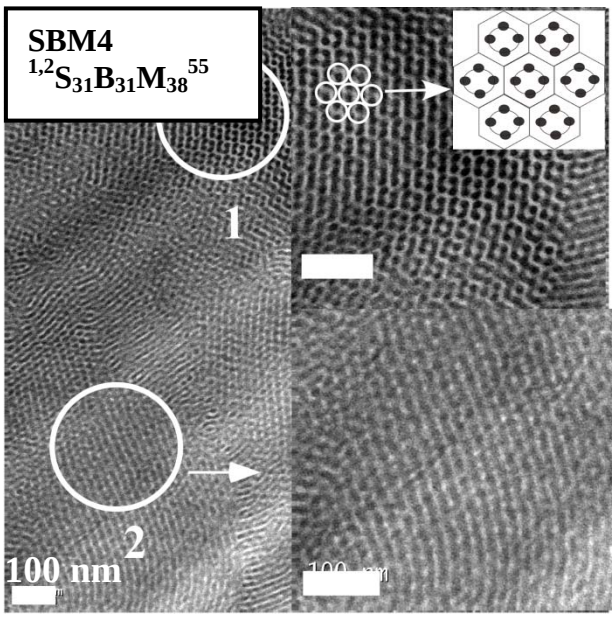

Figure 6.5: *TEM images of $^{1,2}S_{31}B_{31}M_{38}^{55}$ stained in OsO_4 for 3 minutes. The color code, S = gray, B = balck, M = white. The polymer films were casted in $CHCl_3$. In figure, the circled area 1 indicates polybutadiene cylinders. The magnified view of the circle area of 1 is shown in the top inset view where a pseudo hexagonal cylindrical pattern is also sketched. The circled area 2 shows an undulated lamellar pattern. The magnified view of the circle area of 2 is highlighted in the bottom inset view.*

As both polymers consist of similar compositions, molar masses and B microstructures, the dimensions of the different blocks and the long periodicity are comparable. In Table 6.8 different domain sizes and long periodicity of SBM4 and SBM5 calculated from TEM and SAXS data are listed. The results agree reasonably well with each other.

Table 6.8: *Long periodicity and the domain sizes as calculated by TEM and SAXS*

polymer	**S (nm)**	**B (nm)**	**M (nm)**	**SBMB (nm)**	
				TEM	**SAXS**
$S_{31}B_{31}M_{38}^{55}$	12 ± 1	7 ± 1	12 ± 1	40 ± 1	44
$S_{32}B_{27}M_{41}^{43}$	13 ± 1	8 ± 1	11 ± 1	37 ± 1	43

6.2.3 Chain like oriented lamellar morphology

For SBM6 ($^{1,2+,14}S_{31}B_{38}M_{31}{}^{38}$) 'chain' like oriented lamellar patterns were observed (see the TEM images in Figure 6.6a). Very good segregations of different domains can be detected from the TEM image where two B lamellar domains seem to embrace the S domains from both sides. The S domains were found to be narrower (~8 nm) than the M domains (~14 nm). In this TEM image (Figure 6.6a) different areas were highlighted by arrows 1, 2 and 3. Arrow 1 showed the intersection of two B domains bonded from both ends. An isolated S domain seems to embrace by the border of B domains. The M phases reside between the S/B domains. In arrow 2 only a single B domain can be seen which was connected to the S/B domains from both side. Arrow 3 considers the same domain patterns of arrow 1. For a better understanding a sketch of the segregation pattern at different rotation angle is shown in Figure 6.6b. From the top view, same morphology pattern as shown in TEM image can be recognized. For their tilting view (if the domains are rotated 45°), all of the 3 segments (arrow 1, 2, and 3) appear to be narrower. In this case, the isolated S domains will be present in all the three segments forming a chain like structure. Further rotating to 90° will result in a broad middle segment, where the S phase will embrace by border B domains. The S/B domains are connected with the B domains from both sides.

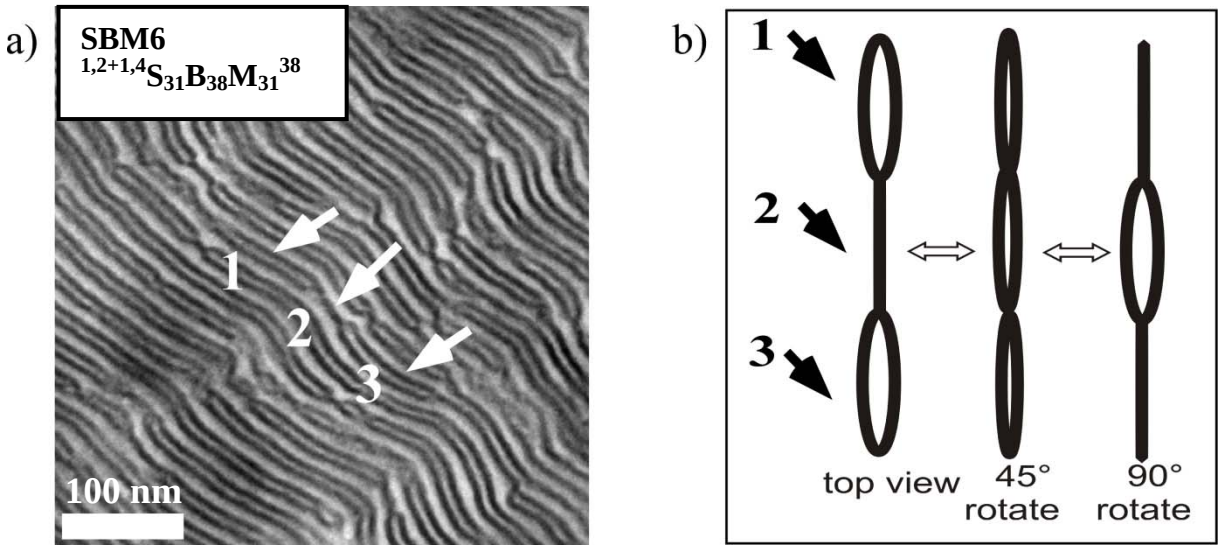

***Figure 6.6**: a) TEM image of $^{1,2+1,4}S_{31}B_{38}M_{31}{}^{38}$. The polymer film was casted in $CHCl_3$ and stained in OsO_4. The color code: S=gray, B=black, M=white. b) Schematic sketch of the chain like domains. The arrow indicates the segments at different rotation view.*

Table 6.9: *Volume fraction ratio and polybutadiene microstructure of* $S_{31}B_{38}M_{31}$[38].

polymer		ϕ_S	ϕ_B	ϕ_M	ϕ_S :	ϕ_B :	ϕ_M	1,2-	1,4-
SBM6	$S_{31}B_{38}M_{31}$[38]	0.23	0.50	0.27	1 :	2.2 :	1.2	34	66

Three possible hypothesis that favor the formation of chain like oriented morphology can be given as follows:

- Low molar mass (38 kg/mol) of the polymer:

The molar mass of the polymer is 38 kg/mol, for that the B repeating units are calculated to be 267. This small B chains are more flexible compared to the S and M; and do not favor the formation of continuous lamellar B domains. However, no supportive data has been found in literature.

- Elastic energy and the ratio of ***1 : 2*** of 1,2- and 1,4-B units:

The differences of elastic energy of 1,2- and 1,4-B could insist to form chain like oriented domains. The higher elastic energy of 1,4-B chains tends to expand along the direction parallel to the domain interface to gain the conformational entropy whereas the lower elastic energy of 1,2-B chains insists to reside perpendicular to the domain interface. As a consequence short B domains are oriented with an isolated S domain. The affect of the ratio at ***1 : 2*** of 1,2- and 1,4-B isomers on the morphology can also be predicted from DSC and DMA analysis. The DSC showed T_g at - 78 °C for the 1,4-B but no T_g for 1,2-B within its range. On the contrary, the DMA showed only one T_g at -26 °C, which was for 1,2-B. The two glass transition temperatures of polybutadiene domains support the individual contribution of 1,2- and 1,4-B on the formation of morphology. The mechanical properties are also hampered for this ratio of 1,2- and 1,4-B isomers, which will be discussed in the section 6.3 of mechanical properties. However, no affect of 1,2- and 1,4-B at a ratio of ***1: 2*** in case of high molar mass polymer, e.g., SBM3($^{1,4}S_{32}B_{32}M_{36}$[170]) can be seen because in SBM3 well segregation of the B domain from the S and M was obtained (see also Figure 6.2e).

- Sample preparation and the annealing time:

The chain like oriented morphology might have been formed during sample preparation. Kim et al.[16] reported an oriented lamellar diblock of polystyrene-*b*-poly (4-vinylpyridine) ($S_{51}4VP_{49}$[39]) where the molar mass of the investigated polymer is identical with the present SBM6. The samples of the reported polymer were prepared by spin coating followed by annealing for 2 days. The resulted morphology shows some oriented lamellae patterns along with the non-oriented lamellae. When the

annealing time is increased to 4 days, 8 days, 10 days and 20 days, the non-oriented lamellae significantly transformed to the oriented ones.

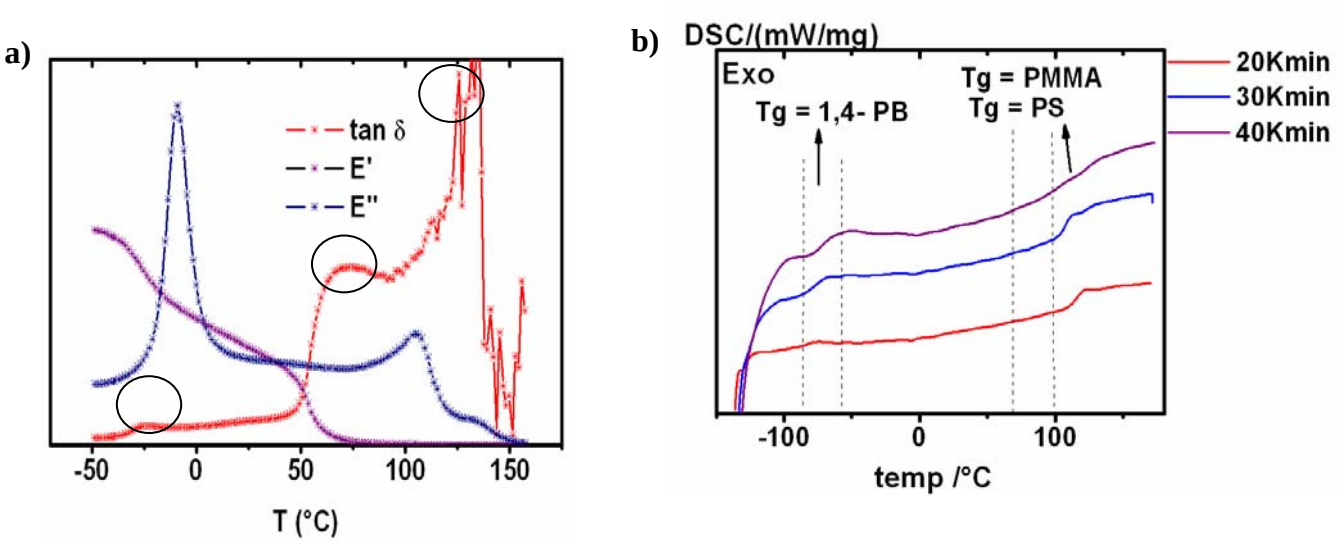

Figure 6.7: *a) DMA curve of $^{1,2+1,4}S_{31}B_{38}M_{31}{}^{38}$ at a temperature range from -50 °C to 160 °. Two T_g indicated by circles at -26 °C (for 1,2-B) and 70 °C (for S). A noisy peak appears at 125 °C (for M). b) DSC curve of $^{1,2+1,4}S_{31}B_{38}M_{31}{}^{38}$. The DSC was measured at the temperature range from -130 °C to 160 °C. Three heating rate (20, 30 and 40 K/min) were applied. Two T_gs at -78 °C (for 1,4-B) and 108 °C (S and M) are recognized.*

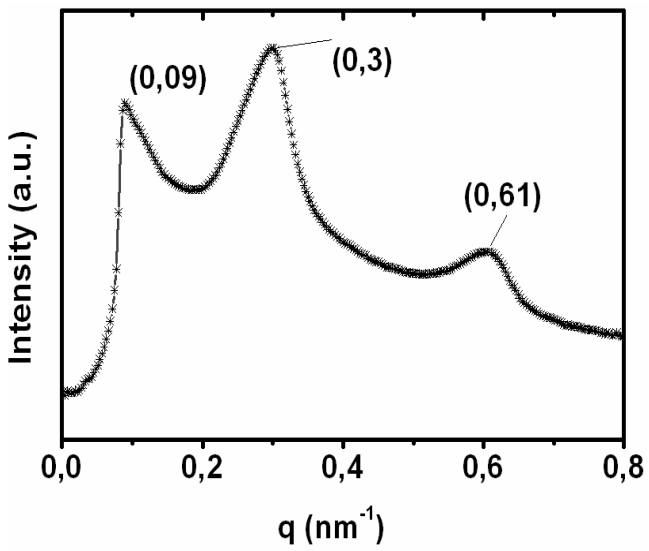

Figure 6.8: *1D-SAXS scattering pattern of SBM6 ($^{1,2+1,4}S_{31}B_{38}M_{31}{}^{38}$).*

In the present investigation, the films of SBM6 were prepared by solvent casting instead of spin coating and were annealed for 2,5 days. Probably the film preparation conditions were not sufficient for good segregations. However, in this work the influence of annealing time at temperatures in analogy to the literature has not been investigated. But SAXS was performed to investigate the morphology further (see in Figure 6.8). No clear structural pattern was recognized from the relative peak positions from the SAXS investigation. The long periodicity for SBMB type lamellar domains were compared with TEM micrographs which shows for n = 1 is 58 nm from TEM whereas 70 nm from SAXS pattern.

6.2.4 Mixed lamellar morphology

The mixed lamellar morphology is obtained in the polymers SBM7 ($S_{30}B_{29}M_{41}^{53}$) and SBM8 ($S_{21}B_{27}M_{52}^{75}$), see Table 6.10 for detail. The SBM7 has almost the same weight fractions of all the three blocks, whereas in SBM8 only the weight fraction of M is higher compared to the other blocks.

From Figure 6.9a and 6.9c, one can see the morphology of SBM7 and SBM8 with zig-zag type lamellae. However, from the images the lamellar domains of S and M cannot be distinguished easily due to the contrast of the TEM images. For a better observation of the domains SAXS is also performed, see Figure 6.9 b and d. The 1D-SAXS pattern of SBM7 shows two scattering peaks at 0.26 nm^{-1} and 0.52 nm^{-1} which shows a relation at 1q* and 2q*. On the other hand, SBM8 shows three distinct scattering peaks at 0.19, 0.38 and 0.58 nm^{-1} which shows the relative positions at 1q*, 2q* and 3q*.

From the interpretation of TEM and SAXS it is not completely clear whether the S and M lamellar domains are mixed or not. The χN of the S and M blocks for SBM7 and SBM8 were calculated by using Equation 6.3. The value for SBM7 is obtained 15.2 and for SBM8 it is 22.2 which are rather large from the Weak Segregation Limit (WSL). For further investigation of the segregation behavior, DSC and DMA were performed. The results are given in Figure 6.10.

Figure 6.10a shows the DMA plot where a very sharp peak at -77,5 °C is observed which is due to the 1,4-B microstructure. Another broad peak has been identified between the T_g range of S and M, as indicated by a circle. Generally, the T_g will be found somewhere between the T_gs of both homopolymers only if the S/M lamellae are mixed. Hence, the end blocks are supposed to form mixed lamellae. The further analysis in the DSC also shows two T_gs at -83 °C and 131 °C (Figure 6.10b) which supports the DMA analysis. In case of SBM8, however, two peaks at 101 °C and 141 °C are

observed (Figure 6.10c), indicating the segregation of S and M domains. Though the peak at 101 °C is rather broad. Nevertheless, two T_g at -82 °C and 128 °C is observed in the DSC curve (see Figure 6.10d). Hence, in SBM8 the mixed lamellae (*ml*) and the non-mixed lamellae (*ll*) seem to co-exist.

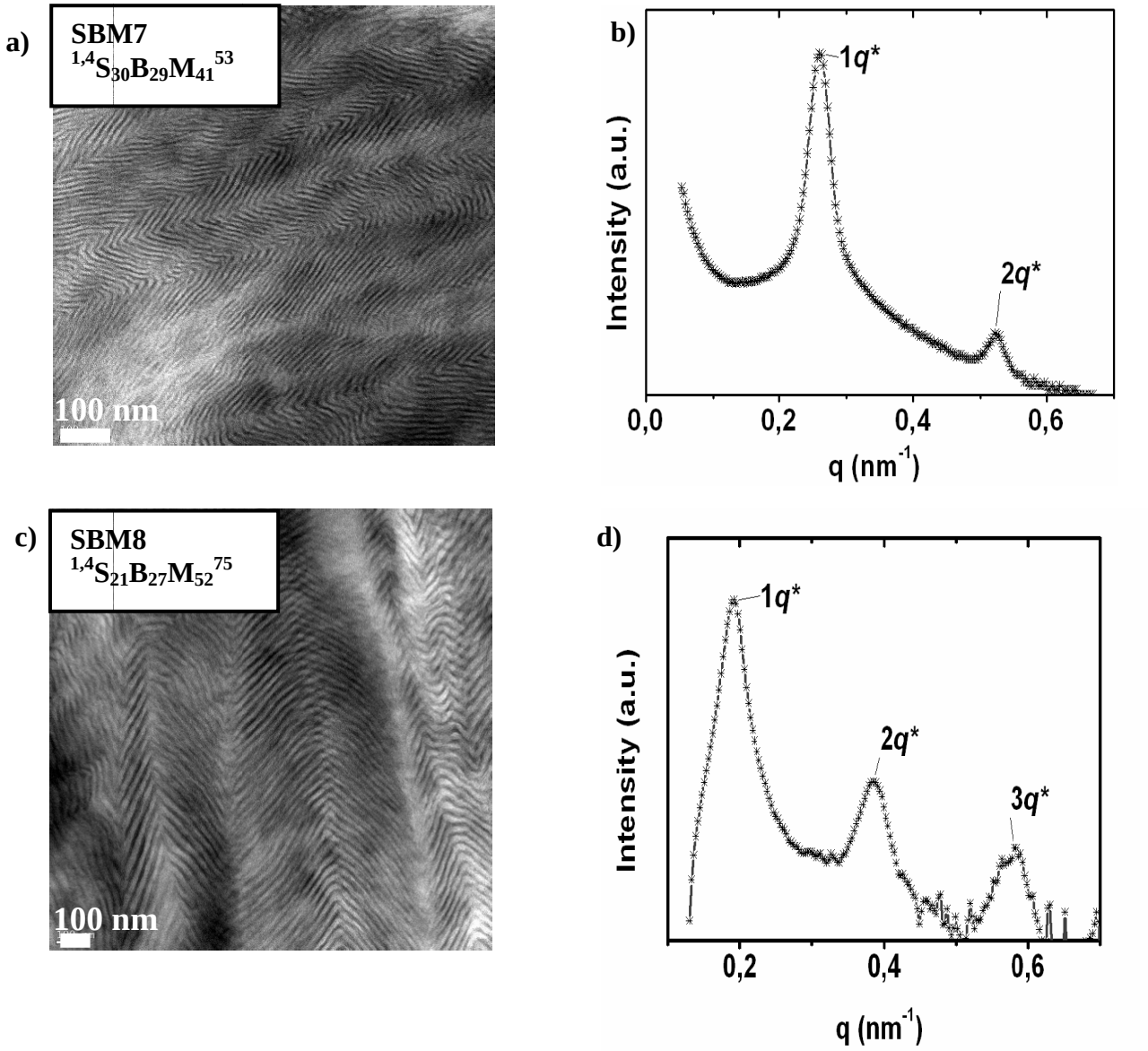

Figure 6.9: *The TEM micrographs of $S_{30}B_{29}M_{41}{}^{53}$ and $S_{21}B_{27}M_{52}{}^{75}$ are given in a) and c). The polymer films were casted in $CHCl_3$ and stained in OsO_4. The color code: S = gray, B = black, M = white. From the TEM images, the mixed S and M lamellar domains are seen. The 1D-SAXS pattern of $S_{30}B_{29}M_{41}{}^{53}$ and $S_{21}B_{27}M_{52}{}^{75}$ are given in b) and d).*

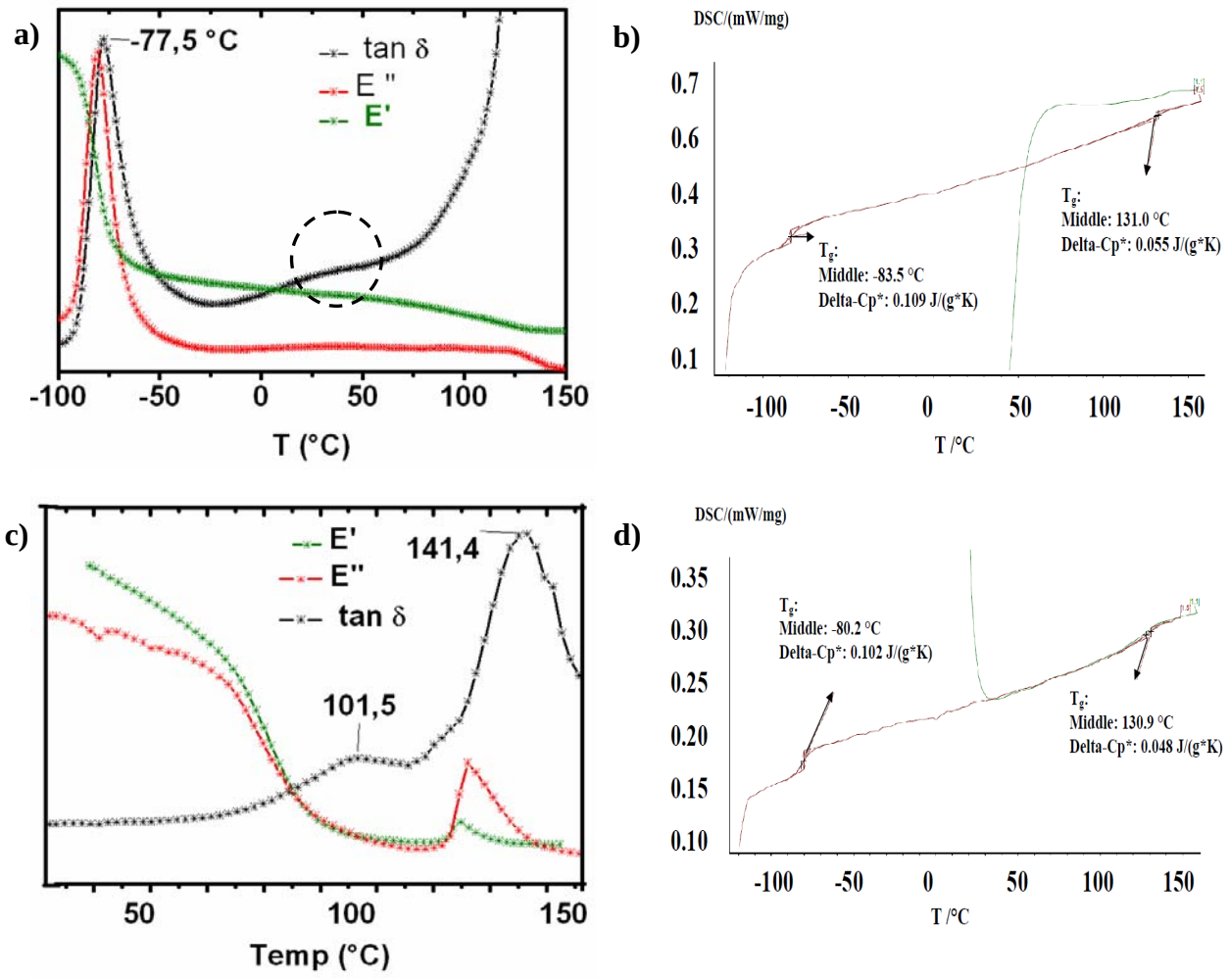

Figure 6.10: *Characterization results of $S_{30}B_{29}M_{41}$[53] and $S_{21}B_{27}M_{52}$[75]. a) shows the DMA plot of $S_{30}B_{29}M_{41}$[53] at a temperature range from -120 °C to 150 °C measured at frequency of 10 Hz. b) shows the DSC curve of $S_{30}B_{29}M_{41}$[53] at a temperature range from -120 °C to 160 °C. Heating rate was 20 K/min. c) shows the DMA plot of $S_{21}B_{27}M_{52}$[75] at a temperature range from 25 °C to 180 °C measured at frequency of 10 Hz. d) shows the DSC curve of $S_{21}B_{27}M_{52}$[75] at a temperature range of -120 °C to 160 °C. Heating rate in DSC was 20 K/min.*

Table 6.10: *Volume fraction ratio and polybutadiene microstructure of the mixed lamellar morphology polymers.*

polymer		ϕ_S	ϕ_B	ϕ_M	ϕ_S :	ϕ_B :	ϕ_M	1,2-B	1,4-B
SBM7	$S_{30}B_{29}M_{41}$[53]	0.24	0.40	0.36	1 :	1.7 :	1.5	16	84
SBM8	$S_{21}B_{27}M_{52}$[75]	0.16	0.37	0.47	1 :	2.3 :	2.9	24	76

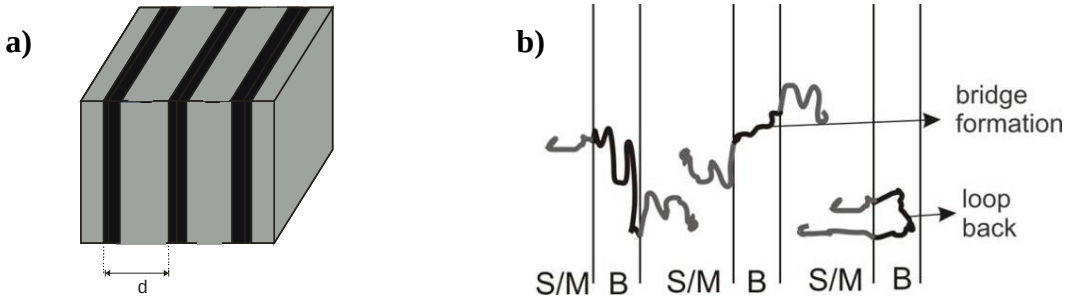

Figure 6.11: *a) Schematic sketch of mixed lamellae (**ml**) where the long periodicity is considered as B(S/M)B. Here, the color code: S/M mixed lamellae = gray, B = black. B) coexisting of mixed lamellae (**ml**) and lamellae (**ll**). The bridge and loop formation of the B domains.*

The schematic structure of mixed lamellar is shown in Figure 6.11. A mixed lamellar phase (*ml*) of the S and M end blocks may arrange itself with the middle B block in two different ways: i) The middle block either forms a bridge between two S/M mixed domains that results in a SBMB type long range order (i.e., lamellae, *ll*), or ii) the B block forms a loop in the same S/M mixed lamellae leading to a coexisting *ml* and *ll* morphology. From the TEM, DSC and DMA results it is understood that the SBM7 forms a mixed lamellae, *ml*, whereas the SBM8 forms coexisting *ml* and *ll*.

To compare the results from SAXS and TEM, the long periodicity of SBMB lamellar domains were calculated. The results are given in Table 6.11 which has a good agreement for both TEM and SAXS results.

Table 6.11: *The domain sizes and the long periodicity of SBM7 ($S_{30}B_{29}M_{41}^{53}$) and SBM8 ($S_{21}B_{27}M_{52}^{75}$) are calculated from TEM images and 1D-SAXS patterns. The domain sizes as well as the periodicity of SBM8 are larger than that of SBM7 because of the higher molar mass of SBM8.*

polymer	**S or M (nm)**	**B (nm)**	**SBMB (nm)**	
			TEM	**SAXS**
SBM7 ($S_{30}B_{29}M_{41}^{53}$)	~7	5	20	24
SBM8 ($S_{21}B_{27}M_{52}^{75}$)	~13	8	22	33

Brinkmann et al.[3] reported the formation of mixed lamellae (*ml*) in $^{1,4}S_{17}B_{52}M_{31}^{35}$ and $^{1,4}S_{30}B_{58}M_{12}^{68}$. In both polymers, the weight percent of B is reported very high ($w_B > 50\%$). Compared to the SBMs reported in literature, the present SBMs have low B contents (w_B = 27-29%). The molar mass of these

polymers ranges from 35 to 75 kg/mol. Despite lower molar mass, the SBM4, SBM5 and SBM6 show very well segregated lamellae. However, all these polymers have higher 1,2- B contents. But in the reported SBMs in [3] including the SBM7 and SBM8, higher 1,4-B contents are predominant. As in 1,4-B has double amount of C-atoms in main chain with double bond compared to 1,2-B, more elastic energy of 1,4-B is favorable to fold back of two endblocks. Thus, the predominant 1,4-B content assists the forming of mixed type endblock lamellae.

The solvent also influences the assembly of mixed lamellae strongly, as reported by Brinkmann et al.[3] In Ref. [3] when casting from $CHCl_3$, mixed lamellae of $^{1,4}S_{17}B_{52}M_{31}{}^{35}$ are obtained. Again, when the solvent was changed from $CHCl_3$ to toluene and THF, the lamellar domains are transformed to different morpholologies, like hexagonal, perforated or undulated cylinders. From the above results and discussion, it is understood that the formation of mixed lamellae (*ml*) or partially mixed lamellae of S and M end blocks are favored when the molar mass of the polymer is low (35-70 kg/mol), the presence of 1,4-B domain is high and the solvent for film casting is $CHCl_3$.

6.2.5 Transitional lamellar morphology

The compositions and polybutadiene microstrcutures of transitional SBMs are listed in Table 6.12. Among the polymers, the SBM9 and SBM11 have asymmetric compositions with higher M domains. For both the polymers the B microstructures are rich in 1,4- B. On the other hand the SBM10 contains a B-block with higher 1,2- microstructure. Moreover, the weight fractions of all the three blocks are found to be equal in SBM10. Total molar mass of these polymers ranges from 54 to 148 kg/mol. The resulted morphology shows a transition of B lamellae to the cylindrical or spherical forms.

Table 6.12: *Volume fraction ratios and polybutadiene microstructures of the transitional lamellar SBMs.*

polymer		ϕ_S	ϕ_B	ϕ_M	ϕ_S :	ϕ_B :	ϕ_M	**1,2-**	**1,4-**
SBM9	$S_{24}B_{25}M_{51}{}^{54}$	0.19	0.34	0.46	1 :	1.8 :	2.4	19	81
SBM10	$S_{32}B_{31}M_{37}{}^{91}$	0.25	0.43	0.32	1 :	1.7 :	1.3	89	11
SBM11	$S_{26}B_{29}M_{45}{}^{148}$	0.20	0.40	0.40	1 :	2.0 :	2.0	14	86

Figure 6.12 a) and b) show the TEM images of SBM9 ($S_{24}B_{25}M_{51}{}^{54}$) where the B lamellae are transformed to cylindrical phases. Some short lamellar domains are twisted along with the B cylinders

as shown in circle 1. In circle 2, well segregated lamellar patterns of the three domains are focused. The B domains are embedded mostly in the S phases. Hence, the S domains tend to become thinner (9 nm) than M domains (16 nm). In circle 3 the distorted B lamellae with cylindrical and ellipsoidal shapes are shown. The diameters of the B cylinders are found to be 12 to 13 nm as calculated from the TEM images.

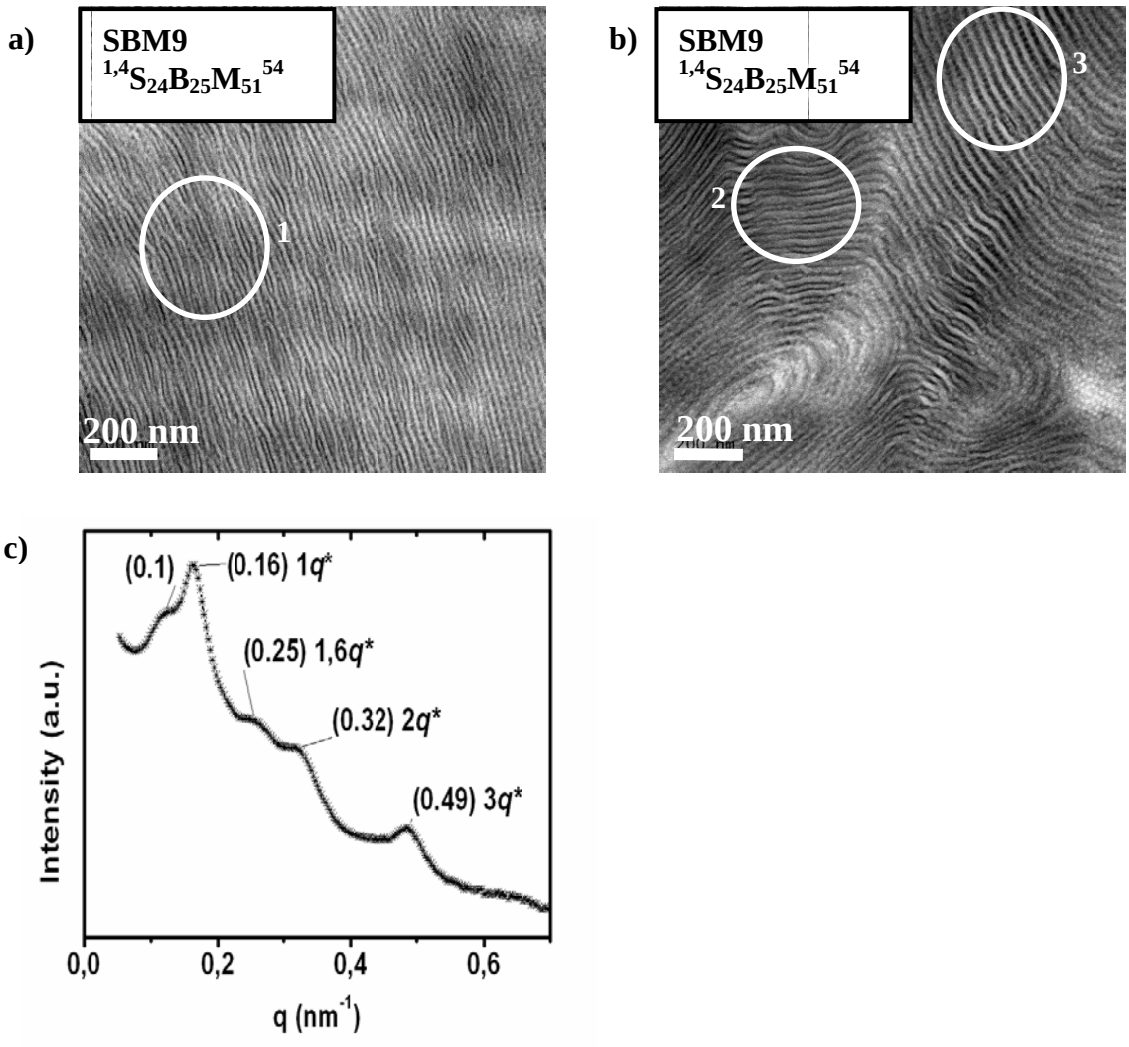

Figure 6.12: *a) and b) shows the TEM micrographs of $S_{24}B_{25}M_{51}^{54}$. The polymer films were casted in $CHCl_3$ and stained in OsO_4. The color code: S = gray, B = black, M = white. Here, circle 1 shows the twisted B lamellae, circle 2 indicates well segregated lamellae, circle 3 shows the transitional B lamellae to cylinders. c) shows the 1D-SAXS pattern of $S_{24}B_{25}M_{51}^{54}$.*

Figure 6.12c shows the 1D-SAXS pattern of $S_{24}B_{25}M_{51}^{54}$. Here, the first peak at 0.1 nm^{-1} appeared at the shoulder of the peak 16 nm^{-1} indicating an artifact for the beamstop. The remaining four peaks are

appeared at the relative positions of 1q*, 1,6q*, 2q*, and 3q*. The relative positions of the first three peaks are very similar to a scattering pattern of hexagonally cylinder. From circle 3 of the TEM image in the Figure 6.12 also the B cylindrical are located with the S and M lamellar domains but they are not completely hexagonally arrayed. The domain spacings of 39 nm obtained from 1D-SAXS scattering peaks via $D = 2\pi n/q^*$ whereas the value obtained 38 ± 3 nm from TEM which give a full agreement of TEM and SAXS interpretation.

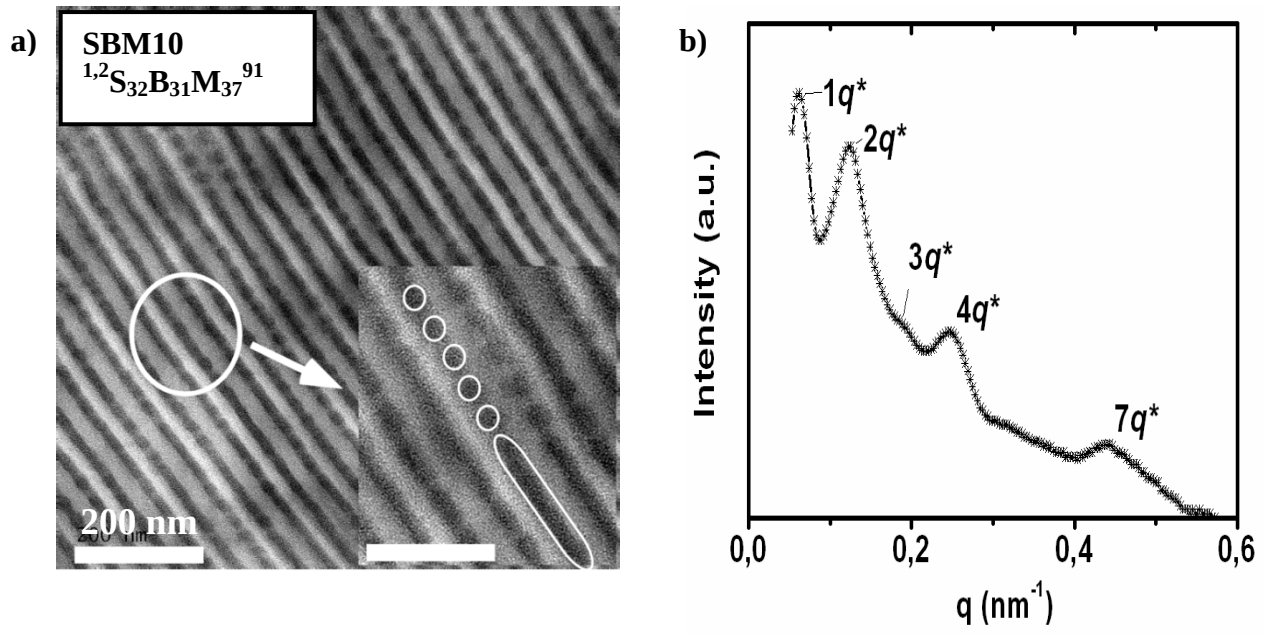

Figure 6.13: *a) the TEM micrograph $S_{32}B_{31}M_{37}^{91}$. The polymer films were casted in $CHCl_3$ and stained in OsO_4. The color code: S = gray, B = black, M = white. The TEM image shows the lamellar domains of the different blocks with transitional B domains. The magnified view of the circle shows co-existance of B spheres with lamellae. b) SAXS pattern of $S_{32}B_{31}M_{37}^{91}$.*

The SBM10 ($S_{32}B_{31}M_{37}^{91}$) also shows the transformation of B lamellae to spherical or cylindrical phases. For this polymer the three domains can be clearly distinguished in the TEM micrographs (Figure 6.13a). The good segregation of the domains is mainly influenced by high molar mass of the polymer (91 kg/mol). In the Figure 6.13b the 1D-SAXS pattern shows the relative positions of the peaks at 1q*, 2q*, 3q*, 4q* and 7q*. The first four peaks resembles lamellar pattern that agrees the images obtained from the TEM images in Figure 6.13a. However, from TEM images the co-existing lamellae and cylindrical morphology can be distinguished.

The domain sizes of the blocks are measured from TEM images as well as from 1D-SAXS (Figure 6.14). Among the lamellae, S domains are found to be broader (24 nm) than the M domains (20 nm),

and B lamellar domains are narrower (15 nm) than the others. The estimated B cylinders are 15-20 nm. The periodic structure is 100 nm long as obtained from 1D-SAXS pattern, whereas it is 80 ± 2 nm when calculated from TEM images.

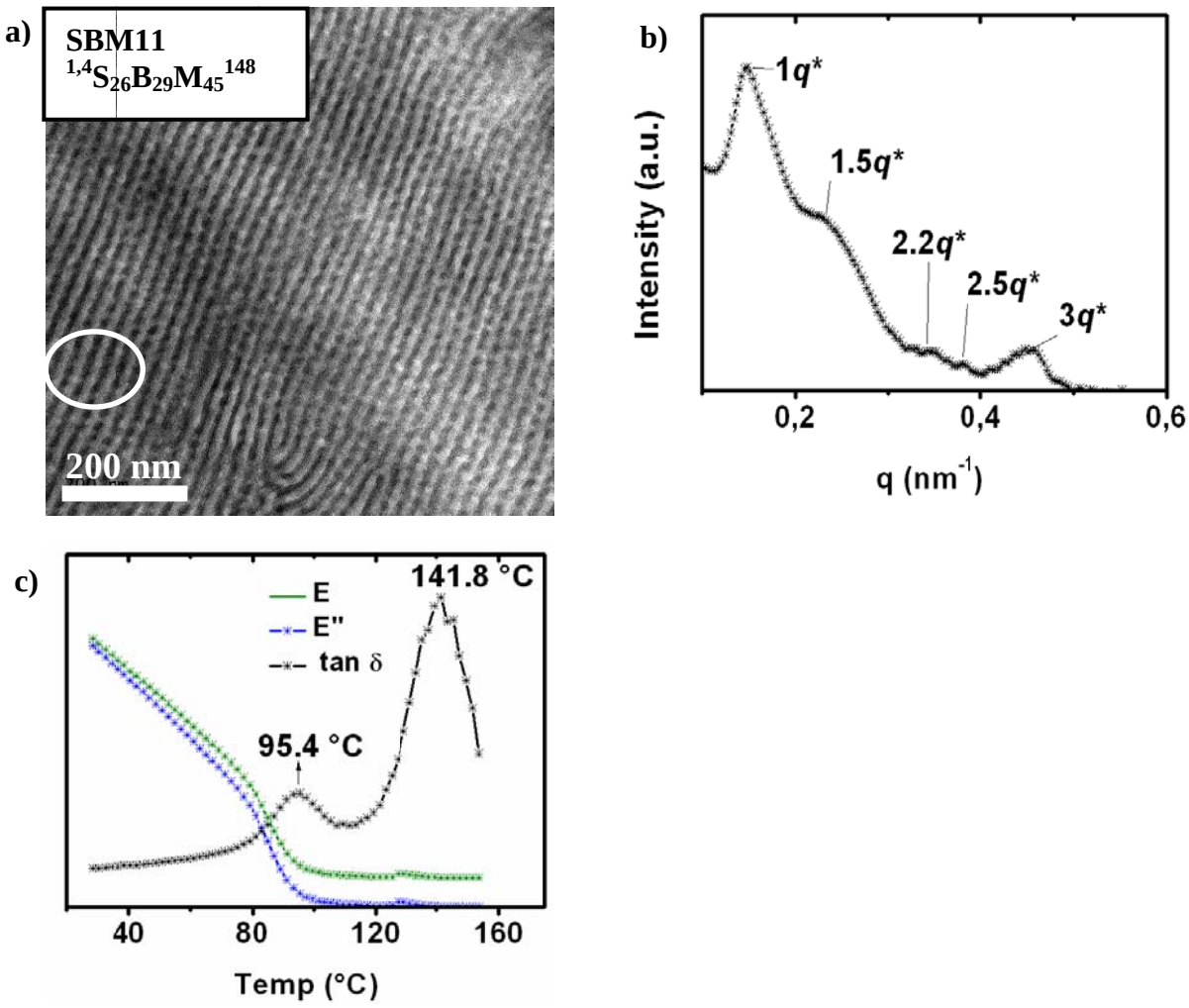

Figure 6.14: *a) TEM and b) 1D-SAXS patterns of $S_{26}B_{29}M_{45}^{148}$. c) Storage modulus, E′, loss modulus, E′′, and the damping factor, tan δ, were monitored in DMA at a constant frequency of 10 Hz against the temperature.*

Figure 6.14a shows the TEM images of the third transitional polymer, SBM11 ($S_{26}B_{29}M_{45}^{148}$) where the transition of B domains from lamellae to cylindrical phases is shown. A clear lamellar pattern is identified from the micrographs. But due to less contrast of the TEM images the S and M domains are hard to distinguish. Hence, to verify the segregation of the S and M clearly the DMA was performed (Figure 6.14c). Two glass transition temperatures (T_g = 95 °C and 142 °C) are detected which were obtained for the segregation of S and M domains. Figure 6.14b shows the SAXS pattern where the lattice peaks with the position ratio of 1q*, 1,5q*, 2,2q*, 2,5q* and 3q* signaling not any particular

structural formation. However, the peaks positions are close to the peaks positions of hexagonally packed cylinders. The characteristic domain spacing (D) of 42 nm for n = 1 calculated via $D = 2\pi n/q^*$ from 1D-SAXS pattern which is quite similar to the D spacing obtained from TEM micrograph (here it is 40 ± 3 nm).

The underlying reason behind the transitional morphology of lamellar to cylindrical or the cylindrical to lamellar domains can be found in literature.[2, 11, 17, 18] Breiner et al.[11] obtained a transitional pattern when a short chain of SB diblock is blended with SBM triblock. The presence of 5% SB at a fraction relation $\phi_S / (\phi_B + \phi_S) \approx 0.43$ tends to form spheres in the S matrix in $S_{21}B_{28}M_{51}$[95].

The same characteristic has been observed for SBM9 ($S_{24}B_{25}M_{51}$[54]) and SBM10 ($S_{32}B_{31}M_{37}$[91]). Almost 37% SB is present in SBM9, whereas in SBM10 the amount of SB is 22%. However, in both cases the composition of SB is ***1:1***. According to Breiner's interpretation, this short chain diblock could result in a spherical or ellisoidal structure.[11] In SBM10, despite the presence of 22% of SB impurities, the B lamellar is not undulated. The high molar mass of SBM10 (89 kg/mol) leads to better segregation, which could not be observed in SBM9 (54 kg/mol) for its lower molar mass.

The undulated deformation of the middle block from a lamellar to a cylindrical morphology is described by Sakurai et al[18]. According to his observation, the transitions of the lamellar B domains proceed via an undulating interface or a B mesh as a transient structure. This structure is appeared just after the coalescence of the cylinder. Another explanation of the transformation state from lamellae to cylinders or spheres is given by Zheng and Wang.[19]. They described the transition behavior of an ABC type triblock by a triangle phase diagram. According to them a lamellar morphology can be seen when all the three blocks have similar volume fractions. If the volume fraction of B (ϕ_B) is decreased in the equilibrium morphology (*ll*) system, the B lamellae transforms to cylindrical or spherical pattern. In SBM11, the relative volume fractions of the three blocks are $\phi_S < \phi_B = \phi_M$. From the above explanation based on Ref [19], it can be postulated that the high volume fraction of middle B block results in a transformation of the morphology from lamellae phase to cylindrical or spherical phase.

Part II (Analysis of Mechanical Properties)

6.3 Mechanical properties of symmetric lamellar SBMs

In this section the mechanical properties of the lamellar SBMs consisting of nearly same weight fractions of the three blocks (symmetric type) are presented. The mechanical properties are discussed correlating the B microstructure and total molar mass of the polymer. In Table 6.13 the tested polymers are summarized along with the detailed constituents and tensile test results. The number of B repeating units and their ratios are also listed for a better overview of the SBMs. The total molar masses of the polymers vary within 38-170 kg/mol and the molar mass of the SM blocks are ranging from 24-115 kg/mol. The SBMs have different polybutadiene microstructures ranging from 16-90% of 1,2-B content.

The tensile curves obtained from the experiments are shown in Figure 6.15. One can see that the polymers with lower x(1,2)% and relatively higher 1,4-B content (e.g., SBM1, SBM3 and SBM7) show increasing stresses during elongation process. In these three SBMs, moderate stress drops occur after yielding. The maximum strain at break is found close to 600% or above. The yield stresses (σ_y) for these polymers show around 15 MPa. On the other hand, the polymers with higher x(1,2)% and relatively higher 1,2-B contents, lower strain hardening is observed. The yield stress (σ_y) is between 28 and 40 MPa, which is rather higher than that of 1,4-B rich SBMs. Among the 1,2-B SBMs, the SBM2 and SBM10 (Figure 6.15b, g) show moderate stress drops after yielding and comparatively lower strains at break (~400%) compared to 1,4.B rich SBMs. For SBM4 where the x(1,2)% is nearly the same and the molar mass of SM is smaller than that of SBM2 and SBM10, a significant stress drop after yield point is observed leading to a strain softening. Comparing the low molar mass SBMs, (e.g., SBM4 and SBM6) with the high molar mass SBMs, (e.g., SBM2 and SBM10), one can see that the lower molar mass SBMs result in lower strains at break compared to the others.

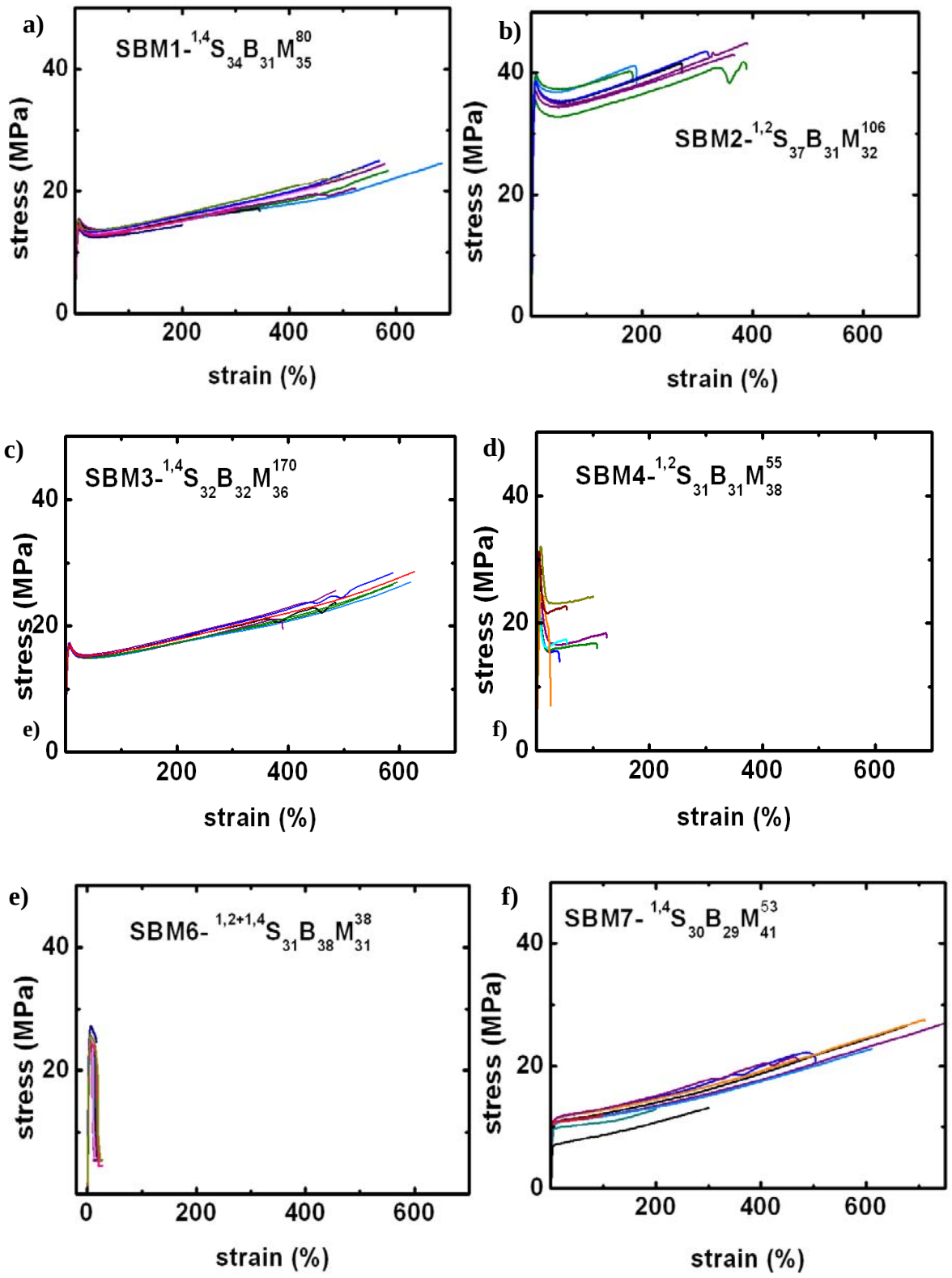
a)
SBM1-$^{1,4}S_{34}B_{31}M_{35}^{80}$
b)
SBM2-$^{1,2}S_{37}B_{31}M_{32}^{106}$
c)
SBM3-$^{1,4}S_{32}B_{32}M_{36}^{170}$
d)
SBM4-$^{1,2}S_{31}B_{31}M_{38}^{55}$
e)
SBM6-$^{1,2+1,4}S_{31}B_{38}M_{31}^{38}$
f)
SBM7-$^{1,4}S_{30}B_{29}M_{41}^{53}$
stress (MPa)
strain (%)
0
20
40
200
400
600

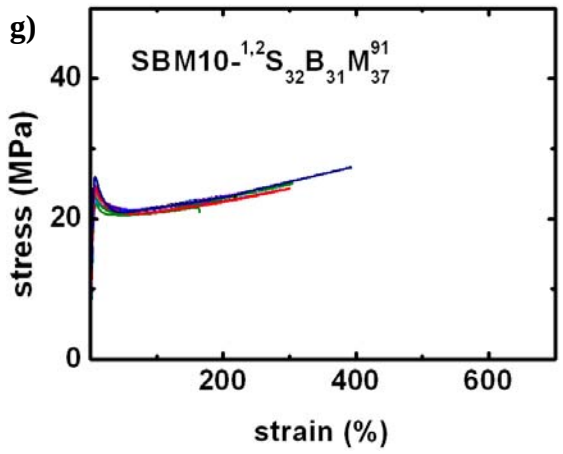

***Figure 6.15**: Stress-strain diagrams of the SBM polymers. Here, a) SBM1-$^{1,4}S_{34}B_{31}M_{35}^{80}$, b) SBM2-$^{1,2}S_{37}B_{31}M_{32}^{106}$, c) SBM3-$^{1,4}S_{32}B_{32}M_{36}^{170}$, d) SBM4 $^{1,2}S_{31}B_{31}M_{38}^{55}$, e) SBM6- $^{1,2+1,4}S_{31}B_{38}M_{31}^{38}$, f) SBM7-$^{1,4}S_{30}B_{29}M_{41}^{53}$, g) SBM10- $^{1,2}S_{32}B_{31}M_{37}^{91}$.*

***Table 6.13:** Microstructural constituents and tensile test results of the symmetric SBMs lamellae.*

Polymer	**No of 1,2-units**	**No of 1,4-units**	***1,2:1,4***	**Mn of SM block kg/mol**	***X* (1,2) %**	***E*, (MPa)**	**ε_B (%)**	**σ_B (MPa)**
SBM7 ($S_{30}B_{29}M_{41}^{53}$)	45	238	***1 : 5***	38	16	230 ± 14	600 ± 100	23 ± 4
SBM1 ($S_{34}B_{31}M_{35}^{80}$)	83	376	***1 : 4***	55	18	460 ± 28	528 ± 100	22 ± 3
SBM3 ($S_{32}B_{32}M_{36}^{170}$)	302	704	***1 : 2***	115	30	523 ± 32	575 ± 57	27 ± 2
SBM6 ($S_{31}B_{38}M_{31}^{38}$)	91	176	***1 : 2***	24	34	251 ± 36	19 ± 7	11 ± 1
SBM2 ($S_{37}B_{31}M_{32}^{106}$)	559	31	***8 : 1***	73	87	832 ± 113	337 ± 82	40 ± 3
SBM10 ($S_{32}B_{31}M_{37}^{91}$)	464	57	***8 : 1***	61	89	697 ± 30	226 ± 75	23 ± 1
SBM4 ($S_{31}B_{31}M_{38}^{55}$)	211	23	***9 : 1***	38	90	527 ± 64	96 ± 37	20 ± 6

A summary of the calculated data from the tensile tests, i.e., tensile modulus (E), stress at maximum (σ_M), strain at break (ε_B) of lamellar type SBMs are listed in Table 6.13. From the observation discussed above it is clear that the microstructural parameters influence the tensile property significantly. For a detailed understanding of the tensile test results, in the following the tensile properties are discussed with respect to the microstructure of B domains as well as the chain length of the glassy SM blocks.

6.3.1 Influence of glassy and rubbery blocks on the elastic modulus

Due to inherent structural properties of S, B, and M domains, the overall elastic modulus for different lamellar structure varies. In Figure 6.16 the elastic behavior of the polymers with respect to molar masses of the glassy SM block and B microstructures is shown. The dependency of tensile modulus on the molar masses of SM blocks can be seen in Figure 6.16a. For increasing molar masses the E modulus also increases. The highest tensile modulus, E = 832 MPa is obtained for SBM2 ($^{1,2}S_{37}B_{31}M_{32}^{106}$) due to it's high molar mass of the polymers and the glassy domains (106 and 73 kg/mol). On the other hand for SBM6 ($^{1,2+1,4}S_{31}B_{38}M_{31}^{38}$) this value is low (E = 251 MPa) because of its low molar mass of the polymer and the glassy domain (38 and 24 kg/mol). However, the tensile modulus for SBM3 has found comparatively low despite the high molar mass of the polymer and the glassy SM domains (170 and 115 kg/mol). This exception is mainly due to the influence of 1,4-B content which are more flexible than the 1,2-B. In following section and in Figure 6.16b the influence of B microstructure on the tensile modulus is described.

An increasing tendency of tensile modulus with the increase of 1,2-B content are noticed from Figure 6.16b. Higher modulus (527 MPa) is obtained for SBM4 ($S_{31}B_{31}M_{38}^{55}$) and lower modulus (230 MPa) is obtained for SBM7 ($S_{30}B_{29}M_{41}^{53}$), despite the fact that the weight fractions and molar masses of the glassy domains of both SBM4 and SBM7 are same (38 kg/mol). For SBM4 90% 1,2-B is present whereas for SBM7 only 16% 1,2-B is present. This means, more flexible 1,4-B domains are dominant in SBM7 than in SBM4. From the analysis of chemical structure of polybutadiene it is reported that the higher presence of 1,2-B results in less orientation and less flexibility compared to 1,4-B. Therefore, elastic modulus is increased if 1,2-B is predominant, (e.g., for SBM4). On the other hand, 1,4-B unit has four carbons in the backbone in one repeating unit, which causes more flexibility and more orientation during tensile test. Hence, lower modulus is obtained (e.g., for SBM7).

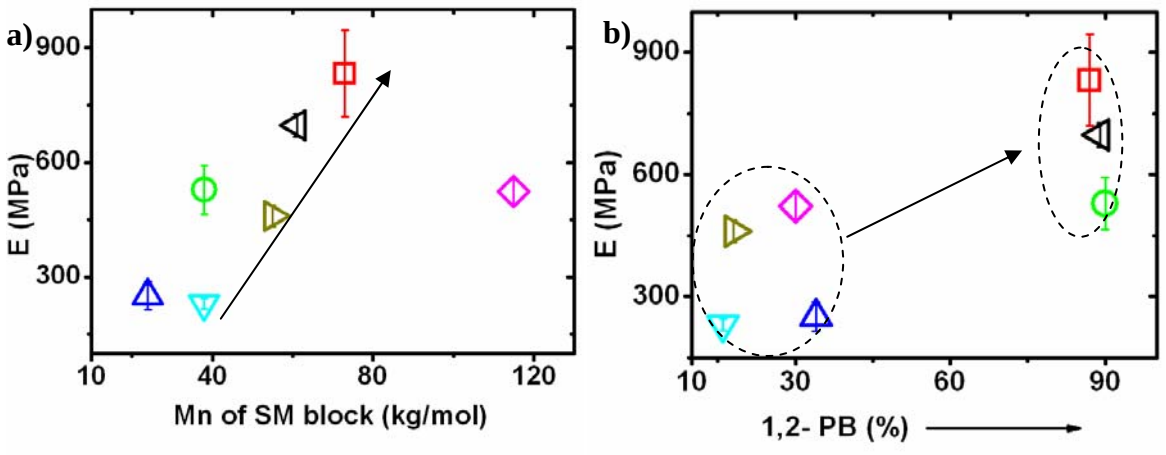

Figure 6.16: *Dependency of the tensile modulus E, on a) molar mass of SM blocks and b) 1,2-B contents of the polymers. Samples codes are* **:** *SBM1 ($^{1,4}S_{34}B_{31}M_{35}^{80}$)= ▷ ,SBM2 ($^{1,2}S_{37}B_{31}M_{32}^{106}$)= □, SBM3 ($^{1,4}S_{32}B_{32}M_{36}^{170}$)= ◇ ,SBM4 ($^{1,2}S_{31}B_{31}M_{38}^{55}$)= ○, SBM6 ($^{1,2+1,4}S_{31}B_{38}M_{31}^{38}$)=△, SBM7 ($^{1,4}S_{30}B_{29}M_{41}^{53}$)= ▽, SBM10 ($^{1,2}S_{32}B_{31}M_{37}^{91}$)=◁.*

An exceptional behavior of B microstructure on the tensile modulus is seen when the ratio of 1,2- and 1,4-B repeating units is close to ***1:2***. In case of SBM3 ($S_{32}B_{32}M_{36}^{170}$), the tensile modulus is almost same as the modulus of SBM4 ($S_{31}B_{31}M_{38}^{55}$) despite very high molar mass of the SM blocks of SBM3 (115 kg/mol) compared to SBM4 (38 kg/mol) is present. From Table 6.13, it has been seen that the ratio's of 1,2- and 1,4- B units is ***1: 2*** in SBM3, whereas it is ***9:1*** in SBM4. Therefore, SBM3 shows comparatively lower tensile modulus than SBM4, although the number of 1,2-units for SBM3 is 302 and for SBM4 it is 211. It is assumed that at this ratio (***1:2***) of 1,2- and 1,4-B repeating units the stiffness of 1,2-B is degraded by more flexible 1,4-B. This observation can also be supported by the tensile modulus for SBM6 ($S_{31}B_{38}M_{31}^{38}$) where the same ratio of the B repeating units (***1:2***) is present. Due to the presence of higher 1,4-B, the tensile modulus is the lowest (251 MPa) in this polymer.

6.3.2 Influence of glassy and rubbery blocks on the stress at break

The stress at break for different molar masses of SM block and B microstructure of SBMs are shown in Figure 6.17. It has been seen from Figure 6.17a that the variation in stress at break is moderately governed by the molar mass of the glassy SM blocks. For example, the lowest stress at break is obtained in SBM6 (11 MPa) due to its low molar mass of SM block (24 kg/mol) whereas in SBM2 this stress is very high (40 MPa), which is mainly due to its high molar mass of SM block (73 kg/mol). The lower stress values (22-23 MPa) are observed in the polymers with the molar mass of SM blocks ranging from 38 to 61 kg/mol, as shown by a circle in Figure 6.17a. In this region the SBMs contain

both the 1,2- and 1,4-B contents with a significant variation, but the resulting σ_B, is same for those polymers (also see the circles in Figure 6.17b). The result indicates that the influence of B microstructure on the stress at break may not be prominent. Again, the SBM10 and SBM4 show low stress at break (σ_B = 20-23 MPa) despite their high content of 1,2-B, where $x(1,2)$ is ≥ 89% (Figure 6.17b). In this case, the low molar mass of SM blocks (38-61 kg/mol) results in lower stress at break.

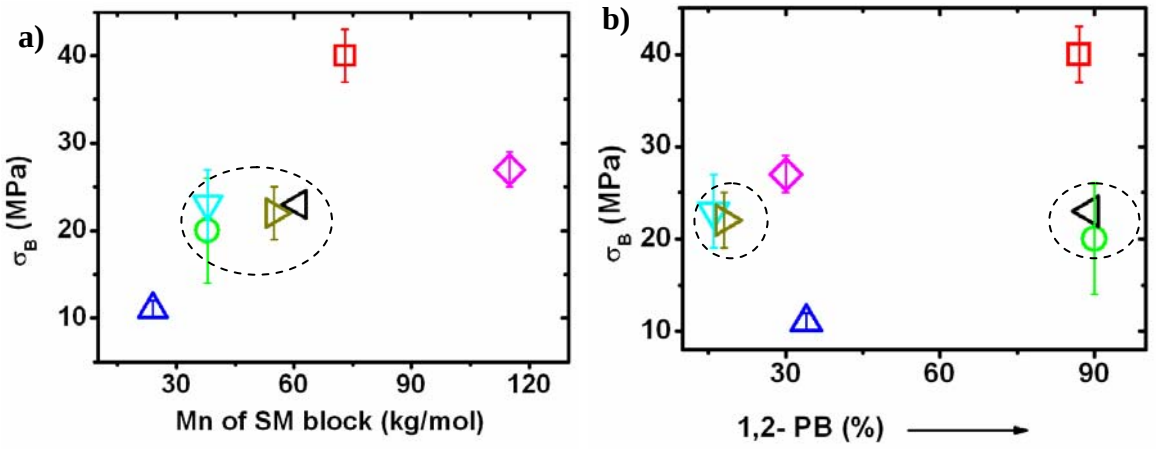

Figure 6.17: *Dependency of stress at break σ_B on the a) molar masses of SM blocks and b) 1,2-B microstructure of the polymers. Samples codes are : SBM1($^{1,4}S_{34}B_{31}M_{35}^{80}$)=▷, SBM2 ($^{1,2}S_{37}B_{31}M_{32}^{106}$)=□, SBM3($^{1,4}S_{32}B_{32}M_{36}^{170}$)=◇, SBM4($^{1,2}S_{31}B_{31}M_{38}^{55}$)=○, SBM6 ($^{1,2+1,4}S_{31}B_{38}M_{31}^{38}$)=△, SBM7($^{1,4}S_{30}B_{29}M_{41}^{53}$)=▽, SBM10 ($^{1,2}S_{32}B_{31}M_{37}^{91}$)=◁.*

6.3.3 Influence of glassy and rubbery blocks on the strain at break

Figure 6.18 shows different strains at break for the polymers containing different polybutadiene microstructure and different molar masses of SM blocks. The influence of final elongation on the molar masses of SM blocks is depicted in Figure 6.18a where an increasing tendency of final strain (strain at break) is noticed for an increasing molar mass. An exception has been noticed for the SBM1 and SBM7 having lower molar masses of SM blocks, 55 kg/mol and 38 kg/mol, respectively. Both the polymers show higher strain at break. This behavior is due to the presence of B microstructure which

can be better explained by the Figure 6.18b. Here, the influence of B microstructure on the strain at break is shown.

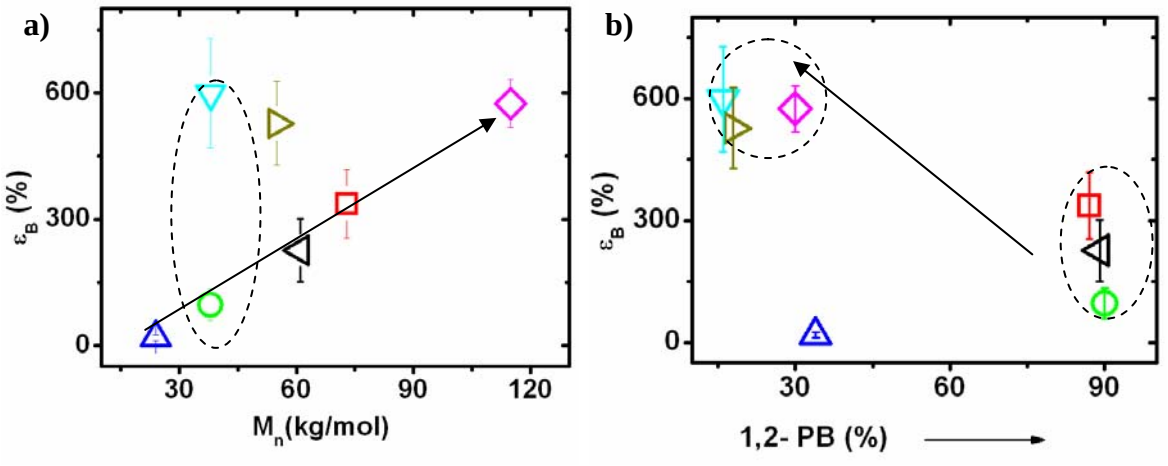

Figure 6.18: *Dependency of the strain at break on the a) molar masses of SM blocks and b) 1,2-B microstructure of the polymers. Samples codes are : SBM1($^{1,4}S_{34}B_{31}M_{35}^{80}$)=▷, SBM2 ($^{1,2}S_{37}B_{31}M_{32}^{106}$)=□, SBM3($^{1,4}S_{32}B_{32}M_{36}^{170}$)= ◇, SBM4($^{1,2}S_{31}B_{31}M_{38}^{55}$)= ○, SBM6 ($^{1,2+1,4}S_{31}B_{38}M_{31}^{38}$)=△, SBM7($^{1,4}S_{30}B_{29}M_{41}^{53}$)= ▽, SBM10 ($^{1,2}S_{32}B_{31}M_{37}^{91}$)=◁.*

An increasing tendency of the strain at break is noticed with an increasing 1,4-B content. As in SBM1 and SBM7 the 1,4-B content is higher (88%), a higher strain at break is accountable. Further influences of the B microstructure are compared for SBM7 and SBM4. In both the polymers the molar masses and the weight fractions of different blocks are same. The results show very high strain at break in SBM7 (ε_B = 600%) for 1,4-B, whereas in SBM4, the strain value is very low (ε_B = 96%) for 1,2-B. For lamellar patterns, the percentage of 1,2- and 1,4-B repeating units also influences the elongation behavior (strain at break) of the polymer. For example, in SBM3 ($S_{32}B_{32}M_{36}^{170}$) 302 units of 1,2-B and 704 units of 1,4-B at a ratio of ***1 : 2*** is present. On the other hand the SBM7 ($S_{30}B_{29}M_{41}^{53}$) has only 45 units of 1,2-B and 235 units of 1,4-B at a ratio of ***1: 5***. Though the molar mass of SBM3 is 3 times higher than the SBM7, the strain at break is almost same (ε_B = 575% and 599%) for both the polymer. Hence, the B domains are more dominant on the strains at break.

6.4 Mechanical properties of asymmetric lamellar SBMs

The asymmetric type lamellar SBMs where the M contents are higher (45 < w_M (%) < 54) than the S and B contents are discussed here. These polymers have a higher content of 1,4- B isomers (86 to 88%). The molar mass of the SM blocks ranges from 42 to 105 kg/mol. The structural constituents

e.g., the number of repeating units and their ratios as well as the mechanical properties, e.g., tensile modulus (*E*), stress at maximum (σ_M), strain at break (ε_B) are listed in Table 6.14.

Table 6.14: *Results of the stress-strain test and the weight percentage of asymmetric type lamellar polymers and number of repeating unit of B domains.*

Polymer Batch no.	**No of 1,2-units**	**No of 1,4-units**	***1,2 : 1,4***	**M_n of SM block kg/mol**	***x*(1,2) %**	***E* (MPa)**	**ε_B(%)**	**σ_B(MPa)**
SBM8 ($S_{21}B_{27}M_{52}^{75}$)	90	285	1:4	54	22	356 ± 31	111	16 ± 1
SBM9 ($S_{24}B_{25}M_{54}^{54}$)	38	232	1:6	42	14	537 ± 51	261 ± 15	28 ± 1
SBM11 ($S_{26}B_{29}M_{45}^{148}$)	111	683	1:6	105	14	554 ± 68	767 ± 21	23 ± 1

In Figure 6.19 the tensile curves of the tested asymmetric SBMs are plotted. The yield stress seems to be the same for SBM8, SBM9, and SBM11 but after the yield point a constant stress for SBM8, while an increase in stress for SBM9 and a reduce of stress for SBM11 are observed. It has been observed that the higher molar mass SBMs show prominent strain softening followed by strain hardening (also seen for the symmetric SBMs in previous section). In SBM8 almost no strain softening and in SBM9 strain hardening are observed.

From the Figure 6.19 one can also see the elongation behavior of the asymmetric SBMs. As the presence of 1,4-B content increases the flexibility of chains, a higher elongation is obtained for the SBMs with a higher 1,4-B content, i.e., more elongation is obtained for SBM11 and SBM9 (with the ratio of 1,2-: 1,4-B = ***1:6***) compared to SBM8 (with the ratio of 1,2-: 1,4-B = ***1:4***). Also notice that the SBM9 and SBM11 have same ratio of 1,2-B : 1,4-B, (i.e. ***1:6*** for both cases) but the SBM11 shows significantly higher elongation at break, ε_B. This higher ε_B of SBM11 is due to its higher molar mass compared to the molar mass of SBM9. Increasing the molar mass increases the strain at break was also seen for symmetric SBMs, recall Figure 6.18a.

For a detailed understanding of the tensile behavior following the mechanical properties are discussed with respect to the presence of constituent.

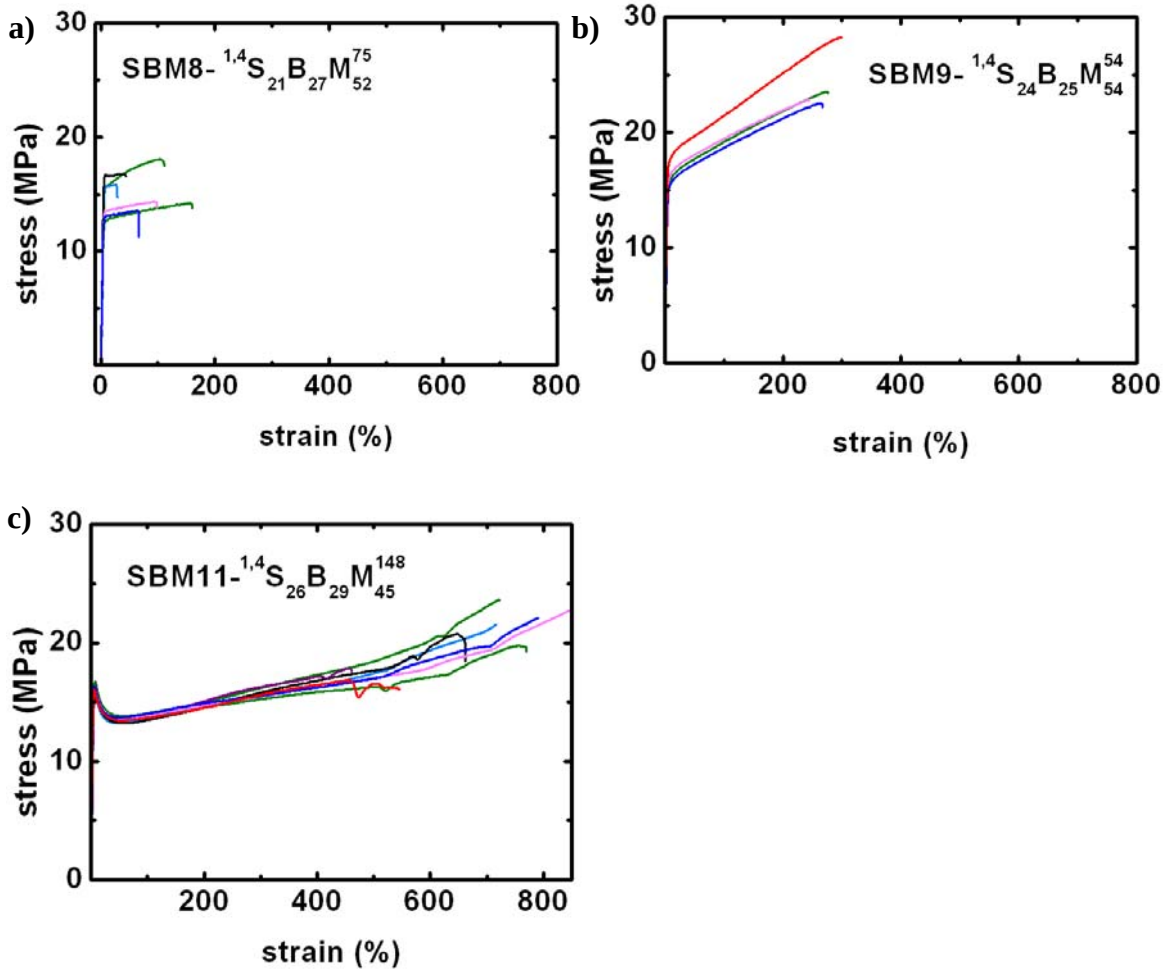

Figure 6.19: *Stress-strain diagrams of the SBM polymers. Here, a) SBM8-$^{1,4}S_{21}B_{27}M_{52}^{75}$, b) SBM9-$^{1,4}S_{24}B_{25}M_{54}^{54}$, c) SBM11-$^{1,4}S_{26}B_{29}M_{45}^{148}$.*

6.4.1 Influence of glassy and rubbery blocks on the elastic modulus

The dependency of the tensile modulus on the molar mass of the glassy SM domains and the polybutadiene microstructure of the polymers are depicted in Figure 6.20. Among the three polymers, SBM9 ($S_{24}B_{25}M_{54}^{54}$) and SBM11 ($S_{26}B_{29}M_{45}^{148}$) show almost the same tensile moduli, although the molar mass of the SM block of SBM9 is lower than that of SBM11. Hence, no dependency of tensile moduli on the molar mass of the glassy domains can be established for asymmetric lamellae (see Figure 6.20a). On the contrary, a dependency of the tensile modulus on the ratio of the B microstructure is observed. The ratio of 1,2- and 1,4- B in SBM8 ($S_{21}B_{27}M_{52}^{75}$) is lower (***1 : 4***) than the ratio of 1,2- and 1,4-B in SBM9 and SBM11 (***1:6***). With a minor increase of 1,2-B content, (the

relative ratio changes from ***1:6*** to ***1: 4***), the stiffness of the polymer decreases very sharply, as can be seen from Figure 6.20b.

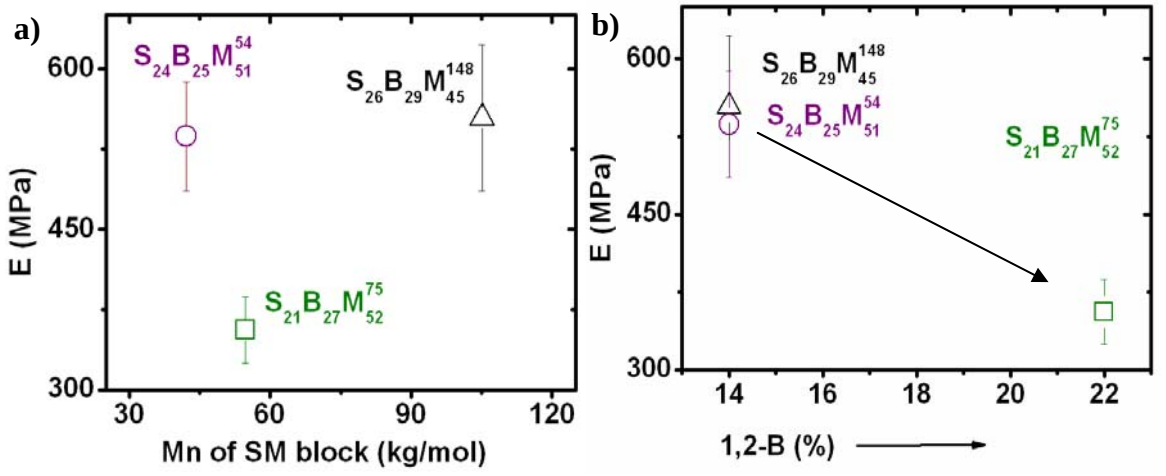

Figure 6.20: *Dependency of the tensile modulus E, on the a) molar mass of SM block and b) 1,2-B microstructure of the polymers.*

6.4.2 Influence of glassy and rubbery blocks on the stress at break

The dependency of stress at break on the total molar mass of SM blocks and the B microstructure are shown in Figure 6.21. Although the molar mass of SM block of SBM11 is higher (105 kg/mol) than that of SBM9 (42 kg/mol), stresses at break for SBM11 is lower, e.g., for SBM11 $\sigma_B = 23$ MPa and for SBM9 $\sigma_B = 28$ MPa. As observed in Figure 6.21a, the molar mass of the polymers does not influence the stress at break. However, in Figure 6.21b, a decreasing trend of the stress at break (σ_B) for increasing 1,2-B microstructures can be observed. For 14% of 1,2- B the stress at break, $\sigma_B = 28$ MPa, is obtained, whereas with a slight increase of 1,2- B (21%) a rapid decrease of stress at break, $\sigma_B = 16$ MPa is noticed.

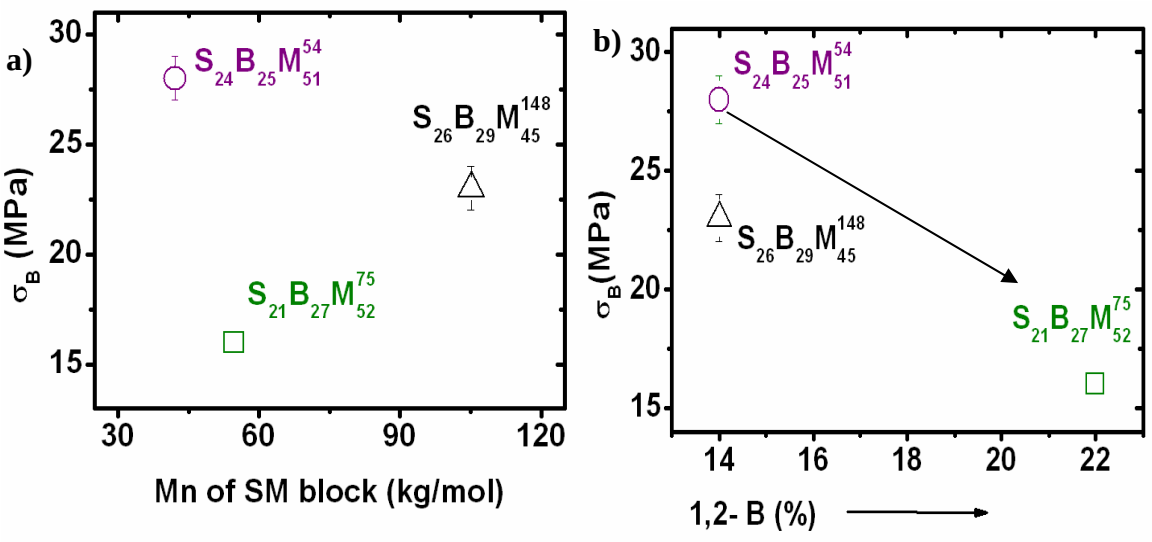

Figure 6.21: *Dependency of the stress at break σ_B on the molar mass of the glassy domains and the. 1,2-B content.*

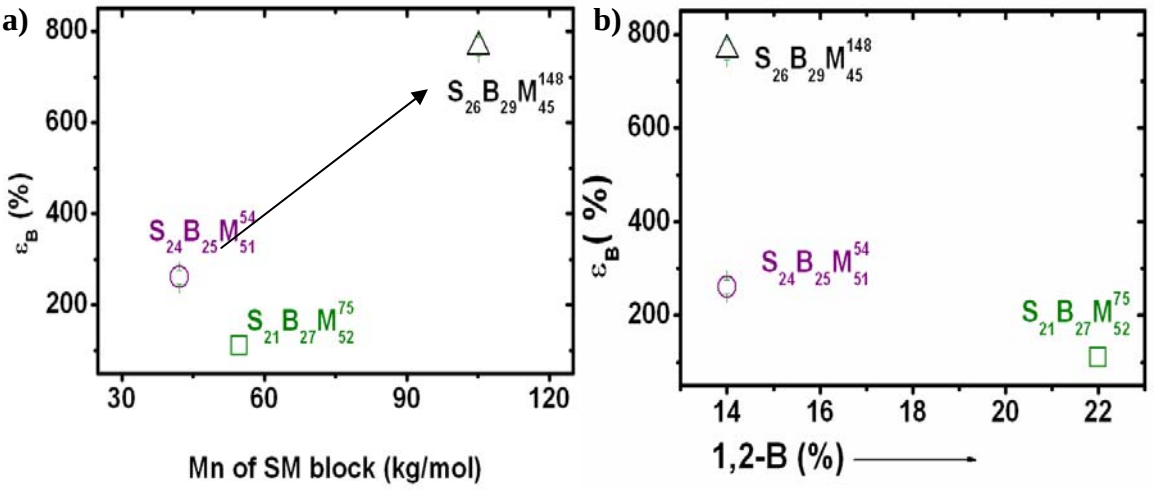

Figure 6.22: *Dependency of the strain at break on the molar mass of the glassy domains and the. 1,2-B content.*

6.4.3 Influence of glassy and rubbery blocks on the strain at break

The dependency of strain at break on the molar mass of the SM blocks and the B microstructure can be understood from Figure 6.22. An increasing tendency of strain at break for SM glassy domains is obtained (see Figure 6.22a). A very high elongation at break (767%) is noticed for SBM11 ($S_{26}B_{29}M_{45}^{148}$) whereas for SBM9 ($S_{24}B_{25}M_{54}^{54}$) it is 261%. This phenomena can be explained with

respect to the number of repeating units of 1,2- and 1,4-B. Both the polymers have the same amount of 1,2-B microstructure (14%) and ratio of 1,2- and 1,4- B (***1: 6***). However, 683 units of 1,4-B are present in SBM11 and only 232 units of 1,4-B exist in SBM9. Hence, the higher elongation at break in SBM11 is mainly due to the high molar mass, i.e., due to the long B chain. Again the lowest elongation at break (111% elongation) is seen in SBM8 ($S_{21}B_{27}M_{52}^{75}$), though the number of 1,4-B repeating units are higher (285 unit) than that of SBM9 (232 units) (Figure 6.22b). This result mostly occurred due to the ratio of 1,2- and 1,4-B which is ***1:4***. Hence, it can be said that the elastomeric properties are mostly influenced by the ratio between the B microstructures as well as the chain length of SM blocks.

6.5 Summary

Different lamellar SBMs have been characterized by TEM and SAXS as well as DMA and DSC. The formation of lamellar morphologies is influenced by the total molar mass and the polybutadiene microstructure of the polymer. For the molar masses ranging from 80 to 170 kg/mol, very well segregated lamellar domains are obtained. Short lamellar domains are found for the molar masses ranging from 40 to 55 kg/mol. Mixed lamellae are obtained mostly when 1,4-B is predominant. Again, the transitions of B from lamellae to cylinder structure can be seen in the SBMs containing a higher 1,2-B and in the the presence of SB residuals. A chain like oriented lamellae is obtained for a polymer, $S_{31}B_{38}M_{31}^{38}$ due to the low molar mass and the ratio of 1,2- and 1,4-B which is ***1:2***.

The mechanical properties are investigated on symmetric and asymmetric polymers with lamellar morphology. In case of symmetric polymers, the results show a significant influence of B microstructures on the elongation behavior. Higher elongation is obtained if the 1,4-B is predominant in SBM. Also, high molar masses favor a higher elongation to break. The tensile moduli are mainly dominated by the total molar mass, the presence of glassy phases, S or M, and higher 1,2- B content. On the contrary, the increasing tendency of stress at break is dominated moderately by an increasing tendency of the total molar mass of the polymers and the glassy domains.

In case of asymmetric SBMs, the tensile modulus and the stress at break strongly depend on the ratio of 1,2- and 1,4-B. Slight increase of the 1,2-B content (relative ratio of 1,2- and 1,4-B changes from ***1:6*** to ***1: 4***) decrease the stiffness of the polymer sharply. On the other hand, the elastomeric properties increase for high molar masses of the glassy SM blocks and for the ratio between the B microstructures when reaches to ***1:4***.

Reference

[1] U. Breiner, U. Krappe, T. Jakob, V. Abetz, R. Stadler, *Polym. Bull.* **1998**, *40*, 219.

[2] U. Breiner, U. Krappe, V. Abetz, R. Stadler, *Macromol. Chem. Phys.* **1997**, *198*, 1051.

[3] S. Brinkmann-Rengel, "Thermoplastic Elastomere auf Basis von ABA und ABC Dreiblockcopolymer", in *am Fachbereich Chemie und Pharmazie*, der Johannes Gutenberg-Universität Mainz, 1998.

[4] U. Krappe, R. Stadler, I. G. Voigt-Martin, *Macromolecules* **1995**, *28*, 4458.

[5] U. Breiner, U. Krappe, E. L. Thomas, R. Stadler, *Macromolecules* **1998**, *31*, 135.

[6] P. Tang, F. Qui, H. Zhang, Y. Yang, *J. Phys. Chem. B* **2004**, *108*, 8434.

[7] K. Arai, T. Kotaka, Y. Kitano, K. Yoshimura, *Macromolecules* **1980**, *13*, 1670.

[8] Y. Mogi, K. Mori, H. Kotsuji, Y. Matsushita, I. Noda., *Macromolecules* **1993**, *26*, 5169.

[9] C. Auschra, R. Stadler., *Macromolecules* **1993**, *26*, 2171.

[10] M. Shibayama, H. Hasegawa, T. Hashimoto, H. Kawai, *Macromolecules* **1982**, *15*, 274.

[11] U. Breiner, "Morphologische Studien zum Phasenverhalten mikrophasenseparierter ABC Dreiblockcopolymer", in *am Fachbereich Chemie und Pharmazie*, der Johannes Gutenberg-Universität Mainz, 1996.

[12] T. Goldacker, "Überstrukturen in Mischungen aus Blockcopolymeren", in *im Fach Chemie der Fakultät für Biologie, Chemie und Geowissenschaften*, Univerrsität Bayreuth, 1999.

[13] K. Jung, "Polybutadien-*block*-polystyrol-*block*-polymethylmethacrylat-Dreiblockcopolymere-Vom Spiel mit der Monomersequenz zu nicht-zentrosymmetrischen Schichtstrukturen." in *an Fachbereich Chemie und Pharmazie*, der Johannes Gutenberg-Universität Mainz, 1996.

[14] C. C. Honeker, E. L. Thomas, *Chem. Mater.* **1996**, *8*, 1702.

[15] J. Brandrup, E. H. Immergut, E. A. Grulke, *Polymer Handbook.* **1999**, *Fourth Edition*.

[16] S. Kim, J. Lee, S. M. Jeon, H. H. Lee, K. Char, B. H. Sohn, *Macromolecules* **2008**, *41*, 3401.

[17] W. Zheng, Z. G. Wang, *Macromolecules* **1995**, *28*, 7215.

[18] S. Sakurai, T. Momii, K. Taie, M. Shibayama, S. Nomura, *Macromolecules* **1993**, *26*, 485.

[19] W. Zheng, Z. G. Wang., *Macromolecules* **1995**, *28*, 7215.

Chapter 07

Influence of Morphology and Polybutadiene Microstructure on SBM Deformation

In this chapter the deformation of the SBM morphology during tensile test are discussed. SBM of symmetrical and transitional lamellar microstructure were investigated especially focusing on the effect of the 1,2-B or 1,4-B on the resulting microstructure after deformation. The SBM copolymers are further organized into a group of low molar mass and a group of high molar mass.

7.1 Deformation of morphology containing 1,2- and 1,4-SBMs: Investigation for low molar mass SBM

7.1.1 Stress-strain behavior of $^{1,2}S_{31}B_{31}M_{38}^{55}$ and $^{1,4}S_{30}B_{29}M_{41}^{53}$

The mechanical properties, the morphologies, and the influence of the 1,2- and 1,4-B contents on the deformation behavior of SBMs are systematically investigated. For this investigation two SBMs, $^{1,2}S_{31}B_{31}M_{38}^{55}$ and $^{1,4}S_{30}B_{29}M_{41}^{53}$ were chosen. A series of tensile tests has been performed for both the polymers, for which the stress-strain curves are shown in Figure 7.1. The molecular compositions and molar masses are the same for both the polymers; however, the B content is different. The $^{1,2}S_{31}B_{31}M_{38}^{55}$ contains 90% of 1,2-B whereas the $^{1,4}S_{30}B_{29}M_{41}^{53}$ contains 84% of 1,4- B.

For the polymer, $^{1,2}S_{31}B_{31}M_{38}^{55}$, the maximum strain at break does not exceed 120%. Only few curves reach strains exceeding 100% before the final failure occurs. Here, two curves show approx. 60% whereas one curve shows less than 30% strain. On the other hand, the polymer $^{1,4}S_{30}B_{29}M_{41}^{53}$ exceeds the strain at break 700%. The curves of all the specimens of this polymer show that the polymer tolerates strains higher than 100%. These characteristic results indicate that the E-modulus as well as the yield stress for $^{1,2}S_{31}B_{31}M_{38}^{55}$ is higher compared to $^{1,4}S_{30}B_{29}M_{41}^{53}$. In case of $^{1,2}S_{31}B_{31}M_{38}^{55}$ a sharp yield drop can be observed after yielding, which is mainly due to a macroscopic necking caused by the

continuous M phase. This typical feature can be seen in the ductile polymers. For higher elongations the stress remains constant up to the final break down of the sample. The steadiness of stress level in the stress-strain curve indicates no strain hardening or network formation, but an intermolecular interaction according to the theory of Meijer et al. [1]

For $^{1,4}S_{30}B_{29}M_{41}^{53}$ an increase in stress occurs under elongation just after yielding (strain hardening). Moreover, in this polymer a moderate necking is observed. From the fundamental understanding of the polymer deformation it can be speculated that when two adjacent continuous phases with highly different mechanical properties (in this case, glassy S or M and rubbery B) are segregated, most of the mechanical forces are absorbed in the elastic domains without distorting the glassy ones. That means the moderate necking is occurred because of the incomplete distortion of the hard S and M domains. The occurring of strain hardening at higher elongations could be explained by an intramolecular interaction of 1,4-B.[2] Such stress-strain behavior with low yield point is a typical feature of a rubbery material. Here the polymer's behavior seems to be dominated by the continuous 1,4-B domains which exist as a lamellar pattern.

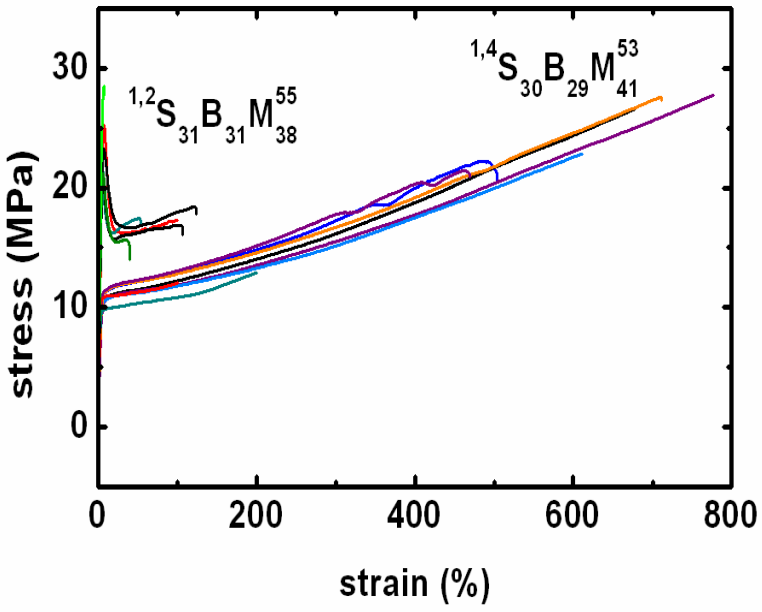

Figure 7.1: *The stress-strain curve of several specimens of $^{1,2}S_{31}B_{31}M_{38}^{55}$ and $^{1,4}S_{30}B_{29}M_{41}^{53}$. $^{1,2}S_{31}B_{31}M_{38}^{55}$ shows high strain softening with low strains at breaks up to 120% whereas $^{1,4}S_{30}B_{29}M_{41}^{53}$ shows low strain softening with higher strains at break up to 700%.*

7.1.2 Morphology of $^{1,2}S_{31}B_{31}M_{38}^{55}$ and $^{1,4}S_{30}B_{29}M_{41}^{53}$ before and after tensile test

a) Morphology of $^{1,2}S_{31}B_{31}M_{38}^{55}$

In Figure 7.2a TEM image of $^{1,2}S_{31}B_{31}M_{38}^{55}$ in the absence of strain is shown. The morphology shows discontinuous B lamellae with a transition to cylindrical pattern. In some areas these B cylinders arrange as hexagonally pattern as can be seen in the circle 1. There are lamellar glassy phase with undulated B lamellae can be recognized in the circle 2. The S domains attach to the B domains and the M domains form a continuous phase surrounding the S and B domains (see section 6.2.2 in chapter 06 for details of it's morphology).

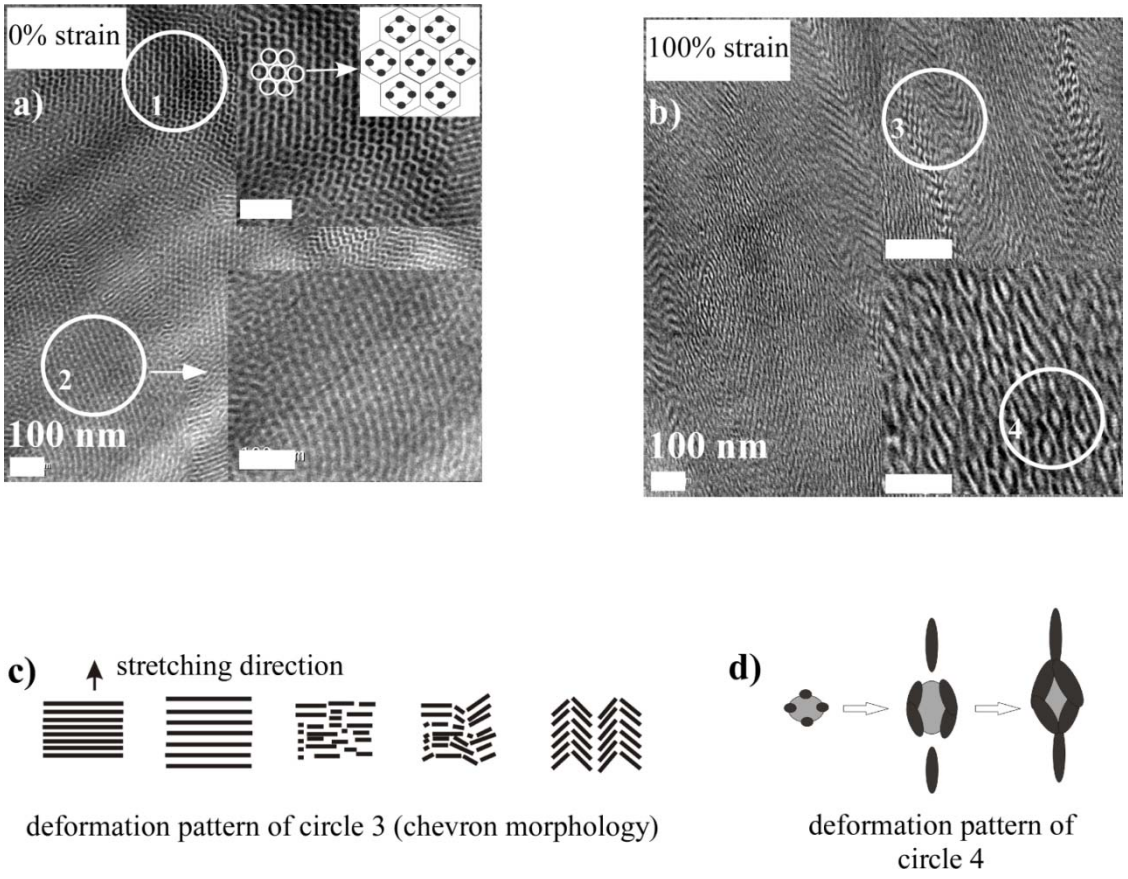

Figure 7.2: *a) The TEM images of $^{1,2}S_{31}B_{31}M_{38}^{55}$. The polymer film was stained with OsO_4. The color code: S = gray, B = black, M = white. circle 1 shows the hexagonally arrayed PB cylinders. Circle 2 shows the lamellar area b) Deformation of the morphology after 100% strain leading to 3) the zig-zag pattern, and 4) the deformed cylindrical pattern. The sketched mechanism of the deformation patterns are given in c) and d).*

The morphology after 100% strain is shown in Figure 7.2b where two magnified TEM images of the deformation patterns are given (see circle 3 and 4). Circle 3 shows a zig-zag pattern of the lamellar domains. According to Hashimoto et al. [3] when the stretching direction is parallel, perpendicular or 45° with respect to the cylindrical domain axis, a chevron structure are formed as the final morphology. Its evolution begins with expanding the lamellar domains along the stretching direction. At the yield point, the S domains are fragmented into smaller regions. These fragmented domains can now orient more easily with the flexible B domains resulting in a zig-zag pattern as sketched in Figure 7.2c.

A schematic sketch of the second type of deformation is given in Figure 7.2d. It is speculated from the TEM image that the pseudo-hexagonally arranged B domains are elongated along the stretching direction. With further stretching, the four B cylinders are further deformed which are connected to their end. Finally, the S domain is isolated by the adjacent B domains as can be seen in the circle 4. Odell and Keller[4] experimented similar type morphology in SBS triblock copolymer where a hexagonally arrayed S cylinders embedded in a rubbery B matrix. On parallel straining, the stress-strain curves displayed a yield behavior at 3% strain, the yielded material became more compliant even at small strains which they explained in terms of breaking up and reformation of the cylinders. Again, Argon and co-workers[5] proposed a two-step craze growth mechanism for SB diblock copolymers having their B domains as hexagonally packed cylinders embedded in the S matrix. In that case, first the material was elastically deformed up to a critical strain then at elevated stresses cavitation was observed within the domains, and finally a necking was occurred with a fibril formation of S matrix. In present polymer as understood the craze formation as well as the distortion of the B domains can be speculated. Furthermore, the stress whitening in the specimens during elongation at around 10% indicates the crazing formation of the glassy domains.

b) Morphology of $^{1,4}S_{30}B_{29}M_{41}{}^{53}$

Figure 7.3a shows a well segregated lamellar pattern with large dimensions of the domains. When the specimens are elongated up to 100% strain perpendicular to the lamellar direction (indicated with the white arrow), only minor distortion are observed in B domains as indicated in Figure 7.3b. Due to the high flexibility of B block a wavy pattern results under deformation. When increasing the elongation upto 300%, the B lamellae transform into a very wavy but still the lamellar domains are not completely distorted. Entanglement of the B domains is accountable in this stage as stress hardening can be seen (see also Figure 7.1).

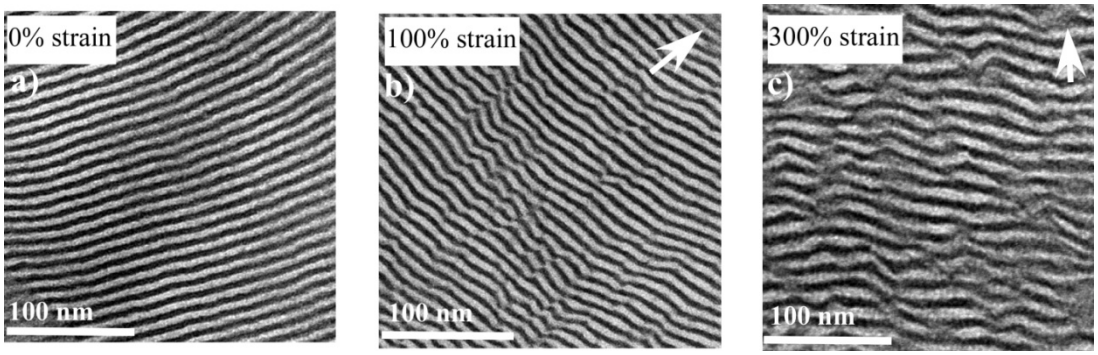

Figure 7.3: *TEM micrographs highlighting the deformation of the morphology of* $^{1,4}S_{30}B_{29}M_{41}{}^{53}$ *at 0%, 100% and 300% strain (white arrow indicates the stretching direction). The wavy B domains are seen at 100% strain while the distorted B lamellae are seen at 300% strain.*

7.1.3 In-situ combination of SAXS and tensile testing for $^{1,2}S_{31}B_{31}M_{38}{}^{55}$ and $^{1,4}S_{30}B_{29}M_{41}{}^{53}$

a) In-situ combination of SAXS and tensile testing for $^{1,2}S_{31}B_{31}M_{38}{}^{55}$

The in-situ SAXS tensile testing of specimens of $^{1,2}S_{31}B_{31}M_{38}{}^{55}$ shows the deformation behavior and the underlying mechanism in greater detail. The results of this experiment are shown in Figure 7.4, which depicts a stress-strain plot as well as four 2D-SAXS images recorded at 0%, 7%, 31% and 53% strain.

In $^{1,2}S_{31}B_{31}M_{38}{}^{55}$ an anisotropic SAXS pattern can be seen at its final deformation. At the initial stage (ε = 0%) due to the randomly oriented domains an isotropic SAXS pattern of two rings is found. The second image was recorded after the yield point (ε = 7%). At this point, both the meridional and equatorial SAXS maximum is deformed in an elliptical manner. A yielding drop occurs for the distortion of the glassy domains. The mechanical forces are absorbed into the rubbery domains causing plastic to rubbery transition at this stage. When the elongation has reached 31%, the outer ring almost disappears and the inner ring turns to an oval. The alteration of the scattering rings commences at a deformation of 31% can be interpreted as breaking down of the rubbery domains which are reoriented to the stretching direction. Finally at an elongation rate of 53% the anisotropic SAXS pattern is found where the equatorial SAXS maximum is highly elongated. In this stage, highly extension occurred in the rubbery domains.

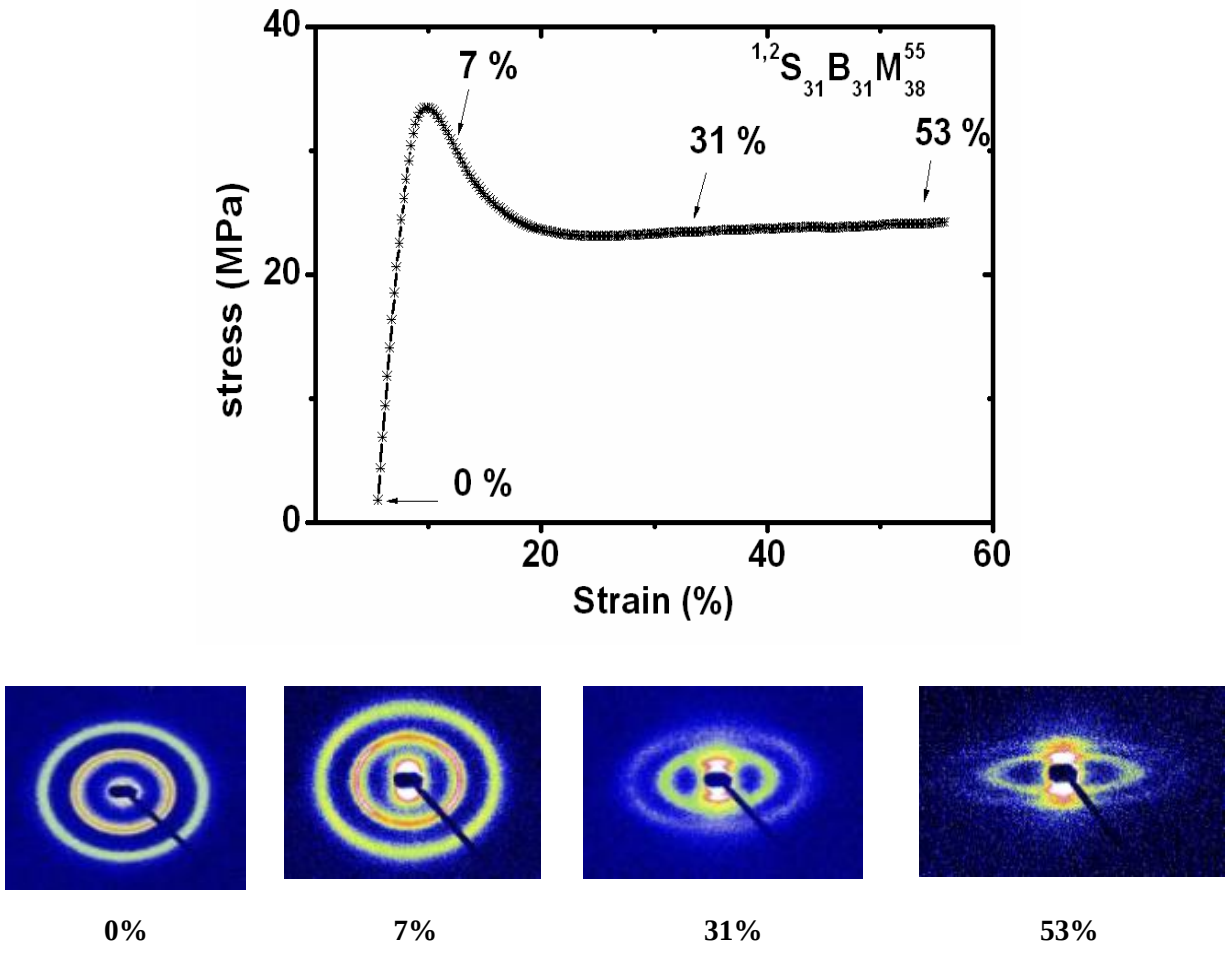

Figure 7.4: *Results of the combination of SAXS and tensile testing for SBM $^{1,2}S_{31}B_{31}M_{38}^{55}$. Stress-strain diagram (top). 2D-SAXS patterns of obtained at strain, (ε) = 0%, 7%, 13%, 53% (bottom).*

The deformation mechanism is further investigated by plotting intensity as a function of the azimuth angle. The so-called azimuthal plot, which indicates a continuous change of the intensity with increasing stretching of the specimens' is shown in Figure 7.5a. At 0% strain, no change of the intensities profile for all azimuth angles can be found indicating the presence of randomly oriented cylindrical domains only. When the strain reaches 7%, the scattering intensities oscillate for angles from 155° to 200°. At the higher elongation of 31%, the intensity maxima for φ = 180° decreases. The effect continues for the highest elongation at 53%. The intensity decrease indicates that a change of the orientation of the deformed domains from meridional to equatorial maxima has taken place. The corresponding change of the interdomain distance during the elongation process can be seen in Figure 7.5b, where the SAXS intensity is plotted against the scattering vector *q* at the strain rates of 0%, 7%,

31% and 53%. Obviously, at 0% strain, two sharp peaks at 0.14 nm^{-1} and 0.24 nm^{-1}appear; their intensity reduces, however at 7% strain. This reduction indicates the tendency that the interdomain spacing increasing along the stretching direction. The intensities further decrease at 31% strain and at 53% no peaks can be detected at all as at this stage the sample's orientation completely broke down. The domain sizes of B before stretching was 10 ± 1 nm which became 5 ± 2 nm after 100% strain. The distance of the long periodicity was changed from 34 ± 1 nm to 27 ± 2 nm as calculated from the TEM image in Figure 7.2.

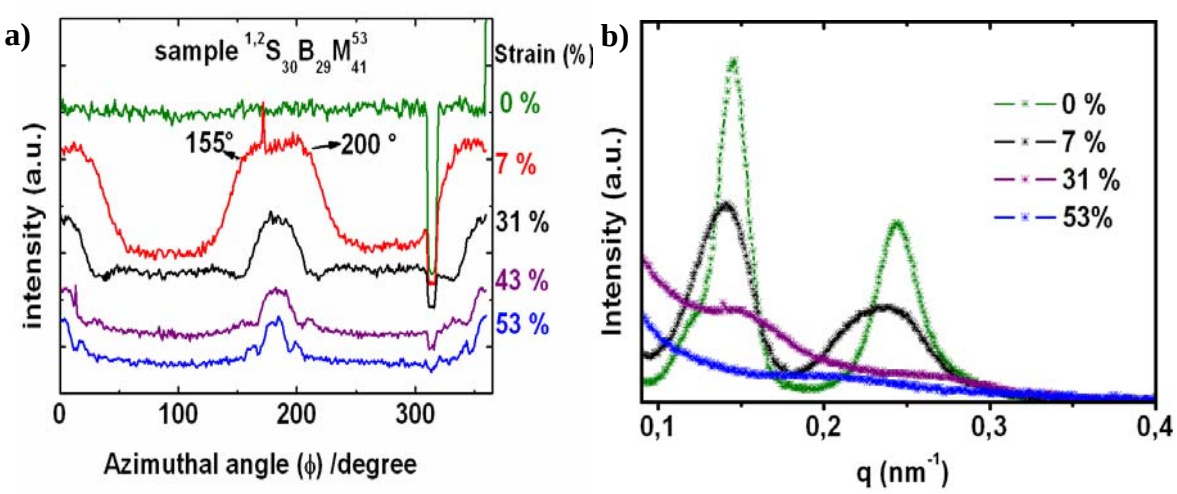

Figure 7.5: *Results of the combination of SAXS and tensile testing for $^{1,2}S_{31}B_{31}M_{38}^{55}$. SAXS results a) intensity vs azimuthal plot for q = 0.14 nm^{-1} show the changes of intensities at azimuth angle with increasing elongation b) 1D-SAXS scattering profiles. Here, the plot shows the intensity decrease of the first two peaks at higher strain rates.*

b) In-situ tensile test-SAXS experiment of $^{1,4}S_{30}B_{29}M_{41}^{53}$

The SAXS images were captured at different strain rates during the in-situ tensile-SAXS experiment (Figure 7.6) of polymer $^{1,4}S_{30}B_{29}M_{41}^{53}$. At 0% elongation, an one ring isotropic SAXS pattern is found. Upon 10% stretching, the yielding occurs and the meridional SAXS maximum tends to shift toward the smaller angles which means that the interdomain distance has increased along the stretching direction. At elongation close to yield point (around 16% elongation) the meridional scattering maximum disappears. This indicates that almost all microdomains originally oriented perpendicular to the stretching direction have changed their orientation. At this stage the four point pattern starts to appear which is well developed at ε = 70%. In this regime, the equatorial SAXS maximum splits completely. This pattern is characteristic for a grain structure in which the lamellar surface is inclined with respect to the stretching direction. The rubbery domains are deformed and oriented to the

stretching direction along with the two end blocks. This deformation can also be seen in the TEM (see Figure 7.3b) where an undulated lamellar pattern is formed.

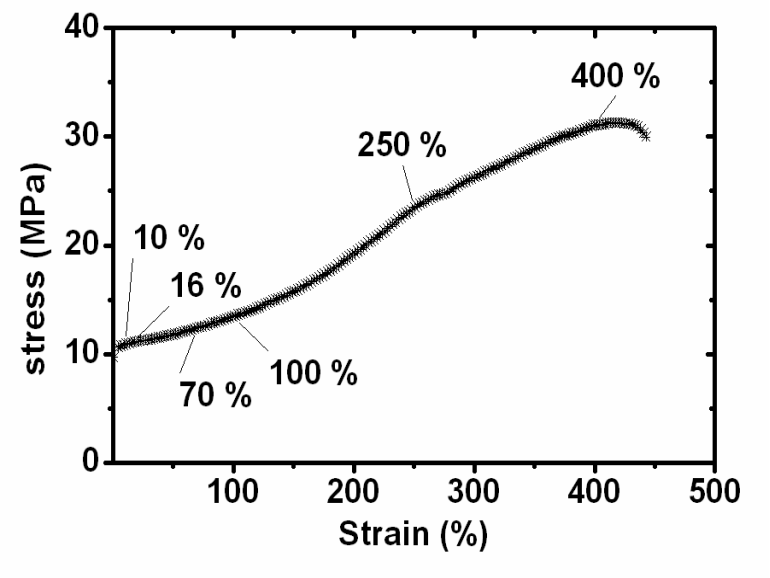

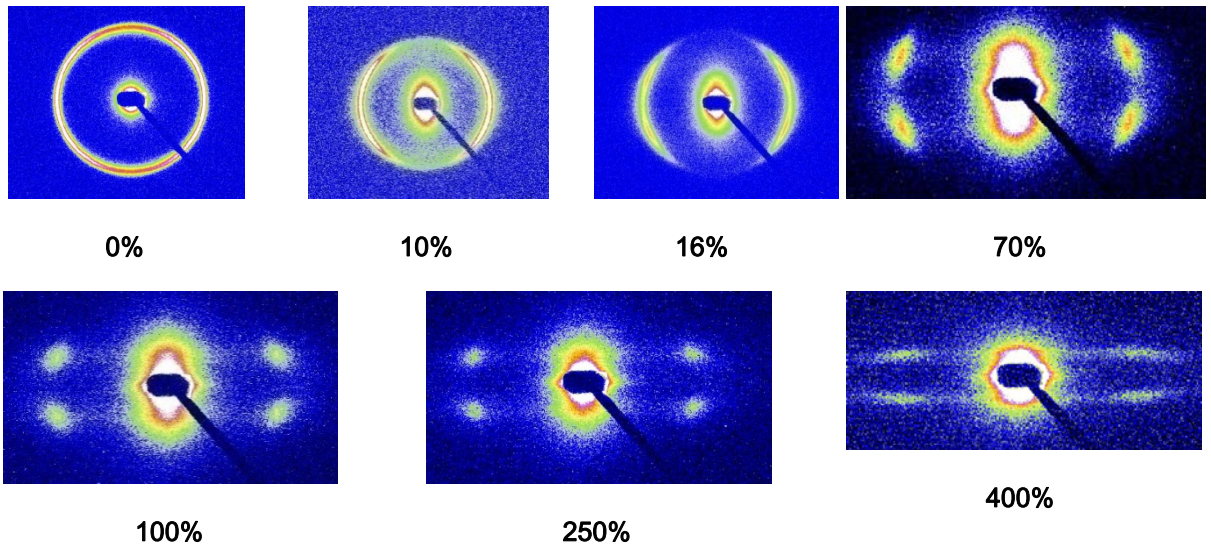

Figure7.6: *Results of the combination of SAXS and tensile testing for* $^{1,4}S_{30}B_{29}M_{41}{}^{53}$*. Top: Stress-strain diagram giving the corresponding elongations at which the SAXS patterns were taken (lower part). Note that the outer ring transforms into a four point lobe pattern at higher elongation.*

At further elongation up to 250%, the scattering lobes tend to elongate parallel to the equator as also can be seen from the TEM image in Figure 7.3c where the lamellar domains are strongly undulated. The spacing parallel to the stretching direction increases with the elongation. When the elongation has reached 400%, the spacing becomes broader and the lobes come close to each other. However, in SBS

block copolymer, at this elongation, the lamellar spacing disappeared according to the investigations by Fujimura et al.[6]. They observed fragmentation and randomly dispersion of the glassy domains in the rubbery B matrix around 400% elongation. Yamaoka et al[7] also observed the same phenomenon in SBS system where the fragmentation of the glassy phase was occurred at high elongation. However, in SBM system, no fragmentation of the glassy domains occurs at this stage due to the bridge formation of B domains which also leads higher elastomeric properties according to Brinkmann et al[8]. This effect can also be realized from Figure 7.6 where the four point lobes recognizable even at high elongation exceeding 400%.

The plot of the intensity versus the azimuth angle for different elongation rates is shown in Figure 7.7. At q = 0.23 nm^{-1} a homogenous intensity profile for all scattering angles (isotropic pattern) is observed in the absence of strain. At 10% elongation, four scattering maxima appear at ϕ =27°, 157°, 203° and 334°. With higher elongation, the four maxima become more distinct and shift to each other at the azimuth angle, ϕ = 10°, 170°, 190° and 350° that indicate the changes of the interdomain distance along the tensile direction.

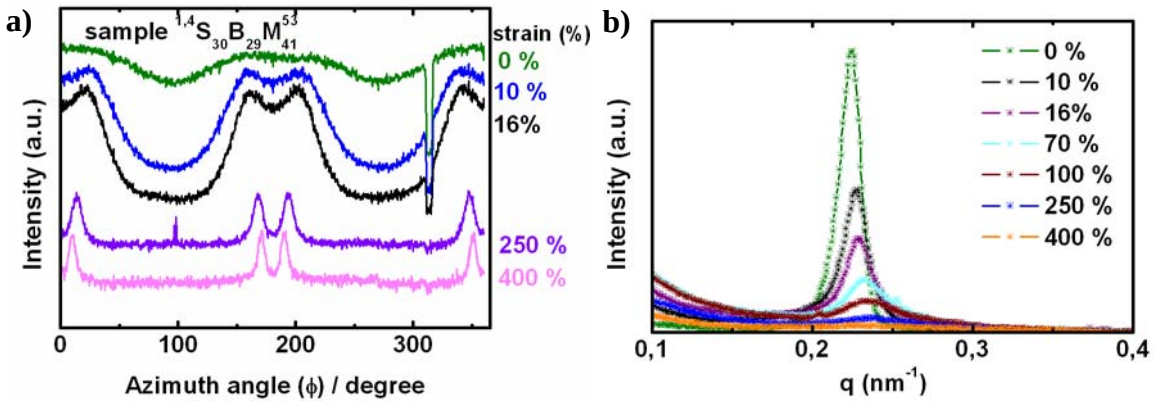

Figure 7.7: *Results of the combination of SAXS and tensile testing for $^{1,4}S_{30}B_{29}M_{41}^{53}$ at 0 %, 10 % and 16 %, 250 % and 400 % strain a) Intensity versus azimuthal plot for q = 0.23 nm^{-1} show the changes of intensities at azimuth angle with increasing elongation and b) 1D-SAXS scattering profiles show the change of intensities at different elongation rate.*

Figure 7.7b shows the 1D-SAXS patterns where the relation between the intensities and the scattering vector, q (nm^{-1}) is depicted at different elongation rate. From this curves the morphologies of the unstretched and stretched specimen can be clearly distinguished. At 0% elongation, the peak is more distinct at a position of 0.23 nm^{-1}. When the elongation reaches 10%, the intensity decreases and shifts to higher q values. At 100% elongation, the intensity is reduced but the peak's width expands. Finally, at 400%, the peak intensity has almost disappeared. These decreasing intensities attribute to increasing

disorder in interdomain distance and to reorientation of the microdomains from the direction perpendicular to the stretching according to Pakula et al.[3] The change of the domain lengths during the stretching process of an alternating lamellae pattern or of the long range order of SBMB under stretch can be calculated from the TEM micrographs.

Table 7.1: *Domain sizes of the different lamellar domains and the long periodicity of* $^{1,4}S_{30}B_{29}M_{41}^{53}$ *after tensile test calculated from the TEM micrograph (see Figure 7.3).*

strain (%)	**TEM**		
	mixed S /M (nm)	**B (nm)**	**(S/M)B(S/M)B (nm)**
0 %	8 ± 1	7 ± 1	33 ± 1
300 %	7 ± 1	6 ± 1	30 ± 1

In Table 7.1, the changes of the domains sizes after 300% strain are given. When no stretching was applied (at 0% strain), the mixed lamellae of S/M domain was larger than the B domains. After stretching upto 300%, the sizes of the domains are decreased. This effect is mostly emphasized in case of the B domains (from 7 nm to 6 nm). This relatively pronounced change indicates the high deformation of the B domains compare to the S and M domains.

7.2 Deformation of morphology containing 1,2- and 1,4-SBMs: Investigation for high molar mass SBM

7.2.1 Stress- strain behavior of $^{1,2}S_{32}B_{31}M_{37}^{91}$ and $^{1,4}S_{34}B_{31}M_{35}^{80}$

Several specimens made-up from these two polymers were tested under tensile loading and the calculated stress-strain curves are plotted in Figure 7.8. In case of $^{1,2}S_{32}B_{31}M_{37}^{91}$ the plots show a maximum strain (strain at break) within 300% - 400% of the total strain. On the other hand for $^{1,4}S_{34}B_{31}M_{35}^{80}$ the highest strain at break is observed at 600% – 700% of the total strain. Both copolymers exhibit a similar E-modulus, however, different yield stresses. The yield point for $^{1,2}S_{32}B_{31}M_{37}^{91}$ is observed at stress of 27 MPa, whereas for $^{1,4}S_{34}B_{31}M_{35}^{80}$ a lower yield point of 17 MPa

was found. The higher yield in $^{1,2}S_{32}B_{31}M_{37}^{91}$ is due to the higher content of non-flexible 1,2-B in the polybutadiene block. For $^{1,4}S_{34}B_{31}M_{35}^{80}$ the B phase is mainly composed of the 1,4-isomer, which results in comparatively lower stresses than the former case. The moderate yield stress via neck formation is occurred for both cases. After the yield point strain softening followed by strain hardening is occurred.

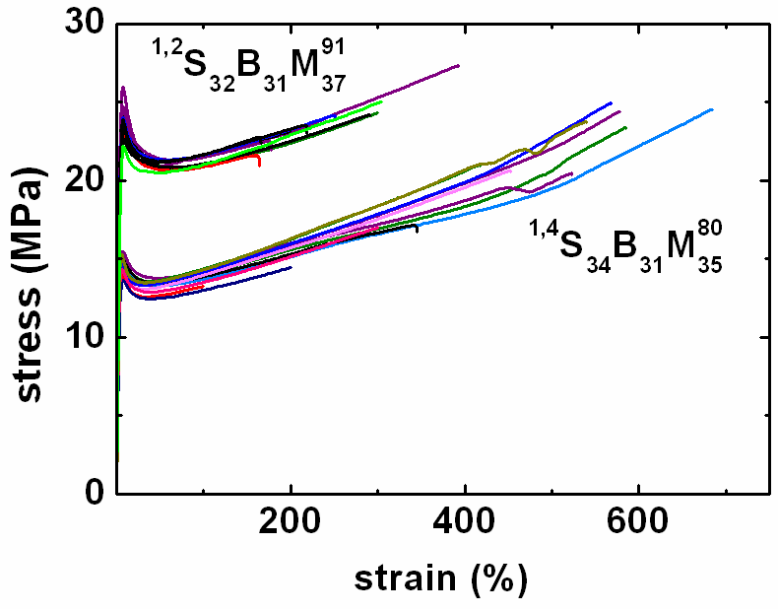

Figure 7.8: *The stress-strain curve of different specimens for $^{1,2}S_{32}B_{31}M_{37}^{91}$ and $^{1,4}S_{34}B_{31}M_{35}^{80}$.For $^{1,2}S_{32}B_{31}M_{37}^{91}$ a pronounced strain softening with high strain at break upto 400% can be seen , whereas for $^{1,4}S_{34}B_{31}M_{35}^{80}$, the strain at break can reach values upto 700%. Obviously, the 1,4-B SBM shows a higher tendency of strain hardening during elongation.*

The large elongation at break is associated with the fragmentation process of the glassy lamellae and a more pronounced tendency of strain hardening.[9] However, for $^{1,4}S_{34}B_{31}M_{35}^{80}$ the strain hardening is more prominent than that of $^{1,2}S_{32}B_{31}M_{37}^{91}$. For $^{1,4}S_{34}B_{31}M_{35}^{80}$, the stress tends to increase monotonically until the specimen breaks. This effect can be clarified by the tendency of entanglements in the 1,4-B domain. According to literature[10] the molar mass of entanglements, M_e of 1,2-B is lower than that of the 1,4-B for same chain length of polybutadiene. As a result, the 1,4-B shows more flexibility which allows the formation of an intramolecular network and shows an increasing tendency to endure stress at high elongation.

7.2.2 Morphology of $^{1,2}S_{32}B_{31}M_{37}^{91}$ and $^{1,4}S_{34}B_{31}M_{35}^{80}$ before and after tensile test

a) Morphology of $^{1,2}S_{32}B_{31}M_{37}^{91}$

The TEM images of a $^{1,2}S_{32}B_{31}M_{37}^{91}$ sample before and after stretching are given in Figure 7.9. Before applying any stretching the morphology, exhibits a very well ordered system of S and M lamellae (Figure 7.9a). However, the B lamellar domains are discontinuous and in some areas they look more like a cylindrical pattern (see the TEM images in Figure 7.9a).

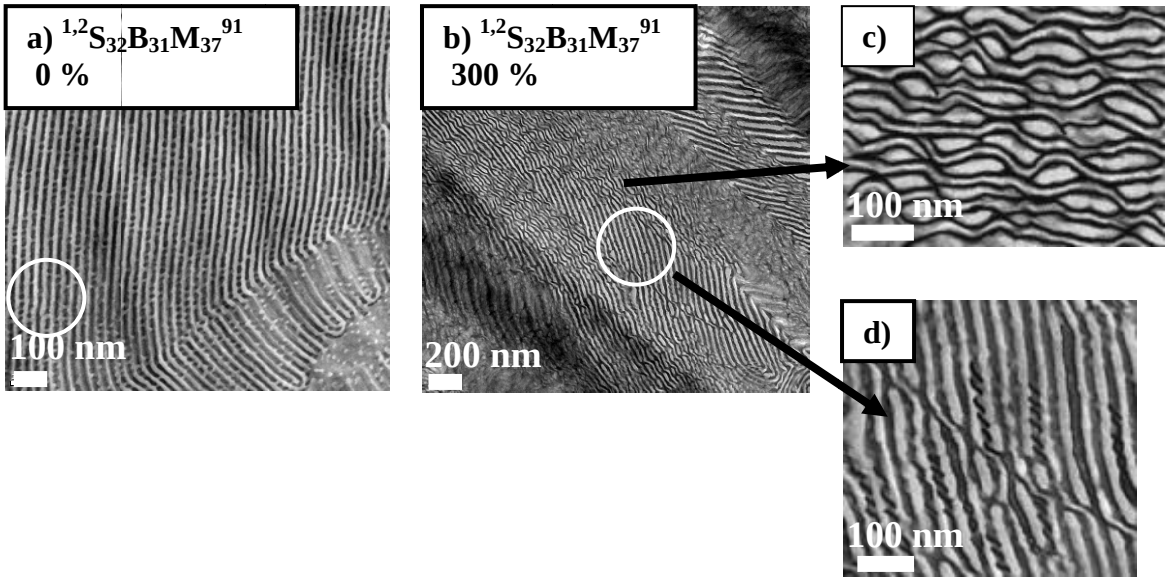

Figure 7.9: *TEM images of $^{1,2}S_{32}B_{31}M_{37}^{91}$ at a) strain 0% where lamellar phases of different domains can be seen. In some places the B phases form cylinder which are disconnected from the lamellar domains. b) at 300% strain, the wavy B domains are observed. c) and d) are the magnification of the TEM images of b) where the deformation of the B domains are highlighted in black*

The deformation of the morphology at 300% strain is highlighted in Figure 7.9b and their magnified view in Figure 7.9(c,d). In the figures the B domains are indicated in black color. Three kinds of deformation patterns can be identified in the image. Firstly, the screw type pattern where the B cylinders are oriented and twisted, as shown in Figure 7.9d. Here, no deformation of the adjacent S and M is observed, but only the B cylinders found to be oriented and twisted like a screw. Secondly, the wavy pattern of B lamellae which are still continuous (see Figure 7.9c). The deformation patterns of the adjacent S and M domains are also similar to the deformation pattern of B domains. The formation of such pattern can be explained as follows. The M exists as a continuous phase whereas the

B exists as discontinuous phase of laminar structure to cylindrical pattern. This discontinuous B phases co-exist alternately with the S phases. As a result, the continuous M phases are deformed at the first deformation stage, according to Stadler et al[11] and yield point is occurred at the high stress at maximum. Then the mechanical force is transmitted to the B rubbery domains. Therefore, the yield drop occurs. After yield drop, the alternating B phases with the S phase causing high stress at higher strain. The discontinuous B domains are deformed to more wavy patterns in that stage. Thirdly, some disordered phases are found in some areas (Figure 7.9b). These disordered phases could stem either from the diffusion of hard domains into the rubbery matrix (*diffuse pattern*) or from an artifact of the TEM micrographs.

b) Morphology of $^{1,4}S_{34}B_{31}M_{35}^{80}$

Figure 7.10a shows the TEM images of $^{1,4}S_{34}B_{31}M_{35}^{80}$, where well segregated lamellae morphology with continuous lamellar domains are observed. The deformed morphology at 300% is shown in Figure 7.10b. A magnified view of the deformed lamellar domains is depicted in Figure 7.10c, where the deformed B domains are highlighted with additional black color. Depending on the stretching direction two types of deformation can be found. If the stretching is parallel to the lamellar domains, the domains become narrow, whereas for perpendicularly stretching to the lamellar domains a chevron like morphology is obtained. This is formed by the combined mechanisms of shearing, kinking, destruction and reorientation of the B lamellae accompanied by fragmentation of the S and M hard phases as described elsewhere[3]. In some cases, the domains are disconnected from their long lamellar domains. The wavy and disconnected domains at high strain also indicate the occurrence of strain hardening at larger elongation.

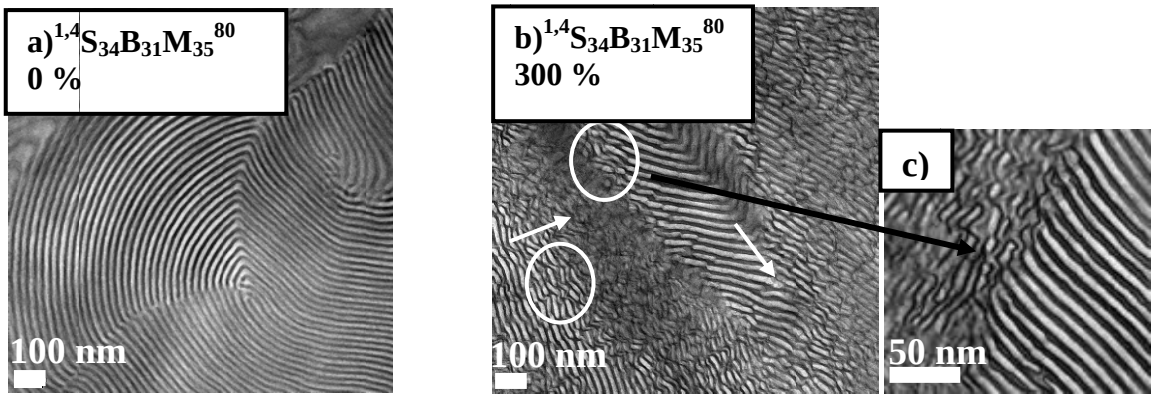

Figure 7.10: *TEM images of $^{1,4}S_{34}B_{31}M_{35}^{80}$at elongation of 0% (a) and 300% (b). a) shows a well segregated lamellae. b) shows the deformation of the lamellar domains after stretching upto 300%. Here, white arrows indicate the stretching direction), c) shows a magnification part of the circled area in b).*

7.2.3 In-situ combination of SAXS and tensile testing for $^{1,2}S_{32}B_{31}M_{37}^{91}$ and $^{1,4}S_{34}B_{31}M_{35}^{80}$

a) In-situ combination of SAXS and tensile testing of $^{1,2}S_{32}B_{31}M_{37}^{91}$

A specimen of $^{1,2}S_{32}B_{31}M_{37}^{91}$ was characterized by in-situ combination of SAXS and tensile testing to investigate the deformation mechanism in greater detail. The tensile curve with 2D-SAXS images are given in the Figure 7.11 where the deformation at certain elongation can be seen.

The development of the scattering pattern with increasing strain is completely different compared to the low molar mass analogues. At 6% strain where yielding occurs, the meridional SAXS maxima start to disappear and the equatorial SAXS maxima is observed which indicates the deformation of the glassy domains. When the strain has been reached 18%, the second scattering ring was almost undetectable. Only the first scattering ring can be found where no equatorial SAXS maximum is observed along the tensile direction. From 6% to 18% of strain, necking and drawing of the glassy lamellae accompanied by shearing in the rubbery phase, so to say 'plastic to rubbery transition' occurs.[6, 12] Again at 31% strain, a symmetric scattering pattern of the first ring appears. The slow increase of the equatorial maximum's intensity continues up to 75% strain. At higher elongations, e. g. at nearly 400%, the equatorial SAXS maximum can still be detected but their close vicinity to the meridional maxima and the beam stop does not allow an evaluation. During the overall deformation process, the intensities were redistributed from equatorial to meridional SAXS maxima, which was mainly due to the deformation, orientation and disorientation of the domains along the stretching direction. This type of anisotropy in deformation behavior resulting from different orientation of lamellae also observed in semicrystalline polymer[9]. Honeker et al.[13] stated similar anisotropic pattern for both large and small strains in the globally oriented samples with a cylindrical morphology. The redistribution of the scattering density which has been noticed in our case, also obtained in a rubber-modified glassy amorphous polymers blend as demonstrated by Jansen et al.[14]. He reported the effects of shear yielding and the absence of cavitation in the polymer blend system as the underlying reason behind such scattering intensity. From above discussion, for the present polymer, $^{1,2}S_{32}B_{31}M_{37}^{91}$, an analogous explanation can be hypothesized.

Due to the homogeneous deformation of the lamellar phases, the resulting lamellar thickness and the long period are decreased. The values are given in the Table 7.2. The changes of the calculated domains sizes from TEM images show that at 0% strain, the M domain is broader than the other two domains. The B domains being the narrowest one. After stretching to 300%, the domain sizes decrease. The decrease is not so obvious in case of the S and M domains, however, high deformation

is pronounced for the B domains (from 12 nm to 7 nm) which also can be seen from the TEM image in Figure 7.9b.

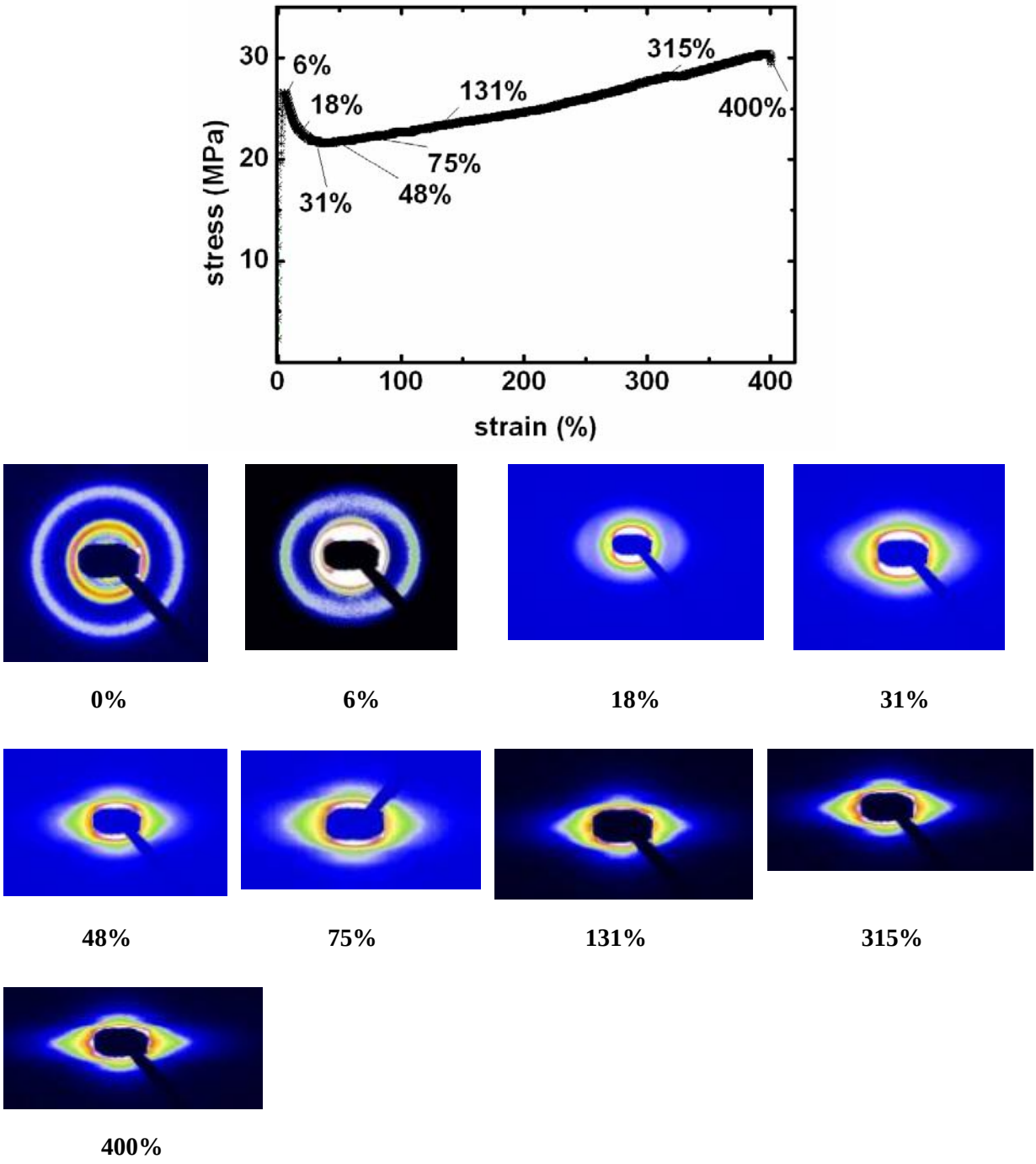

Figure 7.11: *Results of the combination of SAXS and tensile testing for SBM* $^{1,2}S_{32}B_{31}M_{37}^{91}$. *Top: Stress-strain diagram Lower part: SAXS patterns obtained by in-situ tensile test for various elongations. The SAXS patterns deform from isotropic to anisotropic ones.*

Table 7.2: *Domain sizes of the different blocks before and after elongation.*

strain (%)	S (nm)	B (nm)	M (nm)	SBMB (nm)
0 %	14 ± 1	12 ± 1	15 ± 2	56 ± 1
300 %	12 ± 1	7 ± 1	14 ± 1	43 ± 1

The deformation of $^{1,2}S_{32}B_{31}M_{37}^{91}$ morphology was further analyzed by plotting the intensity of the scattered radiation versus the azimuthal angle at the scattering vector (q = 0.16 nm^{-1}) for each elongation rate (Figure 7.12). Up to 6% strain no changes of the intensity are observed, however, for further elongation the intensity maximum raises at 180° (Figure 7.12a). This peak maximum becomes narrow at higher elongations (e. g. 400%), which means the domains are oriented in the direction of 180° azimuth angle. Figure 7.12b shows the relation between the intensities and the scattering vector, q for each different elongation. Increasing the strain up to 6%, the intensity of the 3rd peak starts to diminish, which is in accordance to the disappearance of the meridional SAXS maximum in Figure 7.11. At 18% stain the 3rd peak completely disappears, which means that the domains are starting to become disordered. However, at the same time, the intensities of the 1st and 2nd peaks increase. At 400% elongation only the first two peaks remain. This may be explained by a change of the interdomain distances during orientation-disorientation process.

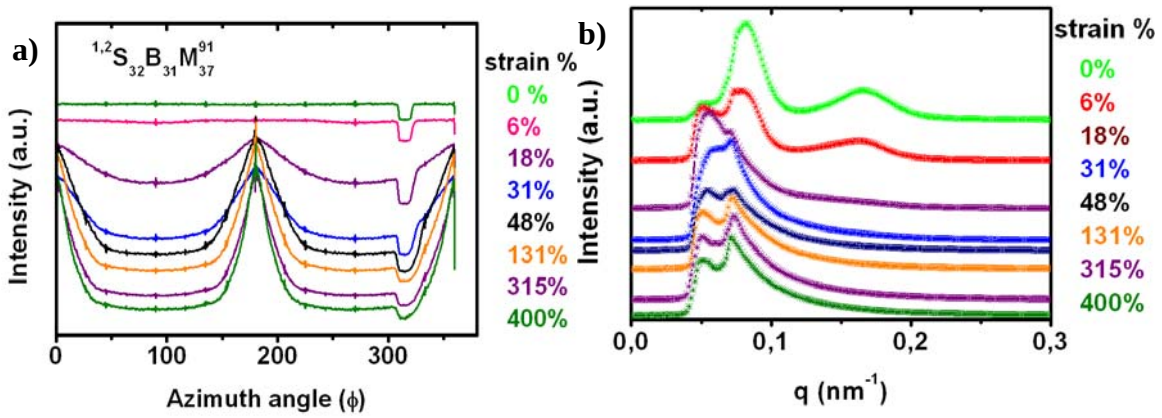

Figure 7.12: *SAXS results obtained by in-situ tensile test of $^{1,2}S_{32}B_{31}M_{37}^{91}$ at 0%, 6%, 18%, 48%, 131%, 315%, and 400% strain a) Intensity vs azimuthal plot for q = 0.16 nm^{-1} show the changes of intensities at azimuth angle with increasing elongation b) 1D-SAXS scattering profiles show the change of intensities at different elongation rate.*

b) In-situ combination of SAXS and tensile testing of $^{1,4}S_{34}B_{31}M_{35}^{80}$

For the $^{1,4}S_{34}B_{31}M_{35}^{80}$ copolymer the sequence of the morphological deformations with increasing elongation are summarized in the SAXS patterns of Figure 7.13. Like in $^{1,2}S_{32}B_{31}M_{37}^{91}$, the disappearance of the meridional SAXS maxima can be observed at 6% strain. The equatorial SAXS maxima are separated into four points at ε = 23%. With a further increase of strain (up to 39%), the four points are totally separated, which indicates a chevron-type deformation structure. The scattering rings near the beam-stop are also deformed and become less blurred in both the parallel and the perpendicular tensile direction. The four point pattern disappears at high elongations (e. g. 156% strain) which indicate that the domains are transformed from the chevron-like type to a random one. Here, the first scattering ring is deformed both in parallel and perpendicular to the tensile direction, which is also an indication of an orientation-reorientation process of the rubbery domains. The same pattern-type can also be found at higher elongations up to 353%. When the elongation is increased up to 470% strain, the scattering ring is further jolted towards the tensile direction.

The deformation can be investigated further by correlating the azimuth angle and the intensity, as shown in Figure 7.14a. At the beginning of stretching, the SAXS pattern is isotropic. When the stretching reaches 6%, a broad maxima at 180° appears, which shows four SAXS maxima at the scattering angles of 0°, 90°, 180° and 270°. At a higher elongation of 469% strain, the intensity maxima at ϕ = 90° and ϕ = 270° have almost disappeared due to the random domain orientation. Only the intensity maxima at 180° are continuously increasing at this stage. The plot of intensity versus *q* (Figure 7.14b) also shows the changes of the inter-domain distance at different strain rates. The intensity of the four scattering peaks decreases continuously with increasing elongation. At 469% elongation, only the first scattering peak can be recognized. The variation of the scattering peaks' intensity can mainly be attributed to the continuous changing of the interdomain spacing during stretching.

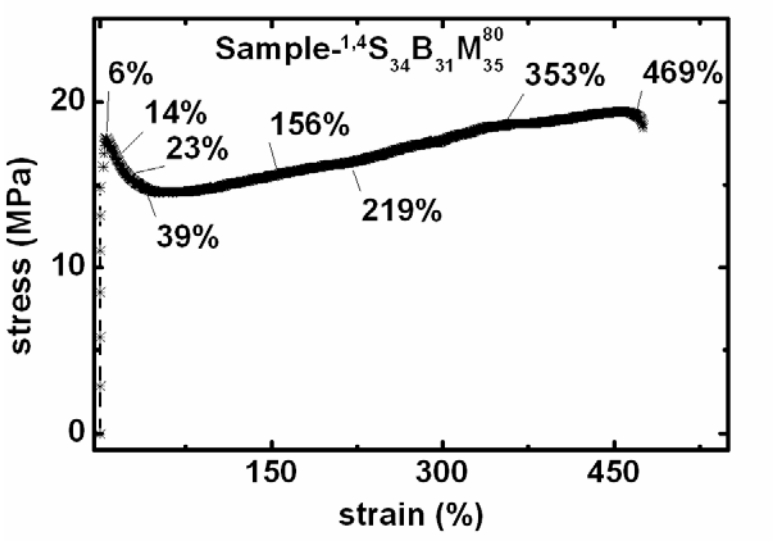

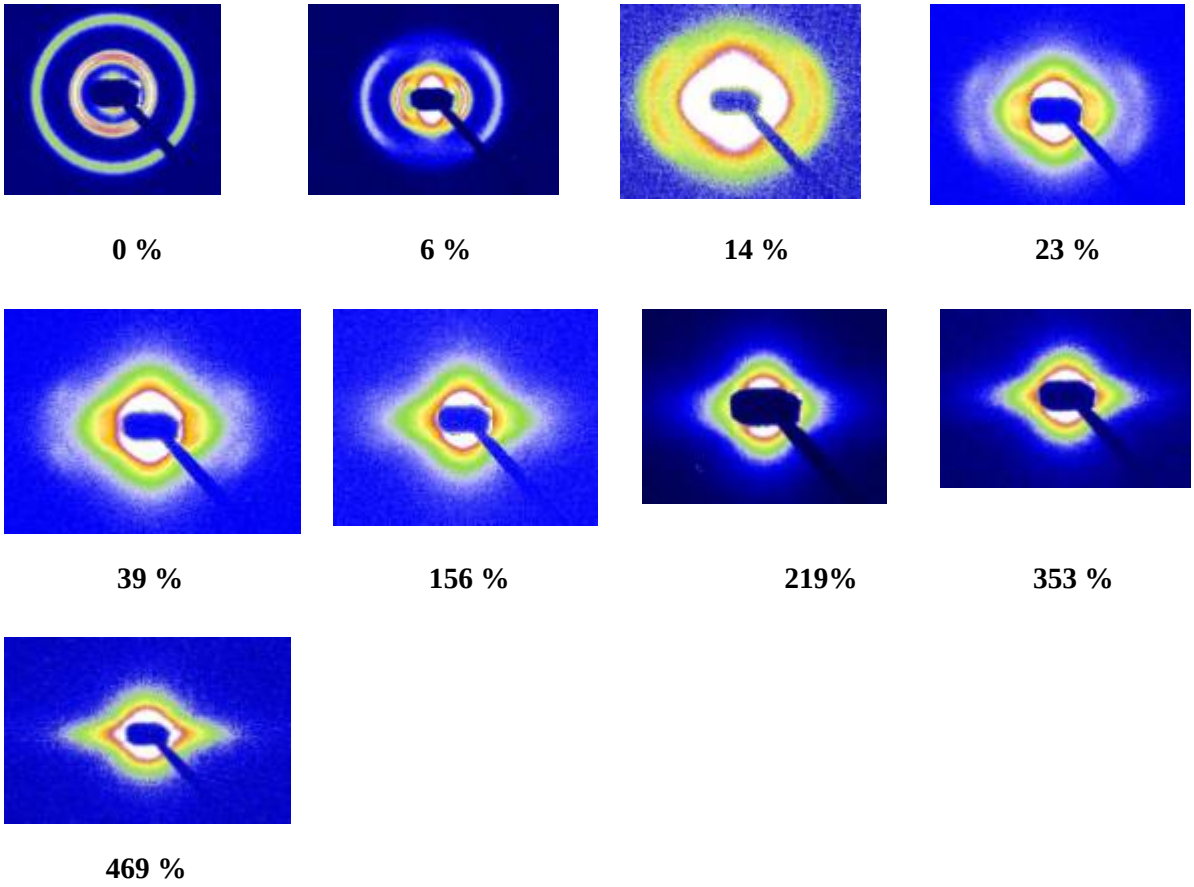

Figure 7.13: *Results of the combination of SAXS and tensile testing for $^{1,4}S_{34}B_{31}M_{35}^{80}$. Top: Stress-strain diagram. Lower part: SAXS patterns obtained at different elongations. The scattering patterns change from isotropic one (at 0%) to a four point lobes-type (at 39%); the latter deforms to an anisotropic pattern at high elongation (at 469%).*

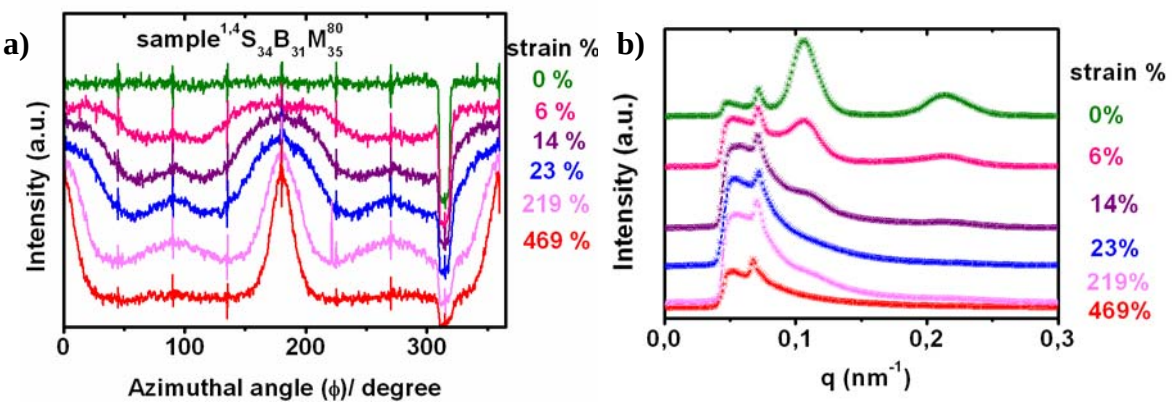

Figure 7.14: *SAXS results obtained by in-situ tensile test of $^{1,4}S_{34}B_{31}M_{35}^{80}$ at 0%, 6%, 14%, 23%, 219%, and 469% strain a) Intensity versus azimuthal angle for q = 0.11 nm^{-1} show the changes of intensities at azimuth angle with increasing elongation b) 1D-SAXS scattering profiles show the change of intensities at different elongation rate.*

The domain sizes were estimated from the TEM image of Figure 7.10. The values are highlighted in Table 7.3. At 0% strain, the M domain has been found broader than that of the S and B domain. The B domain is the narrowest one. It has been seen from the calculated data that all the three domains become 2-3 nm narrow than their previous dimensions.

Table 7.3: *Domain sizes of the different lamellar domains and the long periodicity of $^{1,4}S_{34}B_{31}M_{35}^{80}$ after tensile test calculated from the TEM images (see Figure 7.10).*

strain (%)	**TEM**		
	S (nm)	**B (nm)**	**M (nm)**
0 %	16 ± 2	14 ± 1	19 ± 1
300 %	15 ± 1	10 ± 1	17 ± 1

7.3 Effect of deformation on the 1,2- and 1,4- SBM morphology: Orientation behavior

The orientation factors (P2) (for definition see section 4.8, chapter 04) versus the strain of the four different SBMs are plotted in Figure 7.15. The integrations of the scattering profiles were performed between φ = 90° and φ = 270° in order to avoid any distortion caused by beam-stop. The behavior of P2 mostly shows the orientation of the copolymer phases during elongation process.

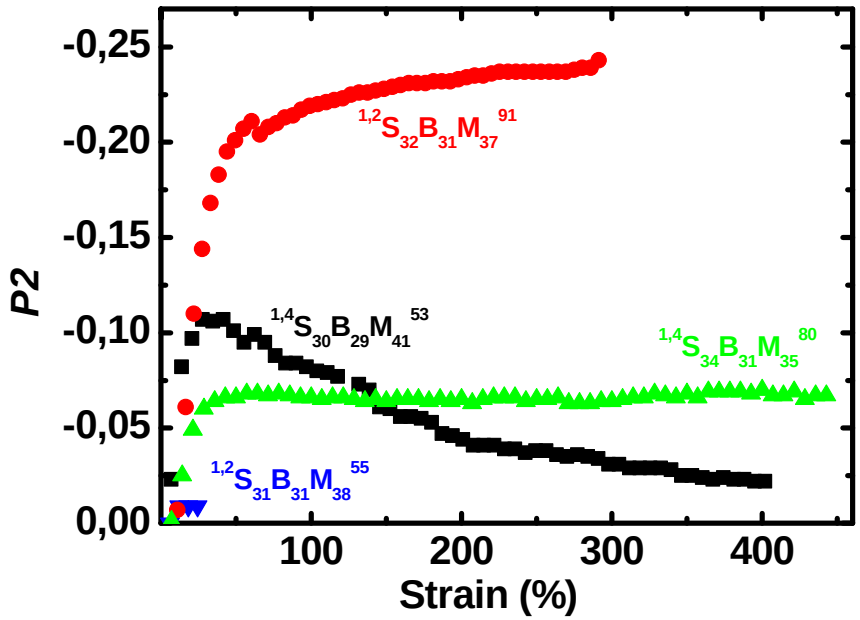

Figure 7.15: *Dependence of the orientation order parameter P2 on the strain for four different SBMs. The orientation factor of* $^{1,2}S_{31}B_{31}M_{38}^{55}$ *shows very close to 0 whereas the value for* $^{1,2}S_{32}B_{31}M_{37}^{91}$ *is -0.25. For 1,4-B SBMs a factor of -0.1 for* $^{1,4}S_{30}B_{29}M_{41}^{53}$ *and of -0.06 for* $^{1,4}S_{34}B_{31}M_{35}^{80}$ *is found.*

Only a very limited number of orientation factors (P2) obtained for $^{1,2}S_{31}B_{31}M_{38}^{55}$ which has been found very close to zero. As the domains are short and brittle, it is assumed that no orientation occurs during elongation. Only the morphology plays the role of deformation according to Thomas et al.[13] For the high molar mass $^{1,2}S_{32}B_{31}M_{37}^{91}$ a totally different orientation behavior is observed. The orientation factor (P2) reaches -0.22 at the first deformation stage which indicates the orientation is partly perpendicular to the stretching direction. With further elongation the lamellar spacing orient more perpendicularly as the orientation factor (P2) decreases in a continuous manner. This deformed morphology was also found in the TEM images in Figure 7.9b where wavy lamellar domains along with zig-zag patterns were observed. One can see from the image that how the B phases turn into a wavy pattern along the direction perpendicular to the stretching after 300% strain are reached.

Comparing the 1,2- SBMs, the 1,4-SBMs obtain lower P2 value. In case of $^{1,4}S_{30}B_{29}M_{41}^{53}$, the P2 reaches -0.10 at the first stage of deformation and then slowly increases to -0.02 at higher strain. This means, during deformation the domains first align along the stretching direction and then orient randomly at higher strains, which can also be seen in the TEM images in Figure 7.3. Again for the high molar mass $^{1,4}S_{34}B_{31}M_{35}^{80}$, the P2 value is -0.06 which remains constant even above 400%

elongation. This means the domains are partly oriented at low strain and this orientation is preserved even at 469% elongation as also can be seen in SAXS images (see Figure 7.13).

Hence, from the above results, it can be concluded that in case of SBM with high molar mass and high 1,2-B content, the orientation is mostly perpendicular to the stretching direction. However, for both low and high molar mass 1,4-SBMs the lamellae are moderately oriented.

7.4 Summary

The effect of deformation on the morphology as well as the stress-strain behavior are discussed for two pairs of SBMs where the 1,2-B to 1,4-B ratio and the total molar mass were varied. In case of 1,2-SBM, a transitional domain structure from lamellar to cylindrical patterns of polybutadiene is observed for the both low and high molar mass SBMs. However, in both 1,4-SBMs, very continuous and well segregated lamellar patterns are obtained.

Due to these morphological differences of the two SBMs, a high stress yielding followed by a stress drop after the yield point with macroscopic necking caused by the continuous M phase is observed in $^{1,2}S_{31}B_{31}M_{38}{}^{55}$. In contrast, a typical rubbery behavior is found for $^{1,4}S_{30}B_{29}M_{41}{}^{53}$ dominated by the much more continuous B lamellar phase. The other two SBMs containing high molar masses show somewhat intermediate mechanical behavior within these two extremes. Figure 7.8 shows high yield drop at low strain for $^{1,2}S_{32}B_{31}M_{37}{}^{91}$. Here, the B phases in the laminar structure are no longer continuous, but alternate with S, resulting an increase of the yield stress at high strain. The reinforcement effect of B is further assisted by the possibility to delocalize the strain. Compared to $^{1,2}S_{32}B_{31}M_{37}{}^{91}$ polymer, the $^{1,4}S_{34}B_{31}M_{35}{}^{80}$ in Figure 7.8 shows moderate yield drop at low strain but higher strain hardening due to the differences of the polybutadiene's 1,2- to 1,4- ratio.

The effect of deformation on the morphology was also investigated by means of SAXS. The scattering patterns are of an anisotropic type in the both 1,2-SBM types for both small and large strains. Contrary, both the low and high molar mass 1,4-SBMs are transformed into a zig-zag structural motif and a four lobe-pattern in 2D SAXS. The discontinuous B domains in the 1,2-SBMs cause a high orientation at the initial deformation stage. On the other hand, the 1,4-SBMs show moderate orientation even at 300% strain. Hence, the B phases become wavy but still the long periodicity of the domains remains unchanged.

The orientation behavior of different domains is assessed with respect to the orientation factor (P2). Very limited number of orientation factor is obtained for $^{1,2}S_{31}B_{31}M_{38}^{55}$ due to the brittleness of the specimens. In case of the high molar mass $^{1,2}S_{32}B_{31}M_{37}^{91}$, the orientation is mostly perpendicular to the stretching direction. A P2 value of -0.22 at initial deformation is found, which decreases at further elongation. This difference of the orientation behavior in $^{1,2}S_{32}B_{31}M_{37}^{91}$ mainly occurs due to long chain domains of 1,2-B which is also reflected in the absence of an extreme brittle behavior like $^{1,2}S_{31}B_{31}M_{38}^{55}$. For SBMs containing 1,4-content, due to the high flexible 1,4-B, the orientations are moderate compared to the 1,2-SBMs. For the low molar mass $^{1,4}S_{30}B_{29}M_{41}^{53}$, the P2 value is -0.10 at the initial deformation state, which increases slowly up to -0.02 at higher elongation. However, in case of the high molar mass $^{1,4}S_{34}B_{31}M_{35}^{80}$, the P2 value is -0.06 at the initial deformation, and it remains constant even at high elongation. The results indicate that the lamellar domains of $^{1,4}S_{30}B_{29}M_{41}^{53}$ are aligned first along the stretching direction, which turns to a random arrangement at higher elongation. Again for high molar mass $^{1,4}S_{34}B_{31}M_{35}^{80}$, the orientation is fairly perpendicular along the stretching direction, which remains steady even at high elongation.

Reference

[1] H. E. H. Meijer, L. E. Govaert, *Prog. Polym.Sci.* 2005, *30*, 915.
[2] J. T. A. Kierkels, *Proefschrift, Technische Universiteit Eindhoven* 2006.
[3] T. Pakula, K. Saijo, H. Kawai, T. Hashimoto, *Macromolecules* 1985, *18*, 1294.
[4] J. A. Odell, A. Keller, *Polym. Eng. Sci.* 1977, *17*, 544.
[5] C. E. Schwier, RA. S. Argon, R. E. Cohen, *Polymer* 1985, *26*, 1985.
[6] M. Fujimura, T.Hashimoto, H. Kawai, *Rubber Chem Technol* 1978, *51*, 215.
[7] I. Yamaoka, M. Kimura, *Polymer* 1993, *34*, 4399.
[8] S. Brinkmann-Rengel, V. Abetz, R. Stadler, E. L. Thomas, *Kautschuk Gummi Kunstoffe* 1999, *12*, 806.
[9] G. H. Michler, R. Adhikari, W. Lebek, S. Goerlitz, R. Weidisch, K. Knoll, *J. App. Polym. Sci.* 2002, *85*, 683.
[10] C. G. Robertson, C. M. Rademacher, *Macromolecules* 2004, *37*, 10009.
[11] R. Weidisch, S. Goerlitz, G. H. Michler, R. Stadler, in *10th Int. Conf. Deformation, Yield and Fracture of Polymers*, Cambridge, UK, 1997.
[12] R. Adhikari, G. H. Michler, W. Lebek, S. Goerlitz, R. Weidisch, K. Knoll, *J. App. Polym. Sci.* 2002, *85*, 701.
[13] C. C. Honeker, E. L. Thomas, *Chem. Mater.* 1996, *8*, 1702.
[14] B. J. P. Jansen, S. Rastogi, H. E. H. Meijer, P. J. Lemstra, *Macromolecules* 2001, *34*, 4007.

Chapter 08

Influence of Residual Precursors on the Morphology and the Mechanical Properties of SBM Triblock Terpolymers

8.1 Introduction

So far in the previous chapters the mechanical and morphological investigations of SBMs were discussed where the polymers were free of any residuals. As in reality some residuals of polystyrene (S) and polystyrene-*b*-polybutadiene (SB) may blended with the targeted SBM triblock. It is needed to be mentioned that these residuals were formed in an insitu reaction during SBM synthesis. Therefore, it is of major interest to explore their effects on the physical properties of the blended diblock on a microscopic (phase separation) and macroscopic (mechanical properties) level. The impact of residual precursor on the SBM microphase separation has been reported by several authors. Ritzenthaler et al[1] investigated the morphology of a SBM triblock where 21% of SB precursors are blended with a epoxy thermoset. The resulting morphology shows an increasing tendency of the domain sizes of the S and B phases within the triblock. Another blending approach was performed by Jaffrennou et al.[2] where different amounts of residual precursors (10%, 20%, and 54% of SB) were present into SBMs and then these SBMs were blended with diisocyanates and macrodiols. When the residuals (ranging from 20-50%) were blended with polyurethane matrix an entirely nanostructured and transparent material was obtained. However, if the content of SB exceeds 50%, the diblock copolymer could no longer be accommodated within the SBM, thereby resulting in a macro-separation of the SB in the SBM matrix. Considering the effects on the SBM morphology discussed above, it would also be fascinating to investigate the effect of remaining S and SB precursor residuals on the macroscopic properties of the resulting polymer. To best of my knowledge, the effect of the residual precursor on the mechanical properties has not been discussed in the literature. Hence, the final chapter of the present thesis will address that question and present an investigation of the mechanical properties and the effect of the deformation process on the final morphology of a SBM system. All polymers that are chosen for this investigation have certain quantity of S and SB residuals. The amount of the SB diblock and S residuals was calculated to range from 19 to 41% by using Deconvolution using a Gaussian curve algorithm of the elugram (RI detector) (see section 10.5 in appendix D).

This chapter is organized in three sections:

i) The morphology of SBM with and without the S and SB residuals is discussed.

ii) The influence of S and SB on the mechanical properties is investigated.

iii) The impact of S and SB on the morphology after deformation is discussed.

8.2 Influence of the S- and SB residuals on the SBM's morphology

8.2.1 GPC results

The presence of residual precursor polymers can easily be detected from the GPC's elugram as shown in Figure 8.1. An overlay of the purified, non-purified SBM and the residual SB diblock are shown in Figure 8.1a). The elugram of crude SBM features a multimodal distribution which indicates that terminations occurred during the synthesis. Within an elution volume ranging from 27.9 to 30.2 mL, a S peak with high intensity and a corresponding molar mass of M_n = 26 kg/mol is observed. Another peak within 29.9 and 27.4 mL (equivalent to M_n = 50 kg/mol) can also be detected as its M_n is almost double compared to the M_n of S, this peak can tentatively be assigned to the product of the S coupling reaction. The SB diblock appears within 27.4 and 26.2 mL (equivalent to M_n^{app} = 83 kg/mol). A very small peak with an apparent molar mass of M_n^{app} =177 kg/mol arises at 25 mL, which may represent the coupling product of the SB diblock precursor. The final SBM triblock appears at an elution volume from 22 to 25.2 mL having a molar mass of M_n^{app} = 388 kg/mol.

After purification almost the entire S precursor is removed, but still 14% of the SB diblock remains. The amount of impurities were calculated by peak deconvolution based on a *Gaussian curve*, (see Figure 8.1b). The weight percentages of the non-purified and purified SBM along with the SB residual blocks are listed in Table 8.1.

Table 8.1: *Weight percentage of impurities present in the SBM triblock (cf. Figure 8.1b).*

Polymer	**% S**	**% SB**	**% SBM**
$S_{51}B_{10}M_{39}$ (non-purified)	30	40	30
$S_8B_8M_{84}$ (purified)	0.5	13.5	86

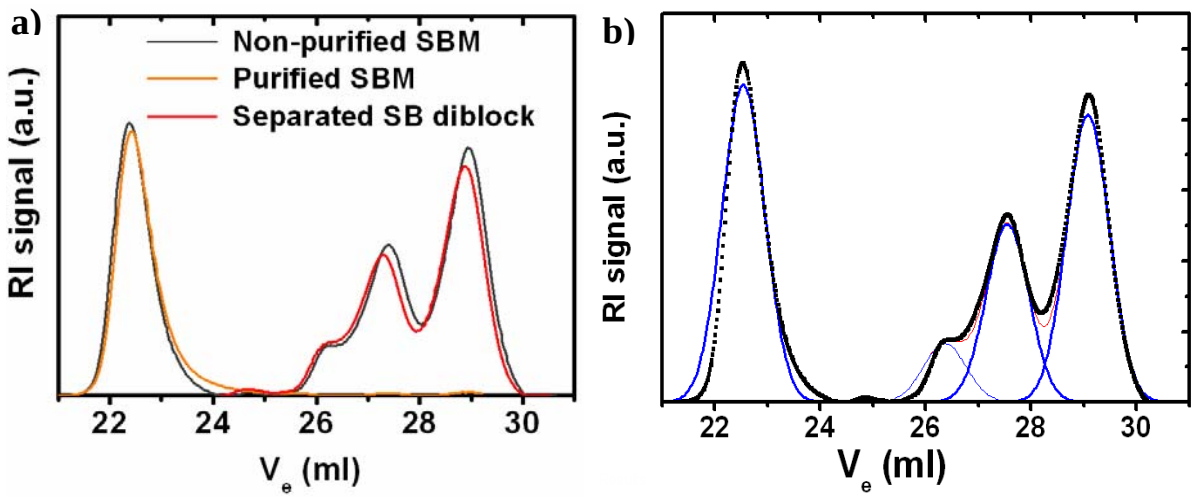

Figure 8.1: *a): GPC elugram (RI signal) of non-purified SBM, purified SBM and the residual SB diblock. b): Deconvolution using a Gaussian curve algorithm of the elugram (RI detector) of sample $S_{51}B_{10}M_{39}$ following procedure in secton 10.5 in Appendix. (━━ before purification, ------ after purification).*

8.2.2 TEM results

The transmission electron microscopy (TEM) images of non-purified $S_{51}B_{10}M_{39}$ after staining with OsO_4 vapor are shown in Figure 8.2 a),b). In the micrographs, the gray color indicates S domains, the black one B domains and the white one represents M domains. The microstructural features are indicated by arrows and numbers in the micrographs of Figure 8.2a) and 8.2b). Some large domains with a diameter ~1 µm are found throughout the sample (cf. Figure 8.2a) arrow 1) and 2), which can mainly be attributed to the residual S polymer. Most of these (30%) are not incorporated within the SBM triblock, however, they assemble as macrodomains analogous to the results reported by Ritzenthaler et al[1]. A detailed observation reveals that the B domains exist as cylinders at the interface of the S macrodomains. This B phase most probably stems from the SB residuals having a composition of $S_{88}B_{12}$. In addition, some large S spheres along with a randomly dispersed B phase are also formed, as shown in circle 5. Some other phases of S and B arranged in a spherical fashion are also identified in the vicinity of arrow 3 and 4. The remaining areas of pure SBM exhibit a morphology that is not influenced by the presence of SB. With its absence, the weight fractions of S and B are comparatively lower than that of M ($S_8B_8M_{84}$) resulting in spherical S and B domains which are randomly dispersed in the M matrix.

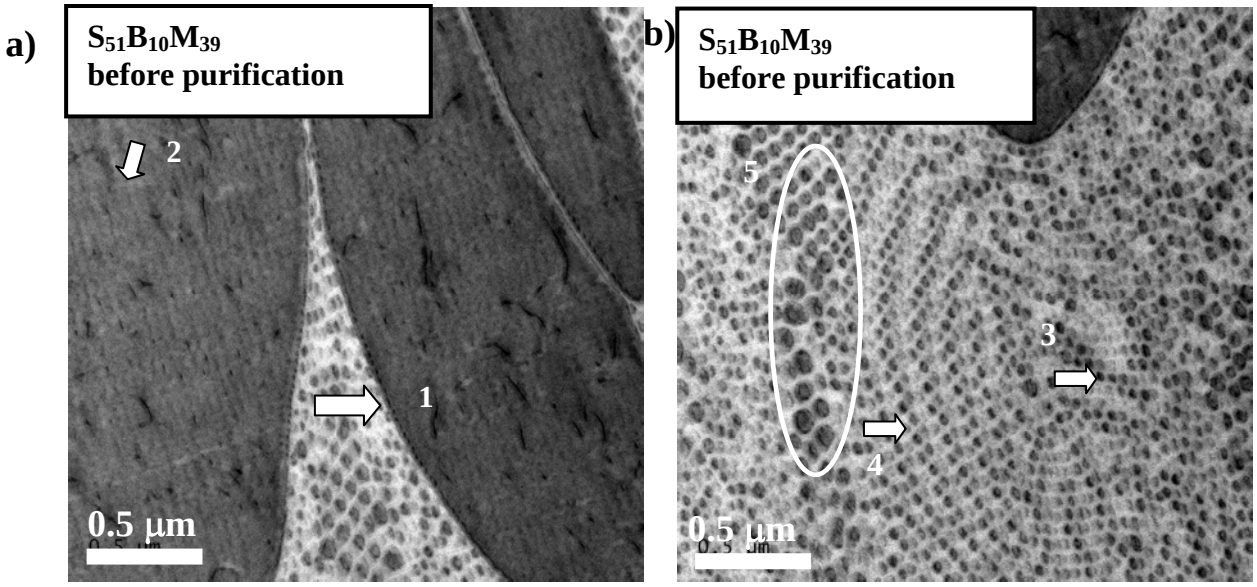

Figure 8.2: *TEM micrographs of non-purified$S_{51}B_{10}M_{39}$ (stained OsO_4, S=gray, B= black, M = white), here 1, 2 represent the S macrodomains embedded with B domains, 3) B spheres 4) S spheres, 5) S spheres embedded with B.*

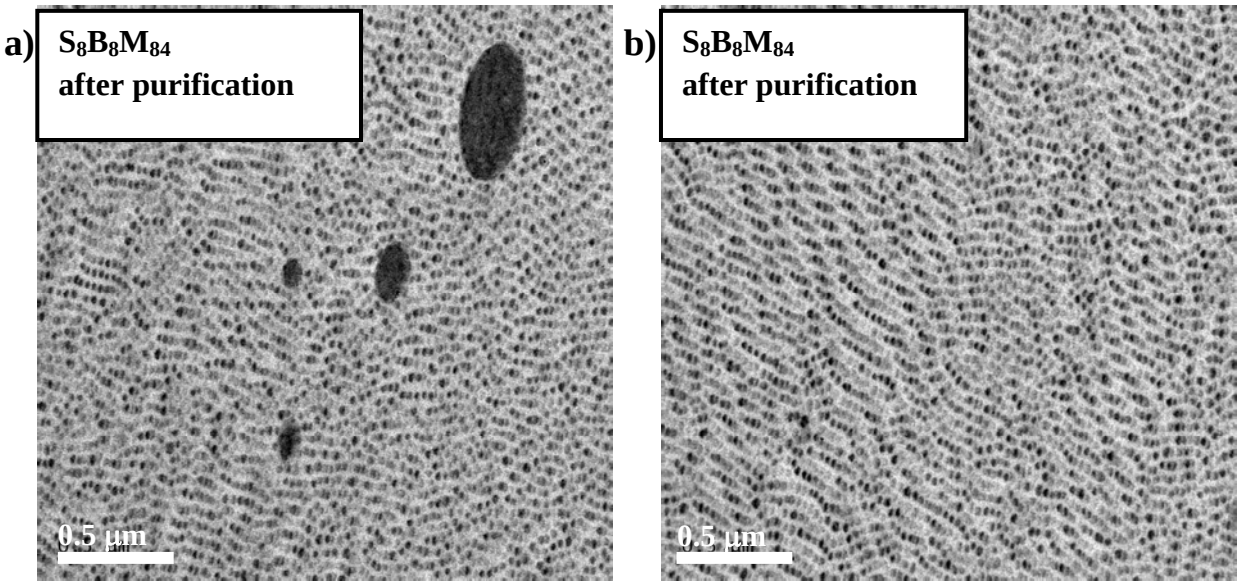

Figure 8.3: *TEM micrographs of pure $S_8B_8M_{84}$. After purification, only few S macrodomains, S and B spheres embedded on M matrix.*

The micrographs of the purified SBM are shown in Figure 8.3. As the weight fractions of S and B are very low compared to M, both the S (~ 24 nm) and B (~ 18 nm) blocks form spheres and they are randomly dispersed in the M matrix. Here, the gray spheres are the S and the black spheres are the B

domains. Still some macrophase separation can be observed in Figure 8.3a) which is mainly caused by the presence of 14% of SB precursor.

8.3 Influence of the S- and SB residuals on the mechanical properties

To investigate the influence of the precursor residuals on the mechanical properties, seven SBM samples of different molar masses ranging from 80 to 312 kg/mol are chosen. The amount of the residuals is ranging from 19 - 41% with a weight fraction of the overall amount of B blocks being 31%. Note, that the 1,2-B content varies from 17% to 89%. All the samples are loaded under tension and the tensile test results, e.g., the Young's modulus, stress and strain at break are evaluated and listed in Table 8.2 along with the SBM composition.

Figure 8.4 shows the tensile curves of the polymers listed in Table 8.2. Depending on the type of stress-strain curve, the samples are divided into three categories. In the first category (polymers a-c), the blends contain 33 to 41% residual precursor and they show a similar pattern of the yield stress with a high strain softening. The yield stress(σ_y) obtained is in the range of 19 to 25 MPa. After strain softening a slow increase of the stress for further elongation is observed. The strain at break reaches values as high as 400%.

In second category (polymers d-f), the contents of residual precursors in an interval from 19 to 24%. From the stress-strain curve, a moderate strain softening but a very high strain hardening during the elongation process is observed. In this case, rather yield stresses are lower (σ_y = 17 to 19 MPa) and strains at break are higher (~ 600 %) compared to the first category. The reason for the higher strains at break of polymers (d-f) are mainly attributed to their lower content of 1,2-B. On the contrary, the polymers (a-c) consists of a higher content of 1,2-B resulting in lower strains at break. In final category (polymer g), the content of residual precursor is 29%. From the stress-strain curve, surprisingly no yield point or strain hardening is observed despite the presence of its high 1,2-B content (88%); the strain at break is already reached at 40% strain. The exception may be explained due to the presence of the precursors in the polymer. One can see from Table 8.2 that in this polymer the content of SB is 9% and that of S reaches 20% whereas in all the other specimens discussed the content of SB exceeds the one of S. Hence, it is assumed that a higher content of glassy S and rigid 1,2-B reduces the elongation at break.

Table 8.2: *Overview of the mechanical properties (Young's modulus, stress, and strain at break), composition, and the weight percentage of the residual precursor.*

Polymers			M_n	*X*(1,2) %	E (MPa)	ε_B(%)	σ_B(MPa)	Impurities SB+ S (%)
a)	◇	$S_{29}B_{31}M_{40}^{90}$	90	35	625 ± 45	342 ± 2	19 ± 1	(37+4)=41
b)	◁	$S_{30}B_{31}M_{39}^{110}$	110	34	567 ± 16	227 ± 65	17 ± 1	(30+4)=34
c)	▽	$S_{32}B_{31}M_{37}^{91}$	89	89	697 ± 30	226 ± 75	23 ± 1	(21+12)=33
d)	□	$S_{34}B_{31}M_{35}^{80}$	80	18	460 ± 28	528 ± 100	22 ± 3	(20+4)=24
e)	△	$S_{32}B_{32}M_{36}^{170}$	170	30	523 ± 32	575 ± 57	27 ± 2	(22+2)=24
f)	▷	$S_{30}B_{31}M_{39}^{113}$	113	17	468 ± 27	522 ± 62	25 ± 2	(18+1)=19
g)	⬡	$S_{39}B_{31}M_{30}^{312}$	312	88	675 ± 24	33 ± 6	21 ± 1	(9+20)=29

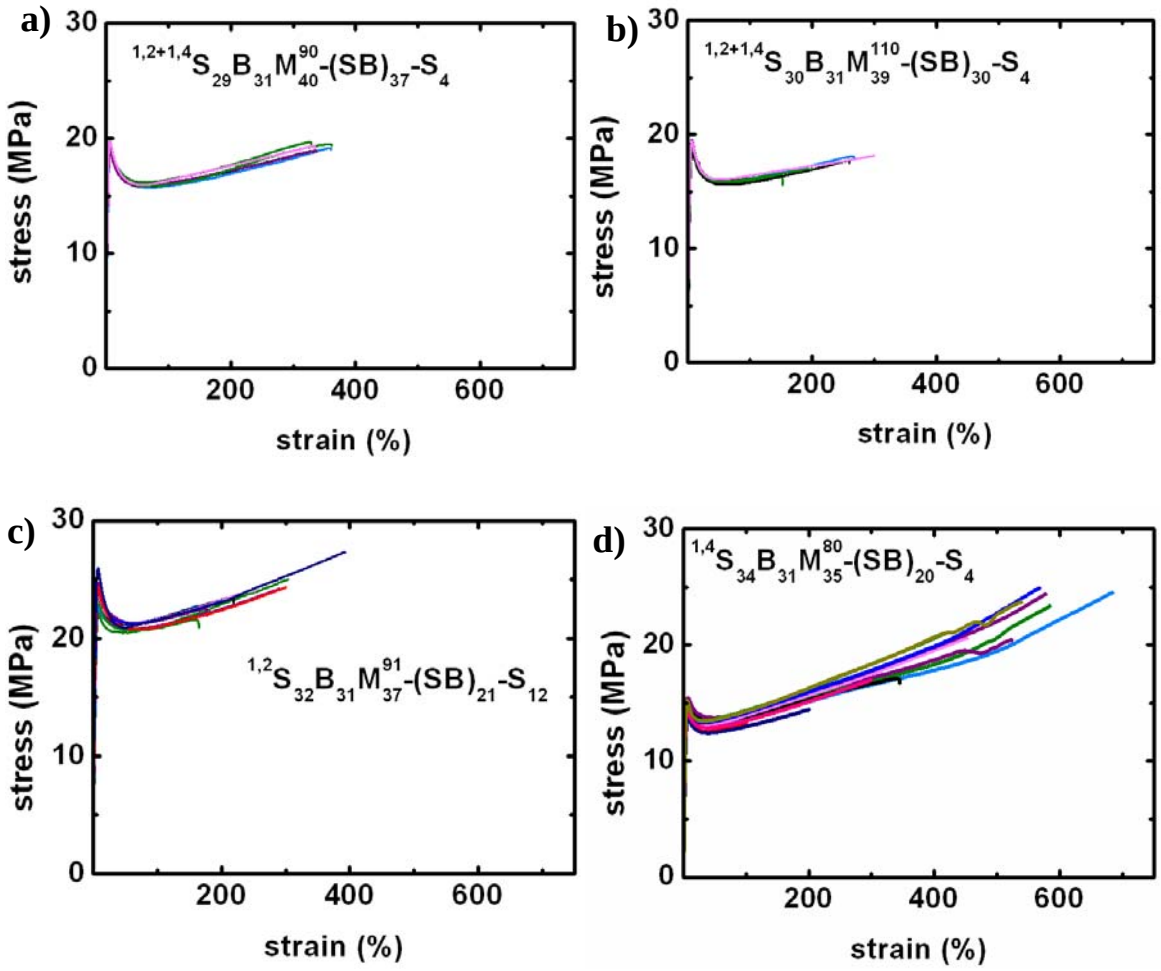

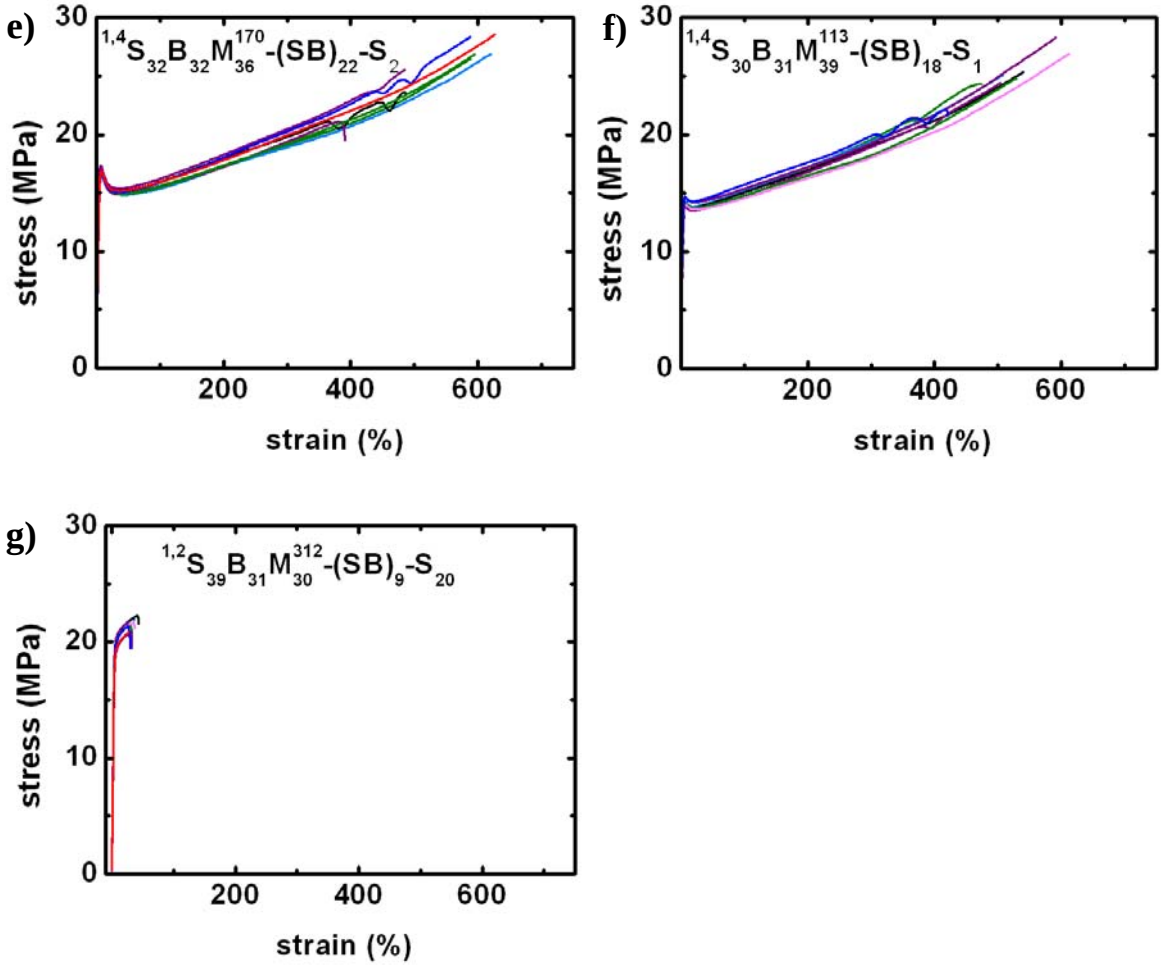

Figure 8.4: *Stress-strain diagrams of SBM polymers. The nomenclature of the polymer is* $^{n}S_xB_yM_z^{m}$-$(SB)_O$-S_P *(n = percentage of B microstructure, x,y,z = weight fraction of the blocks,* $_O$ *= weight percentage of SB residuals,* $_P$ *= weight percentage of S residuals. Here, a)* $^{1,2+1,4}S_{29}B_{31}M_{40}^{90}$-$SB_{37}$-$S_4$*, b)* $^{1,2+1,4}S_{30}B_{31}M_{39}^{110}$-$SB_{30}$-$S_4$*, c)* $^{1,2}S_{32}B_{31}M_{37}^{91}$-$SB_{21}$-$S_{12}$*, d)* $^{1,4}S_{34}B_{31}M_{35}^{80}$-$SB_{20}$-$S_4$ *e)* $^{1,4}S_{32}B_{32}M_{36}^{170}$-$SB_{22}$-$S_2$ *f)* $^{1,4}S_{30}B_{31}M_{39}^{113}$-$SB_{18}$-$S_1$*, g)* $^{1,2}S_{39}B_{31}M_{30}^{312}$-$SB_9$-$S_{20}$*'. [In a and b, the value n = 1,2+1,4 represents the ratio of 1,2- and 1,4-B 1:2]*

A summary of the data from the tensile tests, i.e., tensile modulus (*E*), stress at maximum (σ_M), strain at break (ε_B) of the lamellar type SBMs is listed in Table 8.2. The data also indicate the percentage of the precursor residuals present in the system. From the tensile behavior shown in Figure 8.4, it is obvious that the presence of residuals strongly influences the polymers' tensile properties. Therefore, in the following sections, the different tensile properties are discussed in dependency of the type and content of the residual precursor along especially focusing on the two different B isomers.

8.3.1 Influence of residual precursors and 1,2-B content on the elastic properties

The tensile modulus of the block copolymers in dependency of the fraction of 1,2-B and of the amount of residual precursor is depicted in Figure 8.5a) and 8.5b) respectively. Obviously, the E-modulus slightly increases in both cases. For all polymers investigated, the E-modulus is increased for an increasing fraction of residual precursor (see Figure 8.5a). The polymers,'$^{1,2+1,4}S_{29}B_{31}M_{40}^{90}$-$SB_{37}$-$S_4$'and '$^{1,2+1,4}S_{30}B_{31}M_{39}^{110}$-$SB_{30}$-$S_4$' show a comparatively lower modulus compared to '$^{1,2}S_{32}B_{31}M_{37}^{91}$-$SB_{21}$-$S_{12}$'and'$^{1,2}S_{39}B_{31}M_{30}^{312}$-$SB_9$-$S_{20}$'though the first two polymers contain more precursor residuals (see Table 8.2). This behavior can be explained by the amount of hard S block, here in later case, this amount is 12 and 20%. Figure 8.5b) shows the relation of the E-modulus with the fraction of the1,2-B isomer. With increasing the 1,2-B content the E-modulus is also increases. The polymers $^{1,2+1,4}S_{29}B_{31}M_{40}^{90}$-$SB_{37}$-$S_4$'and '$^{1,2+1,4}S_{30}B_{31}M_{39}^{110}$-$SB_{30}$-$S_4$'contain approximately 34% of 1,2-B whereas in '$^{1,2}S_{32}B_{31}M_{37}^{91}$-$SB_{21}$-$S_{12}$'and'$^{1,2}S_{39}B_{31}M_{30}^{312}$-$SB_9$-$S_{20}$', the content is as high as 88%. Hence, a lower E-modulus can be expected for the polymers'$^{1,4}S_{34}B_{31}M_{35}^{80}$-$SB_{20}$-$S_4$', '$^{1,4}S_{32}B_{32}M_{36}^{170}$-$SB_{22}$-$S_2$', and '$^{1,4}S_{30}B_{31}M_{39}^{113}$-$SB_{18}$-$S_1$'.

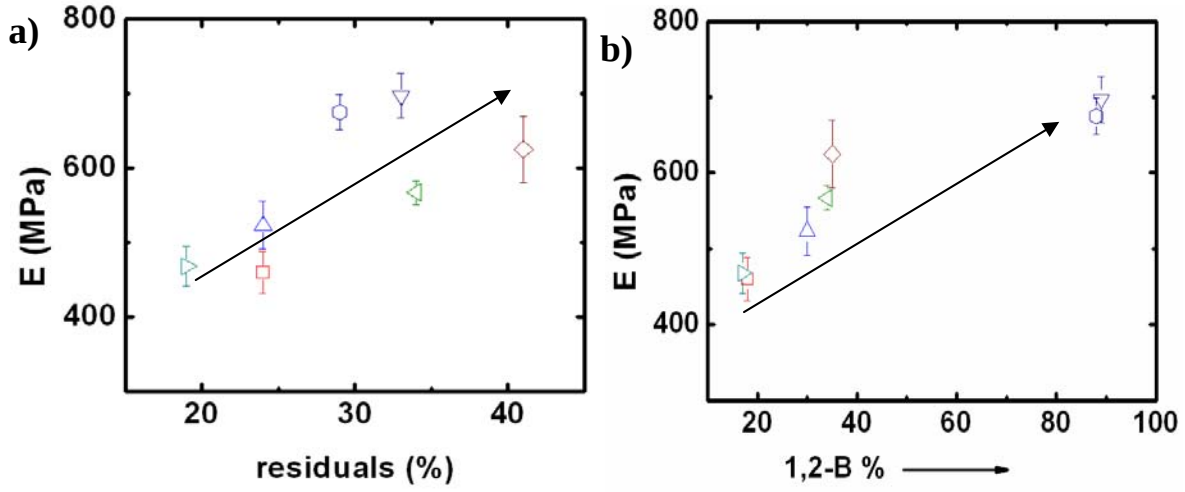

Figure 8.5:*a) Dependency of the E-Modulus of the fraction of residual precursor (a) and the content of the 1,2-B isomer (b). Samples code are:* ◇ = $S_{29}B_{31}M_{40}^{90}$-SB_{37}-S_4 , ◁ = $S_{30}B_{31}M_{39}^{110}$-SB_{30}-S_4 , ▽ = $S_{32}B_{31}M_{37}^{91}$-SB_{21}-S_{12} , □ = $S_{34}B_{31}M_{35}^{80}$-SB_{20}-S_4, △ =$S_{32}B_{32}M_{36}^{170}$-SB_{22}-S_2, ▷ = $S_{30}B_{31}M_{39}^{113}$-SB_{18}-S_1, ⬡ = $S_{39}B_{31}M_{30}^{312}$-SB_9-S_{20}.

8.3.2 Influence of residual precursors and 1,2-B content on the stress and strain at break

In Figure 8.6, the stress at break is plotted against the amount of the residual precursor and against the fraction of the 1,2- B isomer. The stress at break decreases linearly with an increasing amount of residual precursor (see Figure 8.6a).

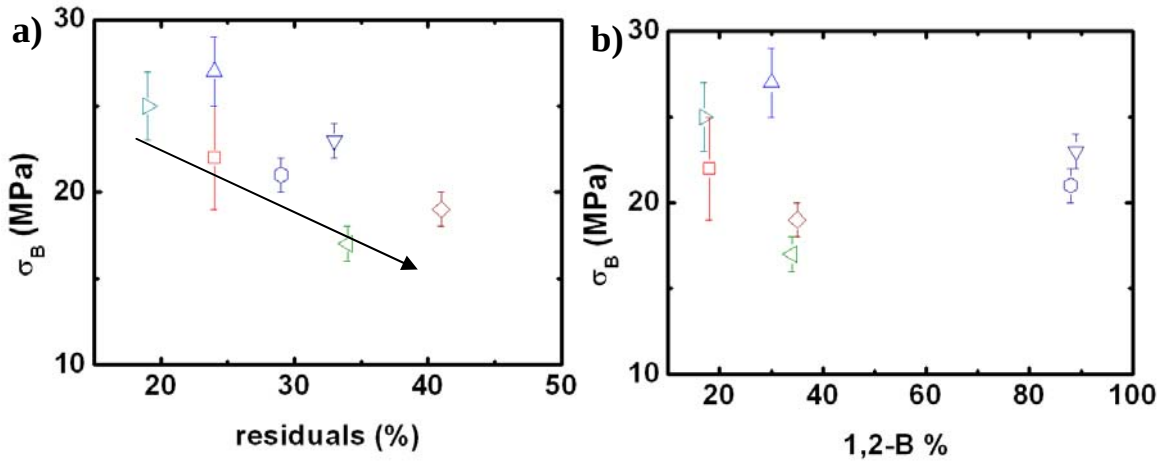

Figure 8.6: *Dependency of the stress at break σ_B on the a) percentage of residual precursor and b) the1,2-B content of the polymers. Samples code are: ◇ = $S_{29}B_{31}M_{40}^{90}$-SB_{37}-S_4 , ◁ = $S_{30}B_{31}M_{39}^{110}$-SB_{30}-S_4 , ▽ = $S_{32}B_{31}M_{37}^{91}$-SB_{21}-S_{12} , □ = $S_{34}B_{31}M_{35}^{80}$-SB_{20}-S_4, Δ =$S_{32}B_{32}M_{36}^{170}$-SB_{22}-S_2, ▷ = $S_{30}B_{31}M_{39}^{113}$-SB_{18}-S_1, ⬡ = $S_{39}B_{31}M_{30}^{312}$-SB_9-S_{20}.*

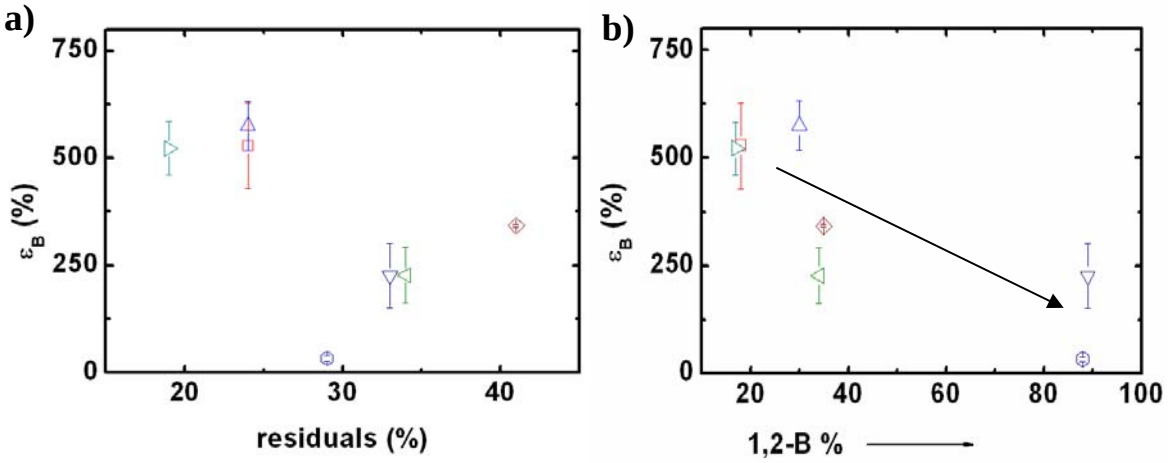

Figure 8.7: *Dependency of the strain at break on the a) percentage of residual precursor and b) on 1,2-B content of the polymers. Samples code are: ◇ = $S_{29}B_{31}M_{40}^{90}$-SB_{37}-S_4 , ◁ = $S_{30}B_{31}M_{39}^{110}$-SB_{30}-S_4 , ▽ = $S_{32}B_{31}M_{37}^{91}$-SB_{21}-S_{12} , □ = $S_{34}B_{31}M_{35}^{80}$-SB_{20}-S_4, Δ =$S_{32}B_{32}M_{36}^{170}$-SB_{22}-S_2, ▷ = $S_{30}B_{31}M_{39}^{113}$-SB_{18}-S_1, ⬡ = $S_{39}B_{31}M_{30}^{312}$-SB_9-S_{20}.*

The maximum stress at break is obtained for polymer '$^{1,4}S_{32}B_{32}M_{36}^{170}$-$SB_{22}$-$S_2$'($\sigma_B$ = 27 MPa) with a precursor content of 24%, whereas the lower stresses are found for polymer '$^{1,2+1,4}S_{29}B_{31}M_{40}^{90}$-$SB_{37}$-$S_4$'($\sigma_B$ = 17 MPa) and '$^{1,2}S_{32}B_{31}M_{37}^{91}$-$SB_{21}$-$S_{12}$' ($\sigma_B$= 19 MPa) both having a higher amount of impurities (see Table 8.2). Figure 8.6b indicates that the stress at break is nearly independent of the type of B isomers (e.g. '$^{1,4}S_{34}B_{31}M_{35}^{80}$-$SB_{20}$-$S_4$',' $^{1,4}S_{30}B_{31}M_{39}^{113}$-$SB_{18}$-$S_1$' and '$^{1,2}S_{32}B_{31}M_{37}^{91}$-$SB_{21}$-$S_{12}$', '$S_{39}B_{31}M_{30}^{312}$-$SB_9$-$S_{20}$').

Figure 8.7 depicts the dependency of the strain at break on the residual precursor content a) and on the fraction of the 1,2- B isomer b). In Figure 8.7a) the interpretation is hampered by the scatter of ε_B especially for higher amounts of residual precursor. However, according to Figure 8.7b) for an increasing 1,2-B microstructure ε_B tends to decrease . The highest elongation at break is observed in case of polymer '$^{1,4}S_{32}B_{32}M_{36}^{170}$-$SB_{22}$-$S_2$' ($\varepsilon_B$ = 575%) whereas polymer '$^{1,2}S_{39}B_{31}M_{30}^{312}$-$SB_9$-$S_{20}$' ($\varepsilon_B$ = 33%) exhibits the lowest elongation at break despite its very high molar mass. Probably this unexpected behavior is caused by its high 1,2-B content. '$^{1,2}S_{32}B_{31}M_{37}^{91}$-$SB_{21}$-$S_{12}$' and '$^{1,2}S_{39}B_{31}M_{30}^{312}$-$SB_9$-$S_{20}$',possess almost the same contents of 1,2-B and residual precursor however the low molar mass polymer '$^{1,2}S_{32}B_{31}M_{37}^{91}$-$SB_{21}$-$S_{12}$' exhibits a higher elongation at break (ε_B = 226%) compared to high molar mass polymer '$^{1,2}S_{39}B_{31}M_{30}^{312}$-$SB_9$-$S_{20}$'. This effect is mainly caused by the type of precursor blended with the polymer. The polymer '$^{1,2}S_{32}B_{31}M_{37}^{91}$-$SB_{21}$-$S_{12}$' is composed of approximately 12% S and 21% SB residual precursor whereas in polymer '$^{1,2}S_{39}B_{31}M_{30}^{312}$-$SB_9$-$S_{20}$' this content accounts to 20% S and 9% SB. As the hard phase lowers the elongation, the higher content of S causes the lower elongation at break in case of polymer '$^{1,2}S_{39}B_{31}M_{30}^{312}$-$SB_9$-$S_{20}$'.

8.4 Influence of residual precursor on the morphology before and after tensile test

8.4.1 Morphology before tensile test

Figure 8.8a) illustrates the TEM images of SBM15 ($^{1,2}S_{39}B_{31}M_{30}^{312}$) where almost 29% impurities are present. The lamellar domains of gray S and white M can clearly be seen from the micrograph. With a careful observation very narrow B domains are found at the S interface marking by arrow 2. Furthermore, in few areas the macrophase separation can be seen in that sample. Circle 1 depicts the

S-phase which is due to the 20% of residual S precursor. Despite this high amount of S homopolymer still the SBM triblock sustains it lamellar type of morphology with domain sizes of 14 ± 1 nm (B), 86 ± 2 nm (S), and 38 ± 1 nm (M) (domain sizes were measured in the circle area 3, Figure 8.8a). The broad S domains are probably caused by the presence of the S and the SB precursor residuals containing 20% S and 9% SB.

Obviously, the S-precursor is embedded in the SBM triblock (where it swells the S-lamellae) and present as co-existent macrophase. The behavior of such type of bicomponent mixtures (ABC triblock + AB, BC or AC diblock) for lamellar systems were described by various researchers.[3-6]Among them Goldacker et al. [5] has demonstrated the different variations how ABC lamellar triblock can be blended with AB or BC diblock components: A centrosymmetric lamellar pattern of ABC CBA AB BA ABC CBA-type may be formed (see Figure 8.8b); however also an aperiodic superstructure may also result where the AB and ABC blocks are arranged in a random manner. The third possibility is the formation of a lamellar type superstructure of both the AB diblock and the ABC triblock. Here, only small volume fractions of the diblock must be present; for larger amounts the lamellar superstructure changes to a superstructure with curved interfaces, such as a co-continuous or cylindrical morphology.

These lamellar-type superstructures can be made-up in two different fashions. Birstein et al. proposed [7] that the AB-diblock (or BC-diblock) is totally located inside the domains and leading to *mixed supperlattice* (see Figure 8.9a). The second type of superlatice was described by Goldacker et al.[6]; here a diblock and a triblock with similar block lengths and comparable interfacial tensions form a lamellar structure where the diblock is not located inside the triblocks' phase, hence a sequence of ABC CBA and AB BA-type will be yielded which is termed as *individual lamellae* (see Figure 8.8b and 8.9b).

In the light of the theories discussed above the TEM images of polymer $S_{39}B_{31}M_{30}^{312}$ (see circle 3 in Figure 8.8a) are strongly indicating the presence of individual lamellae as sketched in Figure 8.9b. It has to be kept in mind that the SB precursor residual is yielded in-situ with the SBM synthesis; hence its chain length is identical to that of the SB's in the SBM triblock. Furthermore, the composition of the SB impurity is calculated as $S_{56}B_{44}^{250}$ which also favors the formation of an individual SB lamellae due to the high molar mass and almost equal weight fractions of the S and B blocks.

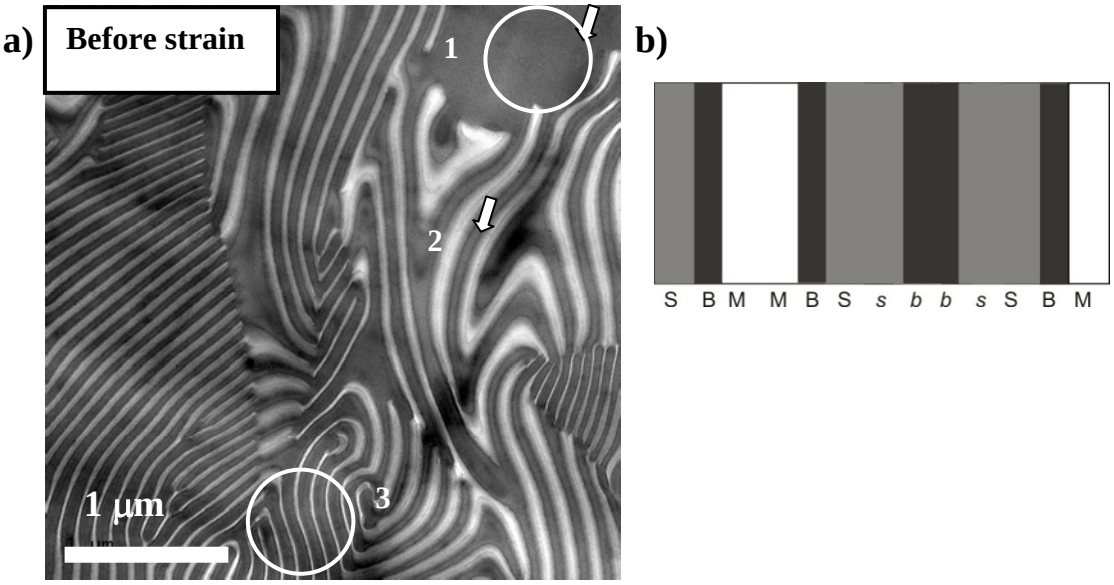

Figure 8.8: *a) TEM micrographs of non-purified* $^{1,2}S_{39}B_{31}M_{30}^{312}$*-*$SB_9$*-*$S_{20}$*. Here, 1 is a macrodomain of S, 2 shows the narrow B domains on the S interface and 3 depicts the lamellar phase of a broad S and a narrow M domain. b) The blending with a SB diblock copolymer symbolized with (**sb**) forms centrosymmetric lamellae.*

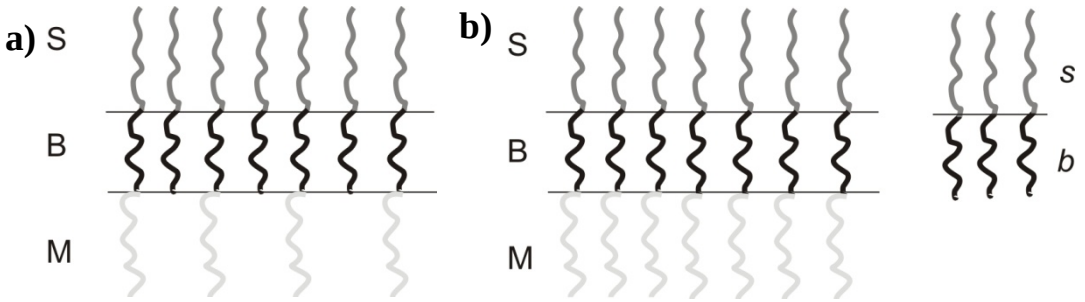

Figure 8.9: *a) Schematic presentation of a possible blendof SBM triblock + SB diblock leading to a **mixed superlattice**. b) The formation of individual lamellae of SBM triblock and SB diblock forms **individual lamellae**.*

8.4.2 Morphology after tensile test

The TEM image of $^{1,2}S_{39}B_{31}M_{30}^{312}$ after performing mechanical testing is given in Figure 8.10a). The deformations of the domains are highlighted by the arrows 1 to 4. When the polymer is stretched parallel to the lamellae direction, the domains are elongated, undulated, and become narrow, (cf. arrow 1 in Figure 8.10a). Again a zig-zag pattern named 'chevron pattern' is observed, as indicated by arrow 2. The deformation pattern of 'chevron morphology' is sketched in Figure 8.10b) for a better

understanding. Such pattern mainly occurs if the lamellar domains are elongated perpendicular to the stretching direction. In some places an U-like pattern (arrow 3) is found, which can be either be an artifact or result from a different projection of the TEM view. Arrow 4 shows the macrophase separation of the S phase. One can notice that the macrophase was not affected even at the high elongations during the tensile tests. Very likely the presence of the S macrophase interferes with a regular deformation eventually resulting in lower strains at break.

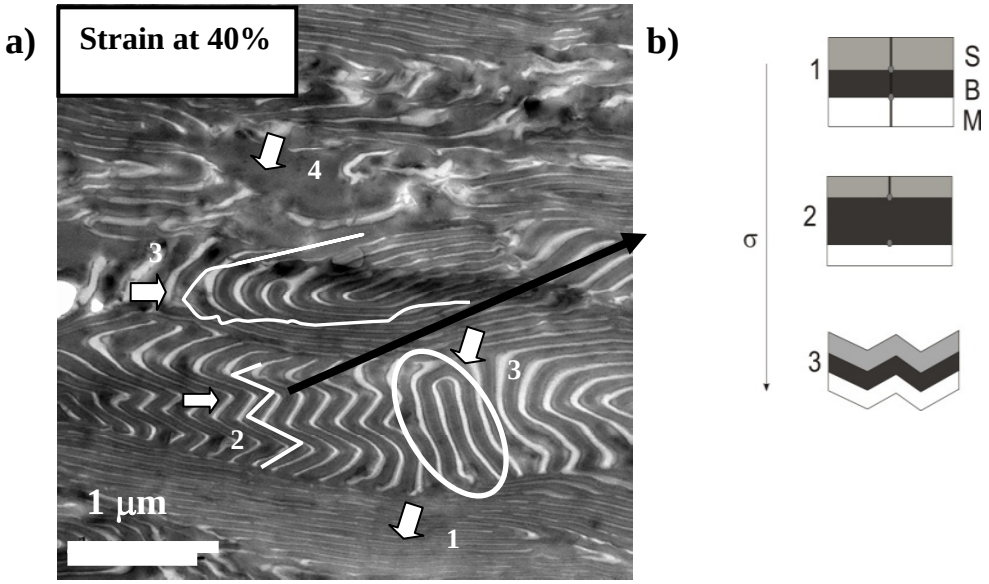

Figure 8.10:*a) TEM micrographs of* $^{1,2}S_{39}B_{31}M_{30}{}^{312}$*-*$SB_9$*-*$S_{20}$ *after tensile test. Here 1) undulated lamellae, 2) zig-zag pattern, 3) U like pattern, 4) macrophases. B) The mechanism of chevron morphology (right)*

Table 8.3: *The change of the domain sizes of S, B, and M blocks after tensile testing.*

domain sizes	**S**	**B**	**M**
before tesile test	86 ± 2	14 ± 1	38 ± 1
after tensile test	87 ± 1	12 ± 2	37 ± 1

The domain sizes after the tensile test were calculated from the TEM images. The dimension of B domain is reduced slightly during the elongation parallel to the lamellar domains. The calculated domain sizes after 33% strain (Fig 8.10a, in the circle indicated arrow 3) of S, B and M blocks are compared to the domain sizes of non-elongated sample indicated in the circle 3, Figure 8.8a. It calculation shows in Table 8.3 that the domain sizes of all the three blocks are almost same even after elongation. This observation can also be explained from the stress-strain curve (see Figure 8.4g) at

maximum strain at break around 33% which might be insignificant to deform the lamellar domains of this polymer.

8.5 Summary

The influence of residual S homopolymer or SB diblock copolymer precursor on the morphology and the mechanical properties were discussed for SBM triblock polymers. When the content of residual precursor exceeds 50%, macrophase separation is occurred (see Figure 8.2). For lower contents of residuals (e. g. 29%) the well-ordered morphology sustains (see Figure 8.8). If the SB precursor is composed of equal weight fractions (e. g. $S_{56}B_{44}^{250}$), it forms an individual lamellae co-existing with the SBM triblock.

To investigate the effects of residual precursor on the mechanical properties, a series of SBM polymers was chosen. The results show that precursor contents ranging from 33 - 41% lead to high yield stresses in combination with only minor strain hardening. The strain at break can reach values up to 400%. When the precursor contents range from19 - 24%, moderate yield stresses with a higher tendency of strain hardening along with strains at break up to 600% can be observed. If the amount of S precursor exceeds that of the SB (see Figure 8.4g), no yield stress and strain hardening can be detected with a strain at break as low as 40%. The E-modulus increases with a higher amount of residual precursor and a higher 1,2-B content, whereas the stress at break decreases with an increasing content of the precursor. Interestingly in case of the strain at break an opposite dependency is observed as it is mainly governed by the type of the B isomers but not by the amount of residual precursor. With increasing the 1,2-B microstructure a decreasing tendency of strain at break is observed.

Reference

[1] S. Ritzenthaler, F. Court, L. David, E. G. Reydet, L.Leibler, J. P. Pascault., *Macromolecules* **2002**, *35*, 6245.

[2] B. Jaffrennou, J. Portal, F. Méchin, J. P. Pascault, *European Polymer Journal* **2008**, *44*, 3439.

[3] L. Leibler, C. Gay, I. Erukhimovich, *Europhys. Lett.* **1999**, *46*, 549.

[4] R. A. Wickham, A. C. Shi, *Macromolecules* **2001**, *34*, 6487.

[5] T. Goldacker, V. Abetz, *Macromolecules* **1999**, *32*, 5165.

[6] T. Goldacker, V. Abetz, R. Stadler, *Macromol. Symp.* **2000**, *149*, 93.

[7] T. M. Birshtein, A. A. Polotsky, V. M. Amoskov, *Macromol. Symp.* **1999**, *146*, 215.

Chapter 09

Summary and Conclusion

In this work correlation between morphology and mechanical properties of different triblock terpolymers of polystyrene-*b*-polybutadiene-*b*-poly(methyl methacrylate), SBM, especially of those having lamellar morphology subtypes (e. g. well segregated lamellae or a transitional lamellar pattern) have been extensively investigated. Moreover, the influence of polybutadiene (B) isomers (which is mainly controlled by the solvent polarity) on the morphology and mechanical properties have been explored. Different polybutadiene isomers were obtained as follows:

- The polymerization was performed either in THF (to obtain predominantly 1,2-B) or in toluene (to obtain a higher content of 1,4-B).
- For both types of polymer's molar masses ranged from 30 kg/mol to 300 kg/mol to allow better segregation of the different domains and an investigation of the influence of the chain length on the polymers' properties.

Among the monomers, the polymerization of styrene (S) and butadiene (B) were controlled easily in all kinds of solvents, however, the synthesis of poly(methyl methacrylate) (M) was troublesome in both polar and non-polar solvents due to high tendency of backbiting and side reactions. The best way to alleviate these reactions in THF was to modulate the reactivity of carbanion chain end by introducing the end-capping reagent, 1,1-diphenylethylene, (DPE), prior to adding M monomer. However, when the synthesis was performed in a non-polar solvent, like toluene, further aggregation complicates the polymerization of M monomer. To overcome this problem, additives or the aluminium catalyst, (di[2,6-di(tert-butyl)-4-methyl phenoxy]isopropyl aluminium, *i*BAl(BHT)$_2$), were used. Unfortunately, in the presence of Al catalyst the targeted polymers' composition was not reached. Therefore, the first two blocks (polystyrene and polybutadiene) were polymerized in pure toluene to increase the fraction of 1,4-B and the terminal M block was performed in a solvent mixtures consisting of THF and toluene in a volume ratio of ***2:1***. Best results in terms of low polydispersity and low content of S and SB residuals were obtained when THF and DPE were added at -30 °C and the M monomer at -60 °C. Eventual traces of non-reacted S and SB precursor polymers were subsequently removed by using theta solvents for the different blocks.

The morphological and mechanical investigations for different lamellar type SBMs in present work are summarized as follows:

9.1. Summary on morphology characterization

- Very well segregation of the lamellar domains for both 1,2- and 1,4- SBM at molar masses ranging from 80 to 170 kg/mol can be obtained.
- Short lamellar domains can be found for the molar masses ranging from 40 to 55 kg/mol.
- Mixed lamellae can be obtained in the polymers containing low molar mass (35-70 kg/mol) and higher contents of 1,4-B.
- A transitional lamellar morphology can be achieved in presence of a significant amount of SB residual precursors. This residual can trigger the transformation of a B lamellar domain-shape pattern to a cylindrical or spherical one especially when the 1,2-B isomer is predominant.
- The chain like oriented lamellae can be obtained in a SBM existing short chain B domains where the ratio of the 1,2- and 1,4-B is ***1:2***.

9.2. Summary on mechanical properties for different subtypes of lamellar SBM

9.2.1 In symmetric type SBM the following conclusion were obtained:

- The polymers with lower x(1,2)% and relatively higher 1,4-B content show moderate stress drops after yielding and an increasing stresses during elongation process. On the other hand, the polymers with higher x(1,2)% and relatively higher 1,2-B contents, higher stress drops and lower strain hardening are observed.
- Higher elongation was obtained if 1,4- B is predominant and the molar masses of SBMs are high.
- The tensile modulus and stresses at break were mainly affected by the nature of glassy domains of the polymers as well as the 1,2- B content. However, the effect of B isomers on the stresses at break is moderately low.
- A strong influence of the ratio of the 1,2- and 1,4-B was observed on the mechanical properties. If the molar mass of the B domains are low and the ratio of 1,2- and 1,4-B is close to ***1:2***, the mechanical properties are found remarkably low.

9.2.2 In asymmetric type SBM the following results can be summarized:

- The molar masses of SM glassy domain had minor influence on the stress behavior.
- Higher elongation was obtained high chain length of SM glassy domains as well as for polymers' molar masses.
- The stress at break and the tensile modulus were strongly influenced by the ratio of 1,2 and 1,4-B. Slight changes of the ratio of 1,2- and 1,4-B from ***1:6*** to ***1:4*** decrease the stiffness of the polymers sharply.

9.3. Comparative studies of stress-strain behavior for two pairs of SBM containing similar molar masses of glassy and rubbery domains.

- In case of low molar mass 1,2-SBM (i.e., $^{1,2}S_{31}B_{31}M_{38}^{55}$) a transitional structures from lamellar to cylindrical domain patterns of polybutadiene was observed. However, in low molar mass 1,4-SBM (i.e.,$^{1,4}S_{30}B_{29}M_{41}^{53}$) very continuous and well segregated lamellar patterns were obtained. As a consequence of the differences between these morphologies, a typical yield point (followed by a drop in stress after yield that indicates macroscopic necking) caused by the continuous M phase in $^{1,2}S_{31}B_{31}M_{38}^{55}$ is observed. In contrast, typical rubbery behavior without any yield point was observed in $^{1,4}S_{30}B_{29}M_{41}^{53}$ due to the much more continuous B phase in the laminar structure.
- The SBMs with high molar masses (i.e., $^{1,2}S_{32}B_{31}M_{37}^{91}$ and $^{1,4}S_{34}B_{31}M_{35}^{80}$) show intermediate stress-strain behavior than the previous pair. A moderate yield and delocalization of strains in both $^{1,2}S_{32}B_{31}M_{37}^{91}$ and $^{1,4}S_{34}B_{31}M_{35}^{80}$ were detected. Only the $^{1,4}S_{34}B_{31}M_{35}^{80}$ showed comparatively higher elongation at break than the others. Such properties were governed mostly by the long chain 1,4-B domains due to their higher flexibility.

9.4. Summary on deformation and orientation behavior of SBM

- In case of 1,2-SBMs (both the low and high molar masses), the transitional B domains were deformed into wavy and screw type patterns after tensile test. In most cases, the B domains were detouched from their lamellar domains and blended homogenously in the S phases. On the contrary, the 1,4-SBM (both the low and high molar masses) deformed to very wavy lamellae after tensile test. In most cases, even at 300% elongation, the long periodicity of the deformed B domains remained unchanged and stress hardening resulted after post-yield elongation.
- The discontinuous B domains in the 1,2-SBMs caused a high orientation at the initial deformation stage. On the other hand, the 1,4-SBMs showed moderate orientation even at 300% strain.
- From SAXS interpretation anisotropic SAXS patterns were observed in case of 1,2-SBMs whereas four point SAXS patterns were obtained for 1,4-SBMs.
- In case of low molar masses SBMs, very limited number of orientation factor (P2) was obtained in $^{1,2}S_{31}B_{31}M_{38}^{55}$due to the brittleness of the polymer. But for $^{1,4}S_{30}B_{29}M_{41}^{53}$, the P2 value was -0.10 at the initial elongation (35%) and -0.02 at the very high elongation (400%). The results showed for $^{1,4}S_{30}B_{29}M_{41}^{53}$ the continuous lamellar domains, which are orientated perpendicularly to the chain axis, have been randomly arranged at higher elongation.
- For high molar masses SBMs, the P2 value for 1,2-SBM ($^{1,2}S_{32}B_{31}M_{37}^{91}$) showed -0.22 which resembled partly orientation of the lamellar domains perpendicular to the chain axis, whereas in case of 1,4-SBM ($^{1,4}S_{34}B_{31}M_{35}^{80}$), the P2 value was -0.06 at the initial elongation (35%), which remained constant even at high elongation (440%). The orientation for this polymer was fairly perpendicular to the chain axis up to the higher elongation.

9.5. Influence of precursor residuals on morphology and mechanical properties

- The precursor residuals (S homopolymer and SB diblock copolymer) have a significant influence on the morphology and the mechanical properties. The

abundance of residuals (e.g. 50%) caused macrophase separated domains in a triblock. For lower contents of residuals (e. g. 29%) the well-ordered morphology sustained.

- If the residual contents ranging from 33 to 41% high yield stresses in combination with only minor strain hardening were observed. The strain at break reached up to 400%.
- For residual contents ranging from19 to 24%, moderate yield stresses with a higher tendency of strain hardening along with strains at break up to 600% can be observed. If the amount of S residuals (e.g. 20%) exceeded the amount of the SB residuals (e.g. 9%), no yield stress and strain hardening were obtained. Also the strain at break was found as low as 40%.
- The E-modulus increased with higher amount of residual precursor and a higher 1,2-B content, whereas the stress at break decreased with an increasing content of the residuals. In case of the strain at break an opposite dependency was observed as the strain at break decreased with an increasing content of 1,2-B isomers but not by the amount of residual precursor.

9.6. Future outlook

The results discussed in this thesis work have unclosed important mechanisms that describe structure-property correlation of B-isomers of SBM triblock terpolymers. The presented work will deliver advance knowledge to endeavor new challenges on understanding the orientation and deformation behavior of the B isomers in other types of morphologies, e.g., helical pattern. The helical pattern shows significant prospects for applications as chiral meso structure that offers potential approaches to the materials exhibiting enantioselective and antiferromagnetic properties. Also the helical pattern can be used as base material for high performance filtration membrane for viruses of the order of 10 nm or more by selectively decomposing the B helical microdomains to create a continuous helical nanochanel having a diameter of nanometer scale. As in recent research activities mostly the structural behavior of the helical pattern were investigated, it would also be in immense interest to study the deformation and orientation behavior of different domain sizes 1,2- or 1,4-B helical domains in-situ SAXS tensile testing and in microscopy, which may provide new information concerning the structural and mechanical behavior.

Zusammenfassung

Im Rahmen dieser Arbeit wurde der Zusammenhang zwischen Morphologie und mechanischen Eigenschaften unterschiedlicher Polystyrol-*b*-polybutadien-*b*-poly(methyl methacrylat), (SBM) Triblockcopolymere untersucht. Ein spezielles Augenmerk richtet sich auf die lamellare Morphologie, wobei auch die Übergangsbereiche dieser Struktur berücksichtigt werden. Weiterhin beinhaltet die Arbeit Untersuchungen zum Einfluss der Isomerie des Polybutadien-Blocks (die durch die Polarität des zur Synthese verwendeten Lösungsmittels gesteuert werden kann) auf die Morphologie und die mechanischen Eigenschaften des SBMs. Die Polymerisation ist entweder in THF (hoher 1,2-polybutadien-Anteil) oder in Toluol (hoher 1,4-polybutadiene Anteil) ausgeführt worden. Da in beiden Fällen molare Massen im Bereich von 30 kg/mol bis 300 kg/mol erreicht werden konnten, erlaubt dies sowohl den Einfluss der Isomerie des B-Blocks als auch den Effekt der Kettenlänge auf die Eigenschaften des Polymers zu untersuchen.

Im Rahmen der Triblocksynthese ist die Polymerisation von Styrol (S) und Butadien (B) ohne größere Schwierigkeiten in üblichen Lösungsmitteln gelungen. Die Synthese des Polymethylmethacrylat-Blocks hat sich sowohl in unpolaren als auch in polaren Lösungsmitteln aufgrund der Neigung des Monomeres zu Nebenreaktionen als schwierig gestaltete. Eine Umgehung der Nebenreaktionen in THF ist durch ein Verkappen des carbanionischen Kettenendes mit 1,1-Diphenylethylen (DPE) vor Zugabe des M-Monomers erreicht worden. In unpolaren Lösungsmitteln (z. B. Toluol) erschweren Aggregationsphänomene die Polymerisation des M-Monomers. Es ist leider nicht gelungen, dies durch Einsatz von Additiven und eines speziellen Aluminium-Katalysators (Di[2,6-di(*tert*-butyl)-4-methylphenoxy]isopropylaluminium*i*BAl(BHT)$_2$) zu umgehen.

Letztlich sind die beiden ersten Blöcke (Polystyrol und Polybutadien) in Toluol hergestellt worden (hoher Anteil an 1,4-B-Isomeren). Danach erfolgte die Polymerisation des M-Monomeren in einer Mischung aus THF und Toluol im Volumenverhältnis ***2:1*** erfolgt. Beste Ergebnisse im Hinblick auf eine geringe Polydispersität und einen geringer Anteil an Precursor-Resten ist durch Zugabe des THF und des DPE bei -30 °C, bzw. des M-Monomers bei -60 °C erzielt worden. Reste der S und SB-Precursorsind schrittweise durch Lösungs-Fällungs-Fraktionierung in theta-Lösungsmittel entfernt worden.

9.1. Morphologische Charakterisierung

- Eine deutliche Phasensegregation in lamellare Domänen kann sowohl im Falle des 1,2- als auch des 1,4- SBM für molare Massen im Bereich von 80 bis 170 kg/mol beobachtet werden.
- Für molaren Massen im Bereich von 40 bis 55 kg/mol nimmt die Länge der Lamellen ab.
- Polymere mit geringen molaren Massen (35-70 kg/mol) und hohem Anteil von 1,4-B organisieren sich in partiell gemischten A/C Lamellen.
- Eine aus Übergangslamellen bestehende Morphologie tritt in Gegenwart von größeren Mengen an SB-Precursor auf. Der Precursor-Rest führt zu Umwandlung der lamellaren B Domänen in eine zylindrische oder kugelförmige Anordnung, speziell bei hohen Anteilen an 1,2-B Isomer.
- Bestehen die B-Domänen aus kurzen Ketten und beträgt das Verhältnis1,2-B:1,4-B etwa ***1:2*** so organisiert sich der Triblock in kettenartig angeordneten Lamellen.

9.2. Einfluss der Symmetrie der Lamellen auf die mechanischen Eigenschaften

9.2.1 Symmetrische Lamelle

- Das Dehnungsverhalten wird wesentlich durch die molare Masse des SBM gesteuert. Hierbei führt eine Erhöhung des 1,4-B Anteils zu einer Zunahme der Dehnung.
- Das Zugmodul wird sowohl durch die Hartphase als auch den 1,2-B-Anteil beeinflusst. Die Bruchspannung hängt stark von der Hartphase ab. Der Einfluss des Isomerenverhältnisses des B-Blocks ist gering.
- Die mechanischen Eigenschaften variieren deutlich mit dem Isomerenverhältnis des B-Blocks. Geringe molare Massen und ein 1,2- zu 1,4-B Verhältnis von ungefähr ***1:2***, resultieren in vergleichsweise schlechten mechanischen Eigenschaften.

9.2.2 Subtyp: asymmetrische Lamelle

- Das Zugverhalten ist weitgehend unabhängig von den molaren Massen der Hartphase.
- Hohe Dehnungen können bei hohen molaren Massen der Hartphase, bzw. des gesamten Triblockcopolymeres erreicht werden.
- Bruchspannung und Zugmodul werden durch das Isomerenverhältnis des B-Blocks beeinflusst. Schon eine geringe Änderung des Verhältnisses 1,2- : 1,4-B von ***1:6*** zu ***1: 4*** vermindert die Steifheit des Polymeres signifikant.

9.3. Untersuchungen des Zug-Dehnungsverhaltens zweier SBM mit glas- und gummiartigen Domänen vergleichbarer molarer Masse

- In einem 1,2-SBM mit geringer molarer Masse ($^{1,2}S_{31}B_{31}M_{38}^{55}$) organisiert sich die Butadienphase im Übergangsbereich zwischen lamellarer und zylindrischer Anordnung. Das entsprechende 1,4-SBM-Isomer ($^{1,4}S_{30}B_{29}M_{41}^{53}$) zeigt demgegenüber eine durchgehend lamellare Morphologie. Im ersten Fall wird eine Fließgrenze (mit der zugehörigen Einschnürung) erreicht, die durch das Vorliegen einer durchgehenden M-Phase erklärt werden kann. $^{1,4}S_{30}B_{29}M_{41}^{53}$zeigt demgegenüber ein typisch gummielastisches Verhalten ohne Fließgrenze, da hier kontinuierliche B-Domänen vorliegen.
- Die Zug-Dehnungsverhalten des SBM mit hohen molaren Massen ($^{1,2}S_{32}B_{31}M_{37}^{91}$ und $^{1,4}S_{34}B_{31}M_{35}^{80}$) deuten darauf hin, dass das im vorherigen Abschnitt genannte Paar eine Art von Grenzfällen absteckt. Eine mäßige Dehnung und eine Verteilung der Spannung kann sowohl für $^{1,2}S_{32}B_{31}M_{37}^{91}$ als auch für $^{1,4}S_{34}B_{31}M_{35}^{80}$ beobachtet werden. Letzteres weist eine höhere Bruchdehnung auf. Es ist anzunehmen, dass dieses Verhalten in den langkettigen 1,4-B Domänen hoher Flexibilität begründet liegt.

9.4. Deformations und Orientierungsverhaltens der SBM

- Im Falle des 1,2-SBM (sowohl für niedrige als auch höhere molare Massen) führt eine Deformation zuerst zu wellen- und schraubenförmigen Anordnungen, die bei weiterer

Deformation zum Abreißen der B-Phase von den lamellaren Domänen-Resten und einer Mischung mit der S-Phase führt. 1,4-SBM kann demgegenüber nur bis hin zu stark wellenförmigen Domänen deformiert werden, sowohl bei niedrige als auch höherer molaren Masse. Die Fernordnung der deformierten B-Domänen bleibt bis 300% Dehnung erhalten und beim Erreichen der Fließgrenze wird eine Verhärtung des Materials beobachtet.

- Die diskontinuierlichen B-Domänen des 1,2-SBMs können schon bei geringen Dehnungen orientiert werden, während im 1,4-SBM bei 300% Dehnungnur ein mäßiges Orientierungsverhaltenerreicht wird.
- Im SAXS wird für 1,2-SBM eine anisotrope Streuung gefunden, während für 1,4-SBM ein 4-Punkt-Muster beobachtet werden kann.
- Der Orientierungsfaktor (P2) der SBM kleiner molarer Massen ($^{1,2}S_{31}B_{31}M_{38}^{55}$) ist bedingt durch die Brüchigkeit des Materials sehr klein. Für $^{1,4}S_{30}B_{29}M_{41}^{53}$beträgt er -0.10 (Dehnung:35%) bzw. -0.02 (maximalen Dehnung: 400%). Dies ist ein Anzeichen, dafür dass sich die Kettenachse senkrecht zu den Lamellen ausrichtet und letztere bei hoher Dehnung zufällig angeordnet sind.
- Der Orientierungsfaktor beträgt für das 1,2-SBM hoher molarer Masse ($^{1,2}S_{32}B_{31}M_{37}^{91}$) P2 = -0.22. Dieser Wert dokumentiert eine teilweise senkrechte Orientierung der Lamellen zur Kettenachse. Für das 1,4-SBM ($^{1,4}S_{34}B_{31}M_{35}^{80}$) wird für Dehnungen von 35 % bis zu 440% ein konstanter Wert von P2 = -0.06 gefunden, der den Schluss zulässt, dass eine senkrechte Orientierung des Polymers zur Kettenachse auch bei höheren Dehnungen aufrechterhalten werden kann.

9.5. Einfluss des Precursor-Rests auf die Morphologie und die mechanischen Eigenschaften

- Rückstände der Precursor-Polymere (S Homopolymer und binäres SB Diblockcopolymer) haben einen deutlichen Einfluss auf die Morphologie und die mechanischen Eigenschaften des SBM/Precursor-Blends. Ist der Anteil an Precursor hoch (z. B. 50%) so findet eine Mikrophasenseparation statt, während bei geringem Anteil die ursprüngliche Morphologie des Triblocks erhalten bleibt.
- Ein Precursor-Gehalt von 33 bis 41% führt zu hohen Fließspannungen bei nur geringer Kaltverfestigung und Bruchspannungen von bis zu 400%.

- Ein Precursor-Gehalt im Bereich von 19 bis 24% resultiert in moderatenFließspannungen mit höherer Neigung zur Kaltverfestigung und Bruchspannungen bis zu 600%. Übersteig der Anteil des S-Precursor (z. B. 20%) den des SB Precursors (z.B. 9%), so kannte weder eine Fließgrenze noch eine Kaltverfestigung beobachtet werden. Auch die Bruchspannungen sind in diesem Fall sehr gering – typischerweise im Bereich von 40%.
- Das Zugmodul scheint mit dem Anteil an Precursor und 1,2-B anzusteigen, während die Bruchspannung mit steigendem Anteil an Precursor abnimmt. Die Bruchdehnung folgt einem gegenläufigem Trend. Hier kann eine Abnahme durch eine Erhöhung des Anteils a 1,2-B Isomeren erreicht werden – allerdings nicht, wenn der Anteil des Precursors zunimmt.

9.6. Ausblick

Im Rahmen dieser Arbeit konnten neue Zusammenhänge zwischen der Struktur des B-Blocks und dem mechanischen Eigenschaftsprofil eines ternären SBM Triblock terpolymers gefunden werden. Die Ergebnisse können mit hoher Wahrscheinlichkeit auf das Orientierungs- und Deformationsverhalten der B-Domänen in anderen Morphologien, wie zum Beispiel der helikalen Anordnung übertragen werden. Eine Organisation des B-Blocks in eine Helix könnte den Weg für eine Vielzahl neuartiger Anwendungen ebnen, z. B. im Bereich der enantioselektiven und antiferromagnetischen Materialien. Weiterhin könnte eine solches Polymer als Ausgangsmaterial für eine Membran zur Abtrennung von Viren dienen, da der typische Durchmesse der Helix (10 nm) den Abmessungen eines Virus entspricht. Gegenwärtig beschränken sich die Forschungsaktivitäten auf die Klärung des strukturellen Verhaltens der Helixstruktur. Eine Untersuchung des Deformations- und Orientierungsverhalten insbesondere in Abhängigkeit der 1,2- bzw. 1,4-B Verteilung auf die Dimension der B-Domänen mittels in-situ SAXS-Zug-Dehnungsmessungen und anschließender Mikroskopie würde das Wissen über potentielle Einsatzmöglichkeiten dieses chiralen Strukturmotivs wesentlich erweitern.

Chapter 10

Appendix

Appendix A.

10.1 Chemicals

All solvents and reagents were obtained from Merck or Sigma-Aldrich and used without further treatment except the following ones. The purification procedures for the chemicals and the solvents are given below.

10.2 Purification of monomers, solvents and reagents

10.2.1 Styrene

Crude styrene was first filtered through a chromatographic column containing Al_2O_3 and further purified by using Bu_2Mg (1.6 M in heptane). To a volume of typically 100 ml of styrene (the styrene level needs to be marked) 8 ml of Bu_2Mg solution were added until a light yellowish color was obtained. Heptane was removed by applying vacuum and continued until the previous marked level was reached. N_2 overpressure was applied on the styrene and it was stored at 4 °C. Prior polymerization styrene was degassed and distilled from that stock solution at its own vacuum pressure.

10.2.2 Methyl methacrylate

Crude methyl methacrylate (MMA) was first filtered through a chromatographic column containing Al_2O_3 and subsequently distilled onto CaH_2 at a pressure of 136-146 mbar. The resulting stock solution was kept under a slight N_2 overpressure and stored at -18 °C. Prior polymerization MMA was degassed and distilled from that stock solution at its own vacuum pressure.

10.2.3 Butadiene

The pre-cleaned reactor where butadiene gas will be condensed was filled with Bu_2Mg (1.6 M in heptane) (10-15 ml per 50 g of monomer) and the solvent was removed in vacuo under gentle heating

resulting in a grayish colored plaque of Bu_2Mg which is soluble in the monomer. Butadiene gas which was previously purified by passing through two subsequent columns filled with the mol sieves (4 Å) and Al_2O_3 was condensed into the pre-reactor under liquid nitrogen cooling. When the butadiene was collected, the flow rate was constantly monitored. Then the butadiene was thawed by removing liquid N_2 bath and stirred for 24 h at a temperature below 0 °C maintaining a slight N_2 overpressure. The low temperature is necessary to ensure that the major part of the monomer is solved in the cleaning solution. Before butadiene was transferred to the reactor its amount was determined volumetrically at -20 °C in a specially designed burette.

10.2.4 Diphenylethylene (DPE)

Custom-made glassware was used to purify and collect DPE to avoid contamination of the distillate. DPE was filled into the source ampoule and *sec*-BuLi (1.4 M solution in cyclohexane) was added dropwise under a N_2 flow until the solution looks reddish. The red color indicates the absense of impurities. Cyclohexane was removed in vacuo; subsequently the DPE was distilled into the collector ampoule at 300-400 °C by using heat gun.

10.2.5 Diethyl ether (Et_2O)

Crude diethyl ether (Et_2O) was first filtered through a chromatographic column and subsequently stirred over CaH_2 for at least one day. The stock solution was stored at 4 °C. Prior usage diethyl ether was degassed and distilled from that stock solution at its own vacuum pressure.

10.2.6 Tetrahydrofuran (THF)

Tetrahydrofuran (THF) were refluxed over potassium for 3-4 days. The solvent was transferred to the reactor one day before the reaction and cooled down to -30 °C. Then 10 ml (1.4 mmol) of *sec*-BuLi (1.4 M solution in cyclohexane) was added dropwise until the solution color became yellowish. When this yellowish color persist for 20-30 minutes, the temperature was raised to 20 °C and the solution

was stirred slowly overnight which lead to the disappearance of the yellowish color indicating pure THF.

10.2.7 Toluene

Toluene were refluxed over potassium for 3-4 days. After transferring toluene to the reactor, 1-2 drops of styrene were added and the solution was titrated dropwise with *sec*-BuLi (1.4 M solution in cyclohexane) until a light orange color appeares. If the color persists for at least 20-30 minutes, the solvent can be regarded as purified. The entire procedure was done at room temperature. The color disappears typically after 12 hours.

Appendix B.

10.3 Instrumentation of the characterization techniques

10.3.1 Nuclear Magnetic Resonance Spectroscopy (NMR)

^{1}H-NMR spectra were recorded using a Bruker Avance 300 spectrometer at 300 MHz employing field strength of 7.0 Tesla, and relaxation times of 2 sec. For each sample, 64 scans were taken with 10.20 μs pulse length. The solvent $CDCl_3$ is used for the all polymer samples at concentrations of 10-30 mg/ml. Tetramethylsilan (TMS) was used as an internal standard. Raw data were evaluated by the MestRe-C (version 4.8.6.0) software package.

10.3.2 Gel Permeation Chromatography (GPC)

GPC measurements were performed at room temperature in THF using 4 PSS SDV gel columns (10^2, 10^3, 10^4, 10^5 Å, 8×300 mm each, PSS GmbH, Mainz, Germany) at a flow rate of 1.0 ml/min (VWR-Hitachi 2130 pump). A Waters 2410 refractive index detector (λ = 930 nm) and a waters UV-detector operated at 254 nm were used for concentration detection. Samples were injected employing a Waters 717 autosampler (injection volume 20 μL). To compensate for flow-rate fluctuations, 20 ppm 2,6-di-tert-butyl-hydroxytoluene (BHT) was added as internal standard to each sample. Raw data were processed using PSS WinGPC Unity software package. Elugrams are flow-rate corrected; polystyrene

calibration was used to calculate the molar mass distributions. Samples were dissolved overnight in the eluent (c = 1g/l).

10.3.3 Transmission Electron Microscopy (TEM)

The bulk morphology of SBM triblock terpolymers was studied by bright field TEM using a FEI Tecnai 20 operated at 200 kV. Films (approx. 0.2 to 0.3 mm thick) were prepared by casting from a 3 wt% solution of the triblocks in chloroform at room temperature. Teflon rings were used for film casting. The solvent was allowed to evaporate slowly within 2-3 weeks to ensure the formation of a highly ordered morphology close to the thermodynamic equilibrium. The resulting films were annealed for 1 day at room temperature, 1 day at 100 °C, 1 day at 140 °C and subsequently slowly cooled down. For the measurement of TEM, thin sections (thickness 20-30 nm) were cut at room temperature using a Leica Ultracut UCT Ultramicrotome equipped with a diamond knife. The thin films were stained by exposure to OsO_4 vapor for 1 to 3 minutes.

10.3.4 Dynamic Mechanical Analysis (DMA)

The DMA was performed on a EPLEXOR instrument. The temperature range was fixed between -120 °C to 160 °C. Temperature sweeps were conducted at a constant heating rate of 3K/min and at a constant frequency of 10 Hz. Static and dynamic load on strain was 0.35% and 0.25%. Tolerance of contact force was 1.5 N. 1 N contact force was applied for every sample.

10.3.5 Differential Scanning Calorimetry (DSC)

DSC was performed using a Netzsch DSC Phoenix. The equipment was calibrated using indium and cyclohexane. Standard aluminum pans of 50 µl were used to encapsulate the samples of 10 mg ± 1 mg. Dynamic heating and cooling scans were performed. The samples were first heated to 160 °C, held for 3 min, cooled down to -120 °C (for SBM of high 1,4-PB content) or -60 °C (for SBM of high 1,2- B content), held at that temperature for another 3 min, and finally heated to 160 °C. The second heating was picked up to evaluate the thermal transitions of the polymer. The middle points of the transitions were taken as glass transition temperature. All the measurements were done under N_2 atmosphere at a constant rate of 20 K/min.

10.3.6 Small Angle X-ray Scattering (SAXS)

The bulk morphology was complementary studied by small angle X-ray scattering (SAXS). In-situ SAXS and stress-strain experiments were carried out at BW4 beamline of DORIS III, HASYLAB at DESY, Germany. The experiment was done at room temperature at marCCD165 detector to capture the 2D SAXS images. The sample – detector distance was set to 4 meter and 1.38 Å X-ray wavelength was used. The tensile test equipment was set up with the beamline which can simultaneously moves upper and lower clamps in opposite directions thus keeping the beam on the same position of the sample during elongation. 5 mm/min strain rate was used during all experiments and in every 35 sec; one 2D SAXS images were collected. Prior to data analysis, background scattering was subtracted from the data and corrections were made through the operating software Fit2D.

10.3.7 Strain-stress experiments

The strain-stress experiments were carried out on a "Zwick" model Z020, with a load cell of 20 kN. The measurements were done with a crosshead speed of 5 mm/min at ambient temperature, according to the standard ASTM D882. The samples have an average dimension of 12 mm x 35 mm x 250 μm.

Appendix C.

10.4 Determination of the number average molar mass of SBM triblock terpolymer in combination of ^{1}H-NMR and GPC

The number of styrene repeating units in the ternary triblock, n(PS), can be calculated from the number average molar mass of the polystyrene precursor, M_n (PS), which can easily be obtained by a conventional GPC measurement. If a S calibration curve is employed, the averages are not apparent ones. In case the S precursor was not isolated, the molar mass assigned to the peak maximum of the S-precursor concentration signal, M_p(PS), may alternatively be used. For a narrow molar mass distribution (which is usually the case in anionic polymerization), the assumption, $M_p(S) = M_n(S) = M_w(S)$, is fulfilled with the error depending on the precursor's polydispersity, $D = M_w/M_n$. For $D < 1.1$, the error will be less than 10 %. Hence, n (S) can be calculated as

$$n(S) = \frac{M_n(S)}{M_S} = \frac{M_p(S)}{M_S} \quad \text{Equation 10.1}$$

With M_S = 104.2 g/mol (molar mass of the styrene repeating unit)

The knowledge of n(S) allows us to normalize the integral values of the ^{1}H-NMR spectram. The normalization constant, k, is calculated from the combined integral value of the five phenyl-protons of styrene, I (Arom)

$$k = \frac{I\,(Arom)}{5.n(S)} \quad \text{Equation 10.2}$$

The determination of the number of butadiene units, n(B), is not so straightforward, as the downfield vinyl peak group combines the contribution of both the 1,4- and the 1,2- isomers, I (B 1,4 & 1,2). As the upfield vinyl peak group solely contains the contribution of the 1,2-isomer, I(B 1,2), the expression for n (B) reads

$$n\,(B) = \frac{[I(B\ 1{,}4\ \&\ 1{,}2) - 0.5.I(B\ 1{,}2)] + I\ (B\ 1{,}2)]}{2.k} = \frac{I\ (B\ 1{,}4\ \&\ 12) + 0.5.I(B\ 1{,}2)}{2.k} \quad \text{Equation 10.3}$$

Taking into account, that the 1,4-isomer contributes two protons to the downfield vinyl peak group, whereas the 1,2-isomer contributes one proton to the downfield vinyl peak group and two protons to the upfield vinyl peak group of the B units. In case of the poly (methyl methacrylate) block, the resonance signal of the methoxy group (3 protons, I(M) may be used to calculate the number of the methacrylic units

$$n(M) = \frac{I\ (M)}{3.k} \quad \text{Equation 10.4}$$

Analogous to Equation 10.1, the overall number average molecular weight of the ternary triblock is calculated by summation of the averages of each block

$$M_n(SBM) = M_n(S) + M_n(B) + M_n(M)$$

$$= M_n(S) + n(B).M_B + n(M).M_{MMA} \quad \text{Equation 10.5}$$

With M_B and M_{MMA} being the molar mass of the butadiene and methyl methacrylate repeat units/monomer.

Appendix D.

10.5 Determination of chemical composition of SBM copolymers by Gel Permeation Chromatography

The calculation of chemical composition of SBM copolymers by Gel Permeation Chromatography (GPC) is only possible if the refraction increments (dn/dc) of the copolymers additively compose that of the homopolymer, i.e.,

$$(dn/dc)_{SBM} = w_S (dn/dc)_S + w_B (dn/dc)_B + w_M (dn/dc)_M \quad \text{Equation 10.6}$$

Again for SB diblock and S homopolymer, the calculated equations are

$$(dn/dc)_{SB} = w_S (dn/dc)_S + w_B (dn/dc)_B \quad \text{Equation 10.7}$$

$$(dn/dc)_S = w_S (dn/dc)_S \quad \text{Equation 10.8}$$

Here, w_S, w_B, and w_M indicate the weight fraction of S, B and M present in the SBM triblock.

The refraction index increment (dn/dc) of homopolymers are obtained from literature.

$(dn/dc)_S = 0.186$ ml/g

$(dn/dc)_B = 0.132$ ml/g

$(dn/dc)_M = 0.089$ ml/g

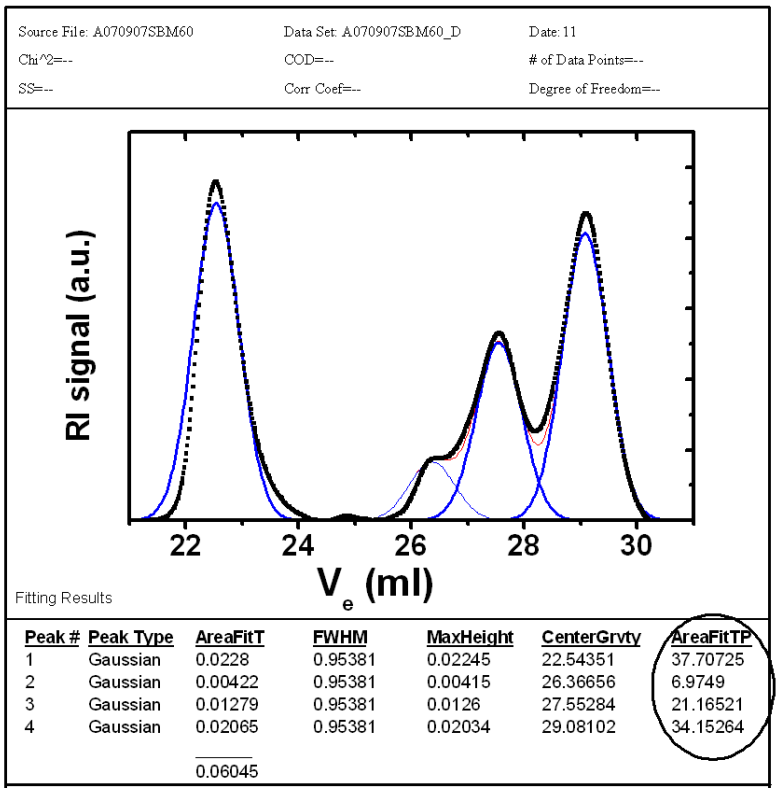

Peak #	Peak Type	AreaFitT	FWHM	MaxHeight	CenterGrvty	AreaFitTP
1	Gaussian	0.0228	0.95381	0.02245	22.54351	37.70725
2	Gaussian	0.00422	0.95381	0.00415	26.36656	6.9749
3	Gaussian	0.01279	0.95381	0.0126	27.55284	21.16521
4	Gaussian	0.02065	0.95381	0.02034	29.08102	34.15264
		0.06045				

Figure 10.1: *Deconvolution using a Gaussian curve algorithm of the elugram (RI detector) to obtain the integration area of the fitting peaks (indicating by circle).*

Taking account of Equation 10.6, the contents of SBM triblock, $M_{(SBM)}$, SB residual diblock, $M_{(SB)}$, and S residual homopolymer, $M_{(S)}$ can be calculated by using the following equations.

$$M_{(SBM)} = \frac{I\,(SBM)}{(dn/dc)_{SBM}} \qquad \text{Equation 10.9}$$

$$M_{(SB)} = \frac{I\,(SB)}{(dn/dc)_{SB}} \qquad \text{Equation 10.10}$$

$$M_{(S)} = \frac{I\,(S)}{(dn/dc)_{S}} \qquad \text{Equation 10.11}$$

Here, I(SBM), I(SB), and I(S) are the area of the peaks obtained by Deconvolution using a Gaussian curve algorithm of the elugram (RI detector) as shown in the circle in Figure 10.1.

Appendix E.

10.6 Mechanical testing data

SBM1 (Batch no 0912103) : $S_{34}B_{31}M_{35}^{80}$

specimens	Et (MPa)	σ_Y (MPa)	ε_Y (%)	σ_M (MPa)	ε_M (%)	σ_B (MPa)	ε_B (%)
1	433	14,5	7,4	15,8	634,8	25,8	579.5
2	430	14,6	7,3	22	540,8	22,0	541,2
3	435	14,5	7,2	14,9	640,9	24,9	524,7
4	513	15,2	6,5	13,4	584,0	23,3	513,4
5	508	15,5	7,1	15,5	522,6	20,4	522,8
6	467	14,8	6,2	14,4	577,7	24,4	577,8
7	460	14,8	6,3	14,9	567,4	24,9	567,9

SBM2 (Batch no 061208_P) : $S_{37}B_{31}M_{32}^{106}$

specimens	Et (MPa)	σ_Y (MPa)	ε_Y (%)	σ_M (MPa)	ε_M (%)	σ_B (MPa)	ε_B (%)
1	862	35,5	7,4	41,8	383,6	40,6	368,9
2	875	31	5,5	32,6	322,7	30,8	329,7
3	812	38,7	7,8	41,6	271,2	39,9	272
4	794	36,9	8	43	365,4	42,8	336,9
5	794	38,5	7,9	44,9	389,3	44,7	389,8
6	839	38,7	7,6	43,5	315,8	42,8	319,4
7	850	39,7	8,5	40,3	177,4	39	183

SBM3 (Batch no 081113) : $S_{32}B_{32}M_{36}^{170}$

specimens	Et (MPa)	σ_Y (MPa)	ε_Y (%)	σ_M (MPa)	ε_M (%)	σ_B (MPa)	ε_B (%)
1	551	16,9	6,3	18,5	620,7	28,5	620,7
2	524	16,9	6,6	16,5	588,6	26,5	588,6
3	519	16,7	6,7	16,9	620	26,9	620,2
4	491	17,2	7,5	18,2	607,7	28,2	607,9
5	550	17,4	6,5	15,5	485,5	25,5	485,5
6	542	16,9	6,5	18,4	588	28,4	588,1
7	483	16,9	7,2	18,6	627,1	28,6	500,3

SBM4 (Batch no 090217) : $S_{31}B_{31}M_{38}^{55}$

specimens	Et (MPa)	σ_Y (MPa)	ε_Y (%)	σ_M (MPa)	ε_M (%)	σ_B (MPa)	ε_B (%)
1	493	21,1	6,4	31,1	6,4	14	66,3
2	609	-	-	27,9	7,2	27,5	119,2
3	614	28,5	7,9	38,5	7,9	27,8	96,5
4	495	23,3	7,3	33,3	7,3	17,8	124,1
5	467	20,6	6,6	37,6	6,6	16,1	107,3
6	548	22,3	5	32,3	5	16,9	85,4
7	461	19,4	6,5	29,4	6,5	14,2	72,3

SBM6 (Batch no 081016) : $S_{31}B_{38}M_{31}^{38}$

specimens	Et (MPa)	σ_Y (MPa)	ε_Y (%)	σ_M (MPa)	ε_M (%)	σ_B (MPa)	ε_B (%)
1	271	22,85	8	22,85	8	13,1	18,4
2	260	19,04	8,45	29,04	24,7	15,6	24,3
3	293	-	-	23,23	9	14,8	17,4
4	238	-	-	28,26	12,8	9	27,5
5	192	26,63	6,9	26,63	28,3	11,2	18,4
6	262	28,7	7,9	28,7	25,7	8,5	15,8
7	253	-	-	28,63	8,5	9,3	16,2

SBM7 (Batch no 090304_P) : ($S_{30}B_{29}M_{41}^{53}$)

specimens	Et (MPa)	σ_Y (MPa)	ε_Y (%)	σ_M (MPa)	ε_M (%)	σ_B (MPa)	ε_B (%)
1	243	-	-	18,5	358,6	26,3	430,5
2	239	-	-	12,2	486,3	19,7	503,5
3	231	-	-	10,6	677,1	26,6	677,2
4	207	-	-	17,8	776,6	22,8	776,7
5	215	-	-	9,8	610,5	22,8	611
6	224	-	-	8,6	710,6	23,3	711,4
7	247	-	-	11,4	463,3	27,3	469,9

SBM8 (Batch no 090225_P) : ($S_{21}B_{27}M_{52}^{75}$)

specimens	Et (MPa)	σ_Y (MPa)	ε_Y (%)	σ_M (MPa)	ε_M (%)	σ_B (MPa)	ε_B (%)
1	390	-	-	16,7	92,2	19,8	130,4
2	369	-	-	15,9	155,9	13,7	160,6
3	348	-	-	18,1	12,5	12,8	102,5
4	334	-	-	17,4	63,9	17,2	96,8
5	366	-	-	14,2	36,9	16,5	83,4
6	354	-	-	18,1	25,7	14,7	88,8
7	319	-	-	15,6	103,4	17,4	120,9

SBM9 (Batch no 090219) : ($S_{24}B_{25}M_{54}^{54}$)

specimens	Et (MPa)	σ_Y (MPa)	ε_Y (%)	σ_M (MPa)	ε_M (%)	σ_B (MPa)	ε_B (%)
1	390	-	-	16,7	92,2	19,8	130,4
2	369	-	-	19,9	155,9	13,7	160,6
3	348	-	-	18,1	12,5	12,8	102,5
4	334	-	-	16,4	63,9	17,2	96,8
5	366	-	-	14,2	36,9	16,5	83,4
6	354	-	-	21,1	25,7	14,7	88,8
7	319	-	-	15,6	103,4	17,4	120,9

SBM10 (Batch no 090310_3P) : ($S_{32}B_{31}M_{37}^{91}$)

specimens	Et (MPa)	σ_Y (MPa)	ε_Y (%)	σ_M (MPa)	ε_M (%)	σ_B (MPa)	ε_B (%)
1	741	22,5	7,2	24,3	264,2	24,1	265,8
2	677	22,9	7,8	23,8	223,6	23,5	225,9
3	684	22,3	7,8	22,5	193,7	22,3	196,6
4	685	21,8	7,4	23,7	262,4	23,6	263,5
5	695	22,6	7,2	22,9	165,2	22,1	169
6	717	21,6	7,9	22,4	200,6	22,1	201,3
7	668	22,2	7,8	25	303,8	25	304,2

SBM11 (Batch no 090317_P) : ($S_{26}B_{29}M_{45}^{148}$)

specimens	Et (MPa)	σ_Y (MPa)	ε_Y (%)	σ_M (MPa)	ε_M (%)	σ_B (MPa)	ε_B (%)
1	517	19,3	6,4	17,1	749,8	27,1	749,8
2	605	19	6,5	17,2	759,1	27,2	759,3
3	490	18,7	5,8	21	773,9	20,8	749,4
4	462	18,7	5,9	18,2	786,9	15,6	786,7
5	554	18,7	6,1	19,1	748,4	27,9	748,6
6	646	19,1	6,3	17,9	792,1	28,4	792,2
7	638	19,1	6,5	18,4	757,8	17,9	763

SBM12 (Batch no 081030) : ($S_{29}B_{31}M_{40}^{90}$)

specimens	Et (MPa)	σ_Y (MPa)	ε_Y (%)	σ_M (MPa)	ε_M (%)	σ_B (MPa)	ε_B (%)
1	659	19,6	6	19,7	326,7	19,5	328,3
2	547	19	7	19,2	359,2	19	360,4
3	586	18,9	6,5	18,9	6,5	18,7	332,8
4	611	18,9	5,9	18,9	6,4	18,8	337,4
5	659	19,7	6,1	19,7	6	19,4	361,4
6	652	19,8	6,3	19,8	6,1	19,2	335,1
7	661	20	6,5	20	6	16,7	325,1

SBM13 (Batch no 081030_P) : ($S_{30}B_{31}M_{39}^{110}$)

specimens	Et (MPa)	σ_Y (MPa)	ε_Y (%)	σ_M (MPa)	ε_M (%)	σ_B (MPa)	ε_B (%)
1	585	18,7	6,7	18,7	6,7	15,6	192,2
2	555	18,8	6,8	18,8	6,8	17,9	237,9
3	561	18,4	6,7	18,4	6,7	17,5	260,1
4	556	19,5	5,9	19,5	5,9	18,4	190,3
5	550	19	6,5	19	6,5	17,4	237,5
6	636	19,4	6,3	19,4	6,3	16,2	235,1
7	531	20	6,5	19,3	6,5	17,1	225,1

SBM14 (Batch no 090326_P) : ($S_{30}B_{31}M_{39}^{113}$)

specimens	Et (MPa)	σ_Y (MPa)	ε_Y (%)	σ_M (MPa)	ε_M (%)	σ_B (MPa)	ε_B (%)
1	466	14,1	6,6	14,4	473,2	24,4	473,6
2	450	14,3	6,6	15,1	506,9	25	50,7,5
3	448	14,1	6,6	15,3	540	25,3	540,3
4	433	13,9	6,8	14,4	503,8	24,4	528,6
5	462	14,2	7,2	14,8	528,1	24,8	612,7
6	475	14	7,3	16,9	612,7	26,9	591,4
7	489	14,6	6,7	18,3	591,3	28,3	419,9

SBM15 (Batch no 091217) : ($S_{39}B_{31}M_{30}^{312}$)

specimens	Et (MPa)	σ_Y (MPa)	ε_Y (%)	σ_M (MPa)	ε_M (%)	σ_B (MPa)	ε_B (%)
1	561	16,7	5,1	16,7	5,1	3,76	7,3
2	695	-	-	22,1	35,2	21,8	35,9
3	693	-	-	22,3	40,7	21,6	43,4
4	708	-	-	21,7	25,3	21,3	26,3
5	678	-	-	21,5	27,8	20,4	31,8
6	661	-	-	21,7	35,2	21,1	36,6
7	636	-	-	20,9	31,2	19,5	32,3

Appendix F.

10.7 Glass transition temperature obtained from DSC and DMA for different lamellar SBMs triblock terpolymers.

Sample code	Batch no	Polymer	DSC			DMA		
			T_g of S	T_g of B	T_g of M	T_g of S	T_g of B	T_g of M
SBM1	091203	$S_{34}B_{31}M_{35}^{80}$	97.9	-87.3	118.5	99.7		141.7
SBM2	061208_P	$S_{37}B_{31}M_{32}^{106}$	103.3	-12.6	130.4	109.4	-7.5	139.3
SBM3	081113_3P	$S_{32}B_{32}M_{36}^{170}$	98.9	-78.3	132.3	105.7		141.7
SBM4	090217	$S_{31}B_{31}M_{38}^{55}$	93.7	-10.5	124	93.4		141.4
SBM5	081128	$S_{32}B_{27}M_{41}^{43}$	90.2	-4.6	125.4			
SBM6	081016	$S_{31}B_{38}M_{31}^{38}$	-	-75.9	124	70	-25.4	134.6
SBM7	090304_P	$S_{30}B_{29}M_{41}^{53}$	-	-85.6	123.1			
SBM8	090225_2P_large	$S_{21}B_{27}M_{52}^{75}$	-	-80.2	130.9	101.5		141.4
SBM9	090219_P_large	$S_{24}B_{25}M_{51}^{54}$				102	-25	132.2
SBM10	090310_3P	$S_{32}B_{31}M_{37}^{91}$	99.7	-13.2	127.8	99.7		141.7
SBM11	090317_P	$S_{26}B_{29}M_{45}^{148}$	-	-88.5	122.9	93.4		141.3
SBM12	081030	$S_{29}B_{31}M_{40}^{90}$				105.7		141.8
SBM13	081030_P	$S_{30}B_{31}M_{39}^{110}$	97	-82.4	126.2	103.8		141.8
SBM14	090326_P	$S_{30}B_{31}M_{39}^{113}$	97.6	-85	133.1	101.7		143.7
SBM15	091217	$S_{39}B_{31}M_{30}^{312}$	102.4	-13.5	129.5	109.7		141.8

Appendix G.

10.8 Summarize of the estimated interaction parameter, volume fraction ratio, percentage of the B microstructure and the resulted morphologies of SBMs.

Sample code	polymers	$\chi_{SB}.N_{S+B}$	$\chi_{BM}.N_{B+M}$	$\chi_{SM}.N_{S+M}$	ϕ_S	ϕ_B	ϕ_M	ϕ_S:	ϕ_B:	ϕ_M	X(1,2-B)	X(1,4-B)	morphology
SBM1	$S_{34}B_{31}M_{35}^{80}$	44,83	75,96	22,23	0.26	0.43	0.31	1 :	1.6 :	1.2	18	82	well segregated lamellae
SBM2	$S_{37}B_{31}M_{32}^{106}$	61,31	97,37	29,40	0.29	0.43	0.28	1 :	1.5 :	1	87	13	well segregated lamellae
SBM3	$S_{32}B_{32}M_{36}^{170}$	95,20	166,39	46,59	0.25	0.43	0.32	1 :	1.7 :	1.3	30	70	well segregated lamellae
SBM4	$S_{31}B_{31}M_{38}^{55}$	29,84	53,92	15,31	0.24	0.42	0.33	1 :	1.8 :	1.4	90	10	well segregated short domain lamellae
SBM5	$S_{32}B_{27}M_{41}^{43}$	21,60	40,21	12,67	0.25	0.38	0.37	1 :	1.5 :	1.5	89	11	well segregated short domain lamellae
SBM6	$S_{31}B_{38}M_{31}^{38}$	23,68	39,58	9,48	0.23	0.50	0.27	1 :	2.2 :	1.2	34	66	chain like oriented lamellae
SBM7	$S_{30}B_{29}M_{41}^{53}$	27,21	51,57	15,19	0.24	0.40	0.36	1 :	1.7 :	1.5	16	84	mixed lamellae
SBM8	$S_{21}B_{27}M_{52}^{75}$	32,74	78,61	22,23	0.16	0.37	0.47	1 :	2.3 :	2.9	24	76	mixed lamellae
SBM9	$S_{24}B_{25}M_{51}^{54}$	23,30	53,99	16,42	0.19	0.34	0.46	1 :	1.8 :	2.4	19	81	transitional lamellae
SBM10	$S_{32}B_{31}M_{37}^{91}$	48,81	86,33	24,76	0.25	0.43	0.32	1 :	1.7 :	1.3	89	11	transitional lamellae
SBM11	$S_{26}B_{29}M_{45}^{148}$	72,45	150,10	42,52	0.20	0.40	0.40	1 :	2.0 :	2.0	14	86	transitional lamellae
SBM12	$S_{29}B_{31}M_{40}^{90}$	47,75	90,08	25,08	0,23	0,42	0,35	1:	1.8:	1.5	35	65	-
SBM13	$S_{30}B_{31}M_{39}^{110}$	59,02	108,96	30,63	0,23	0,43	0,34	1:	1.9:	1.5	34	66	-
SBM14	$S_{30}B_{31}M_{39}^{113}$	60,63	111,93	31,47	0,24	0,42	0,34	1:	1.8:	1.4	17	83	-
SBM15	$S_{39}B_{31}M_{30}^{312}$	184,19	280,20	86,44	0,30	0,43	0,27	1:1	1.4:	1	88	12	lamellae

Acknowledgement

First of all, I would like to thank Prof. Dr. Volker Abetz for giving me the opportunity to pursue my PhD in the '*Institute of Polymer Research*' at Helmholt-Zentrum Geesthacht and to be my supervisor. I would like to express my gratitude for his patience and persistence with me in the duration of my work. His support, guidance and encouragement helped me to develop my understanding in the field of block copolymer's morphology and also made this PhD work possible.

Secondly, I would like to thank my co-supervisor Prof. Dr. Peter F.W. Simon for his great patience and willingness to supervise my daily work. Without his support and his expertise in the organic synthesis my work would be hard to format so nicely. His systematic working for achieving scientific success encouraged me to work hard during these years.

I feel deeply indebted to my department head Dr. Volkan Filiz. Though I got him as a co-supervisor only for a few months but within this short time he helped me a lot to organize the results and to finalize my thesis.

I am very much grateful to Clarissa Abetz for hard working to obtain so nice TEM micrographs from my polymers which helped me a lot during discussing my result. Thanks to Heinrich Böttcher for performing the mechanical testing of all my polymers. I appreciate his patience specially during measurements of some rubbery elastomers. I am also deeply indebted to Dr. Adriana Boschetti-de-Fierro for her caring approach to me. She always allowed me to do SAXS experiment in DESY with her group PMM. My warm thanks to Dr. Julio Albuerne who helped me a lot not only to evaluate the SAXS results but also in many other cases.

Many thanks to Silvio Neumann and Dr.Thomas Emmler for DSC and NMR measurements, Maren Brinkmann for doing the GPC, Dr. Sérgio Funari, Dr. Ulla Vainio and Jan Perlich for their help during SAXS measurement in HASYLAB.

Among my group members, I specially thanks to Brigitte Lademann. From the very beginning to the very end of my working, she helped me in the lab during anionic polymerization. Her patience, sometimes very nice ideas during my experiment assisted me to synthesis in a good way.

I feel also indebt to Prof. Dr. Mady Elbahri with whom I am presently working in the department of Nanochemistry and Nanoengineering. His great patience and friendly attitude gave me enough chance to complete my PhD writings.

During this long period of staying in Germany, I have many great moments with my colleagues and friends. My warm thanks to Sabrina, Nahide and Dragutin for their support during these years. I have my pleasure to introduce Shahid, Maab, Shahin, Usman, Sofia, Adina, Sara, Bach and my other friends to share my days during staying in Geesthacht.

Financial support from the German Research Foundation (Deutsche Forschungsgemeinschaft (DFG) is also greatly acknowledged.

Finally, I am very much grateful to my Parents, Brothers and Sister for their continuous support and encouragement during these years.